




University of
Stavanger

Faculty of Science and Technology

MASTER'S THESIS

Study program/ Specialization: MSc in Petroleum Geoscience Engineering	Spring semester, 2012 Open
Writer: Kriswandani	 KRISWANDANI (Writer's signature)
Faculty supervisor: Chris Townsend (University of Stavanger & Total E&P Norge AS) External supervisors:	
Title of thesis: Log Typing and Electro-facies Interpretation in Ekofisk Field	
Credits (ECTS): 30	
Key words: chalk, electro-facies, dense zone	Pages: 235 + Front pages: 9 + CD Stavanger, June 2012

Log Typing and Electro-facies Interpretation in Ekofisk Field

Kriswandani

Department of Petroleum Geosciences Engineering – University of Stavanger

ABSTRACT

Recognition of the dense zones in Ekofisk field is clearly observed from well logging through a specific peak in the neutron-density log. These zones appear to be intercalated in porous clean chinks in the middle part of the Ekofisk formation, at the border of the Ekofisk-Tor Formation and in the middle part of the Tor formation. The thick zone between the Ekofisk and Tor formation that is a so called tight zone is found continuously within the Central Graben basin. On the Ekofisk field, this zone is suspected to be a very good conductor for cold injected water compared to the clean porous chalk intervals. By recognizing these zones, a more integrated new well planning (completion and placement) together with the field development schemes to more efficiently drain the field is possible to implement.

Log responses of gamma ray and density that is combined with the values of Young's Modulus and Poisson's ratio from 5 wells (2/4-A-6, 2/4-B-19 A, 2/4-K-22, 2/4-K-4 and 2/4-X-32) are used to characterize the different chalk types within the Ekofisk field. These responses group the rock into 8 types, which comprise 3 types of tight clean chalk, 3 types of clay-contaminated tight chalk and 2 types of clean porous chalk. In a different scale, wells with mineralogy analysis links the electro-facies to the elements that may be responsible for the different chalk reservoir quality. The defined electro-facies in the Ekofisk and Tor formations have also been checked against data from core analysis and measurements of pressure, fractures and permeability to better characterize the physical properties of the electro-facies.

By the means of 72 wells completed with e-facies, the trend of dense zones in specific layers (EM2, EM4, EEU, EEM, EEL and TBU) is examined. A spatial analysis of each e-facies is performed in order to be able to extrapolate the facies distribution throughout the field. The resulting model is validated by using 3 blind-test wells, completed with electro-facies and core description, which not are accounted for in the modeling.

The result of the study is a map of facies proportion for each of the stratigraphic layers within the Ekofisk field and a facies model of certain stratigraphic layers. In the EM2 and EM4 layers, the pattern of lateral facies change can hardly be recognized qualitatively indicating a random-patchy facies distribution. In the EE layer, the facies population suggests an unsystematic lateral facies distribution. However, a distinct belt of more dense facies of East-West orientation can be demonstrated in the northern and southern areas of the Ekofisk field in the TBU layer.

Keywords: chalk, electro-facies, dense zone

List of Contents

Abstract	ii
List of Contents	iii
List of Figures	v
List of Tables	vii
List of Appendix.....	viii
Acknowledgements.....	ix
1 Introduction	1
2 Data and Methodology	7
2.1 Log Typing for Electro-facies Interpretation.....	8
2.2 Data Analysis for Facies Modeling.....	11
3 Geological Setting and Sedimentation of Chalk	15
3.1 Geological Setting	15
Tectonic Activity	17
Direction of Sedimentation related to Tectonic Activity.....	18
3.2 Sedimentation of Chalk	18
Reworking of the Sediment	23
Rock Geomechanics.....	25
4 Data Preparation and Result.....	26
4.1 Data Preparation.....	26
4.2 Result	28
4.2.1. Log Typing	28
4.2.2. Facies Modeling	32
5 Quality Check and Observation	33
5.1 Log Typing.....	33
5.2 Statistical Observation of Geomechanical Response and Rock Properties..	36
5.2.1. Facies to porosity	36
5.2.2. Porosity vs. Young's Modulus	37
5.2.3. Porosity vs. Poisson's Ratio.....	38
5.2.4. Porosity Distribution by the Function of Depositional Type	39
5.2.5. Facies Distribution by the Function of Depositional Type.....	40
5.3 Facies Evolution throughout the Field.....	41

Layer EM2	41
Layer EM4	42
Layer TBU	42
Layer EE.....	42
5.4 Facies Modeling	44
5.5 Facies Characterization.....	47
5.5.1. Observation 1(2/4-M-23 and 2/4-M-24)	47
5.5.2. Observation 2 (2/4-X-37 and 2/4-X-32)	48
5.5.3. Observation 3 (2/4-C-11 and 2/4-K-11 A).....	49
5.5.4. Observation 4 (2/4-K-13 T3)	50
6 Discussion.....	51
6.1 Facies Classification	51
6.2 Facies Characterization.....	54
Water Weakening	54
Porosity Preservation.....	56
Reservoir Connectivity and Fracturing	58
6.3 Sedimentation	59
6.4 Facies Modeling	59
7 Conclusion.....	61
References	62

List of Figures

Figure 1.1	Norwegian chalk province	1
Figure 1.2	Lithostratigraphy of North Sea chalk	2
Figure 1.3	Regressive-transgressive of Late Cretaceous sequences	3
Figure 1.4	Dense zones at different interval.....	5
Figure 1.5	Stratigraphy unit in the Ekofisk field.....	6
Figure 2.1	Illustration of rock's elastic measurement	7
Figure 2.2	Example of KNN attraction sets	9
Figure 2.3	KRI used in the study.....	10
Figure 2.4	Illustration of vertical variogram	12
Figure 2.5	Illustration of variogram	13
Figure 2.6	Workflow of the study	14
Figure 3.1	Map showing the Highs and Zechstein salt	15
Figure 3.2	Diagram Illustrating Palaeogeography in north-western Europe.....	16
Figure 3.3	Schematic diagram of North Atlantic rift system during Late Jurassic	17
Figure 3.4	Trace-fossil of Maastrichtian chalk.....	19
Figure 3.5	Development of nodular chalk and hardgrounds.....	20
Figure 3.6	Schematic process of pressure-solution	21
Figure 3.7	Formation of lenticular chalk.....	22
Figure 3.8	Different appearance of fracture.....	23
Figure 3.9	Resedimentation process and the resulted feature	24
Figure 4.1	CDF and PDF of GR, RHOB, YMOD and POIS.....	27
Figure 4.2	Sensitivity on normalization	27
Figure 4.3	Statistics of log response for 123 facies model	28
Figure 4.4	3D chart of 3 facies model	29
Figure 4.5	Statistics of log response for 1-8 facies model	30
Figure 4.6	3D chart of 8 facies model	30
Figure 4.7	Example of map of facies proportion	31
Figure 4.8	Variogram analysis of 123 facies model with its major direction	32
Figure 4.9	Example of continuous facies model of layer EEM.....	33

Figure 5.1	Well section of 2/4-X-32 comparing electro-facies and mineralogy.	36
Figure 5.2	Histogram of porosity filtered by type of facies	37
Figure 5.3	Plot of porosity vs. Young's modulus.....	38
Figure 5.4	Histogram of porosity vs. Poisson's ratio	39
Figure 5.5	Histogram of porosity filtered by depositional type	40
Figure 5.6	Histogram of depositional type filtered by facies.....	41
Figure 5.7	Map showing well location and well section of 2/4-X-32; 2/4-X-12 and 2/4-X40 for 123 facies model.....	44
Figure 5.8	Well section of 2/4-X-32; 2/4-X-12 and 2/4-X40 for 1-8 facies model	45
Figure 5.9	Illustration of the error in the blind test.....	46
Figure 5.10	Qualitative QC using 2/4-A-8 in the 1-8 facies model	47
Figure 6.1	Plot of mineralogy analysis	52
Figure 6.2	Histogram of porosity filtered by facies	52
Figure 6.3	Well section of 2/4-X-32 with STM	53
Figure 6.4	Proportion of depositional type to porosity	56
Figure 6.5	Porosity vs depth classified by carbonates content	57

List of Tables

Table 2.1	Summary of dataset, methodology and QC used in the study.....	14
Table 4.1	Facies change due different smoothing	26
Table 4.2	Facies change due to different sampling rate	26
Table 4.3	Facies change due to normalization	28
Table. 5.1	P50 from 1-8 facies model	34

List of Appendix

Appendix 2.1	Wells with complete logging data	66
Appendix 2.2	Mineralogy analysis of 2/4-X-32 and 2/4-A-8	67
Appendix 2.3	Variogram analysis to determine cell size	68
Appendix 3.1	Isochron map	74
Appendix 3.2	Seismic Line.....	75
Appendix 4.1	Wells with data cleaning and handling; and Sensitivity result	76
Appendix 4.2	Map of proportion of facies	83
Appendix 4.2.1	Map of facies proportion from 123 model (Well log)	83
Appendix 4.2.2	Map of facies proportion from 123 model (Upscaled Well log)	110
Appendix 4.2.3	Map of facies proportion from 1-8 model (Well log).....	137
Appendix 4.2.4	Map of facies proportion from 1-8 model (Upscaled Well log) .	164
Appendix 4.3	Variogram analysis of 3 facies model	191
Appendix 4.4	Variogram analysis of 8 facies model	197
Appendix 4.5	Parameters from variogram analysis of 3 and 8 facies model	215
Appendix 5.1	Well correlation	217
Appendix 5.2	Observation from well section.....	220
Appendix 6.1	Well section of 2/4-M-17 and 2/4-M-18	226
Appendix 6.2	Trend of facies in layer EEU	227
Appendix 6.3	Water imbibition issue on 2/4-C-11 A	231

Acknowledgement

The author would like to thank Chris Townsend and Lutz Seiffert for defining this thesis project and for patiently sharing the knowledge and experience throughout the project, and Mats Skaug for providing the reviews and comments in detailed of the report. The author would also like to thank the management of Total E&P Norge who granted him the opportunity to work throughout the thesis period.

Stavanger, June 2012

Kriswandani

1 Introduction

The prolific chalk province of the North Sea Central Graben that extends in Danish, Norwegian and UK sectors was deposited during Upper Cretaceous to early Paleocene (Fig. 1.1). This area has been explored since 1966; the first discovery was the Kraka field in the Danish sector. On the Norwegian sector, the first discovery was the giant Ekofisk field in 1969. The first discovery on the UK sector was the Machar field, which was discovered in 1976. During the following years, Eldfisk, Tor, Valhall and Hod were found on the Norwegian sector (Surlyk, 2003).

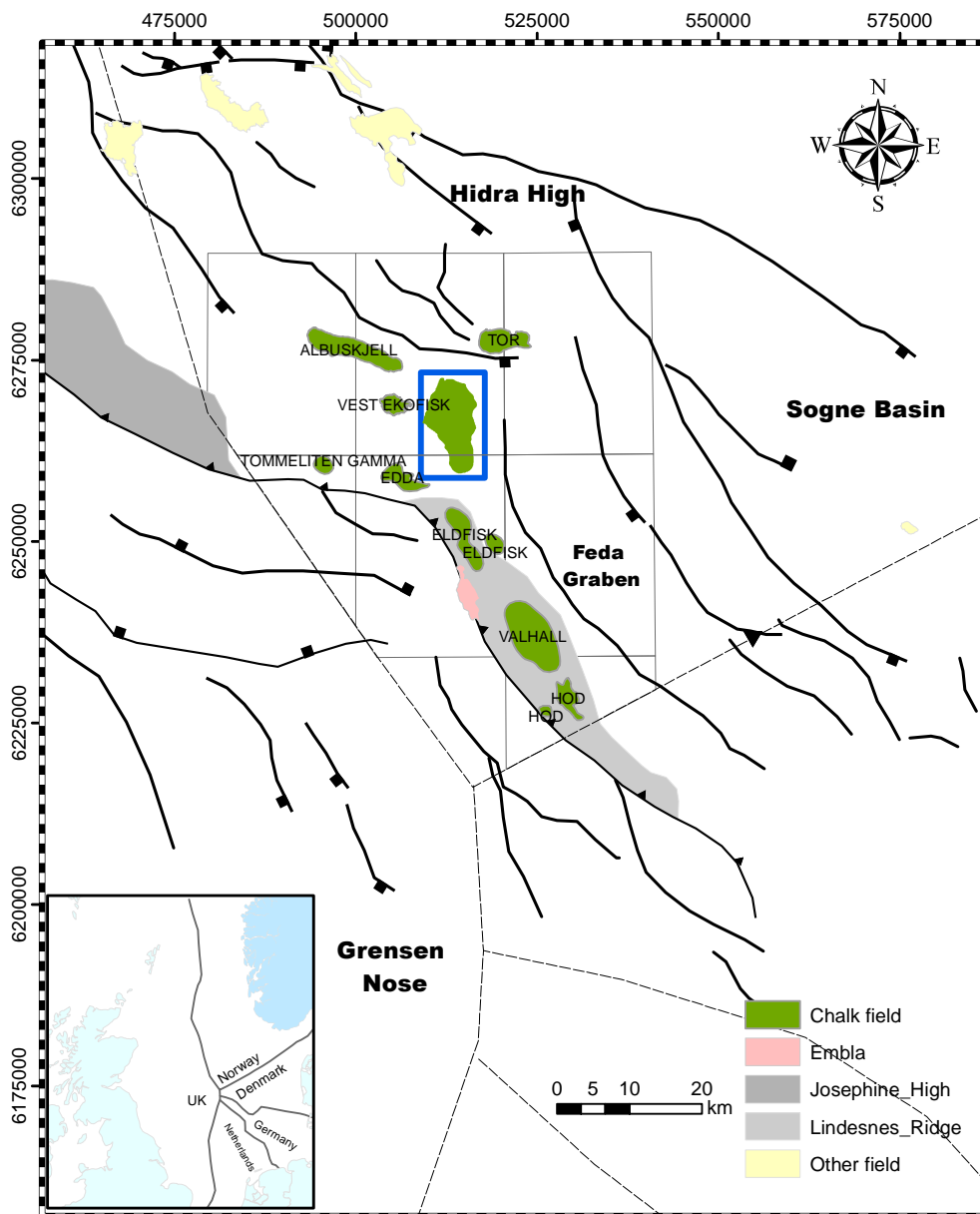


Figure 1.1. Norwegian chalk province (blue box is the area of study of the Ekofisk field)

The lithostratigraphy of the Norwegian sector divides the chalk group into several formations. The Cenomanian Hydra formation was deposited at the base of the group and in contact with Zechstein group in some areas. A marl sequence on top of the Hydra formation marks the boundary to the Turonian to Campanian in Hod formation, which acts as a reservoir in the Valhall, Hod and Eldfisk fields. On top of the Hod formation, the Maastrichtian deposits of the Tor formation are marked by thick clay sequence. The Tor formation is found extensively in the Central Graben basin and is the most productive series in most of the Norwegian chalk fields (Andersen, 1995). On the top of the group, Ekofisk formation is deposited in Danian age (Fig. 1.2).

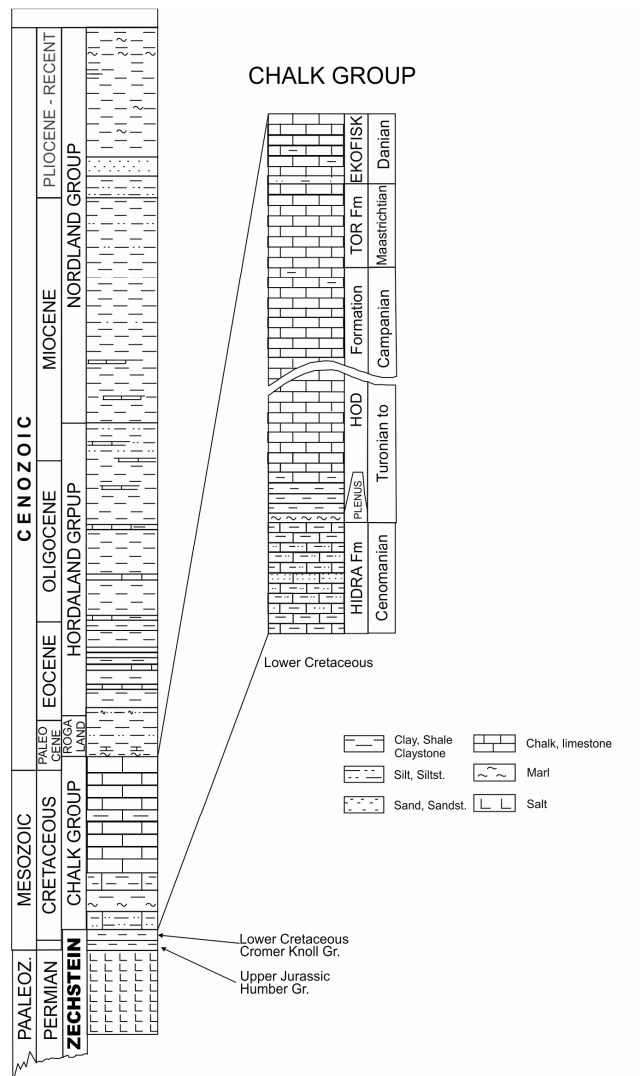


Figure 1.2. Lithostratigraphy of North Sea chalk (D'Heur, 1985)

In regional scale within Central Graben, a so called 'Ekofisk tight zone' presents in the border between the Ekofisk and Tor formations. The thickness and degree of the tightness of the zone can vary from one place to another. This zone represents a turnover of the sea level change that took place between Maastrichtian and Danian age (Kennedy, 1980). The relatively deep regression enabled the input of terrestrial deposits in a deep water chalk environment (Fig. 1.3).

The age between Maastrichtian-Danian might also represent the starting point of a strongly reduced or ended of chalk deposition. The chinks deposited during the Danian time period (i.e. the Ekofisk formation) are mostly found to have the same signature as the chalk deposited during the Cretaceous. Scholle and Arthur (1990) compiled data from pelagic limestones in the Circum Atlantic western Tethyan region and found a drop in $\delta^{13}\text{C}$ of c. 1‰ at the transition from the Maastrichtian into Danian. This is interpreted as a reflection of probable faunal and floral changes.

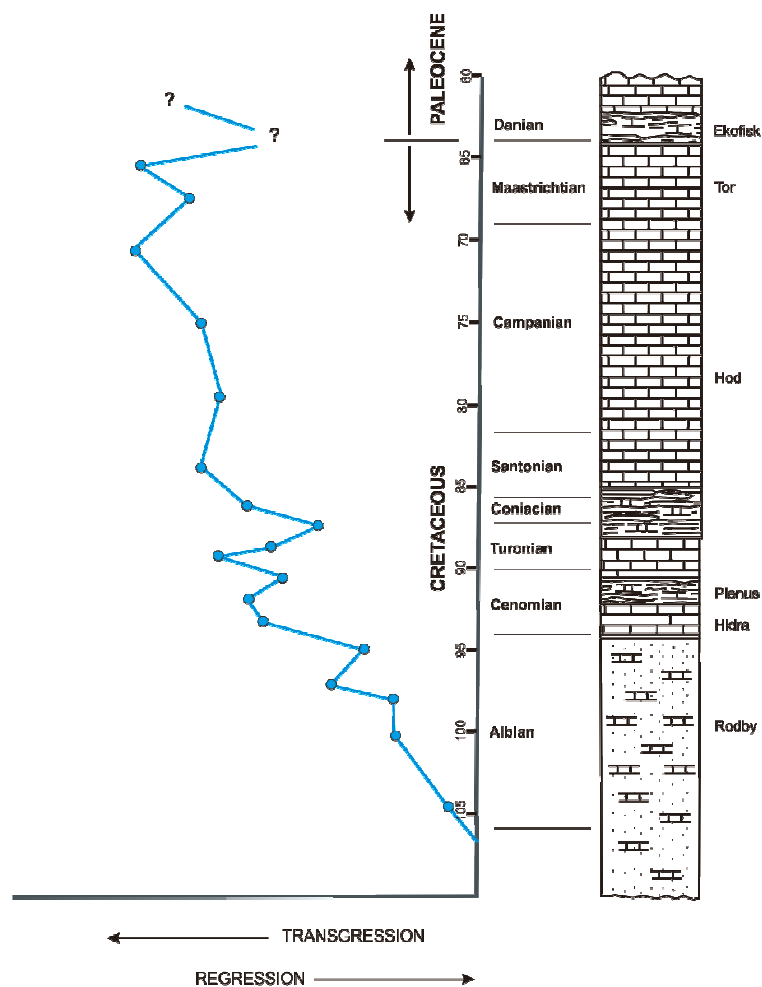


Figure 1.3. Regressive-transgressive of Late Cretaceous sequences in north-west Europe (Kennedy, 1980)

On a well scale, the Ekofisk tight zone (EE) is recognized by high Gamma Ray (GR) and density (RHOB) readings. In the normal chalk zone, GR reading is at level of 6 API; but it can jump to 16 API in front of the tight zone (Fig. 1.4). This zone is also marked by a increase in the density (RHOB) from 2.1 g/cc, in the porous chalk zone, to as much as 2.3 g/cc in the tight zone (EE). Even if the zone has a very low porosity, it appears as a good marker throughout the basin.

A more detail subdivision of the EE zone has provided a better interpretation of the different rock types (Fig. 1.5). The upper part of the Ekofisk tight zone (EEU) is typically signed by low GR and high RHOB readings. The middle part (EEM) exhibits high GR reading and high RHOB, while the bottom part (EEL) is more unique as the log signature changes and becomes the combination of the log response of EEU and EEM.

In Ekofisk field, there also seems to be dense zones in the middle of Ekofisk formation and in the middle of Tor formation beside the thick dense zone in Ekofisk-Tor boundary. Two intervals in the middle of Ekofisk field, known as Ekofisk Middle 2 (EM2) and Ekofisk Middle 4 (EM4), are recognized through the small peaks of RHOB and neutron (NPHI). The same signature of logs also present at Tor B Upper (TBU).

Understanding the different rock types is important especially when the field comes into production. A fast water-conductive rock, which as observed at 2/4-C-11 A, has indicated that not all of the chalk has the same productive manner. This indicates a different correlation is at place between the rock properties to the different dense zone.

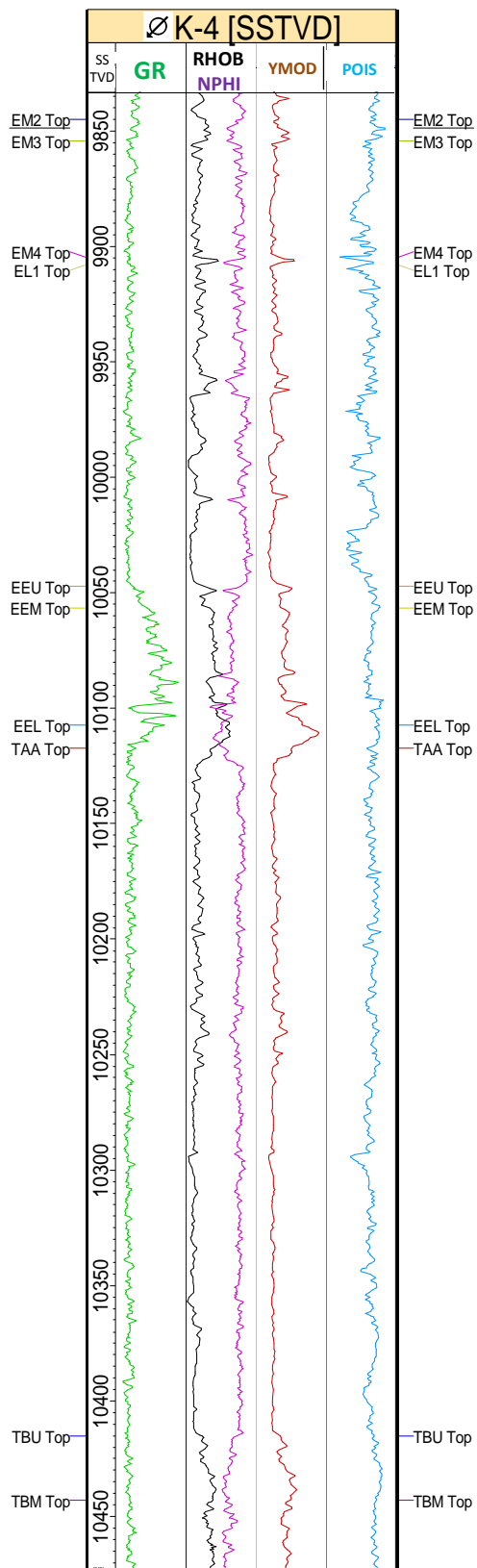


Figure 1.4. Dense zones at different intervals signed with density peak and anomaly values for Poisson's ratio and Young's modulus

stratigraphy		
EKOFISK formation	UPPER	EA1_U
		EA1_M
		EA1_L
		EA2
		EA3_U
		EA3_M
		EA3_L
	MIDDLE	EM1
		EM2
		EM3
		EM4
	LOWER	EL1
		EL2
EL3		
TIGHT zone	EEU	
	EEM	
	EEL	
TOR formation	TA	TA_A
		TA_B
		TA_C
		TA_D
		TA_E
	TB	TB_U
		TB_M
		TB_L
	TC	TC_U
		TC_M

Figure 1.5. Stratigraphy unit in the Ekofisk field

This study focuses on grouping the different rock type of chalk and that includes recognizing the different dense zone in Tor and Ekofisk formation in Ekofisk field. In well scale, the result of the grouping is to be correlated to fracture and reservoir connectivity. In field scale, a map of rock type proportion is produced for qualitative interpretation regard to the lateral change of the facies. Then a more detail facies modeling in certain zone (EM2, EM4, EEU, EEM, EEL and TBU) where dense zone presents is performed to better understand the spatial distribution of the facies and that also to feed the reservoir simulation.

2 Data and Methodology

In this study, the grouping of rock type is based on the log response of GR, RHOB, together with Young's modulus (YMOD) and Poisson's ratio (POIS) values. GR is used to separate the rock based on its radioactive quantity, notably chalk and clay. RHOB is used to measure the degree of the compaction applied to the rock. YMOD describes the stiffness of the rock or the rock's resistance against being compressed. POIS indicate the degree of the stress contained by the rock.

Poisson's ratio is the ratio of lateral strain to longitudinal strain for the application of an increment of longitudinal stress (Fig. 2.1). This property is derived from dipole excitation of the sonic log. The source causes a package or volume of wellbore fluid to be pulsed unidirectionally perpendicular to the borehole axis (whereas traditional monopole has a radial expanding wave). With low frequency dipole excitation, the measured shear velocities of slow formations becomes viable (Fjær, E., et al.,2008).

Theoretically, Poisson's ratio is measured by:

$$POIS = \frac{\text{Lateral Strain } (\Delta r)}{\text{Longitudinal Strain } (\Delta L)}$$

From dipole sonic, it is derived from:

$$POIS = \frac{0.5 \times R^2 - 1}{R^2 - 1} \quad \text{where } R = \frac{DT_s}{DT_c}$$

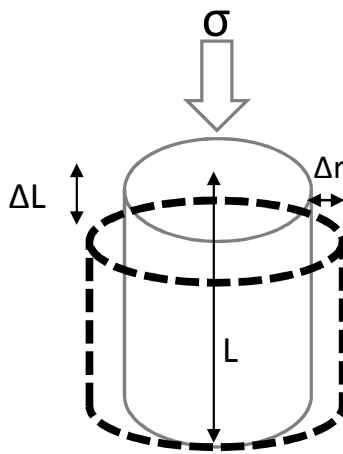


Figure 2.1. Illustration of rock's elastic measurement

Young's modulus is defined as the relationship between the uniaxial stress and uniaxial normal strain. From experiments, Young's modulus can be measured by:

$$YMOD = \frac{\text{Applied Stress}}{\text{Normal Strain}} = \frac{\sigma}{\Delta L / L}$$

In well logging, it is calculated using Poisson's ratio:

$$YMOD = 2 \times N \times (1 + POIS)$$

where N is shear modulus of an empty rock frame that can be derived from :

$$N = \frac{F / A}{\tan x}$$

with $\tan x$ as the fractional strains of length

The background for using these dataset is to be able to differentiate the degree of chalk purity with its corresponding elastic properties. This will be useful in order to address the different rock properties (permeability and fracture) with regards to different chalk qualities which may not be explained by a simple law. As some chinks may behave ductile or brittle depending on the rock components, the method used for measuring the rock properties for one rock type may be quite unique compared to the method used to measure the rock properties for another rock types.

The dataset in this study contains of 72 wells completed with GR, RHOB, YMOD and POIS (Appendix 2.1) and 2 wells with mineralogy analysis (Appendix 2.2).

2.1 Log Typing for Electro Facies Interpretation

Based on the logs combination of GR, RHOB, YMOD and POIS, an electro-facies analysis is possible to build using Multi-Resolution Graph-Based Clustering or MRGC (Ye, 2000) which is provided in Geolog6 using the Facimage application. The method works by using multi-dimensional dot-pattern-recognition based on non-parametric K-Nearest-Neighbour (KNN) and graph data representation. This method is able to automatically recommend the optimal number of clusters, but it also provides the flexibility to the user to produce as many clusters as needed and re-group them to sensible number of facies (Ye, 2000).

In log clustering, the log samples are characterized by two indexes (NI and KRI) which describe the neighboring relationship.

1. Neighboring Index (NI)

NI is a parameter that indicates how strong a point attracts (or get attracted by) the other individual points in its surroundings regarding to the position of each point. As the index depends on the value of KNN (K-Nearest-Neighbour) or the size of the dataset, the NI of a point may change accordingly (Fig. 2.2). After assigning the NI value, the points can be grouped into small datasets with the highest NI value as the barycenter. The higher the value of NI, the closer the point is to the kernel (mode) of a cluster (Ye, 2000). This is mathematically represented as:

$$NI_n(x) \approx \sum_{n=1}^{N-1} \exp\left(-\frac{m}{\alpha}\right)$$

where:

- $(N-1)$ is the size of data set
- x is the m^{th} NN of y , $m \leq N-1$, and $\alpha > 0$
- y is n^{th} NN of x
- α is a smoothing (resolution) parameter

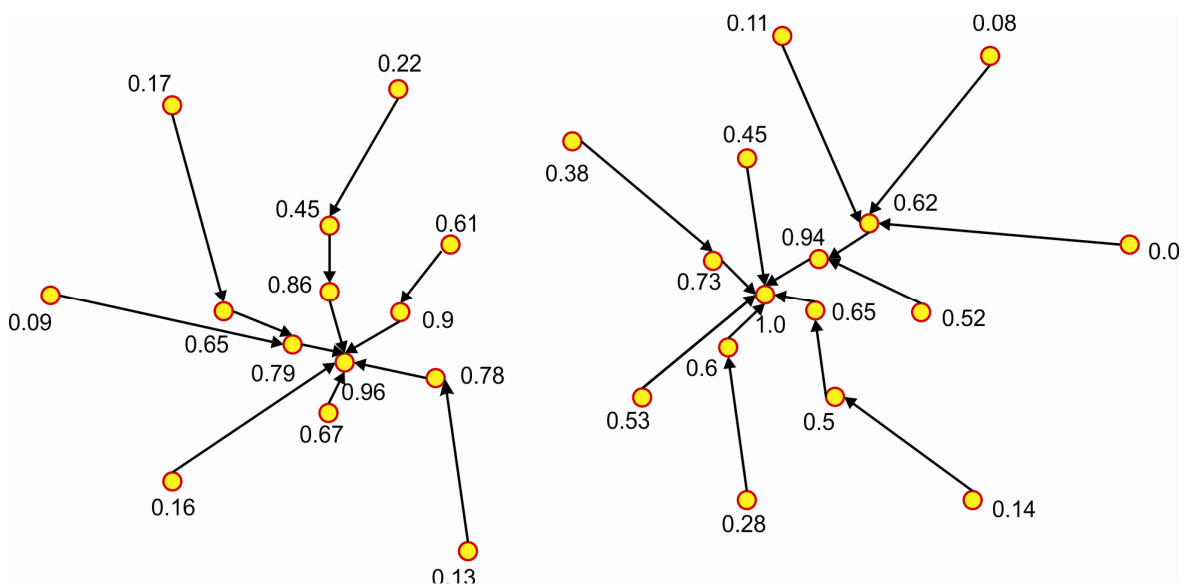


Figure 2.2. Example of KNN (K-Nearest-Neighbour) attraction sets with numbers of neighboring indexes (Ye, 2000)

2. Kernel Representative Index (KRI)

This method is able to propose several optimal numbers of clusters corresponding to different resolutions. The result will be organized in a hierarchical way so that the clusters of higher resolution always are sub-clusters of the low resolution clusters (Ye, 2000).

NI can identify local modes, valleys or minimums, while the KRI can identify the optimal number of the cluster. On top of that, it is very important to check whether each point in the KRI is representative. This is why the flexibility to re-group comes in place. However, points with the best values of KRI will be selected as final cluster kernels by default.

KRI of x is calculated as:

$$KRI(x) = NI(x)M(x)D(x, y)$$

where:

- $M(x, y) = m$ if y is the m th neighbor of x .
- $D(x, y)$ is the distance between x and y .

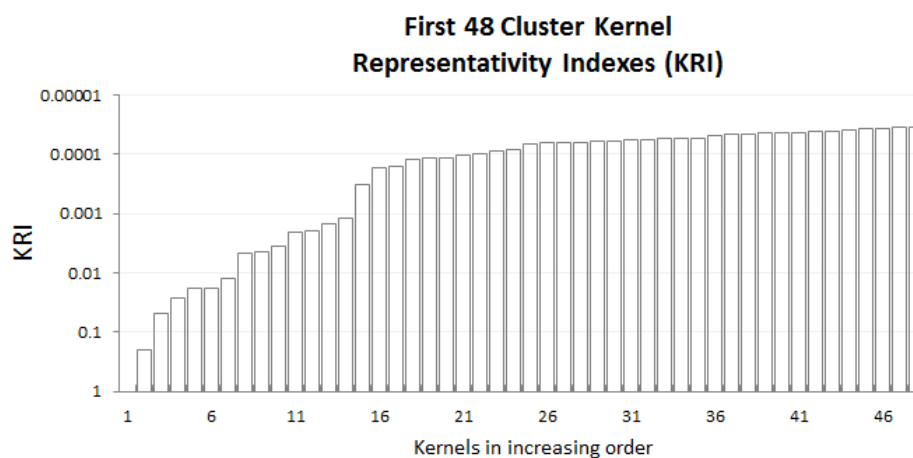


Figure 2.3. KRI used in the study

A different way of quality check is possible to perform by using another application within the software of Similarity Threshold Method (STM). This application enables one to check whether if the interpreted facies is covered in the training dataset (reference dataset). It implies to the correctness of wells used in training data set which should normally represent all the possible

facies that may appear in the field. This method may also indicate the possible presence of some specific facies that has been penetrated by certain wells.

This study uses un-supervised facies interpretation which may lead to an un-unique solution of rock type grouping. In order to quality check the resulted groupings (on a different scale), a well (2/4-X-32) completed with mineralogy analysis is compared side by side to hint the possible elements responsible for certain groups of electro-facies. By doing so, the sedimentary facies which is complex and also affected by diagenesis and tectonism (Ye, 2000) can be compared with the electro-facies that is based on sets of log responses.

In order to understand the physical meaning contained by each facies, the data acquisition from well logging is attached next to the facies interpreted. A plot of pressure data from Repeat Formation Pressure (RFP) is used to quantify the physical meaning of the facies. This observation is combined with the plot of fracture intensity to give a clearer picture of the rock properties within certain rock types.

2.2 Data Analysis for Facies Modeling

In the data analysis, variograms have been chosen to check the relationship of the variation in a property as a function of the separation distance between the data points. In this analysis, two points that are close together are assumed to be more likely to have similar values than points far from each other. In any condition of the data (different or similar), the variogram can be used to model the way two points are correlated (Schlumberger, 2011). In this study, this method is used intensively to predict the continuity of the facies.

The first step of facies modeling is to upscale the interpreted electrofacies to a certain vertical size of 3D model. The analysis of the cell size is performed by the means of vertical variograms with a data resolution of 0.5 ft or equal to the resolution of the log sampling (the lateral x and y size of the cells remain unchanged). It depends on the heterogeneity of the facies contained and each layer may have different cell sizes (Appendix 2.3).

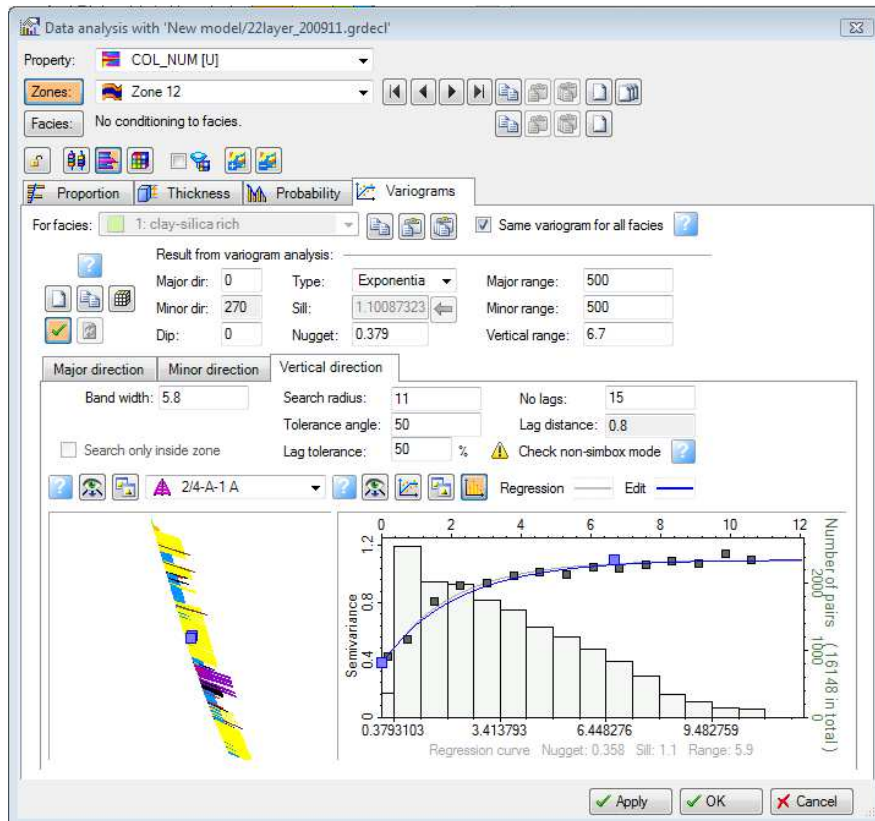


Figure 2.4. Illustration of vertical variogram

From the vertical variogram analysis, the proper vertical size of the cells can be obtained. This may reduce the possibility of losing the important details of the facies change in the vertical direction. At the same time, the analysis will reduce the load on the computer when facies are propagated throughout the field. The criteria used for the correct layering size is that the lag distance should be 1-2 times of the sampling rate, hence giving a grid layering less than $\frac{1}{2}$ of the vertical range.

In this study, the algorithms for upscaling the logs were the:

- Average method of “Most of” as the correct sizing of the grid layering is assumed to be known from the vertical variogram analysis.
- Treat log of “As lines” where the sample values will be weighted by the distance between samples.
- Method of “Neighbor cell” where log values are averaged and then assigned to the penetrated cell(s) without any constrains.

In order to be able to propagate the facies from 70 wells throughout the field, a more detailed data analysis were required. The analysis consisted of a statistical relationship in the major

direction which refer to the major sedimentation within the area and minor direction which refers to the localized direction of sedimentation. From this analysis, a range from the major and minor directions will be used to model the spatial distribution of the facies. The curve matching of variogram model type and nugget is also performed in this stage. In these models, the dip is kept at 0 and sill is normalized to 1 (Fig. 2.5).

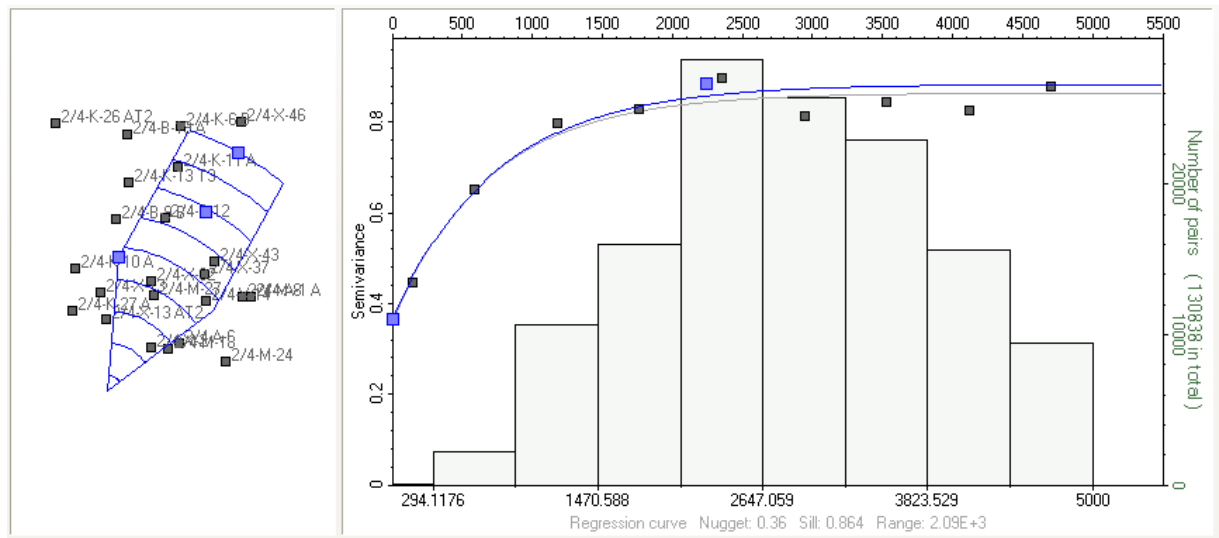


Figure 2.5. Illustration of variogram (major direction of N29E, major range of 2244 m and nugget of 0.36)

The determination of the direction of sedimentation in this study is strongly influenced by the observation of the tectonic activity and the way the sediment was deposited within the region. From previous studies reviewing the seismic stratigraphy of the region (Gennaro, 2011); it is possible to identify the location of the sediment source and the orientation of the deposition. This may however vary from one facies to another case by case.

The algorithm used to propagate the facies is the Sequential Indicator Simulation (SIS). It works based on stochastic pixel models that use upscaled cells as a basis for facies types to be modeled. The variogram built in the data analysis constrains the distribution and connectivity of each facies type (Schlumberger, 2011).

A total of 70 wells are taken into account in the facies modeling. There are two wells excluded from the dataset in order to provide the tool to validate the resulting facies model. With the same purpose, one well (2/4-A-8) with mineralogy analysis is used to check the reliability of the

model. In the end, the issue of the fast water imbibition on 2/4-C-11 A is also considered for the model validation.

The dataset are summarized as follow:

Table 2.1. Summary of dataset, methodology and QC used in the study

	Log Typing	Facies Modeling
Methodology	MRGC	SIS with variogram
Dataset	GR, RHOB, YMOD, POIS	Upscaled facies using 3 and 8 model facies
Reference well	2/4-A-6, 2/4-B-19 A, 2/4-K-22, 2/4-K-4, 2/4-X-32	All 72 wells, except 2/4-X-12 and 2/4-X-40
Quality Check	Core data from 2/4-X-32	2/4-X-12, 2/4-X-40 and core data from 2/4-A-8

The step and workflow of the study is represented as:

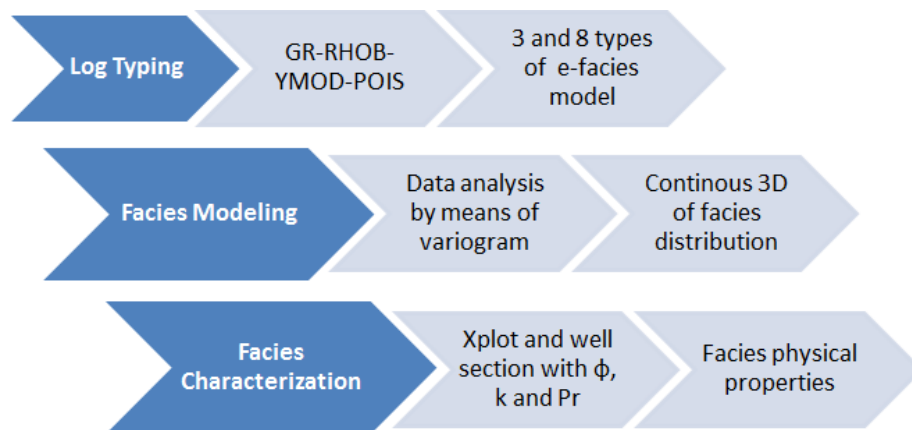


Figure 2.6. Workflow of the study

3 Geological Setting and Sedimentation of Chalk

3.1 Geological Setting

The crustal movements begun in the Late Permian and continued into Early Triassic, where a basin commenced forming in the North Sea (Fig. 3.1). This period is related to the initiation of the break-up of the Pangea supercontinent in the Triassic. In the North Sea, this activity subdivided the region into southern and northern basins by the east-west trending elongated Mid-North Sea and Ringkøbing-Fyn Highs (Nystuen, 2008).

The condition in North Sea during Late Permian was mostly dry. But the rifting allowed the Boreal Sea to extend southwards and flood the two great basins (Nystuen, 2008). With the climate remaining hot and arid, vast amounts of water evaporated and initiated the remaining water to become oversaturated with salt. This process later on formed the Zechstein salt within the basins (Worsley, 2008).

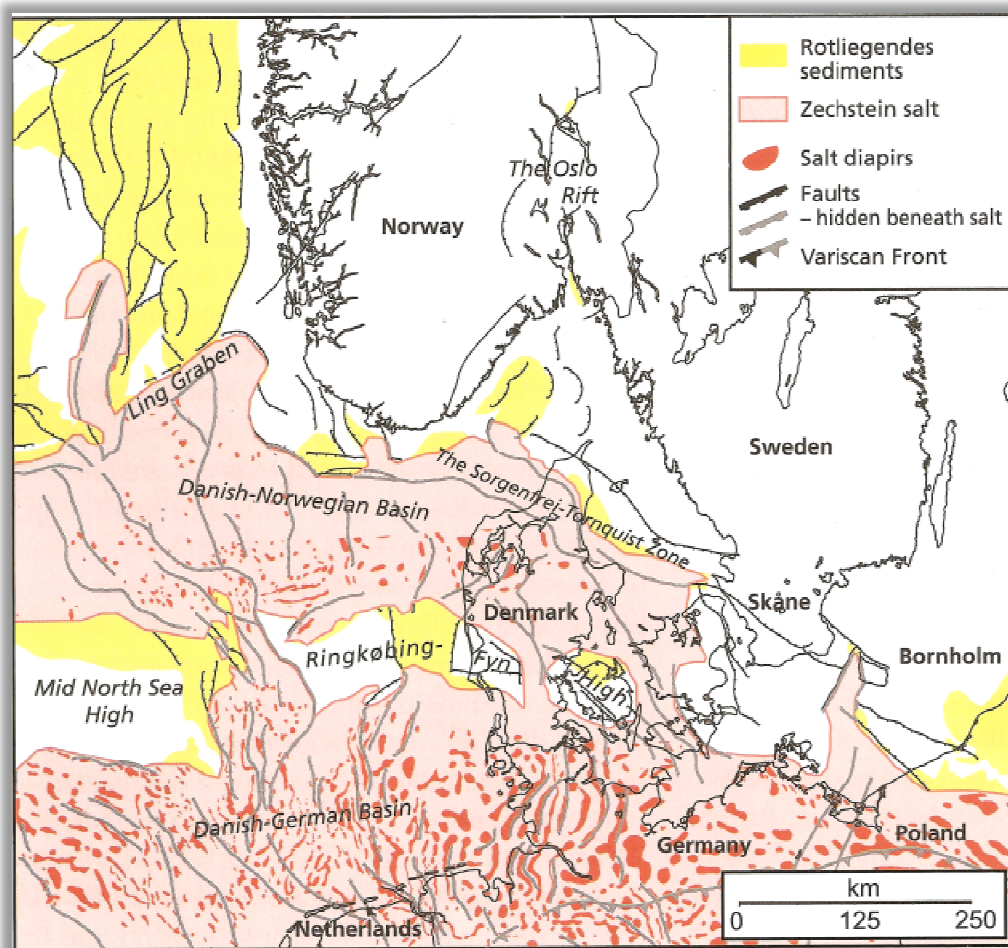


Figure 3.1. Map showing the Highs and Zechstein salt (Larsen, 2008)

In the Triassic, the northern part of the North Sea was surrounded by the hills and low-lying mountains of mainland Norway (Nystuen, 2008). These elevated areas became the sediment source of sands, gravel and muds to the North Sea basin (Fig. 3.2).

During the Early and Middle Jurassic, the North Sea became sub-merged as the fragmentation of the old Permian-Carboniferous Pangean supercontinent continued, with the break-up axis migrated progressively northwards to the central Atlantic Ocean. This provided the areas close to Norway to be subjected to a period of less tectonic activity (Johannessen, 2008). During this period, the climate changed from arid to humid, which led to a sedimentation that was dominated by gravel, sand and mud from the mainland (Fig. 3.2).

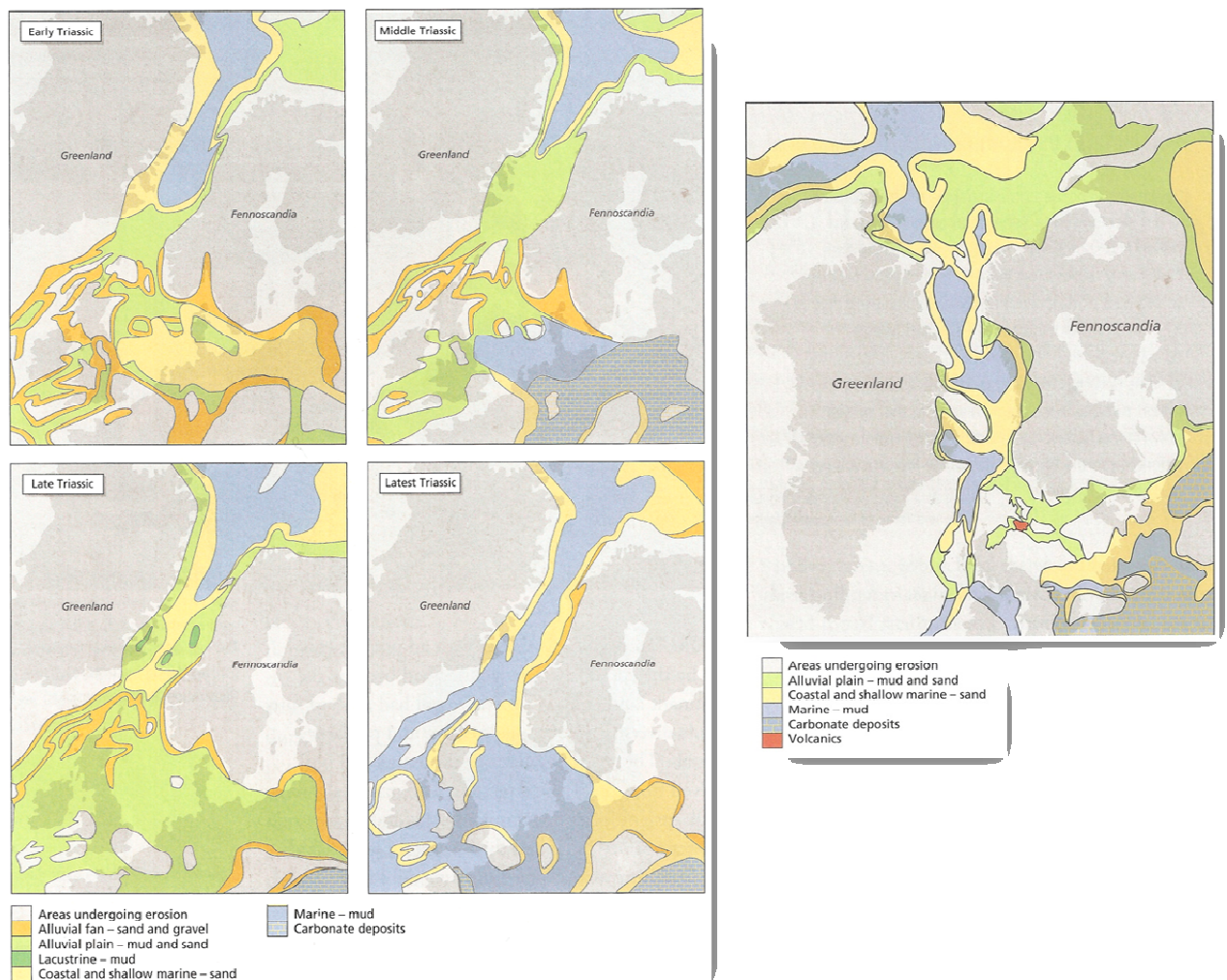


Figure 3.2. Diagram Illustrating Palaeogeography in north-western Europe. On the left is during Triassic (Nystuen, 2008) and on the right is during Middle Jurassic (Johannessen, 2008)

In the late Jurassic, the sea-floor spreading in the Mid-Atlantic branched into the North Sea, resulting in a rift characterized by an elongate and continuous appearance from North Sea to the Barents Sea, which represented a renewal of the older Permo-Triassic rift (Fig. 3.3). Compared to the precursor Permian-Triassic rift, which was continental, the Late Jurassic break-up involved deeper subsidence and was localized within a narrower zone (Nøttvedt, 2008). During the rifting in this period, the deep Central Graben basin was formed before it eventually got filled by Late Cretaceous-Early Paleogene chalk sediments.

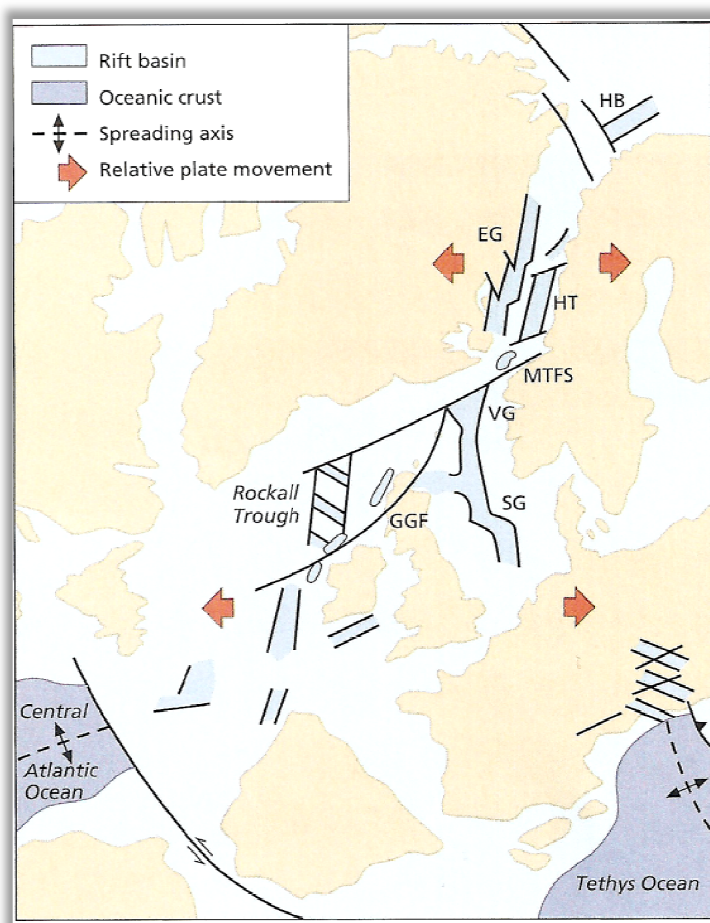


Figure 3.3. Schematic diagram of North Atlantic rift system during Late Jurassic (SG=Central Graben, VG=Viking Graben, HT=Halten Terrace, EG=East Greenland Basin, HB=Hammerfest Basin, GGF=Great Glen Fault, MTFZ=Møre-Trøndelag Fault Zone) (Nøttvedt, 2008).

Tectonic Activity

In the Late Cretaceous, the Central Graben was influenced by thermal relaxation and subsidence along the main boundary faults (Ziegler, 1990). During this period until Lower Paleocene, the surrounding basin margins acting as relatively stable platforms. However due to NNE-SSW compressional events that lead to the inversion of existing Upper Jurassic faults,

which created anticlines and structural highs such as the Lindesnes Ridge (Cartwright 1989). In addition to the inversion, the ductile behavior of the Zechstein salt also created diapirs and salt domes structures along the major basement faults (Knott, 1993; Oakman & Partington, 1998).

The study area of the Ekofisk field is located in middle part of chalk province in the Norwegian sector in the Central Graben (Fig. 1.1). The field is a result of piercing diapirs of Zechstein salt and is characterized by upturned reservoir beds that are deformed during the salt piercement (Zanella, 2003). Trapped towards the overlying shales, the field extends 13 km N-S and 7 km W-E. It deposited sediment from Maastrichtian age of Tor formation and Danian age of Ekofisk formation.

Direction of Sedimentation related to Tectonic Activity

The inversion that created the Lindesnes Ridge was significantly active during Santonian age in Late Cretaceous. From the previous study of "Seismic Stratigraphy of the Chalk Group in the Norwegian Central Graben, North Sea" by Gennaro, 2011, isochron maps from the Lindesnes Ridge imply that the sediment deposition in this area was significantly reduced in this period; while thick sediment was deposited in the heart of graben (Appendix 3.1). This observation is supported by a relative northwards shift of the depocenter in the graben during the Cenomanian-Coniacian.

From Santonian age and forward, the main deposenter remained in the middle of the Central Graben with a NW-SE orientation. During Campanian and Lower Maastrichtian, the activity of the ridge was not as significant as during Santonian. This is indicated by the relatively thick Campanian and Lower Maastrichtian sediment sequence on the ridge. In Upper Maastrichtian to Danian, the ridge resumed to be active and seemed to act as sediment source for the graben.

Seismic lines (Appendix 3.2) also indicate that the Lindesnes Ridge became the source of sediment for the Central Graben from Maastrichtian and onwards through the prograding clinoforms of the Tor formation. The SW-NE orientation of the clinoforms is relatively perpendicular to the strike of the ridge. This observation implies that the sediment have been transported across the wide slope of the ridge during a drop in the sea level during the upper Maastrichtian period.

3.2 Sedimentation of Chalk

During the high sea level in Late Cretaceous, most of today's continental areas of NW Europe were flooded by water. This period was combined with reduced terrigenous input, warm temperature and normal water salinities that enabled a widespread chalk deposition (Scholle, 1977; Surlyk, 2003). The chalk deposits roughly covered ~30% of the European continent in the

same successions that may reach a thickness of 2 km in the depocenter of Central Graben (Scholle, 1977; Ziegler, 1990)

During the chalk deposition, the water depth is assumed to have been between 180-450 meters (Van den Bark, 1980). The coccoliths reached the seafloor by slow settling from suspension as faecal pellets (Andersen, 1995). When the coccolith debris first settles, the porosity is about 70%, forming watery carbonate ooze (Hardman, 1977).

This primary pelagic chalk is thereby subject for bioturbation by shallow-burrowing benthic invertebrates that facilitate gradual dewatering and early compaction (Fig. 3.4). The trace fossils that represent the burrowing of diverse benthic communities occupy a succession of substrates that changes through time (Bromley and Ekdale, 1986; Bromley, 1996). In addition to the bioturbation, have the petrophysical properties been affected by the lithological composition and water-driven diagenetic processes as the deposits have been buried to more than 3000 m.

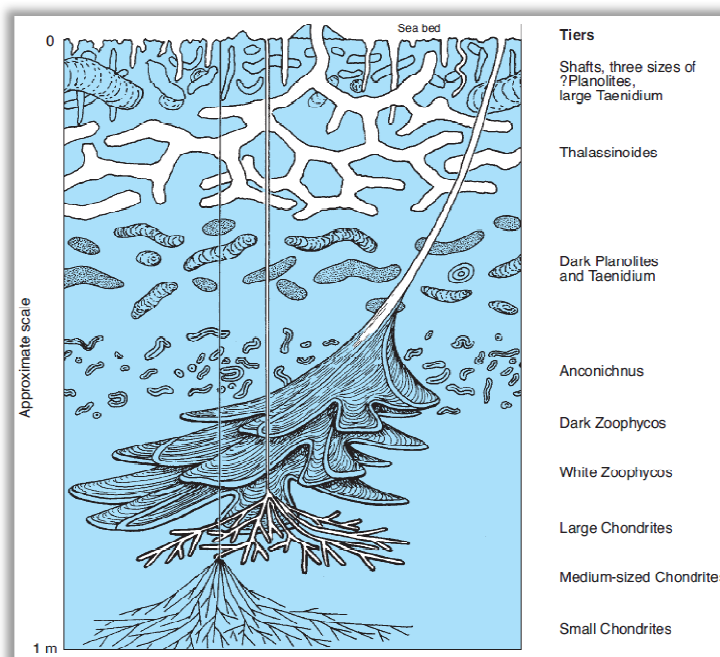


Figure 3.4. Trace-fossil of Maastrichtian chalk (Surlyk, 2003)

Flint nodules in the succession are a result from precipitation of silica formed in *Thalassinoides* burrows. These burrows were formed during times of slow deposition or non-sedimentation. In this system, silica may originate from skeletal elements of siliceous sponges, radiolarian and/or diatoms. The flint is composed of microcrystalline quartz and represents a late diagenetic phenomenon. The process of flint formation was initiated by the dissolution of biogenic opaline silica and subsequent re-precipitation of cristobalite (opal CT) that started at the early stage of the diagenesis (Surlyk, 2003).

Hardgrounds develop due to breaks in sedimentation that may represent periods of time where sedimentation rate were often low (Fig. 3.5). This event is a consequence of long exposure of sediment-water interface which initiate dissolution and other diagenetic process notably cementation and replacement of carbonate by glauconite and phosphate (Scholle, 1977). Discrete nodules are then created few decimeters below the interface. The condition of continuous growth and fusion of the nodules into layers may result in the forming of a incipient hardground. The layer may become a true hardground if it is exposed to erosion basis the sea floor (Surlyk, 2003).

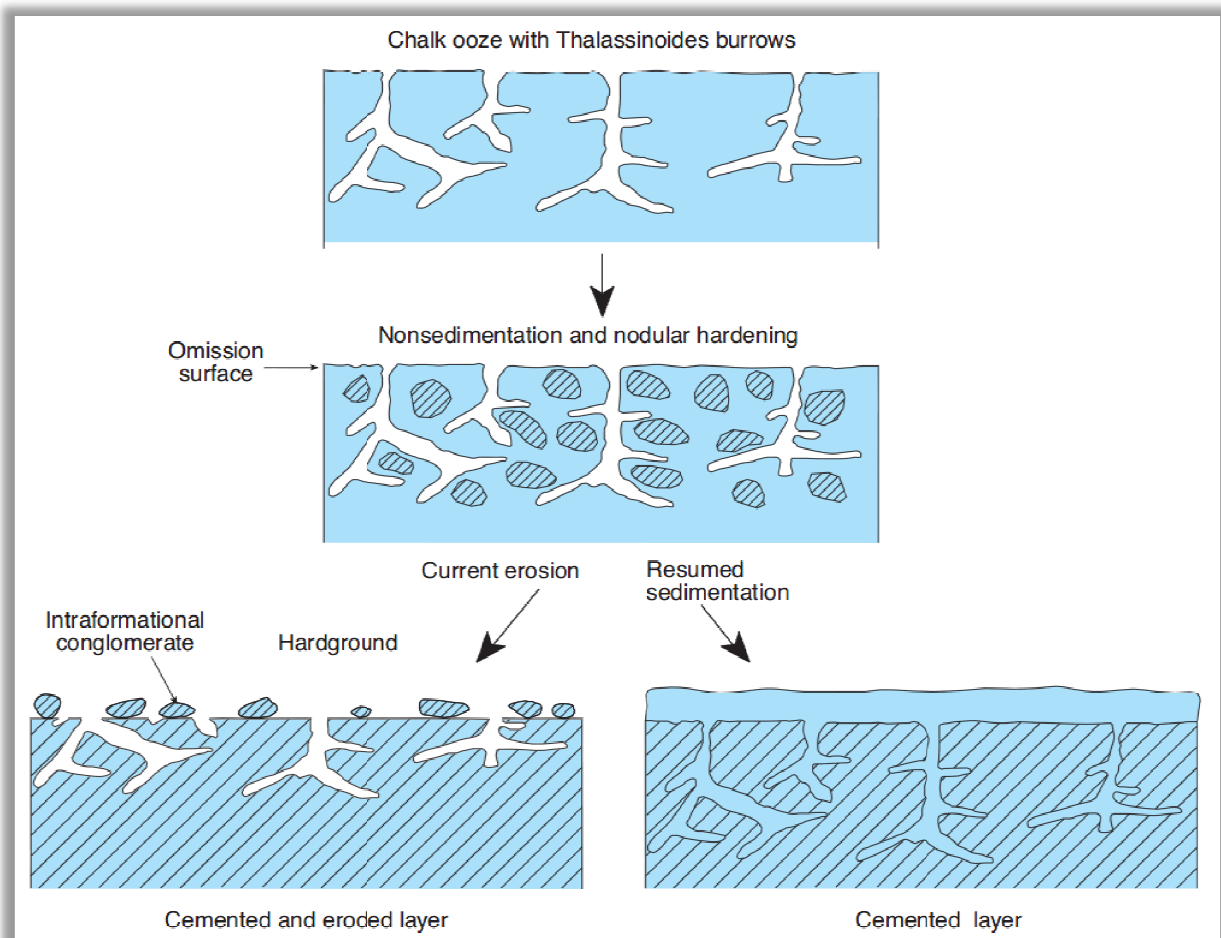


Figure 3.5. Development of nodular chalk and hardgrounds (Surlyk, 2003)

When burial depths exceed about 1000 m pressure solution occur (Neugebauer, 1973) as a result of the deformation of individual mineral grains and precipitation of material in pore spaces (Fig. 3.6). This process may be one of the primary processes responsible for the local production of dissolved material that precipitates as cements during diagenesis and burial cementation (Hudson, 1975; Wong and Oldershaw, 1981).

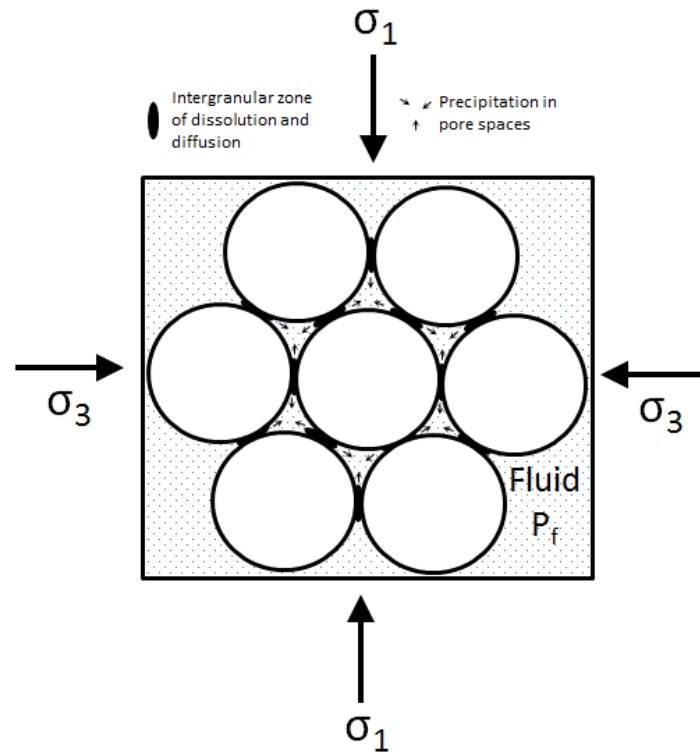


Figure 3.6. Schematic process of pressure-solution in grain to grain contact and pore space (Hellmann, 2002)

Features related to the development of pressure-solution have been widely observed such as diagenetic lamination, lenticular chalk and stylolites (Surlyk, 2003). Diagenetic lamination is characterized by dark, parallel, irregularly wrinkled, pressure-solution seams (Fig. 3.7). Wanless (1979) suggested that the laminae can be considered as micro-stylolites. Lenticular chalk consists of small ellipsoidal bodies or lenses of relatively pure chalk surrounded by wispy, clay-rich solution seams. Stylolite is formed from solution seams once the porosity falls to less than about 25%; even though stylolite can also occur in higher porosity chalk (Scholle, 1977). Stylolite are normally absent in clay rich chinks, as for example in the Ekofisk formation (Maliva and Dickson, 1992). Surlyk (2003) suggested that the forming of stylolite can act as initiation points for tension-gash fractures, the so-called stylolite-associated fractures (Fig. 3.8).

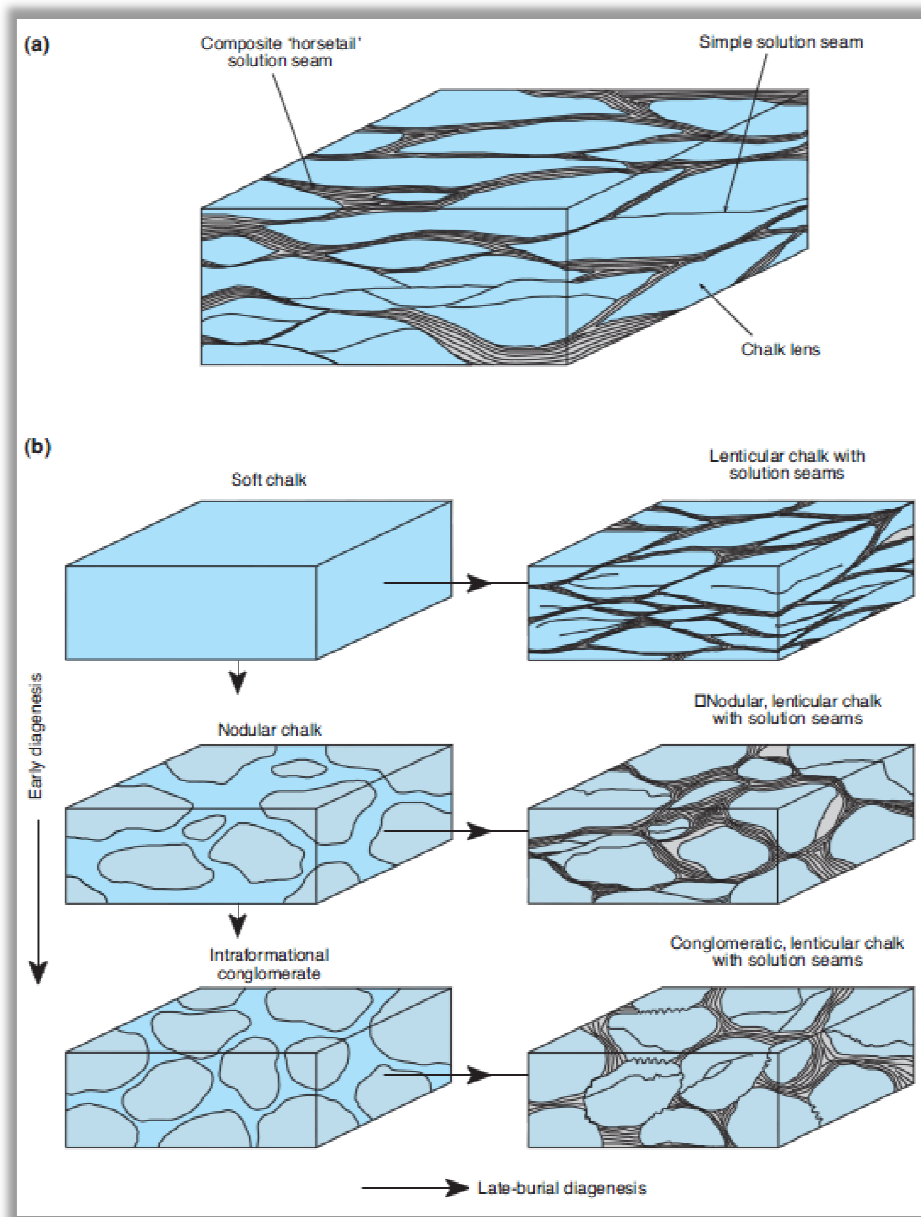


Figure 3.7. Formation of lenticular chalk with dissolution seam in early and Late-burial diagenesis (Surlyk, 2003)



Figure 3.8. Different appearance of fracture. Left is tectonic-related fracture and right is stylolites-associated fracture (Brekke and Olausen, 2008)

Reworking of the Sediment

Another process, apart from diagenesis, involved in the chalk deposition is sediment reworking (Fig. 3.9). The instability of the chalk was created by the subsided basin and uplifted zones of inversion that influenced the thickness of chalk throughout the basin (Andersen, 1995). These series of tectonic activities involved in producing allochthonous accumulations that comprise slide, slump, debris flow and turbidity flows (Kennedy, 1980).

In slides and slumps, a semi-consolidated mass of material moves along a basal plane of failure while retaining some internal coherence (Kruit, 1975). Sliding is a mostly translational movement with little or no internal deformation (Martinsen, 1994) which makes it difficult to identify in cores. Slumping includes a degree of internal deformation of bedding planes or rotational movement (Kruit, 1975). In debris flow, the dominant clast support mechanism was cohesive matrix strength and it normally incorporates poorly lithified clasts that disintegrated progressively during the downslope transport (Surlyk, 2003). In turbidite, which is characterized by the destroyed fabric due to the high turbiditic current, that might have given the newly re-deposited rock a higher porosity than the source material (Andersen, 1995).

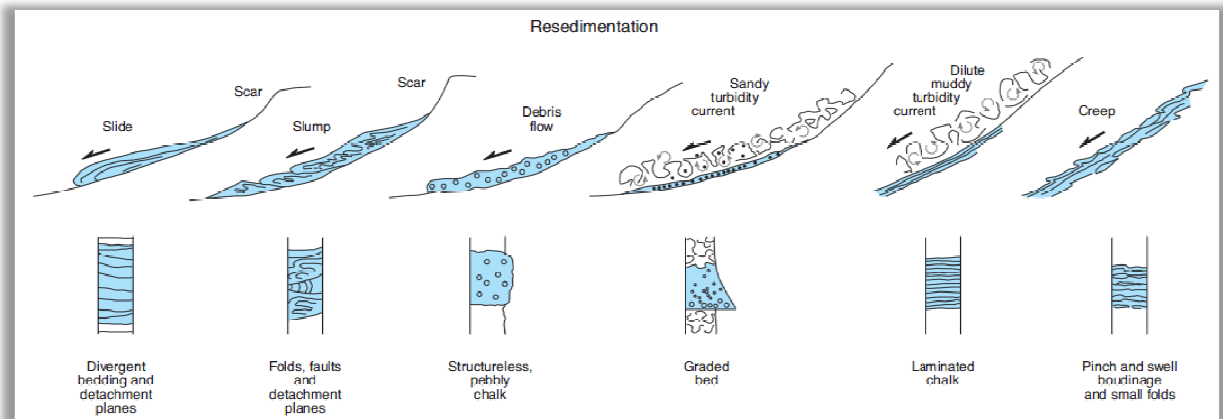


Figure 3.9. Resedimentation process and the resulted feature (Surlyk, 2003).

The following preceding studies of chalk suggest that the reworking of chalk influence the quality of chalk as potential reservoirs. It has been suggested that the mass-movement deposits retain a higher porosity than the primary, hemipelagic chalks (Schatzinger, 1985; Hatton, 1986). The thick-rapid sedimentation, combined with minor bioturbation that only occurred at the surface has been suggested to produce high porosity chalk (Bramwell, 1999). Disintegration of weak and early diagenetic cement during reworking may also be responsible for the higher porosity chalk (Taylor and Lapre, 1987).

However, Maliva and Dickson (1992) studied chalk from Eldfisk field and found that the mode of deposition has little influence on porosity. They rather found that the content of non-carbonates are significant. They added that variations in the porosity at similar depths of burial may reflect the differences in the content of microcrystalline quartz. This supports the positive correlation between the occurrence of low-porosity zones and non-carbonate insoluble residues in the Tor and Ekofisk formation of the Eldfisk field.

In 2002, Rogen and Fabricius found that for a given porosity, the content of clay and silica has significant influence on permeability in chalk. Fabricius and Borre (2007) also suggested that the presence of cemented microfossils and pore-filling silicates causes local variations in porosity of chalk.

Kennedy (1987b) suggested a strong correlation between clay content and poor reservoir quality. Generally, the presence of clay prevents early lithification as it inhibits growth of early cement as point contacts between carbonate grains fail to develop. This prevents local pressure solution and associated spot-welding of grains (Mapstone, 1975). During deeper burial, crushing of weakly welded carbonate grains result in greater compaction, more rapid solution and chemical compaction. The presence of clay thus enhances compaction, expulsion of pore fluid and subsequent loss of porosity (Surlyk, 2003).

Rock Geomechanics

In this study, geo-mechanical log by means of Young's modulus and Poisson's ratio is used as reference to discriminate the facies. Two of the factors affecting the mechanical strength of chalk are silica and clay. Halleux (1985) suggested that silica plays a role in rock mechanical strength. Higher silica content increases the Young's modulus and the yield stress for chalk.

In 1998, Mavko et al. suggested that v_p and v_s are unequally influenced by mineralogy and pore structure. Thus, correlating porosity with v_p/v_s ratio may give information on the content of quartz and clay. The v_p/v_s ratio itself can be reflected in the dynamic elastic parameter, ν , also known as Poisson's ratio.

As mentioned above, the clay plays a major role in chalk diagenesis. As stress on the chalk builds up during burial, clay flakes becomes oriented normal to the major stress direction enhancing the degree of compaction. In the end this may relate to the apparent of high rock density.

The pure chalk is generally very weak mechanically, with little to no cementation, while the impure chalk has greater mechanical strength due to the cementation provided by the silica or calcite overgrowths (Andersen, M. A., 1995).

In the study presented by Gennaro (2011) that reviews the dense zones, five main dense zone lithotypes have been identified:

- (1) argillaceous chalk
- (2) flint;
- (3) silicified chalk
- (4) incipient hardground
- (5) stylolitised chalk.

The study was also supported by mineralogy analysis from core data that reveal various sedimentary and early and post depositional diagenetic processes by sediment supply, sea level fluctuations and climatic change. In a different scale, these defined facies will be compared to the result of this current study; having understanding that density and geomechanical properties (Young modulus and Poisson's ratio) are a direct function of chalk constituents and terrigenous component.

4 Data Preparation and Result

4.1 Data Preparation

Prior to discriminating the logs into several clusters, some wells needed some data cleaning and handling. Wells included in this category are listed in Appendix 4.1. Due to poor wellbore conditions that might question the reliability of the data, certain log intervals were erased. In addition to that, wells with strong noise showing very dense data records and extreme peaks were smoothed to a specific level (Appendix 4.1).

The effect of smoothing in this study is assessed to measure how much the log grouping may change. The procedure is first to determine the base case from 5 wells with training data (defined-reference data), which result in 6 simplified groups (Appendix 4.1). Using the same dataset, the logs were smoothed by 3, 5 and 7 times, before the new facies models are created. The 3 cases of facies models are compared to the reference facies at every single depth (Appendix 4.1). This procedure was only applied to the 5 wells with training data. In the maximum mode, the facies interpretation may change by around 8% due to the smoothing (Table 4.1).

Table 4.1. Facies change due different smoothing

Type	Facies change SM3	Facies change SM5	Facies change SM7
Min	0%	0%	0%
Average	2%	3%	3%
Max	8%	9%	8%

By applying a different handling such as changing the sampling rate in order to reduce the noise of the data, more error or dissimilar facies appear compared to those interpreted in the reference facies. This assessment is based on a sampling rate of 1, 1.5 and 2 ft; while the reference facies had a sampling rate of 0.5 ft. When using the same procedure of comparing facies changes as for the case of smoothing, the error created due to different sampling rate may reach 10-11% in the maximum mode (Table 4.2).

Table 4.2. Facies change due to different sampling rate

Type	Facies change SR 1 ft	Facies change SR 1.5 ft	Facies change SR 2 ft
Min	0%	0%	1%
Average	2%	3%	3%
Max	7%	10%	11%

In order to have the same reference of logging tool reading, the logs of Gamma Ray (GR), density (RHOB), Young's modulus (YMOD) and Poisson's ratio (POIS) are normalized to a certain values from the reference well. This is done due to the fact that not all of the logs were run using the same reference or calibration (Fig. 4.1). Different logging speeds may also give different data resolution, due to this a sampling rate of 0.5 ft is used for all the logs.

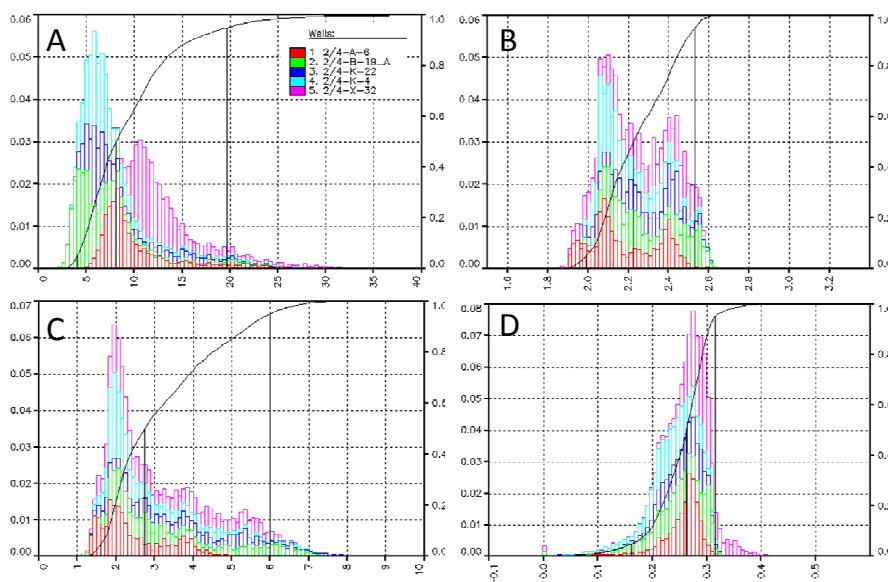


Figure 4.1. CDF and PDF of (A) GR in API, (B) RHOB in gr/cc, (C) YMOD in MPsi and (D) POIS (dimensionless)

Well 2/4-K-4 is used as reference for all the wells to be normalized to because it is part of the training dataset well and has a complete log dataset, including caliper. The normalization is done to match the distribution of P5, P50 and P95 of the wells to the P5, P50 and P95 of the reference well by shift and stretch. Since the re-distributed data from the normalization may be interpreted differently, a sensitivity study is done by 3 cases to assess how far the facies can change due to the normalization (Fig. 4.2).

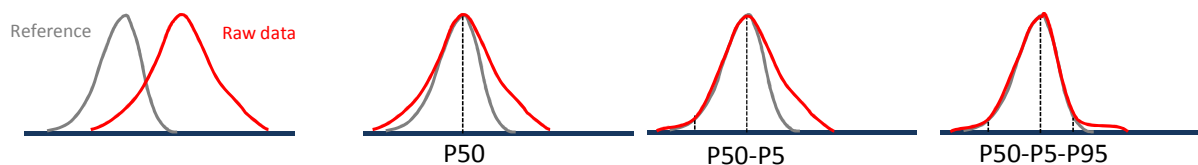


Figure 4.2. Sensitivity on normalization. First, second and third is to match P50, P50-P5 and P50-P5-P95, consecutively. The latter is chosen for final normalization.

The result of the different ways of normalization show that the most affecting factor to facies change is the RHOB, which generate a change of 12% in maximum mode (Table 4.3). The other parameters such as GR, YMOD and POIS maintain the facies change below 9%. Due to this, the GR, YMOD and POIS normalization will follow P50-P5-P95; while the RHOB may be normalized differently for some wells (Appendix 4.1).

Table 4.3. Facies change due to normalization

GR				RHOB			
Type	Facies change P50	Facies change P50-P5	Facies change P50-P5-P95	Type	Facies change P50	Facies change P50-P5	Facies change P50-P5-P95
Min	0%	0%	0%	Min	0%	0%	0%
Average	3%	3%	3%	Average	4%	4%	4%
Max	7%	7%	8%	Max	11%	12%	12%

YMOD				POIS			
Type	Facies change P50	Facies change P50-P5	Facies change P50-P5-P95	Type	Facies change P50	Facies change P50-P5	Facies change P50-P5-P95
Min	0%	0%	0%	Min	0%	0%	1%
Average	2%	2%	3%	Average	2%	2%	3%
Max	8%	9%	7%	Max	7%	7%	9%

4.2 Result

4.2.1 Log Typing

Combination of log response of GR, RHOB, YMOD and POIS are clustered into 3 main electro-facies, when are clustered by criterias of high-low GR; high-moderate-low RHOB and YMOD; high-low POIS (Fig. 4.3). Facies 1 is described as low GR, high RHOB, high YMOD and high POIS, and accounts for 38% of the data population. Facies 2 is characterized by high GR, moderate RHOB and YMOD; and low POIS, and represents 17% from the overall dataset. Facies 3 is clustered with low GR-RHOB-YMOD-POIS and represents 44% of the sample dataset.

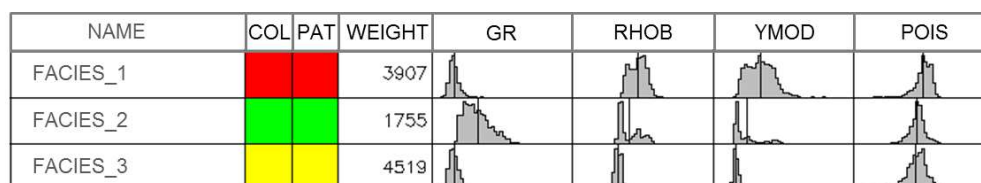


Figure 4.3. Statistics of log response for 123 facies model

In order to better describe the facies, a 3D view can portray the position of the clusters and the boundary between the facies (Fig. 4.4). In a plot of GR-RHOB-POIS, the cloud of Facies 1 (red) is located on the left-corner of the box showing an area with low GR, high RHOB and large coverage of POIS. On the same side of the box, in the area of low RHOB, Facies 3 (yellow) is concentrated. Facies 2 (green) takes side on the high GR and covers large area of RHOB and POIS.

In a GR-RHOB-YMOD plot, the 3 facies are located exactly like in the GR-RHOB-POIS plot. The only difference is that they are now re-distributed and have a lens-kind of shape which is driven by the value of the YMOD.

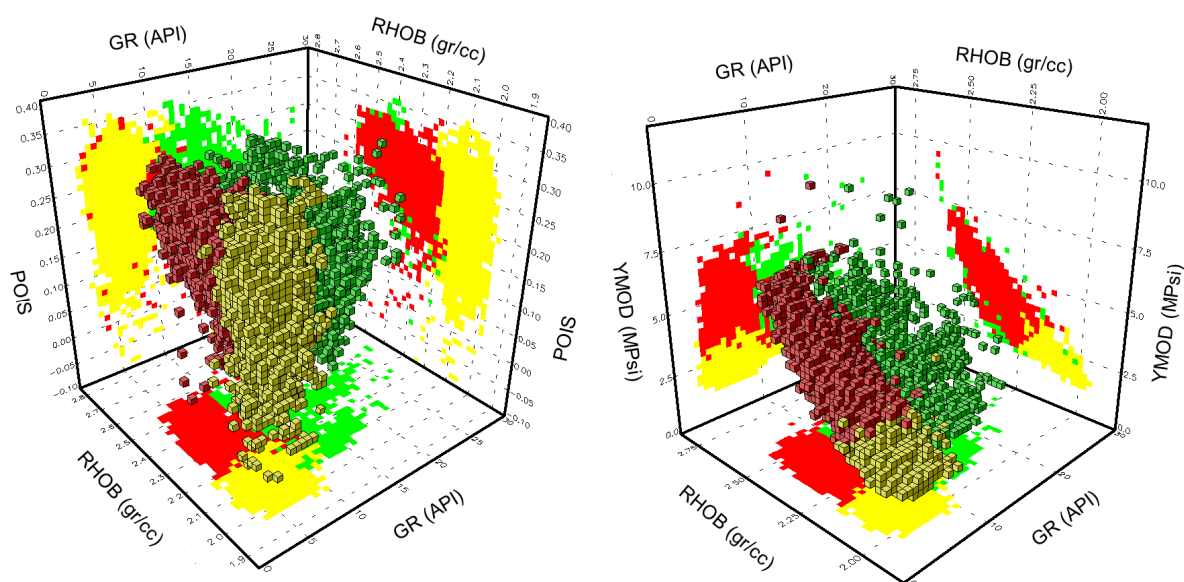


Figure 4.4. 3D chart of 3 facies model (legend in Fig. 4.3)

In order to observe the evolution of each facies, the 3 facies models are subdivided into 8 facies models. Facies 1 and 2 are broken down into 3 models each by decreasing values of RHOB, YMOD and POIS, while Facies 3 is subdivided into 2 models by decreasing values of POIS (Fig. 4.5).

In the 8 facies model, the separation of each facies is stricter and the noise in the distribution can therefore be minimized. The largest population is owned by Facies 3A (39%) which has a similar response as Facies 3 in the 3 facies model. The least population is held by Facies 2A with only 3% of the overall dataset.

NAME	COL	PAT	WEIGHT	GR	RHOB	YMOD	POIS
FACIES_1A			1414				
FACIES_1B			816				
FACIES_1C			1677				
FACIES_2A			279				
FACIES_2B			461				
FACIES_2C			1015				
FACIES_3A			3932				
FACIES_3B			587				

Figure 4.5. Statistics of log response for 1-8 facies model

In 3D view of GR-RHOB-POIS, Facies 1 and Facies 2 are subdivided into 3 clouds which are separated by increasing RHOB (Fig. 4.6). Facies 3 is subdivided into 2 (yellow and blue) and can be seen in decreasing values of POIS. Similar for the plot of GR-RHOB-YMOD, the big cloud of Facies 3 is now divided into 3 smaller clouds (light red, red and dark red). The large group of Facies 2 is also subdivided into 3 facies (light green, green and dark green).

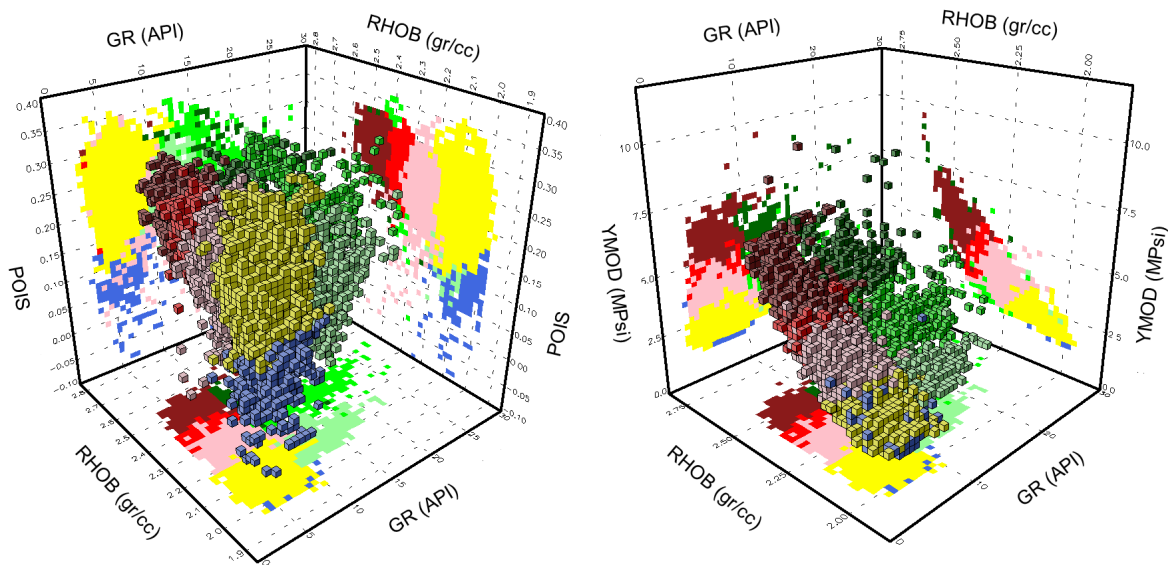


Figure 4.6. 3D chart of 8 facies model (legend in Fig. 4.5)

Using the data from 5 reference wells, the algorithm used to cluster the logs response is trained which in this study result in 3 and 8 facies models. This logic is propagated to the rest of the wells that has 4 dataset of normalized logs. It is applied to a total of 72 wells that comprise 16 horizontal wells and 56 deviated wells spread throughout the field.

Having assigned the facies to all depth intervals, the thickness of each facies can be calculated. For each layer, the proportion of the facies thickness can be defined and attached to the location where the well penetrates the layer. The map of the facies proportions which is represented in pie charts for all layers is then produced throughout the field (Fig. 4.7 and Appendix 4.2).

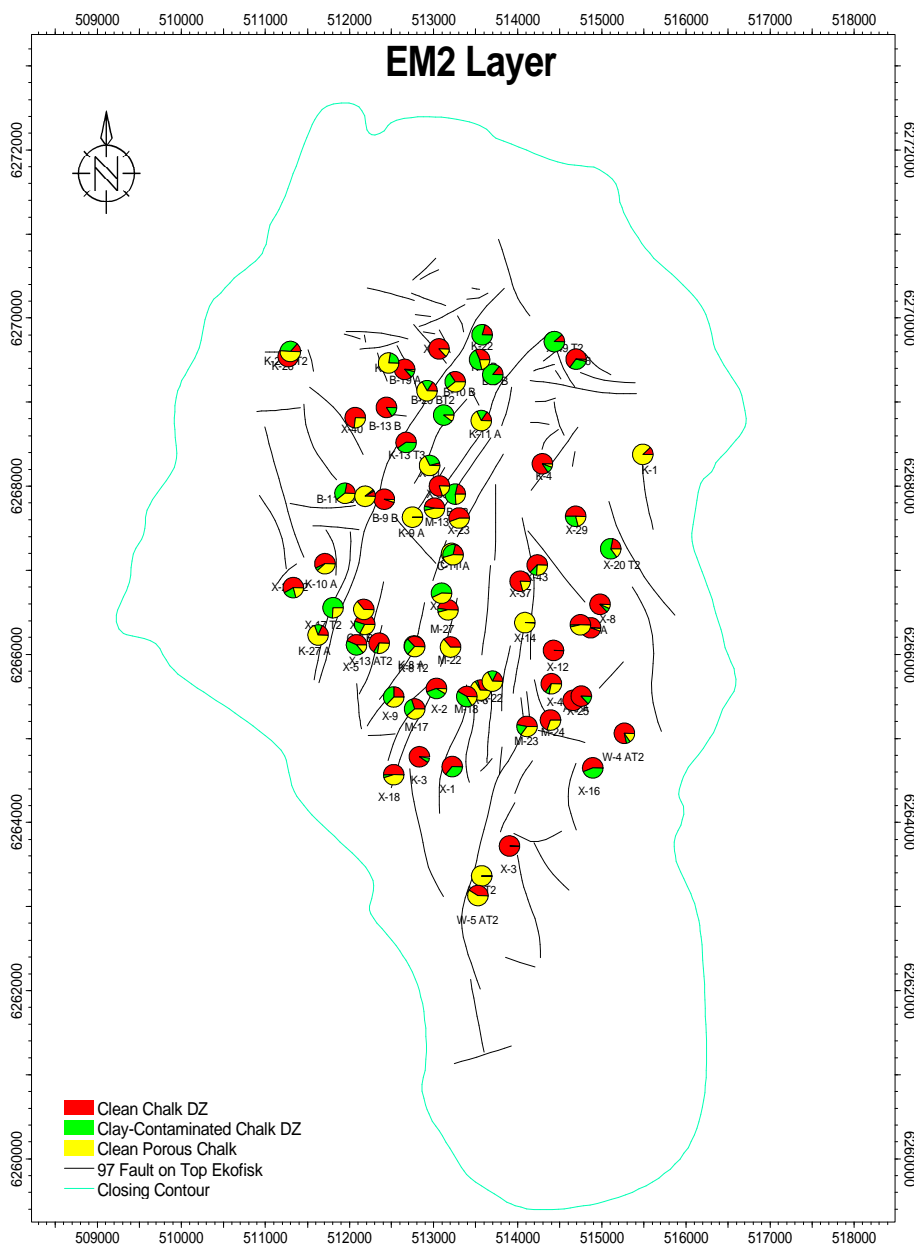


Figure 4.7. Example of map of facies proportion (taken from 123 facies model of layer EM2)

4.2.2 Facies Modeling

Large dataset of facies interpretation enables the investigation of spatial analysis related to the facies distribution pattern. This study is conducted using variogram analysis and performed for each facies in the layer where significant dense zone are presents, notably layer EM2, EM4, EEU, EEM, EEL and TBU (Fig. 4.8). The first step is to use 3 upscaled facies models which are more simple and aimed at obtaining the big picture of the distribution. The second step uses the final facies interpretation of 8 upscaled models.

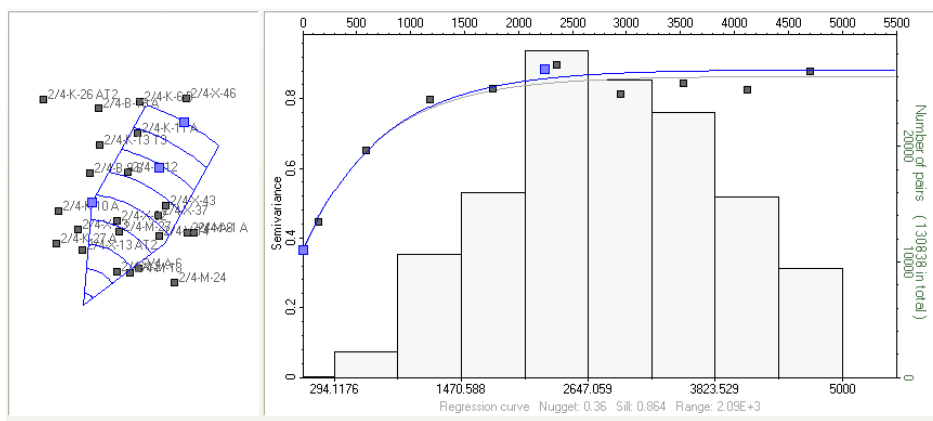


Figure 4.8. Variogram analysis of 123 facies model with its major direction of N29E (taken from layer EEM on Facies 2)

The resulting parameters from this modeling can be used to build a continuous 3D facies mode, which comprises the direction of sedimentation, range, curve type and the nugget (Appendix 4.5). The quality of the model is checked by a variogram that exhibit how the curve match the data (Appendix 4.3 and Appendix 4.4). Assuming that the orientation and pattern of sedimentation is known, one can use the 3D model to statistically identify the facies relationships by using the data from the 72 wells.

The continuous facies model is divided into 6 zones in layer EM2, 6 zones in layer EM4, 3 zones in layer EEU, 25 zones in layer EEM, 4 zones in layer EEL and 7 zones in layer TBU. The result presented here is taken from first zone of layer EEM (Fig. 4.9).



Figure 4.9. Example of continuous facies model of layer EEM predicted from wells (wells indicated by black dots)

6 Quality Check and Observation

6.1 Log Typing

Among the data cluster interpreted in 123 facies model, a bi-modal distribution is created in Facies 2. RHOB is concentrated into two segments:

- One with relatively low RHOB that is dominating the population
- One with relatively high RHOB and is relatively fewer (Fig. 4.3)

In addition to the RHOB segmentation, the distribution of YMOD is skewed to right (positive skew) leaving a very long tail with low frequency. In the 3D view, the cloud of Facies 2 covers a large area of RHOB, which almost is equal to the sum of the area of Facies 1 and Facies 3.

In the 8 facies model, the subdivision of Facies 1 (A, B & C) exhibit consistent patterns of RHOB and YMOD (Table. 5.1). At the same value of GR, the parameters are decreasing by 0.1 gr/cc for RHOB and 1 MPsi for YMOD. The POIS remain high for Facies 1A and 1B, but is relatively low for Facies 1C.

Within Facies 2, the response of Facies 2C is consistent with low GR, RHOB, YMOD and POIS. An obvious change occurs in Facies 2A where the GR value is slightly higher together with very high RHOB and YMOD. The POIS of Facies 2A is also considered high. On the contrary, Facies 2B that has the highest GR in the group show lower RHOB and YMOD compared to Facies 2A.

Within Facies 3, the GR of Facies 3A has the same trend as Facies 1 (low RHOB, YMOD and POIS). Facies 3B shows higher GR response compared to Facies 3A. However, in such a GR value, the YMOD and especially the POIS show anomalously very low values. In 3D view of GR-RHOB-POIS (Fig. 4.6), Facies 3B is exclusively clustered on the bottom of the cloud. While in the GR-RHOB-YMOD plot, Facies 3B is hidden inside the cloud of Facies 3A.

Table 5.1. P50 from 1-8 facies model

Statistics of 8 Facies Model						
P50	GR (API)	RHOB (gr/cc)	YMOD	POIS	Weight	Frac. Weight
Facies_1A	6.1	2.43	5	0.27	1414	0.14
Facies_1B	6	2.35	4	0.27	816	0.08
Facies_1C	6	2.23	3	0.23	1677	0.16
Facies_2A	12.3	2.46	5.3	0.25	279	0.03
Facies_2B	16.2	2.33	3	0.22	461	0.05
Facies_2C	10.7	2.11	2	0.21	1015	0.10
Facies_3A	6	2.1	2	0.22	3932	0.39
Facies_3B	6.8	2.1	1.8	0.12	587	0.06
					10181	1.00

Using the data from the mineralogy analysis of one of the 72 wells included, a comparison of the facies can be done based on the log responses to the elements contained in the

corresponding facies (Fig. 5.1). The reference well for this interpretation is 2/4-X-32 which has a mineralogy analysis that covers the intervals from EEU to TAC.

Within layer TAB and TAC, the mineralogy analysis indicate that the intervals are dominated by clay-poor and stylolitized chalk. These intervals are signed with high calcite (96% by average), very low quartz content (4% in maximum) and a clay content (1%). The points of stylolites and clay-poor chalk coincided with Facies 3A from log response, which is grouped by low GR, RHOB, YMOD and POIS.

On the layer EEL, three points of mineralogy analysis (3248.9 m, 3248.9 m and 3249.2 m) indicate 3 different interpretations. They are reported as calcite cemented chalk, argillaceous laminated chalk and chalk with flint nodule. The calcite cemented chalk and the chalk with flint nodule are described to contain high calcite (>90%) and low clay content, while the argillaceous laminated chalk is reported to contain low calcite (62%), high quartz (14%) and high clay (17%).

The log response of the EEL interval is quite complex. In general, it is an interval with high GR values, but at the particular depth where the points were sampled, a bump of GR appears. The density is relatively high, something which is signed by the crossover with NPHI. However this interval is marked with a very low POIS and a relatively high YMOD. Compared to the facies from log response, the points are coincided with Facies 1C and Facies 3B.

At the bottom part of the EEM layer, two points (at the same depth 3245.2 m) are indicated as chalk with flint nodule and clay-poor chalk. The mineralogy of flint nodule is not reported, while the clay-poor chalk contains 97% calcite, low quartz and clay. From the log response, these points belong to Facies 1C, which is described with low GR and relatively high RHOB.

The thick EEM layer at 3235 m is classified as chalk with micro-quartz associated with clay minerals. The layer contains 27% quartz, low calcite at 64% and 6% of clay. Interestingly, the other point of chalk with micro-quartz associated with clay minerals (at 3230 m) contains higher calcite (80%), lower quartz (14%) and lower clay (3%).

The point at 3235 m is positioned in a thick continuous Facies 2C which is grouped by high GR and relatively high RHOB, while the point with more calcite content (at 3230 m) coincided with Facies 2C with lamination of Facies 3A.

In layer EEU, chalk with flint nodule is reported. This point contains 80% calcite, 11% quartz and 6% clay. This point coincided with Facies 1C, that is characterized by low GR and relatively high RHOB.

Well: 2/4-X-32

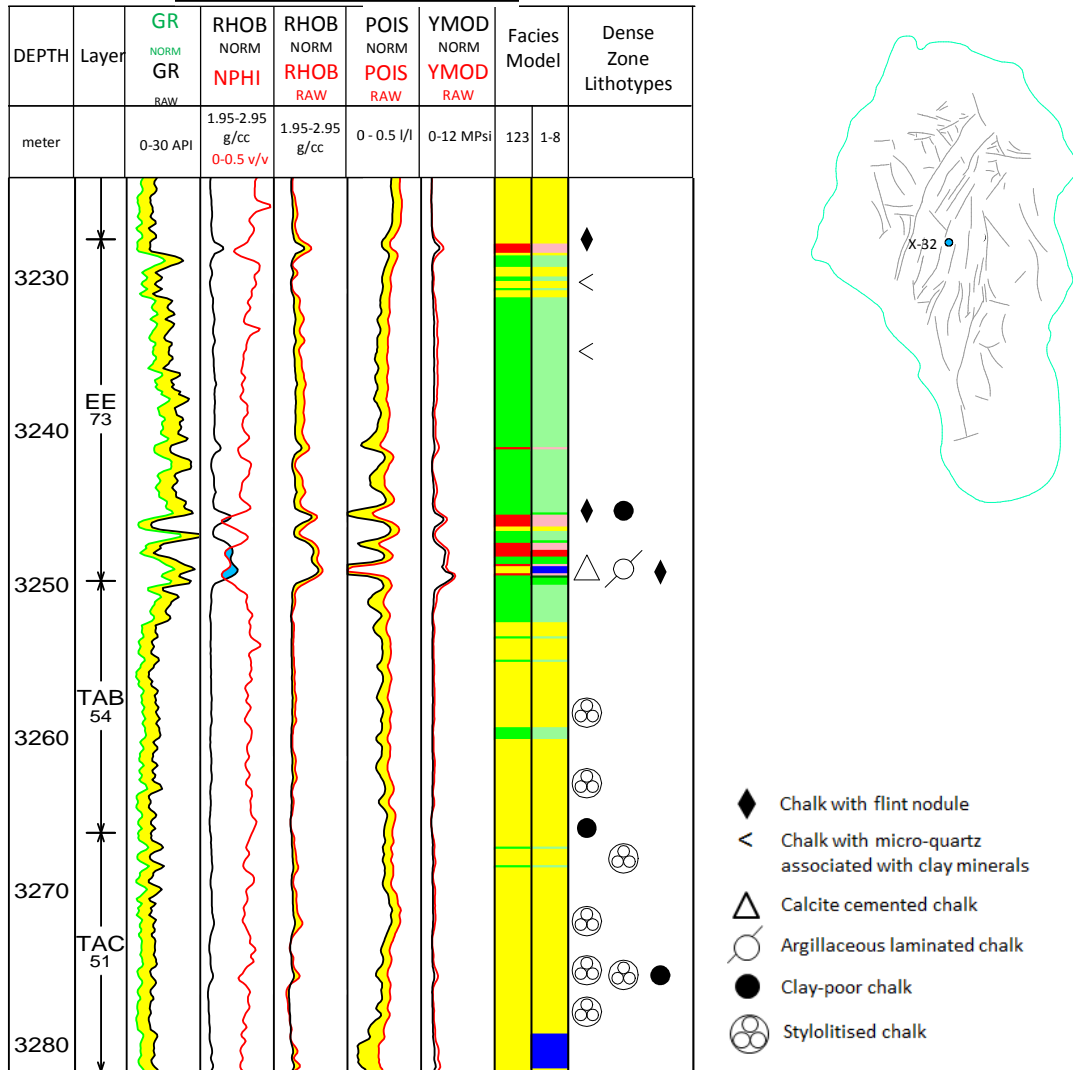


Figure 5.1. Well section of 2/4-X-32 comparing electro-facies and mineralogy analysis (legend of facies is from Fig 4.3 for the 123 model and from Fig. 4.5 for the 1-8 model)

6.2 Statistical Observation of Geomechanical Response and Rock Properties

6.2.1 Facies to Porosity

This observation is to investigate whether the facies interpreted from the well log has a preference to group in certain porosities or water saturations. Only Facies 1 to Facies 2 are used as they correspond to high RHOB-YMOD and POIS.

In Ekofisk formation, the pattern of facies distribution changes at different water saturations (Fig. 5.2). Levels with water saturations below 50% are dominated by facies with low RHOB-YMOD-POIS (Facies 1C and Facies 2C). In the levels with water saturation above 50%, facies with very high RHOB-YMOD-POIS (Facies 1A and Facies 2A) is very dominant compared to the previous group with low water saturation. This pattern is quite obvious at porosities of 10%-15%.

In Tor formation, the trend of the Ekofisk formation repeats where intervals with low water saturation are dominated by low RHOB-YMOD-POIS. It can be seen also that Tor formation is very minor with Facies 2 where it is grouped by high GR value.

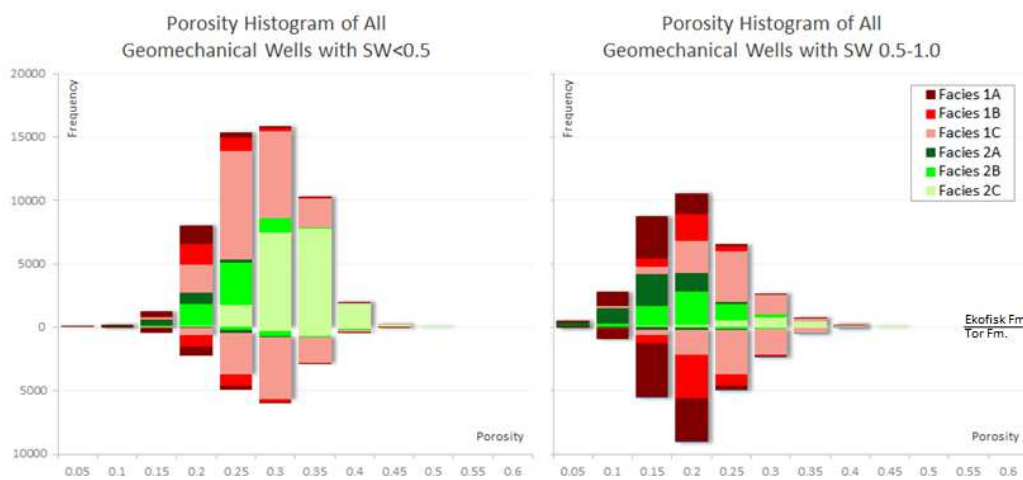


Figure 5.2. Histogram of porosity filtered by type of facies

6.2.2 Porosity vs. Young's Modulus

This plot is used to see the characteristic of each formation in response to the rock resistance against being compressed. The effect is also checked by changing of water saturation.

In the Ekofisk formation, the values of Young's Modulus are more spread at any value of water saturation (Fig. 5.3). At small porosity values, Young's modulus can be very heterogeneous. As the porosity is getting higher, the trend is concentrated to reach similar value of Young's modulus. For samples with high water saturation, the trend of Young's modulus value is relatively smaller than the samples with low water saturation. This trend is quite consistent at any value of porosity.

In the Tor formation, the plots of Young's modulus exhibit the same pattern as those in Ekofisk formation. The only difference is that the points are more concentrated rather than widely

spread like in the Ekofisk formation. In addition to that is the maximum value of Young's modulus in the Tor formation less than the maximum value in the Ekofisk Fm. This might be related to the fact that there are more samples with very low porosity in the Ekofisk formation compared to the Tor formation.

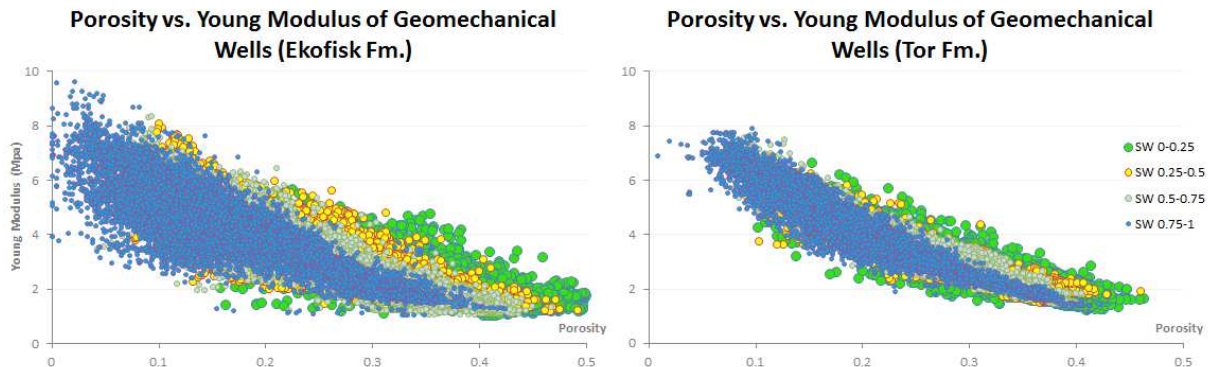


Figure 5.3. Plot of porosity vs. Young's modulus

6.2.3 Porosity vs. Poisson's Ratio

In this histogram, Poisson's ratio is distinguished by porosity, water saturation and different formation (Fig. 5.4). In general, both Ekofisk and Tor formations are dominated by 0.2-0.3 and 0.3-0.4 of Poisson's ratio. In both formations, the highest frequency of Poisson's ratio is at 35% porosity for water saturations below 50% and at 20% of porosity for water saturations above 50%.

The main difference is that at water saturations below 50%, the rocks with higher Poisson's ratio are more frequent in the Ekofisk formation than in the Tor formation. This is applied for any value of porosity. At a different scale, this pattern repeats for water saturations above 50% where the proportion of data with high Poisson's ratio is relatively higher in the Ekofisk than in the Tor formation.

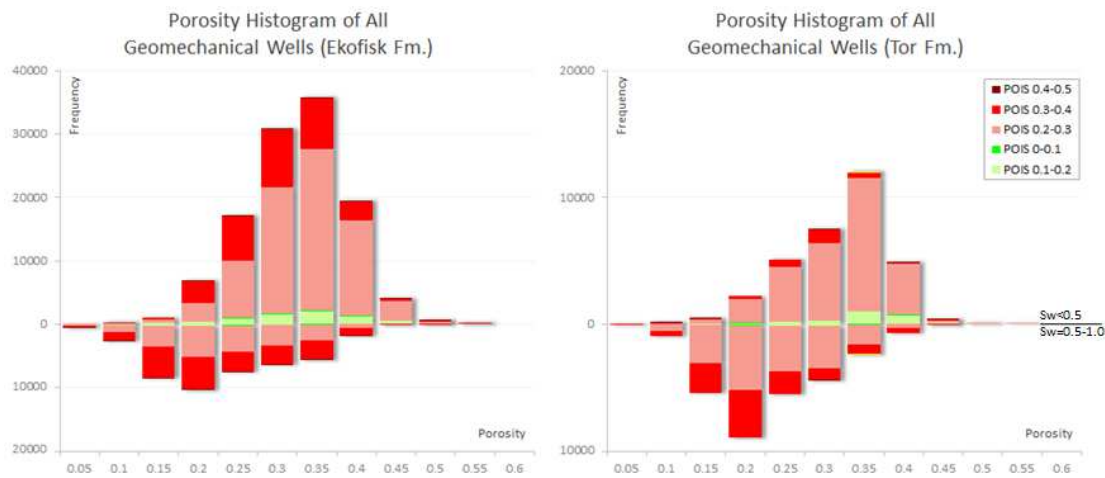


Figure 5.4. Histogram of porosity vs. Poisson's ratio

6.2.4 Porosity Distribution by the Function of Depositional Type

The porosity distribution is used to check whether porosity preservation is a function of certain type of depositional flow as reviewed in the chapter 4. The data is from 7 wells (2/4-A-6, 2/4-B-12, 2/4-B-19 A, 2/4-K-4, 2/4-K-26, 2/4-X-32, 2/4-X-47) which is completed with geomechanical logs and core analysis (Fig. 5.5).

In the Ekofisk formation, high porosity values (35%-45%) are overlapped by high frequency debris flows are rare mud flows. The debris flow is also associated with porosities ranging from 20%-30%. But in these cases the, the frequency of debris flows is not as high. Slump and pelagic chalks exhibit a similar magnitude of porosity preservation (25%-35%). Turbiditic flow types, which covers a large range of porosity values (10%-40%) is most likely to have a preservation around 35%.

The Tor formation shows a different pattern compared to the Ekofisk formation. The debris flows in Tor dominantly covers the large range of porosities (20%-40%) and even some with porosities lower than 20%. Mud flow and slump exhibits quite the same pattern as the Ekofisk formation, while the turbidite flows exclusively exhibits porosities of 35%-40%, even though the population is not as large. Pelagic chalks are absent in the Tor Fm.

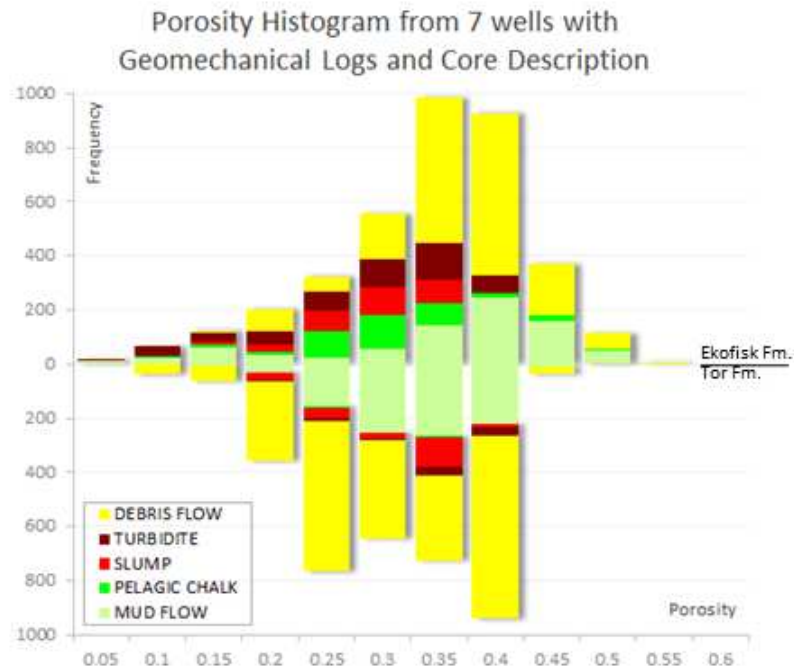


Figure 5.5. Histogram of porosity filtered by depositional type

6.2.5 Facies Distribution by the Function of Depositional Type

The samples taken from the 7 wells comprise 3661 points from the Ekofisk formation and 3590 points from the Tor formation. From both formations, the most dominant depositional type is debris and mud flows (Fig. 5.6). Turbidites are quite frequent in Ekofisk, but they are rarely seen in the Tor formation. Pelagic chalks can be found in the Ekofisk, but they are absent in the Tor formation. Slumps can be found in both formations.

In the Ekofisk formation, debris and mud flows can comprise of various facies. More than 50% of these types of flows contain Facies 3A (low GR-RHOB-YMOD-POIS). Facies 2A (very high RHOB-YMOD-POIS) is only present in the mud flows, while Facies 2C is more common in debris flows. In a smaller proportion, pelagic chalks and slumps also contain significant amounts of Facies 3A. The turbidites are the most complex, where it in a small number of frequency contains all type of facies.

In the Tor formation, slumps are almost 100% within Facies 3A, which also is dominated by debris and mud flows. Facies 1B and Facies 1C (low to intermediate RHOB-YMOD-POIS) are also commonly found in these types of flows, but it is only in debris flow where Facies 1A (very high RHOB-YMOD-POIS) is found.

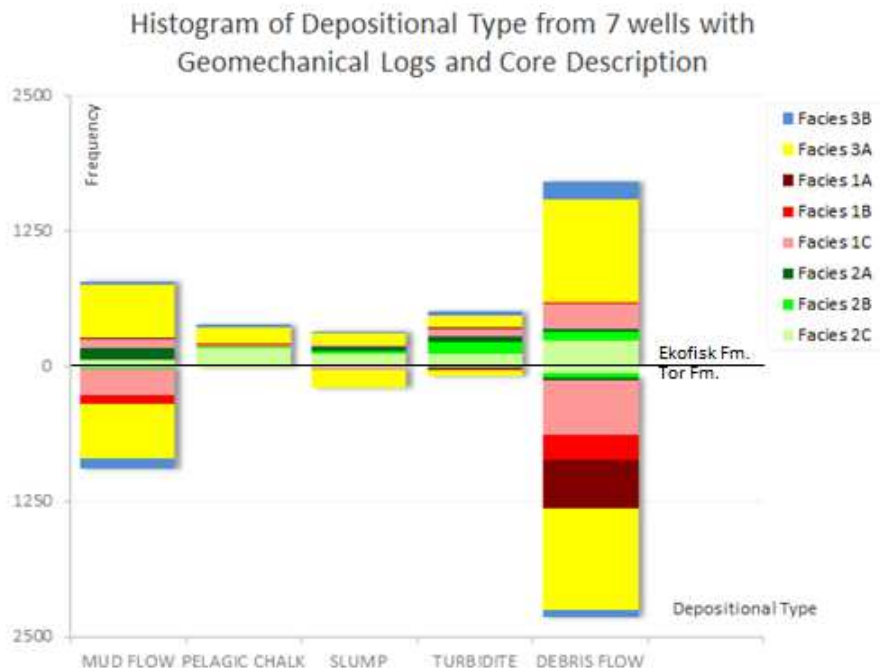


Figure 5.6. Histogram of depositional type filtered by facies

6.3 Facies Evolution throughout the Field

Well 2/4-C-6 B, 2/4-C-11 A, 2/4-B-12, 2/4-K-4 and 2/4-X-46 which all are oriented southwest-northeast has been chosen to represent the evolution of facies throughout the field (Appendix 5.1). These wells are among the oldest wells with geomechanical data logged in period Sep-83 to Jan-95, with the exception of 2/4-X-46 which was logged in Jan-97. The wells are flattened to each layer and are tied to 9000 ftTVD. Then a more detail observation is done for the EE layer.

Layer EM2

The thickness of layer EM2 changes gradually in the southwest-northeast direction. EM2 is relatively thick on C-6 B, B-12 and X-46. Between these wells, on the location of C-11 A and K-4, this layer is thinning. In terms of facies change, Facies 1C is consistently found on all the wells. This facies is found to be a more dense facies in the northeast part of the field that is signed by well X-46.

Facies 2B is found on C6 B, B-12 and X-46. In the area between those wells where C-11 A and K-4 are located, Facies 2B is absent. Instead, a blocky Facies 1C fill the interval in C-11 A and K4. A minor Facies 3A is also found on the middle and southwest part of the Ekofisk field.

Layer EM4

This layer is thick in well C-6 B, thinning in C-11 A, very thick in B-12, turning back to thin in K-4 and again very thick in X-46. The pattern of thickness changes is quite significant between the wells.

The facies change from Facies 3A on C-6 B and C-11 A to Facies 1C on B-12 and K-4. A more dense facies (Facies 1A) is found on X-46. Small intervals of Facies 2B and 2A is also found on X-46, these are not found on the other wells.

Layer TBU

In general the layer is very thick in the southwest to the middle part of the Ekofisk field, while it is thinning in the northeast part of the field, where K-4 and X-46 are located.

In TBU, all of the wells indicate Facies 1, but the quality of facies changes abruptly. In well C-6 B, the facies is dominated with Facies 1A and 1B. In well C-11 A, Facies 1C that is less dense becomes dominant, while a quite similar proportion of Facies 1A, 1B and 1C is observed in well B-12. In well K-4, Facies 1B and 1C present, while the northeast part of the field have a continuous Facies 1A.

Layer EE

Layer EE has a more gradual change of thickness relatively to layer EM. In well C-6 B, the thickness is around 60 ft with 3 cycles of fining and coarsening upward with turnovers in the middle of the layer. The facies is marked by thick and laminated Facies 1C and 1B in EEU, Facies 2B with some laminations of Facies 1C and 1A in layer EEM, and thick Facies 1A in layer EEL.

In well C-11 A, the thickness of layer EE is decreased to around 45 ft with 3 cycles of fining upwards and 2 cycles of coarsening upwards. In terms of facies, this well is filled with Facies 1B in the top and Facies 2B in the bottom of EEU. In layer EEM, a continuous Facies 2B is presents. Layer EEL is filled with lamination of Facies 1C, Facies 2A and Facies 2B.

In well B-12, which is located in the middle of the Ekofisk field, the thickness of layer EE is constant at the level of 45 ft. However, the sequence is decreased to 2 cycles of fining upward and coarsening upward. In EEU, a thin Facies 1C presents, while layer EEM is filled with a thick and continuous Facies 2B. In EEL, Facies 2A becomes dominant and laminated with Facies 1A.

In well K-4, the thickness of layer EE increase to around 58 ft. The cycles are also increased to 3 fining upward and 2 coarsening upward. In terms of facies, layer EEU is filled by Facies 1C with some laminations of Facies 2B and 3A. Layer EEM is remained with continuous Facies 2B, while

the pattern of B-12 repeats for the EEL layer. The only difference is that the laminated facies from K-4 is less dense than those on well B-12.

On well X-46, the thickness of the layers is slightly decreased from those in K-4. The cycles have resumed to 3 fining upward and 3 coarsening upward. The facies pattern is similar to the pattern in well C-6 B. The only difference is that in X-46, the facies in layer EEU is less dense, this is illustrated by Facies 3A and Facies 2C.

Different points of view can be derived from the other sections completed with porosity and water saturation logs. Well C-11 A is located structurally updip to the other wells. In the Ekofisk formation, this well has the least amount of Facies 1C. After C-11 A, the next wells located structurally updip are B-12, K-4 and C-6 B. This sequence follows the pattern of wells with more and more amounts of Facies 1C.

A gradual facies change is observed in interval EL2 to EEU. Well C11 which is updip is filled with Facies 3A, while well B-12 (located slightly downdip) is filled with Facies 3A and some laminations of Facies 1C. Well K-4 (located 50 ft downdip) has more laminations of Facies 1C and well C-6 B (almost 300 ft structurally downdip) is signed with a thick Facies 1C. This section is not in the same stratigraphy unit in X-46, which is included in the North Lobe.

The pattern of facies change in the Ekofisk formation repeats in the Tor formation. For example in the intervals TAA to TBU, wells in updip location (such as C-11 A, B-12 and K-4) have a thick and quite continuous Facies 3A. Among these 3 wells, the lamination of Facies 1C are more dense in the well located most downdip. Well C-6 B is located almost 400 ft downdip and on the bottom part of TAC, the lamination of Facies 1C becomes frequent. This interval coincides with a higher water saturation. Well X-46 has a high water saturation and is filled with very dense facies in these intervals.

From TBU to TCU, these wells are dominated by facies 1. However the degree is changing from well to well. There are indications that the most dense facies is related to zone with high water saturation as for example in well C-6 B in these intervals.

6.4 Facies Modeling

Among the 72 wells completed with interpreted facies, only 70 wells are taken into account in the facies modeling. Well 2/4-X-12 located in the middle part of the field and 2/4-X-40 located in the northwest of the field is randomly excluded from the dataset (Fig. 5.7). Because of that, the facies created on the cells penetrated by the wells rely on the algorithm introduced in the facies modeling.

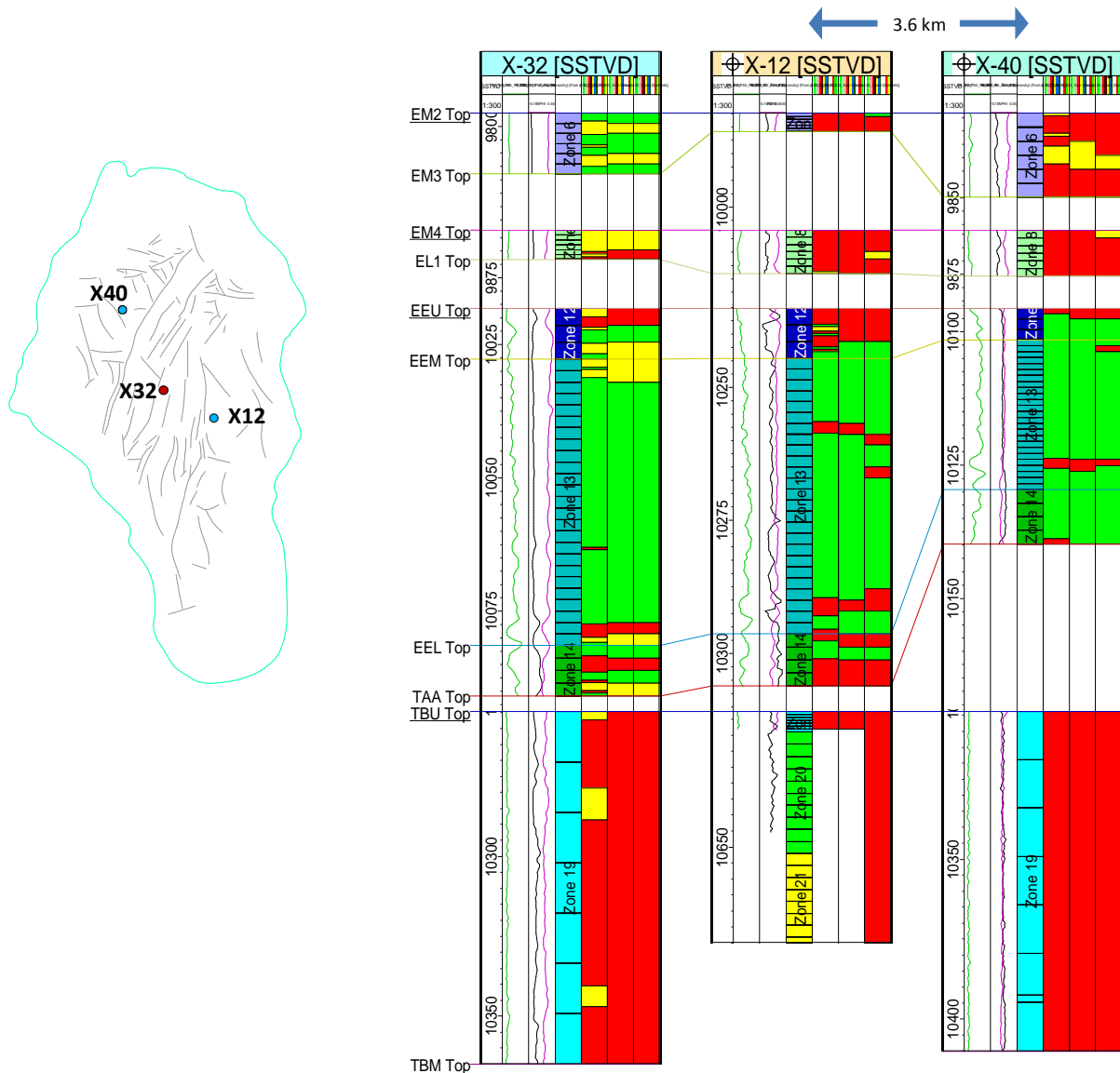


Figure 5.7. Map showing well location (left) and Well section of 2/4-X-32 as reference; 2/4-X-12 and 2/4-X-40 as quality control for facies modeling in the 123 model (right). The first track to the 7th track is SSTVD (ft), GR (0-30 API), RHO (1.95-2.95 gr/cc)-NPHI (0-0.5), zonation, facies well log, facies upscaled, facies from modeling

The same procedure is also applied for the 1-8 facies modeling. Using different data analysis, the quality of facies match in the 123 model may not be the same with those in the 1-8 model. Well 2/4-X-32 is displayed to represent the wells that are taken into account in the modeling (Fig. 5.8). In the case of these wells, the well data is honored and gives a result of the modeling that is exactly the same as the upscaled facies.

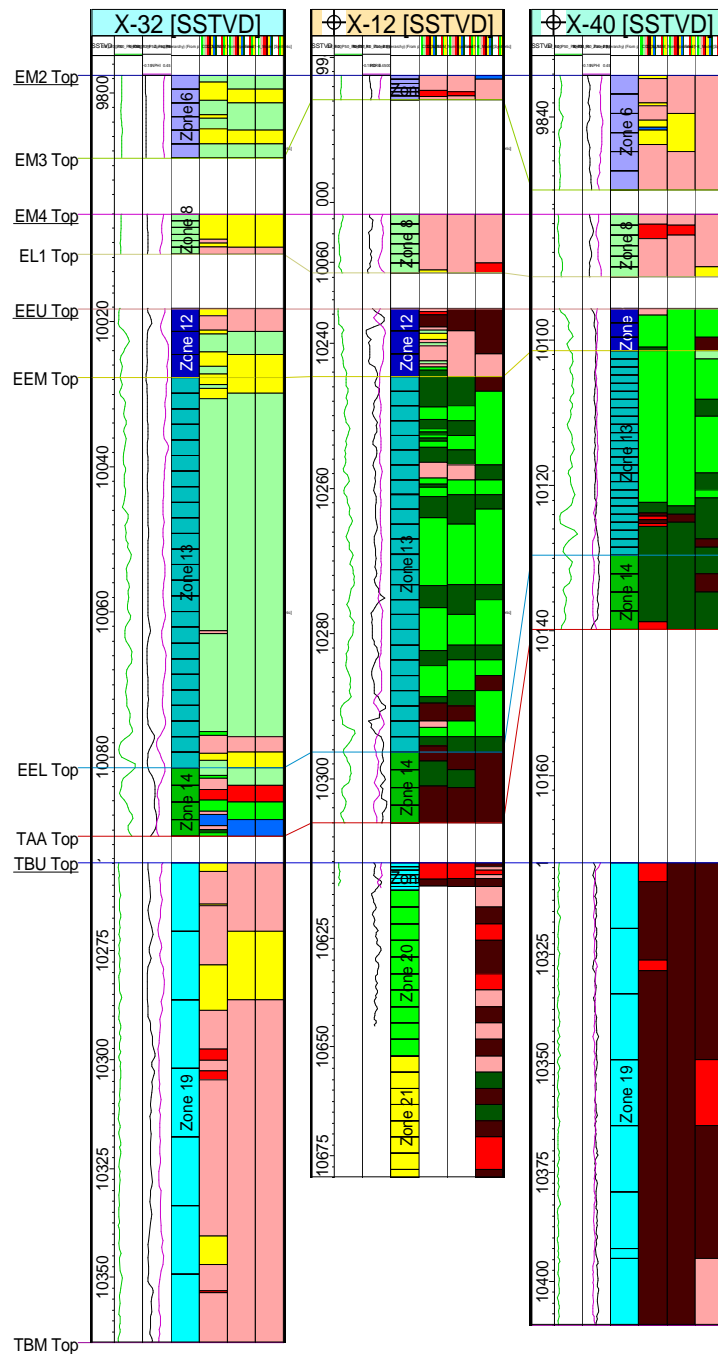


Figure 5.8. Well section of 2/4-X-32 as reference; 2/4-X-12 and 2/4-X-40 as quality control for facies modeling in the 1-8 model (legend of track in Fig. 5.7)

In both of the 123 model and 1-8 model, there may be some discrepancy between the facies from well data to the facies from the result of model propagation on well 2/4-X-12 and 2/4-X-40. However the difference is maintained to be below 40% (mismatch facies thickness divided by total facies thickness) of for 1-8 model. In the 123 model, the difference may be lower than 30% as it is more simple with not many facies to model. The objective to proceed with this QC is to be able to measure the quality of the model specifically on the northwest and southeast parts of the field where the wells are present.

A quantitative comparison of facies modeling is also performed using well with mineralogy analysis, but not completed with geomechanical logs. Well 2/4-A-8, which is located in the relatively southern part of the field (Fig. 5.9) may indicate the reliability of the model in this area. The quantitative quality check is done by comparing the facies generated from the modeling with the lithotypes interpretation.

The points of chalk with micro-quartz associated with clay minerals in layer EE are identified with various calcite content. The first point at 3205 m is identified with 90% of calcite, 8% quartz and 0.5% clay, while the second point at 3207.4 m contains 66% of calcite, 25% of quartz and 8% of clay. The third point at 3211.1 m consists of 52% of calcite, 36% of quartz and 11% of clay. All of the points coincide with Facies 2B which is clustered by high GR, RHOB, YMOD and POIS.

The point on top of EE is identified by chalk with flint nodule with no reported mineralogy. This coincides with Facies 1C. There is no point analyzed from EM4, but the logs show low GR and low RHOB with distinct separation of RHOB-NPHI. This interval is modeled with Facies 3A. One point at EM2 is identified with chalk cemented with nano-quartz (21% of calcite and 79% of quartz), this point coincided with Facies 1C.

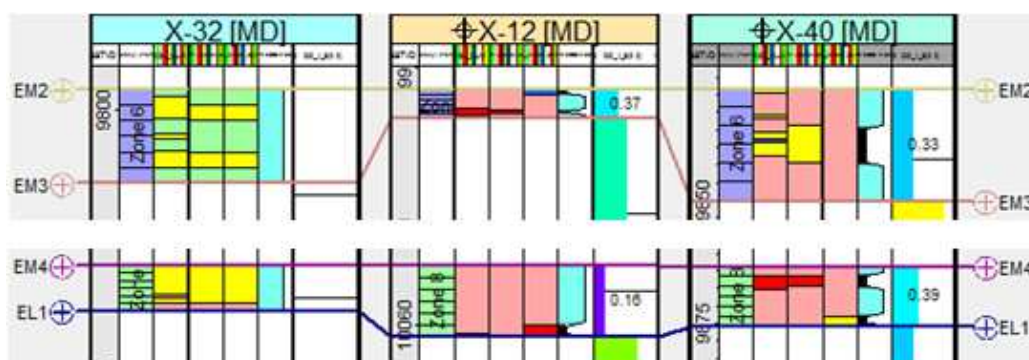


Figure 5.9. Illustration of the error in the blind test. The first track to the 7th track is depth (ft), zonation, facies well log, facies upscaled, facies from modeling, QC of facies upscaled-facies modeling (blue is match, black is un-match), and percentage of error

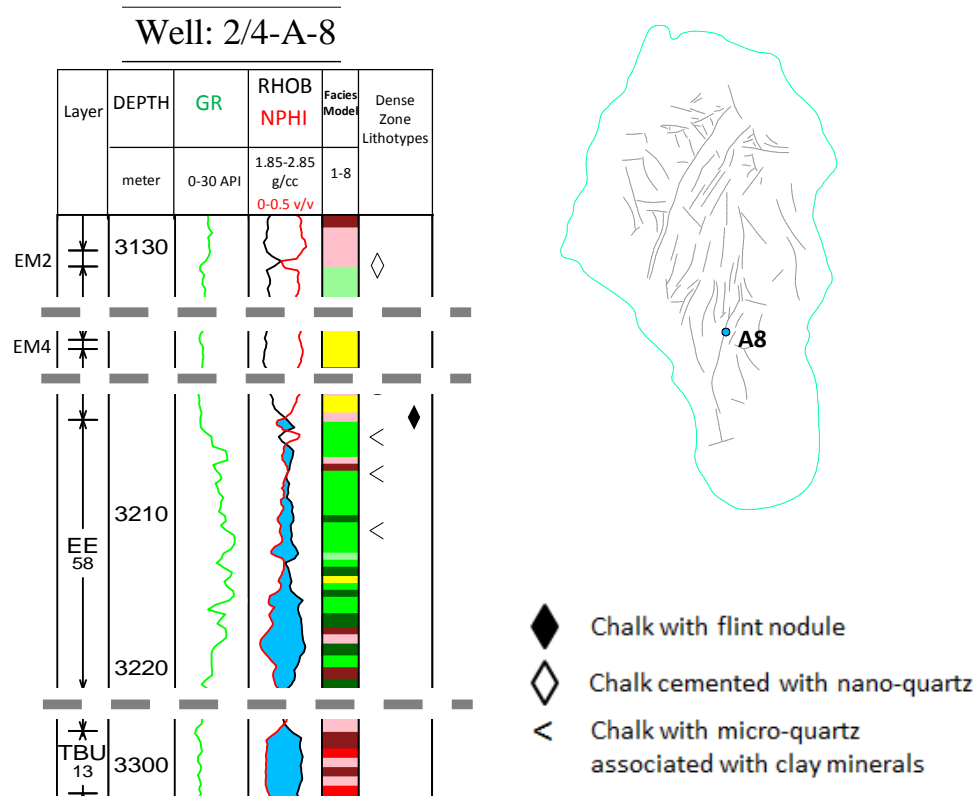


Figure 5.10. Well section of 2/4-A-8 in 1-8 facies model (legend of the facies from Fig. 4.5)

6.5 Facies Characterization

6.5.1 Observation 1 (2/4-M-23 and 2/4-M-24)

Well M-23 and M-24 are located in the southern part of the Ekofisk field and are approximately 300 m apart (Appendix 5.2). Both the wells were drilled in 2005 by a 4 months difference.

Well M-23 that was drilled earliest shows a gradual increase of pressure by depth in all the layers of the Ekofisk formation (Appendix 5.2). This well penetrates some intervals with Facies 1C in layer EM and EL; and Facies 3B in layer EA and EM; with the most dominant facies is Facies 3A. A negative pressure gap of 500 psig occurred at the contact of Ekofisk to Tor formation, where a thick Facies 2B presents in layer EE. The same trend of pressure increment by depth repeats in the Tor formation. In the Tor formation, a thick Facies 1C appear at the top of TAA with some lamination of Facies 3A. The dominant facies in the Tor formation is Facies 3A where it ceases at TBU. It is then dominated by Facies 1 (1A, 1B and 1C) from TBU to TCU.

Well M-24 shows a different pressure regime compared to well M-23. From EA, the pressure decrease consistently by 1000 psig to EM2. In these intervals, the dominant facies is Facies 3A. Then from EM2 down to EE, the pressure increases normally with depth. In these intervals, strong sequences of Facies 1C in Facies 3A appear in the EL layer. On the contact to the Tor formation, a positive pressure gap of 600 psig appears. In the Tor formation, the pressure exhibit the same trend as in M-23 where Facies 3A dominates in TAA to TAD and Facies 1 (1A, 1B and 1C) dominates in TAE to TCU.

In this section, the sequences of Facies 1C in Facies 3A in layer EL in well M-23 can also be found on well M24. The only difference is that in well M-23, the sequences have a water saturation of approximately 70%, while they have a water saturation less than 10% in well M-24.

In layer TAE of well M-23, the interval is filled with a continuous Facies 3A. The water saturation log shows the water saturation changes from high to low in this interval. But in well M-24, the TAE interval is filled with a continuous Facies 1C. In addition to that, on well M-24 lamination of Facies 1C also occurs on layer TAD. The water saturation log shows that the TAE in this well has the same water saturation as the ones in well M-23. But the contact of high-low water saturation has changed to a more updip position by more than 50 ft SSTVD

6.5.2 Observation 2 (2/4-X-37 and 2/4-X-32)

Well X-37 and X-32 are located in the middle of the Ekofisk field and are separated by approximately 900 m (Appendix 5.2). Both wells were drilled in 2001 by 7 month difference.

Well X-37 indicates the same pressure trend as in well M-24 where the pressure decreases by depth with a gradient of -0.7 psig/ft from layer EA to EM2 in the Ekofisk formation. On this well, from EM1 to EEU, Facies 1C repeats strongly with some minor of Facies 2C in layer EM. After the positive gap in layer EE, the pressure trend resumes in the Tor formation. In this formation, the relatively thick Facies 2 (2A, 2B and 2C) is laminated in Facies 1.

The pressure regime in well X-32 is similar to the regime in well M-23. In the Ekofisk formation, the dominant facies is Facies 3A. In layer EL, a more continuous Facies 3A is observed even though the contact of high-low water saturation is far above at EM4. In the Tor formation, Facies 3A is presents until TBU. From TBU to TCU, facies is dominant with some intervals of Facies 3A, while Facies 2 is absent. On top of that, there is one interval at TAD with Facies 3A has a low water saturation while the top and bottom of this interval have been flooded by water.

6.5.3 Observation 3 (2/4-C-11 and 2/4-K-11 A)

Well C-11 is located in the middle of the Ekofisk field and has a distance less than 100 m to the nearest fault (Appendix 5.2). This well is completed with Formation Micro Scanner (FMS) log that enables one to see the correlation of fractures to facies.

In the Ekofisk formation, this well is dominated by Facies 3A, with a quite thick Facies 2C in EM1 and some laminations of Facies 3B and Facies 1C. On the bottom part of EL3 and top part of EEU, a quite thick Facies 1C is presents. The layers in this formation have a very low water saturation. The FMS log indicates that, throughout Ekofisk formation, the fractures are concentrated at the bottom of EL3 and top of EEU where Facies 1C is presents.

In the Tor formation, a thin Facies 1C occurs at the top of TAA. Then Facies 3A fills the interval of TAA until TBU, followed by Facies 1C from TBU to TCU. Along layer TAB to TAD where Facies 3A appear, the FMS indicate minor fractures, but at the border to and in the middle of Facies 1C, the fracture intensity becomes very dense.

From RFT data, points in the Ekofisk formation show normal gradual pressure increase with depth. The pressure trend is shifted by approximately 20 psig after it reaches the Tor formation. The pressure then decreases by depth with a gradient of -1.5 psig/ft. The trend changes in the middle of TBU and form a gradient of 2 psig/ft.

Well K-11 A is used for comparison to well C-11. In this well Facies 3A occurs very thick and continuous from layer EA to EM4. The FMS log indicates that these layers are free of fractures. In the layer EL, the FMS log indicates very minor fractures where it coincided with Facies 1C.

Layer EE in this well is more dense than layer EE on C11 where it is indicated by a dark green color of Facies 2A. From the FMS log, this interval is characterized by more thick and continuous fractures compared to C-11, which is characterized by a spiky fracture signature.

From layer TAA to TBU, this well is dominated by two facies. Facies 1C is found to be thick and continuous in the TAA layer. Facies 3A is found to be continuous in TAC to TAE interval. Nevertheless the FMS log does not indicate any fractures in front of Facies 1C.

In well C-11, fractures are indicated to stop in the middle of Facies 2B in layer EE. This is also the case for well K11 A. But the thickness where the fractures are absent is greater in C-11 compared to the thickness of the fracture free interval in well K-11 A.

6.5.4 Observation 4 (2/4-K-13 T3)

Well 2/4-K13 T3 is located quite in the middle of the Ekofisk field and is located by less than 100 m from the major fault (appendix 5.2). This well encounter the fault around layer EE, thus this layer is missing. This well is used to see how the correlation of facies to permeability, which is taken from well test data. There is no FMS log in this well.

The Ekofisk formation is dominated with Facies 2C from layer EA to EM3. Facies 3A, with sequences of Facies 1C appear from EM4 to TAB. Well test data indicate that EM1 to EM3, where Facies 2C occurs, have low permeability values even though the porosity is slightly higher compared to those in layer EL. Layer EL, where sequences of Facies 1C occur, have a much better permeability even though the porosity is relatively lower.

The same pattern is also observed in the Tor formation. Permeability values at TAB-TAC is very low and coincided with good porosities and Facies 3A. In layer TB, where Facies 3 appears, the permeability is much higher.

In well K-11 A in layer EA to EM3, where Facies 3A dominates, the permeability is in a low range. But in front of layer EL, where Facies 1C is present, the permeability is much higher. This pattern repeats in the Tor formation with a different magnitude.

7 Discussion

7.1 Facies Classification

The classification of facies interpreted based on logs response is taken from the mineralogy analysis and the geomechanical properties. A plot of calcite, quartz and clay is chosen to represent the main component identified in the rock (Fig. 6.1). This is then combined with the clustered data to improve the classification.

From the 123 model, the facies is classified into:

- 1) Clean chalk dense zone (red)
- 2) Clay-contaminated chalk dense zone (green)
- 3) Clean porous chalk (yellow)

From the 1-8 model, the classification falls into:

- 1) Clean chalk with high silica content (dark red)
- 2) Clean chalk with moderate silica content (red)
- 3) Clean chalk with low silica content (light red)
- 4) Chalk with moderate clay content (dark green)
- 5) Chalk with high clay content (green)
- 6) Chalk with low clay content (light green)
- 7) Clean porous chalk (yellow)
- 8) Soft chalk (blue)

The mineralogy analysis of “stylolitized chalk” and “clay-poor chalk” is clustered in a quadrant that is characterized with high calcite, low quartz and low clay content (yellow). These points coincide with Facies 3A with low GR-RHOB, Young’s modulus and Poisson’s ratio. A statistical plot indicates that this facies is related to the best reservoir with high porosity (Fig. 6.2). Facies 3A is classified as clean porous chalk.

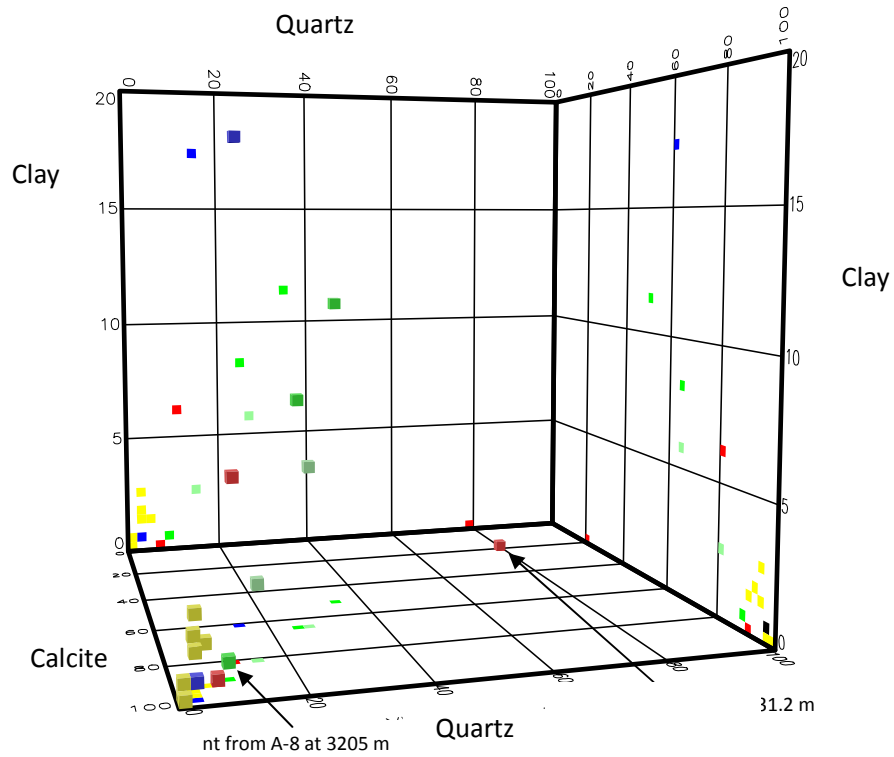


Figure 6.1. Plot of mineralogy analysis (color legend is analogy with color code for facies)

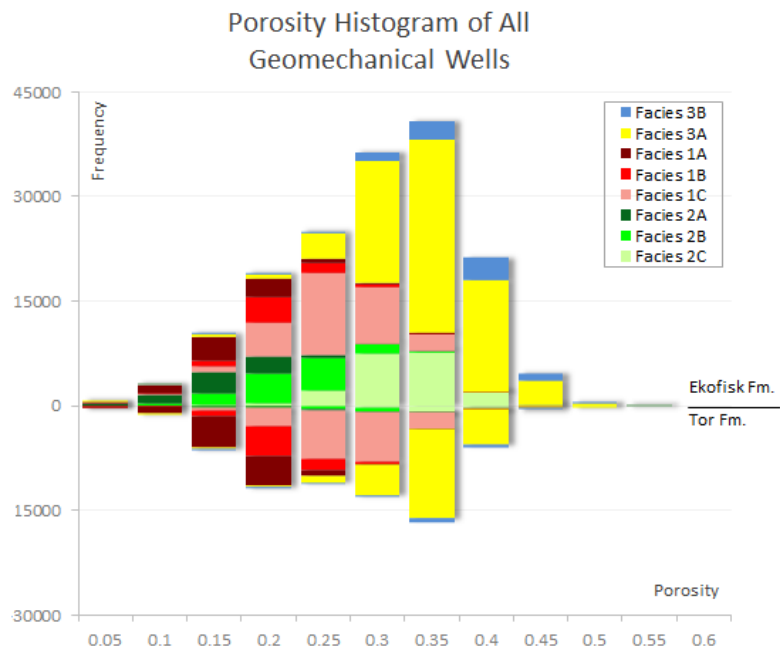


Figure 6.2. Histogram of porosity filtered by facies

In the same group, Facies 3B has similar characteristic as Facies 3A. However, this facies is attached to two different interpretations of mineralogy analysis. In Fig. 6.1, these points are in blue, and are interpreted as “calcite cemented chalk” (very low clay content) and “argillaceous laminated chalk” (very high clay content). This inconclusive mineralogy interpretation coincides with poor quality of log clustering that is indicated by Similarity Threshold Method (STM) analysis (Fig. 6.3). At this point, the correlation between the facies from log typing to the mineralogy analysis may be very poor.

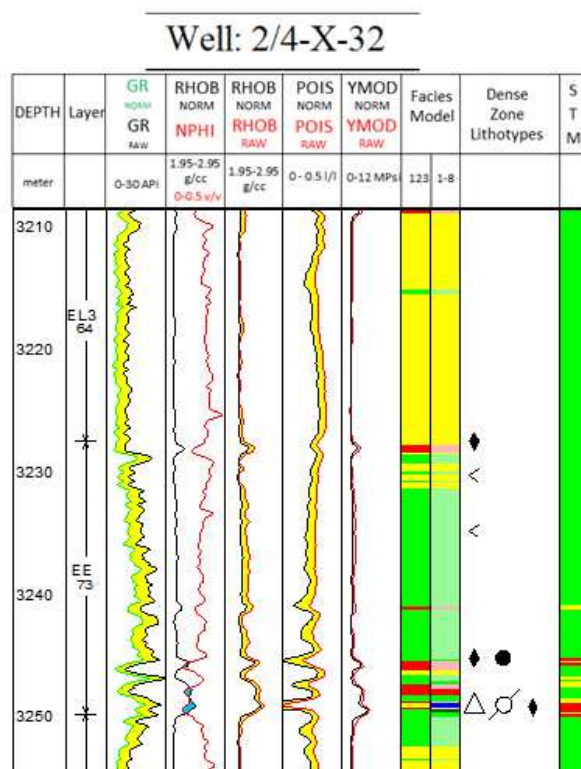


Figure 6.3. Well section of 2/4-X-32 with STM (green is good, yellow is moderate, red is poor correlation)

For the case of Facies 3B, interpretation from geomechanical characteristic is used. The most typical parameters for this facies is very low Young’s modulus and Poisson’s ratios. The Young’s modulus indicates that the rock is not resistive against applied stress in vertical direction. Meaning that the rock can easily be shortened when a uniaxial pressure is applied. Poisson’s ratio indicates that the vertical change of the rock is more important than the lateral change. This indicates that the rock is flexible and able absorb the external forces applied. Due to this the facies is classified as soft chalk.

The mineralogy analysis of “Chalk with micro-quartz associated with clay minerals” consistently coincides with Facies 2C in well X-32 (light green) and Facies 2B in well A-8 (green). The trend

indicates that the points from X-32 have a low clay content (2-6%) and quartz content (14-27%). While the points from A-8 have a higher clay content (8-11%) and quartz content (25-36%). This leads to the classification of “Chalk with low clay content” for Facies 2C, “Chalk with high clay content” for Facies 2B and “Chalk with moderate clay content” (not represented in the mineralogy analysis) for Facies 2A. The quartz content that is responsible for the density differences is represented by a color scale. The darker the color, the denser the facies will be. However the point from 3205 m, in well A-8 (Fig. 6.1), indicates that the classification might be more complex than what is proposed here.

Most of the points interpreted as “chalk with flint nodule” coincided with Facies 1C (Fig. 6.3). One of the points has a similar composition as “clean porous chalk” (Fig. 6.1). While another one, have more clay and less calcite. In well A-8 the sample at 3131.2 m, in layer EM2, is interpreted as “chalk cemented with nano quartz”. This point contains huge amounts of quartz and is thus anomalously positioned in a different quadrant in Fig. 6.1. However this typical mineralogy component is not caught by the resolution of the logs.

Facies 1 that is low on GR and high RHOB, Young’s modulus and Poisson’s ratio is interpreted to be the result of the quartz content and possibly the different compaction of calcite (not discussed in this study). The change in amount of quartz content is represented by the gradual changes of RHOB-YMOD-POIS. Thus, this group is classified as “clean chalk with high/moderate/low silica content”.

The grouping of facies to become 8 clusters is considered to represent the different chalk properties of the Ekofisk field, where two main dense zones are represented by Facies 1 and Facies 2. The different quality degrees are defined by the changes of density and geomechanical properties. The clean and porous chalk are also distinguished distinctly from the dense zones.

7.2 Facies Characterization

Water Weakening

Statistics shows that the dense zones are centered in rock with high water saturation (Fig. 5.2). This pattern is quite obvious for the “chalk with moderate clay content” (Facies 2A) in the Ekofisk formation and also the “clean chalk with high silica content” (Facies 1A) in the Ekofisk and Tor formations. The assumption that chalks get weakened due to contact with water may explain what is portrayed in the statistic.

The pattern that the weakened chalk due to water is not straightforward. In Observation 1, the TAE interval in the Tor formation indicates this phenomenon. Well M-23 is considered to be in

communication with well M-24 in this interval, something that is shown by the same pattern of pressure data. Well M-23 is structurally updip and appears to have a transition zone of water to oil in the TAE interval that is interpreted to be “clean porous chalk”. In well M-24 that was drilled 4 months after and located structurally updip, is interpreted to be “clean chalk with low silica content”. At level the oil-water contact is shallower by around 40 ft while the degree of water saturation remains the same. This shows that the rock experience changes of elastic properties with time when the rock is in contact with water, but not in the first time.

However, the pattern of the weakening chalk due to contact with water is not so obvious in the Ekofisk formation. In Observation 1, the relative same portion of “clean chalk with low silica content” can be found in well M-23 and M-24 in the interval EL1 to EEU. In the downdip well (M-24), the interval is filled with hydrocarbons, while the updip well (M-23) has a high water saturation. The facies remains to be “clean porous chalk” in both wells, as if the elastic properties of the rock are not affected by the amount of water contained.

This pattern repeats in Observation 2 for the interval EL1 to EEU. In this section, the rock properties in well X-32 is not deteriorated due water, given that the facies remains to be “clean porous chalk”. Instead the amounts of dense facies are more frequent in well X-37, which is structurally updip and rich in hydrocarbon.

The more water resistant rocks in the Ekofisk formation might explain why the Ekofisk formation is less sensitive to water. This is represented by the distribution of Young’s modulus and Poisson’s ratio. In Fig. 5.3, the distribution of Young’s modulus in the Ekofisk formation covers a larger area at any porosity value compared to the distribution in the Tor Formation. The values of Young’s modulus are also frequently larger in the Ekofisk compared to the Tor formations. This indicates that the Ekofisk formation is more heterogeneous in terms of elements contained in the rock. This may explain the stronger variations in Young’s modulus in the Ekofisk formation. This is supported by the histogram in Fig. 5.2 that indicate that the Ekofisk formation is more heterogenous with different facies than the Tor formation.

The histogram in Fig. 5.4 also shows the different degree of heterogeneity of rock in the Ekofisk and Tor formations. In the Tor formation, the data is dominated with homogenous populations of Poisson’s ratio at a range of 0.2-0.3 and relatively much less for Poisson’s ratio at 0.3-0.4. In the Ekofisk formation, data with Poisson’s ratio of 0.3-0.4 are more frequent than in the Tor formation. As Poisson’s ratio depends on the element contained in the rock (notably quartz), the Ekofisk formation is mechanically stronger than the Tor formation.

Due to this the possible solution of having “chalk with silica content” in the Ekofisk formation in low water saturations is probably due to the diagenetic process after the chalk deposition. As discussed in Chapter 4, the silica may be precipitated from skeletal elements in *Thalassinoides*

burrows. In such case, the Ekofisk formation is more rich in various elements which provide the mechanical strength against water. While in the Tor formation, the rock is more homogenous and clean by which it is more reactive to water.

Porosity Preservation

The hypothesis that porosity is preserved as a function of type of depositional flow only is not completely obvious in this study (Fig. 6.4). For example in the Ekofisk formation, debris flows can be quite significant to produce 20% and 40% of porosity. This is also the case for mud flows where porosities of 15% and 45% are quite frequent in the bin. However, turbidite, slump and pelagic chalk seem to be in the same group that produces low porosity.

In the Tor formation, debris flow does not show a consistent trend for porosity preservation because it is dominant both in low porosity and high porosity. Mud flows seem to be quite dominant to produce high porosities, while slump and turbidites not are significant in the Tor formation.

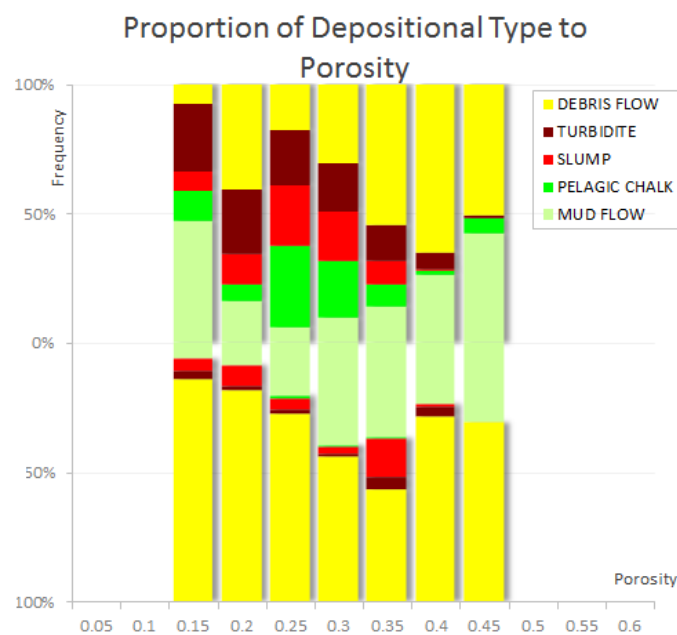


Figure 6.4. Proportion of depositional type to porosity from 7 wells with geomechanical log and core description filtered at 15%-45% of porosity

The indication that the depositional type is not unique to produce certain rock types is also displayed in Fig 5.6. In the Ekofisk and Tor formations, debris flows can be involved in any type

of rock from “porous clean chalk” to “clean chalk with high silica content”. This is also repeated in mud flow types of deposition.

When analyzing the mineralogy against to the porosity preservation (Fig. 6.5), the pattern in well A-8 is more obvious than in well X-32. The data with high carbonate content is relatively grouped in high porosity cluster. Well A-8 is located in the southern part of the field (Fig. 5.9) and all the points are with low water saturation (<15%) except those in the box.

The pattern in well X-32 is not distinct. Points with high non-carbonate content are as the same level of porosity like the points with low non-carbonate content. This well is located in the middle of the field (Fig. 5.1) and the points all have a high water saturation by more than 70%. Most of the points on the X-32 well were sampled from the Tor formation. This may explain the inconsistent trend of porosity that is strongly influenced by the water.

This implies that the porosity preservation not is a function of a factor. The type of depositional flow may produce certain patterns of porosity distribution. But the process after sedimentation may change the initial picture of porosity from depositional type since the mineralogy elements affect the degree of porosity preservation or deformation. Water saturation also seems to be involved to the end product of the porosity.

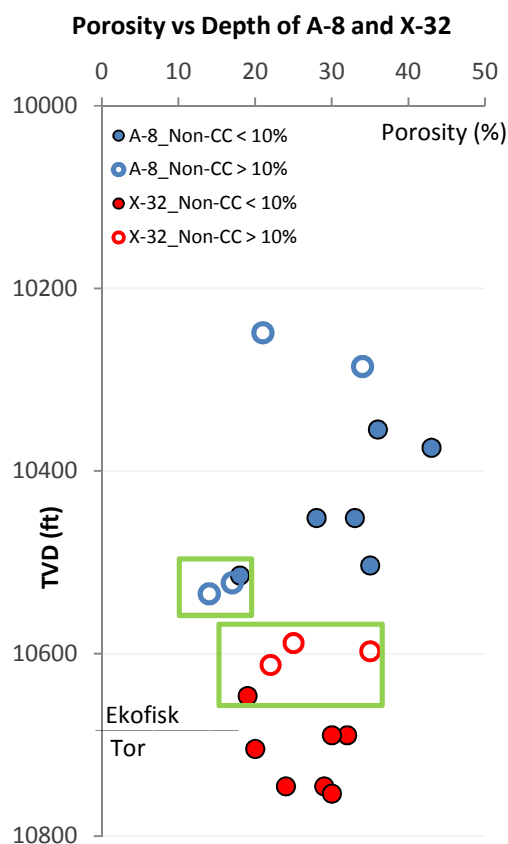


Figure 6.5. Porosity vs depth classified by carbonate content (box = layer EE)

Reservoir Connectivity and Fracturing

Well sections in Observation 1 and 2 explain the characteristic of the Facies “chalk with clay content”. In layer EA1 to EL3 of the Ekofisk formation, there is no evidence that this facies act as a reservoir barrier. The indications from pressure data show that the complete sealing due to the presence of this facies is not obvious. Nevertheless, with regards to the thickness and sequences, reservoir heterogeneity and certain degrees of disconnectivity may be present.

However, the presence of Facies “chalk with clay content” in respect to the thickness may act as a reservoir barrier. This applies for Facies 2C (chalk with low clay content) and Facies 2B (chalk with high clay content) which generally isolate the Ekofisk from the Tor formation. This is indicated by the gap of pressure trends between the Ekofisk and Tor formation. The degree of the sealing may not be homogenous as the pressure gap not is the same from area to area.

In the Tor formation which is dominated by clean chalk facies, the evidence of sealing capability of Facies 2 “chalk with clay content” is not obvious. An example from well X-32 in Observation 2 indicates that the relatively thick Facies 2 is not sealing.

Similar with Facies 2, Facies 1 in the Ekofisk and Tor formations does not indicate a complete sealing (Observation 1 and 2 in Appendix 5.2). But the presence of this facies may be related to the localized relatively higher and thick water saturation compared to the intervals above and below (Appendix 6.1). The lense feature of water saturation in well M-17 and M-18 in layer EM seem to be linked to the shift of the pressure regime. The lense suggest that if the intervals above and below are disconnected to a certain degree.

In its relationship of certain type of facies to fractures, well C-11 and K-11 A in Observation 3 are representative. This observation indicates that the fracture intensity can be correlated to certain facies. In the case of C-11 and K-11 A, the facies with dense zones (Facies 1 and Facies 2B) are strongly correlated with fracture. In well K-11 A, this give an effect to the communication between the Ekofisk and Tor formations.

A surprising observation in K-11 A indicate that fractures correlate to Facies 2A “chalk with moderate clay content” in layer EE and not to Facies 1 “clean chalk with silica content” in interval EL1 to EEU and TAA to TAC. This can be explained by permeability from the well test data. When overlapping the well test data from this well, an anomalous permeability value appears in front of intervals with Facies 1C (Observation 4).

The same pattern is also observed in well K-13 T3, which does not have FMS log, but is completed with well test analysis. Similar with C-11 and K-11 A, this well also exhibits a strong correlation between facies and fractures.

7.3 Sedimentation

In Layer EE, the thickness is gradually changed from southwest to the middle and to the northeast part of the field. The different sequences throughout the area indicate that not all of the area was deposited in exactly the same layer. At the edge of the field (in the location of C-6 B and X-46), more sequences (both for fining upward and also coarsening upward) are found compared to the middle. This corresponds to the fact that thicker chalk sequences are found at the edges of the field.

The period of layer EE deposition took place when the sea level decreased quite strongly between Maastrichtian and Danian (Fig. 1.3). In this period, given the change of cycles throughout the field, the sedimentation of clay might come from the west and east part of the field where stable platforms existed, while the middle part of the field acted as deep basin where deposition occurred.

In layer EEU, the facies distribution is interpreted in 4 quadrants: west, north, east and south (Appendix 6.2). The west and north quadrants are relatively dominated by Facies 2 (chalk with clay content), while the east and south quadrants are identified to have significant Facies 1 (chalk with silica content). The difference among the quadrants is that the west and south quadrants are dominated by more dense facies relative to those in the north and west quadrants.

Layer EEM which is major in Facies 2 is interpreted to have 2 contour lines. The first line (dashed) is less dense than the second line (continuous). From the north to the first line, the area is dominated by Facies 2B (chalk with high clay content). The between the first contour and second contour is dominated by Facies 2C (chalk with low clay content). The area in the south or close to the second contour is described to have more of Facies 2A (chalk with moderate clay content).

Layer EEL is dominated by Facies 1A (clean chalk with high silica content), Facies 2A (chalk with moderate clay content) and Facies 2B (chalk with high clay content). The combination of Facies 1A and 2A is well distributed almost throughout the field. This indicates that the silica is well spread in this layer, both in the sequence of chalk and clay. A clear signature within this layer is that the less dense area is domination of Facies 2B in the middle of the field.

7.4 Facies Modeling

The final validation of the facies model uses the water imbibition issue in well C-11 A and production data from well C-8 A. Well C11 A was drilled in 1994 and well logging surveys were

performed 18 times in a period of 11 years in order to observe the behavior of the water flow. Well C-8 A was drilled in 1994 and has already experienced water breakthrough. The surrounding injector wells are K-9 A drilled in 2007 and K-5 drilled in 1988. Among these wells, only C-11 A and K-9 A are completed with geomechanical data.

The pressure data show that well C-11 that was drilled early in Sep-86, indicate higher pressure than the later drilled wells such as K-9 T3 (that is used to represent the area of well K-9 A as no RFT on this well) and K-5 in 1988. Well C-8 A was drilled in 1994 and also show some declines of pressure together with well C-11 A. In the area of K-5 and K-9 T3 (K-5) there is some degree of connection between the Tor and Ekofisk formation. But the connection is less than in the area of C-11, C-11 A and C-8 A, which is indicated by the pressure gap between the two formations.

The intersection of continuous facies are made from well K-9 A to C-8 A and K-5 to see the evolution of facies throughout the wells (Appendix 6.3). In the 123 model, Facies 1 of “chalk with silica content” appear continuously from well K-9 A to C-8 A in layer EEU. In layer EEM, facies of “chalk with clay content” dominates. In layer EEL, thin facies 1 of “chalk with silica content” presents continuously. With different proportions this pattern repeats in the section from well K-5 to well C-8 A.

A more detail evolution of the facies is shown in the 1-8 model. From well K-9 A to C-11 A, the area between the wells are indicated to be more dense both in layer EEU and EEM. However, the pattern reverses for layer EEL where the less dense rocks are present in between the wells.

From well K-5 to C-11 A, more dense facies appear close to C-11 A in layer EEU. But in layer EEM, more dense facies are located close to K-5. A continuous facies 1C appear between these two wells.

The non-homogenous velocity of the water imbibition displayed in C-11 A section also indicates that some intervals might not have been properly drained by the water. The EL intervals which are filled with “clean porous chalk” does not have the same water saturation (or residual oil saturation) compared to the EM intervals that have “chalk with silica content”. As have been observed before, the water lenses in the EM corresponding to Facies 1 may create anomalies of pressure regimes so that the pressures in the clean porous chalk intervals are slightly lower (Appendix 6.1).

A map view used to better understand the water flow paths, a layer corresponding to EEU is presented (Appendix 6.3). It is proposed here that the water has relatively a direct path from K-9 A to C-8 A and C-11 A. However this is not the case for the path from K-5 where Facies 2B may block the water path. If this is the case the flow path will then be towards the south before it turns westwards.

8 Conclusion

In this study log combinations of GR, RHOB, Young's modulus and Poisson's ratio distinguish the different rock type within the Ekofisk field in 3 main and 8 specific types. The 3 simplified facies interpretations divide the chalk in clean porous chalk, clean chalk dense zone and clay-contaminated chalk dense zone. The 8 more detailed facies interpretations are used to portray the evolution of facies change by the difference degree of rock parameters compliance to the log responses and log values.

The rock type classification is based on grouping of log responses and mineralogy analysis of calcite, clay and quartz content; from which characteristic of each facies is derived in its relationship to porosity, reservoir connectivity and fractures. The clean porous chalk represents the best reservoir with its high porosity; the clay-contaminated chalk dense zone provides the sealing-capability rock and the clean chalk dense zone is strongly correlated to the fracture appearance.

The evidence of water to influence the rock mechanical properties during pre and post-production is quite obvious. The water does not affect the mechanical properties of the Ekofisk formation as important as the effect to the Tor formation. The fact that the Ekofisk formation is more heterogenous than the Tor formation seems to be responsible to the different reaction to water.

The pattern of facies change in layer EM2 and EM4 can hardly be recognized qualitatively both in small and large spacing, indicating random-patchy distribution. This may lead to the random facies-related fracture and localized areas with high water saturation. As a consequence, some degrees of pressure difference in layers that is penetrated by wells are observed.

In the qualitatively defined distribution, the facies population in layer EE suggests an unsystematic repetition of facies relationship. In the EEU layer, the more clay-contaminated chinks that may provide some disconnection are more frequent in the NW area of the Ekofisk field, while the more dense chinks that may act as fast water-conductor rocks are present in the SE area of the field. In the EEM layer, the degree of sealing-ability rock changes from the dense (north) to be less dense (middle) and more dense (south). In the EEL layer, most of the areas are most likely fractured with some degree of disconnection in the small areas of the Ekofisk field.

A distinct pattern of more dense facies oriented west to east in the northern and southern areas of the Ekofisk field can be observed in the TBU layer, generally within the Tor formation.

List of References

1. Andersen, M. A. 1995. Petroleum Research in NORTH SEA CHALK. Stavanger. Rogaland Research, 179 p.
2. Bramwell, N.P., Caillet, G., Meciani, L., Judge, N., Green, M. and Adam, P. 1999. Chalk exploration, the search for a subtle trap. In: *Petroleum Geology of Northwest Europe: Proceedings of the 5th conference* (Eds A.J. Fleet and S.A.R. Boldy), pp. 911–937. Geological Society of London, London.
3. Brekke, H. and Olaussen, S. 2008. High seas and low horizons. In: *The Making of a Land – Geology of Norway*. Trondheim. Norsk Geologisk Forening, 418-441.
4. Cartwright, J.A. 1989. The kinematics of inversion in the Danish Central Graben. *Geol. Soc. London Spec. Publ.*, 44, 153–176.
5. Bromley, R.G. 1996. *Trace Fossils. Biology, Taphonomy and Applications*. Chapman & Hall, London, 361 pp.
6. Bromley, R.G. and Ekdale, A.A. 1986. Composite ichnofabrics and tiering of burrows. *Geol. Mag.*, 123, 59–65.
7. D’Heur, M., “Tor”, in *Geology of the Norwegian Oil and Gas Fields*, Spencer, A. M., et al., Editor. Graham & Trotman: Stavanger, Norway 1985, 129-142.
8. Fabricius, I.L. & Borre, M.K. 2007. Stylolites, porosity, depositional texture, and silicates in chalk facies sediments. Ontong Java Plateau – Gorm and Tyra fields, North Sea. *Sedimentology*, 54, 183–205.
9. Fjær, E., Holt, R. M., Horsrud, P., Raaen, A. M. and Risnes, R. 2008. *Petroleum related rock mechanics* (2nd edition). Elsevier.
10. Gennaro, M., Wonham, J. P., Gawthorpe, R., Sælen, G., *Seismic stratigraphy of the Chalk Group in the Norwegian Central Graben, North Sea*. 2011. Dissertation thesis.
11. Halleux, L., Detiege, C., Poot, B., Schroeder, C., Monjoie, A., Debande, G. and DaSilva, F., “Mechanical Behavior of Chalks”. Paper presented at the 1985 (Second) North Sea Chalk Symposium, Stavanger.
12. Hardman, R. F. P. and Eynon, G., “Valhall Field – A Structural/Stratigraphic Trap”. Paper MNSS/14 presented at the 1977 Norwegian Petroleum Society Mesozoic N North Sea Symposium, Oslo, Norway.
13. Hatton, I. R. 1986. Geometry of allochthonous Chalk Group members, Central Trough, North Sea. *Marine and Petroleum Geology*, Vol. 3, 79-98.
14. Hellmann, R., Renders, P. J. N., Gratier, J. P. and Guiguet, R. 2002. Experimental pressure solution compaction of chalk in aqueous solutions. Part 1. Deformation behavior and chemistry. The Geochemical Society, Special Publication No. 7.
15. Hudson J. D. 1975. Carbon isotopes and limestone cement. *Geology* 3, 19-22.

16. Johannessen, E. P. and Nøttvedt, A. 2008. Norway encircled by coastal plains and deltas. In: *The Making of a Land – Geology of Norway*. Trondheim. Norsk Geologisk Forening, 356-383.
17. Kennedy, W. J., “Aspects of Chalk Sedimentation in the Southern North Sea Reservoir Rocks”. Paper presented at the 1980 Sedimentation of North Sea Reservoir Rocks Conference, Geilo. Norwegian Petroleum Society.
18. Kennedy, W.J. 1987b. Sedimentology of Late Cretaceous-Palaeocene chalk reservoir, North Sea Central Graben. In: Brooks, J. & Glennie, K.W. (eds.) *Petroleum Geology of North West Europe*. Graham & Trotman, 469–481.
19. Knott, S.D., Burchell, M.T., Jolley, E.J. and Fraser, A.J. 1993. Mesozoic to Cenozoic plate reconstruction of the North Atlantic hydrocarbon plays of the Atlantic margins. In: *Petroleum Geology of Northwest Europe: Proceedings of the 4th Conference* (Ed J.R. Parker), pp. 953-974. The Geological Society of London, London.
20. Kruit, C., Brouwer, J., Know, G., Schöllnberger, W. and van Vliet, A., “Une Excursion Aux Cones D’alluvions en Eau Profonde D’age Tertiaire Pres de San Sebastian”. Paper presented at the 1975 9th International Conference on Sedimentology, Nice.
21. Larsen, B. T., Olaussen, S., Sundvoll, B., Heeremans, M. 2008. Volcanoes and faulting in an arid climate. In: *The Making of a Land – Geology of Norway*. Trondheim. Norsk Geologisk Forening, 260-303.
22. Maliva, R.G. & Dickson, J.A.D. 1992. Microfacies and diagenetic controls of porosity in Cretaceous/ Tertiary chalks, Eldfisk Field, Norwegian North Sea. . *American Association of Petroleum Geologists Bulletin*, 76, 1825–1838.
23. Mapstone, N.B. 1975. Diagenetic history of a North Sea chalk. *Sedimentology*, 22, 601–613.
24. Martinsen, O. J. 1994. Mass Movements. 127-165 in *The Geological Deformation of Sediments*. Maltman, A. (editor). (London: Chapman and Hall).
25. Neugebauer, J., “The Diagenetic Problem of Chalk. The Role of Pressure Solution and Pore Fluids”. *Neues Jahrbuch Geol Palaeontol Abhandl*, 143: 2, 1973, 223-245.
26. Nystuen, J. P., Müller, R. Mørk, A. and Nøttvedt, A. 2008. From dessert to alluvial plain – from land to sea. In: *The Making of a Land – Geology of Norway*. Trondheim. Norsk Geologisk Forening, 330-355.
27. Nøttvedt, A. and Johannessen, E. P. 2008. The source of Norway’s oil wealth. In: *The Making of a Land – Geology of Norway*. Trondheim. Norsk Geologisk Forening, 384-417.
28. Oakman, C.D. & Partington, M.A. 1998. Cretaceous. In: *Petroleum Geology of the North Sea* (Ed. by K. W. Glennie), 294–349. Blackwell Scientific Publications, Oxford.

29. Ramberg, I. B., Bryhni, I., Nøttvedt, A. and Rangnes, K. (eds.) 2008, *The Making of a Land – Geology of Norway*. Trondheim. Norsk Geologisk Forening, 624 p.
30. Røgen, B. & Fabricius, I.L. 2002. Influence of Clay and Silica on Permeability and Capillary Entry Pressure of Chalk Reservoirs in the North Sea. *Petroleum Geoscience*, 8, 287–293.
31. Schatzinger, R. A., Feazel, C. T. and Henry, W. E. 1985. Evidence of re-sedimentation in chalk from the Central Graben, North Sea. Deep-water Carbonates. Society of Economic Petrologists and Mineralogists, Core Workshop, No. 6.
32. Schlumberger, 2011. Property Modeling Manual of Petrel 2011.
33. Scholle, P. A., and Arthur, M.A. 1980. Carbon isotope fluctuations in Cretaceous pelagic limestones: potential stratigraphic and petroleum exploration tool. AAPG Bull., 64:67-87.
34. Scholle, P. A., Chalk Diagenesis and Its relation to Petroleum Exploration: Oil from Chalks, a Modern Miracle?. AAPG Bulletin, V 61. NO. 7, 1977, 982-1009.
35. Surlyk, F., Dons, T., Clausen, C. K. and Higham, J. 2003. Upper Cretaceous. In: *The Millennium ATLAS: PETROLEUM GEOLOGY of the CENTRAL and NORTHERN NORTH SEA*. London. The Geological Society of London, 490-547.
36. Taylor, S.R. and Lapré, J.F. 1987. North Sea chalk diagenesis: its effect on reservoir location and properties. In: *Petroleum Geology of North West Europe*. (Eds J. Brooks, and K. Glennie). Graham & Trotman, London, 483–495.
37. Van den Bark, E. and Thomas, O. D., “Ekofisk: First of the Giant Oil Fields in Western Europe”, in *Giant Oil and Gas Fields of the Decade 1968-1978*, AAPG Tulsa: 1980, 195-224.
38. Wanless, H. R. 1979. Limestone response to stress: pressure solution and dolomitization. *Journal of Sedimentary Petrology*, Vol. 49, 437-462.
39. Wong P. K. and Oldershaw A. 1981. Burial cementation in the Devonian, Kaybob reef complex, Alberta, Canada. *J. Sediment. Petrol.* 51, 507-520.
40. Worsley, D. and Nøttvedt, A. 2008. Vast lowland plains, coal and salt. In: *The Making of a Land – Geology of Norway*. Trondheim. Norsk Geologisk Forening, 260-329.
41. Ye, S. J., Rabiller, P. 2000. A new tool for electrofacies analysis: Multi-Resolution Graph-Based Clustering, SPWLA, 41th Annual Logging Symposium, June 4-7.
42. Zanella, E and Coward, M. P. 2003. Structural Framework. In: *The Millennium ATLAS: PETROLEUM GEOLOGY of the CENTRAL and NORTHERN NORTH SEA*. London. The Geological Society of London, 87-124.
43. Ziegler, P.A. 1990. *Geological Atlas of Western and Central Europe*. Geological Society Publishing House, Bath, 1–239 pp.
44. <http://www.spec2000.net/10-elastic.htm>

APPENDIX

Appendix 2.1 Wells with complete logging data

No	Well	Logging date
1	2/4-A-1 A	Jan-88
2	2/4-A-4 A	Mar-89
3	2/4-A-5 T2	Apr-86
4	2/4-A-6	May-86
5	2/4-B-10 B	Apr-02
6	2/4-B-11 T2	Jun-02
7	2/4-B-12	Sep-83
8	2/4-B-13 B	Sep-05
9	2/4-B-19 A	Apr-85
10	2/4-B-20 BT2	Oct-04
11	2/4-B-3 B	May-04
12	2/4-B-9 B	Aug-02
13	2/4-C-11	Aug-86
14	2/4-C-11 A	Jun-94
15	2/4-C-6 B	Jan-95
16	2/4-K-1	Jul-89
17	2/4-K-10 A	May-98
18	2/4-K-11 A	Mar-98
19	2/4-K-13 T3	May-85
20	2/4-K-21 A	Oct-08
21	2/4-K-22	Sep-85
22	2/4-K-26	Feb-90
23	2/4-K-26 AT2	Sep-06
24	2/4-K-27 A	Jun-08
25	2/4-K-3	Nov-95
26	2/4-K-4	Sep-84
27	2/4-K-6 B	Dec-08
28	2/4-K-8 A	Aug-95
29	2/4-K-8 T2	Dec-89
30	2/4-K-9 A	Apr-07
31	2/4-M-13	Oct-06
32	2/4-M-17	Feb-05
33	2/4-M-18	Jan-05
34	2/4-M-22	May-05
35	2/4-M-23	Mar-05
36	2/4-M-24	Jun-05

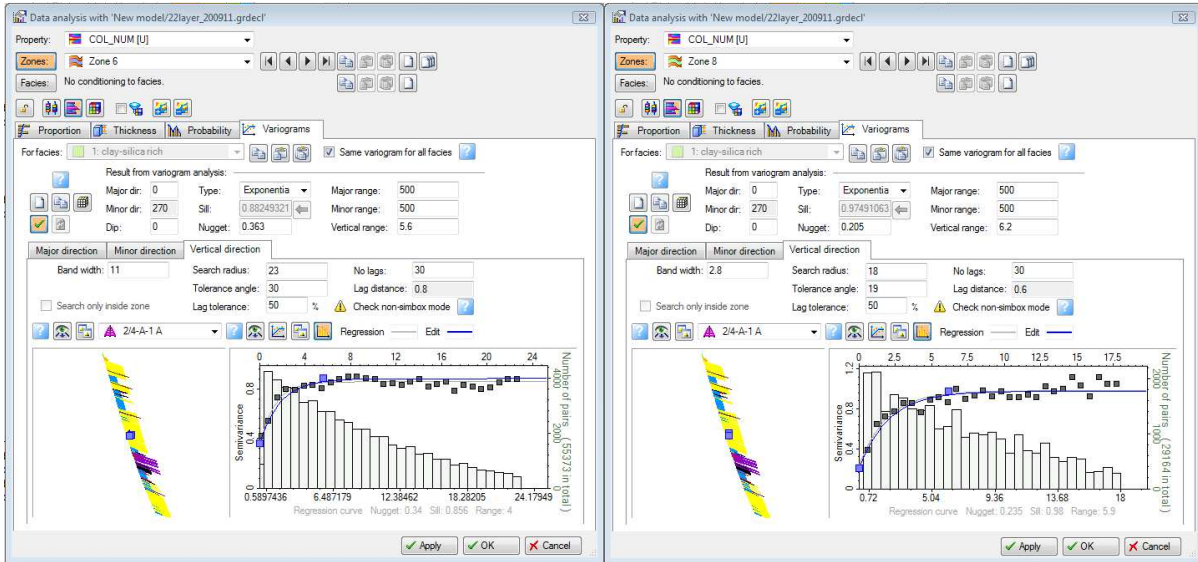
No	Well	Logging date
37	2/4-M-27	Aug-06
38	2/4-M-8	Oct-07
39	2/4-W-4 AT2	Sep-90
40	2/4-W-5 AT2	Oct-03
41	2/4-X-1	Nov-97
42	2/4-X-12	Mar-98
43	2/4-X-13	Mar-02
44	2/4-X-13 AT2	May-04
45	2/4-X-14	Jun-03
46	2/4-X-16	Apr-99
47	2/4-X-17 T2	Jul-01
48	2/4-X-18	Nov-01
49	2/4-X-2	Apr-98
50	2/4-X-20 T2	Dec-00
51	2/4-X-22	Nov-03
52	2/4-X-23	Jan-04
53	2/4-X-25	Feb-04
54	2/4-X-27 T2	Jun-99
55	2/4-X-29	Jan-03
56	2/4-X-3	Aug-97
57	2/4-X-31	Dec-97
58	2/4-X-32	Apr-01
59	2/4-X-36	Jan-98
60	2/4-X-37	Oct-01
61	2/4-X-4	Mar-97
62	2/4-X-40	Apr-98
63	2/4-X-41	Oct-03
64	2/4-X-43	Feb-05
65	2/4-X-45	Feb-97
66	2/4-X-46	Jan-97
67	2/4-X-47	Jul-97
68	2/4-X-48 T2	Feb-02
69	2/4-X-49 T2	Nov-02
70	2/4-X-5	Feb-98
71	2/4-X-8	Dec-96
72	2/4-X-9	Apr-97

Well	Sample ID	Core Depth ft	Denise Zone	Quartz	Calcite	Ankerite	Apatite	Pyrite	Barite	Anatase (mass%)	Kaolinite	Muscovite	Illite & micas	Insoluble residue at HCl 15%	Clays	Micas/smectite or chlorite/smectite (% of total clay)	Illite & micas	Kaolinite
A8	A8-240	10240	Chalk cemented with nano-quartz	-	-	-	-	-	-	-	-	-	-	-	-	-	-	-
A8	A8-249	10249	Chalk cemented with nano-quartz	16.7	81.1	0	0.2	0.1	0	0	0.9	0	0	18.1	1	0	0	100
A8	A8-273	10273	Chalk cemented with nano-quartz	78.7	20.6	0	0.1	0.1	0	0	0.2	0	0	79.9	0.3	0	0	100
A8	A8-286	10286	Chalk with micro-quartz associated with clay minerals	24.3	71.1	0	0.3	0.2	0	0	1.9	0	0	27.9	1.9	0	0	100
A8	A8-355	10355	Clay-poor chalk	1.7	97.2	0	0.2	0	0	0	0.3	0	0	1.4	0.3	5	5	90
A8	A8-375	10375	Clay-poor chalk	2.2	96.4	0	0.2	0	0.2	0	0.2	0	0	2.4	0.2	5	15	80
A8	A8-423	10423	Stylitised chalk	-	-	-	-	-	-	-	-	-	-	-	-	-	-	-
A8	A8-452-3-1	10452.3	Chalk with flint nodule	2.7	95.2	0	0.3	0.1	0	0	0.6	0	0	4	0.6	5	5	90
A8	A8-452-3-2	10452.3	Stylitised chalk	3.1	93.8	0	0.4	0.2	0	0	1.3	0	0	5.5	1.3	5	5	90
A8	A8-504	10504	Clay-poor chalk	4.7	89.6	3.8	0.2	0	0	0	0.2	0	0	4.7	0.2	0	15	85
A8	A8-511	10511	Chalk with flint nodule	-	-	-	-	-	-	-	-	-	-	-	-	-	-	-
A8	A8-515	10515	Chalk with micro-quartz associated with clay minerals	8.6	89.8	0	0.2	0.1	0	0	0.5	0	0	9.6	0.5	0	20	80
A8	A8-523	10523	Chalk with micro-quartz associated with clay minerals	25.3	65.7	0	0.3	0.4	0	0	3.8	0	1.2	33.8	8	10	10	80
A8	A8-535	10535	Chalk with micro-quartz associated with clay minerals	35.8	51.7	0	0.4	0.5	0	0.1	4.8	0	3.5	47.8	11.3	5	10	85
X32	X32-589	10589	Chalk with flint nodule	10.9	80.6	0	0.3	0.2	0	0.1	5.5	0	0.3	19.7	6.3	5	5	90
X32	X32-598	10598	Chalk with micro-quartz associated with clay minerals	14	80.8	0	0.2	0.2	0	0	2.5	0	0	19.9	2.6	0	5	95
X32	X32-613	10613	Chalk with micro-quartz associated with clay minerals	27	64.2	0.8	0.2	0.6	0	0.1	4.9	0	1	37.4	5.9	5	5	90
X32	X32-647-1	10647	Chalk with flint nodule	-	-	-	-	-	-	-	-	-	-	-	-	-	-	-
X32	X32-647-2	10647	Low porosity clean chalk	1.6	97.5	0	0.1	0.1	0	0	0.2	0	0	8.4	0.2	0	0	100
X32	X32-659-1	10659	Calcite cemented chalk	2.9	96.4	0	0.1	0.1	0	0	0.4	0	0	3.6	0.5	0	10	90
X32	X32-659-2	10659	Argillaceous laminated chalk	14.7	61.6	0.8	1.2	2.8	0	0.2	9.8	0	5.2	36.9	17.5	5	5	90
X32	X32-660	10660	Chalk with flint nodule	7.2	91.8	0	0.1	0	0	0	0.2	0	0	2.3	0.3	0	5	95
X32	X32-690-1	10690	Stylitised chalk	4.3	90.4	0	0.6	0.5	0	0	2.3	0	0.1	5.5	1.2	0	5	95
X32	X32-690-2	10690	Stylitised chalk	3.4	94.1	0	0.2	0.1	0	0	1.1	0	0	8.9	2.4	0	5	95
X32	X32-705-1	10705	Stylitised chalk	2.5	94.6	0	0.2	0.1	0	0	1.2	0	0	4.6	1.3	0	0	100
X32	X32-705-2	10705	Stylitised chalk	1.3	96.8	0	0.2	0	0	0	0.4	0	0	1.7	0.4	0	0	100
X32	X32-705-3	10705	Stylitised chalk	-	-	-	-	-	-	-	-	-	-	-	-	-	-	-
X32	X32-715	10715	Clay-poor chalk	-	-	-	-	-	-	-	-	-	-	-	-	-	-	-
X32	X32-721	10721	Stylitised chalk	-	-	-	-	-	-	-	-	-	-	-	-	-	-	-
X32	X32-734-1	10734.5	Stylitised chalk	1.9	96.6	0	0.2	0	0	0	0.5	0	0	2.2	0.6	0	0	100
X32	X32-734-2	10734.5	Stylitised chalk	1.4	97.3	0	0.2	0	0	0	0.3	0	0	1.7	0.4	0	0	100
X32	X32-745	10745	Stylitised chalk	-	-	-	-	-	-	-	-	-	-	-	-	-	-	-
X32	X32-746-1	10746	Clay-poor chalk	1.4	98.3	0	0.2	0	0	0	0.1	0	0	0.3	0.2	0	0	100
X32	X32-746-2	10746	Stylitised chalk	2	93	0	0.6	0.3	0.1	0	1.8	0	0	5.6	1.9	5	0	95
X32	X32-754	10754	Stylitised chalk	0.8	99.1	0	0.1	0	0	0	0	0	0	2.2	0.1	-	-	-

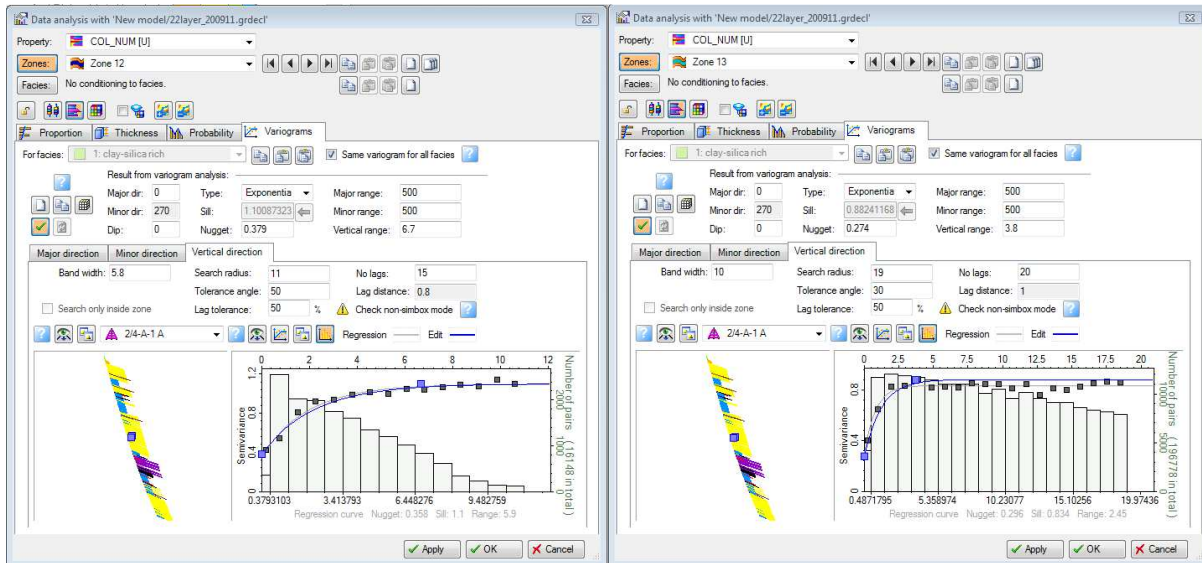
Appendix 2.2 Mineralogy Analysis of 2/4-X-32 and 2/4-A-8

Appendix 2.3 Variogram analysis to determine cell size

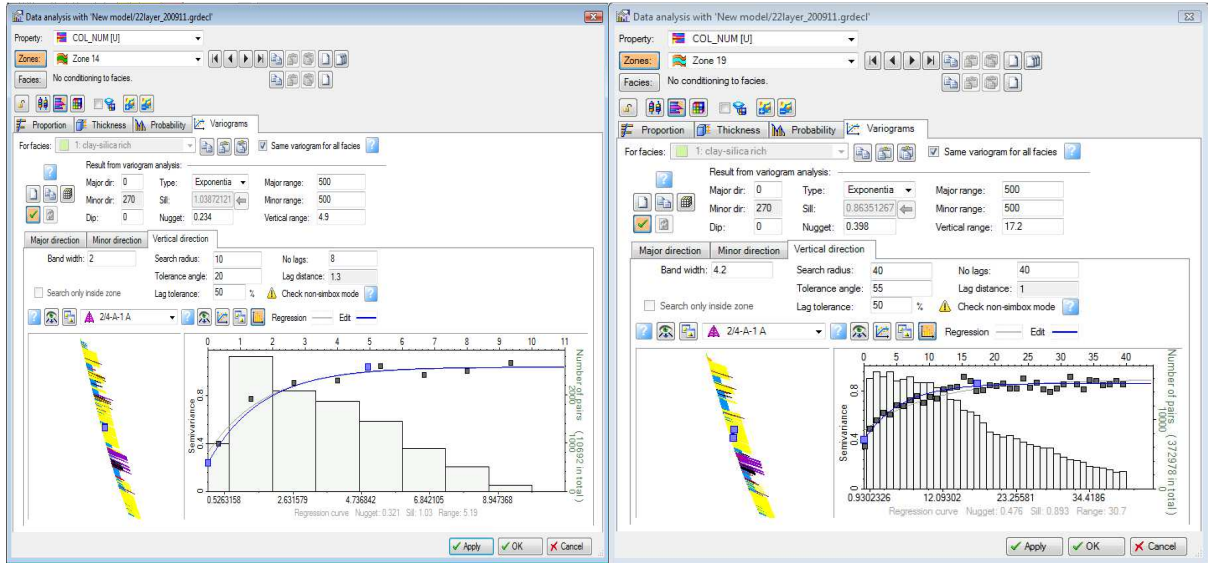
Interval with Dense Zone



Layer EM2 (left) and Layer EM4 (right)

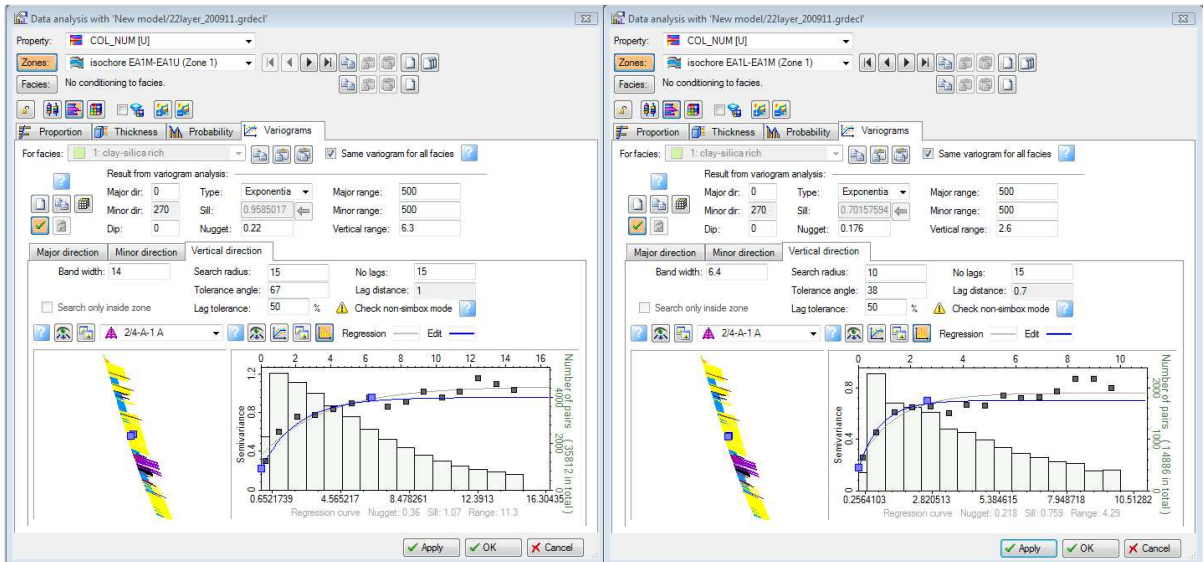


Layer EEU (left) and Layer EEM (right)

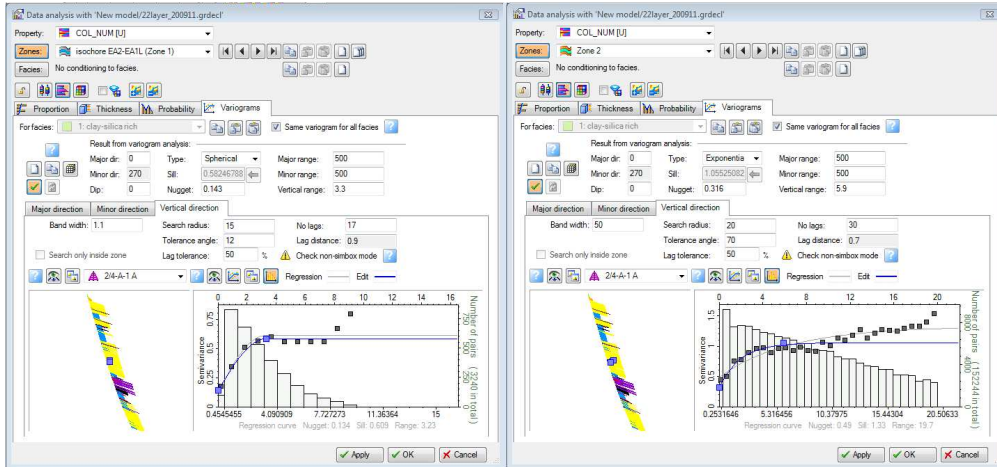


Layer EEL (left) and Layer TBU (right)

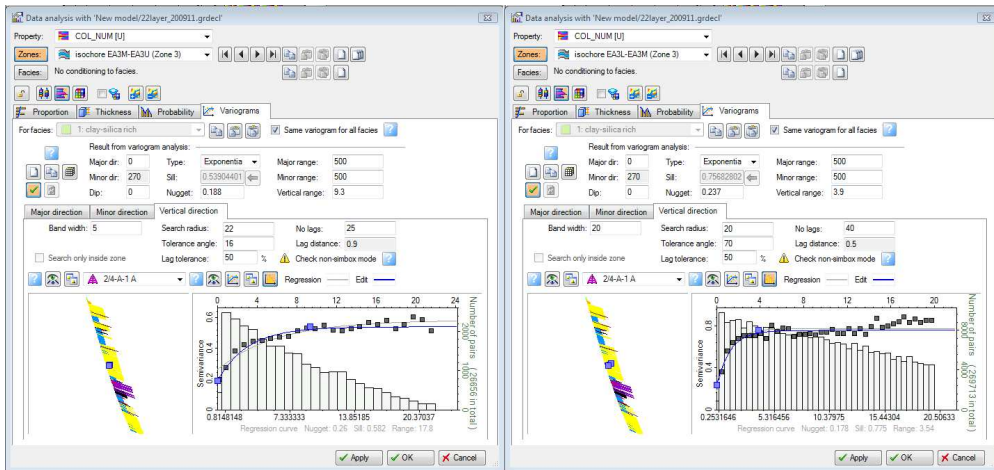
The rest Interval



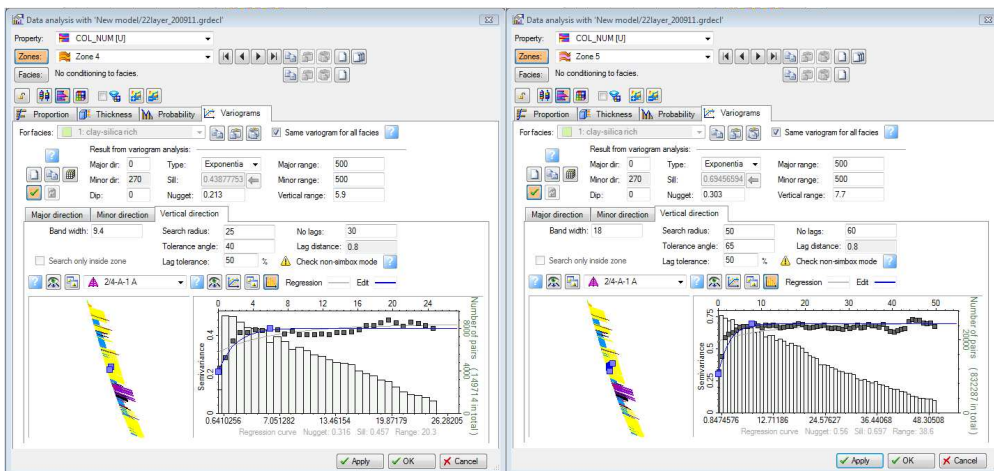
Layer EA1U-EA1M (left) and Layer EA1M-EA1L (right)



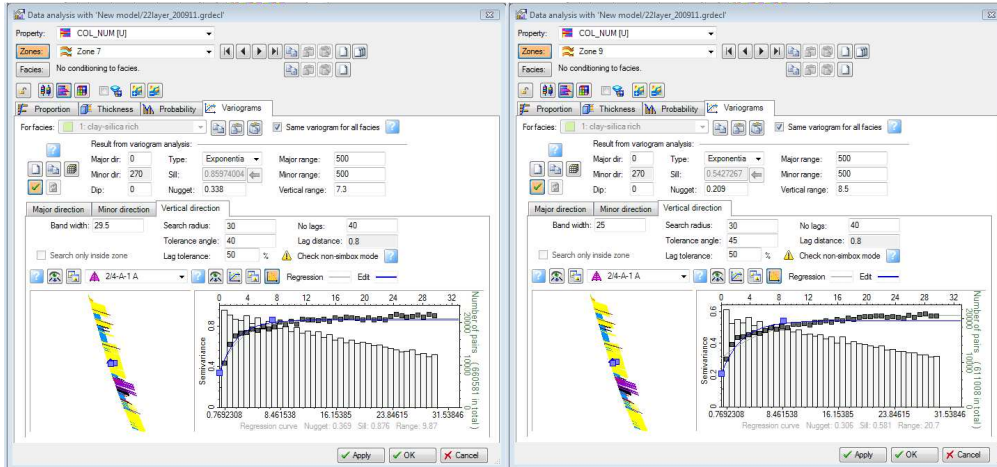
Layer EA1L-EA2 (left) and Layer EA2 (right)



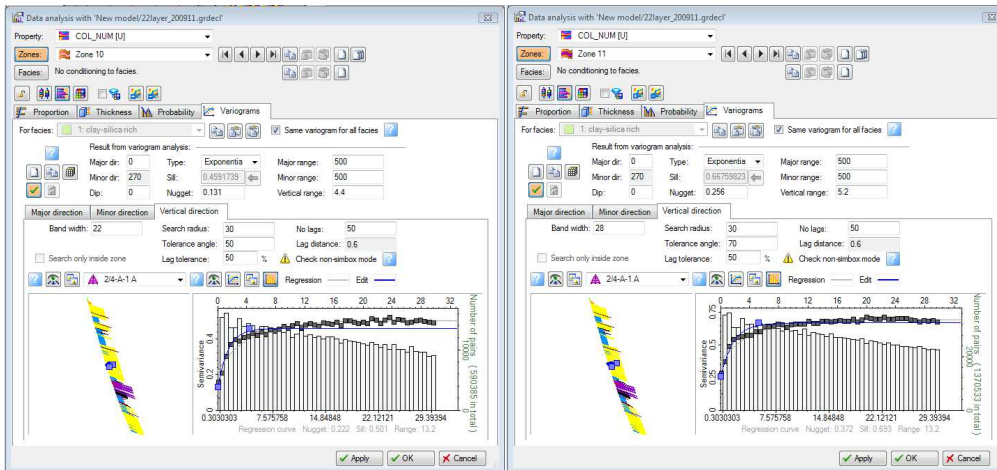
Layer EA3U-EA3M (left) and Layer EA3M-EA3L (right)



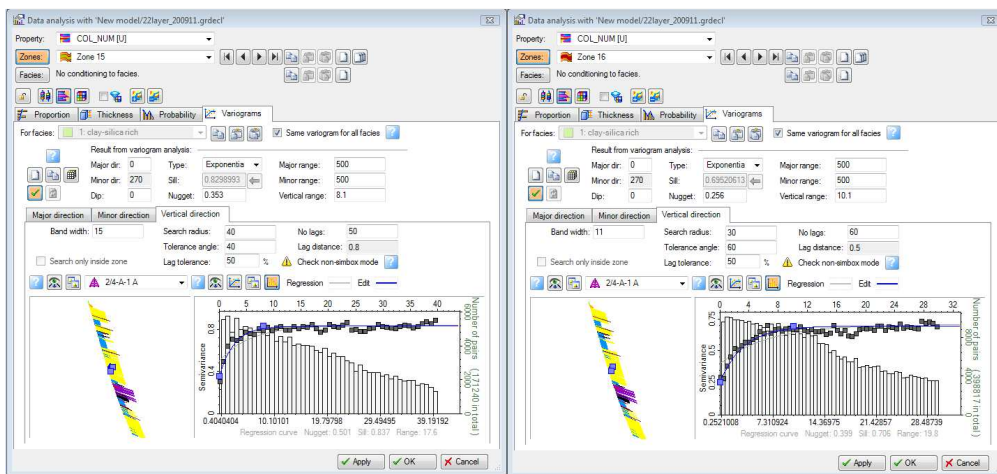
Layer EA3L (left) and Layer EM1 (right)



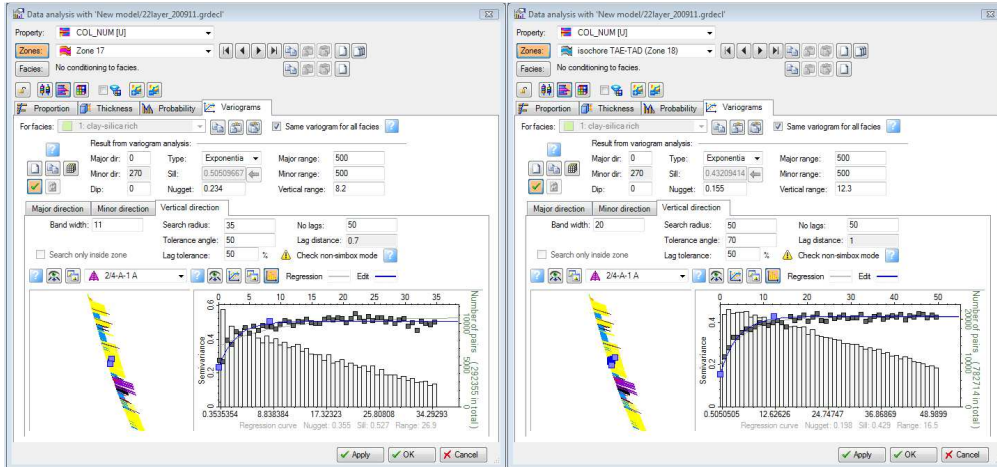
Layer EM3 (left) and Layer EL1 (right)



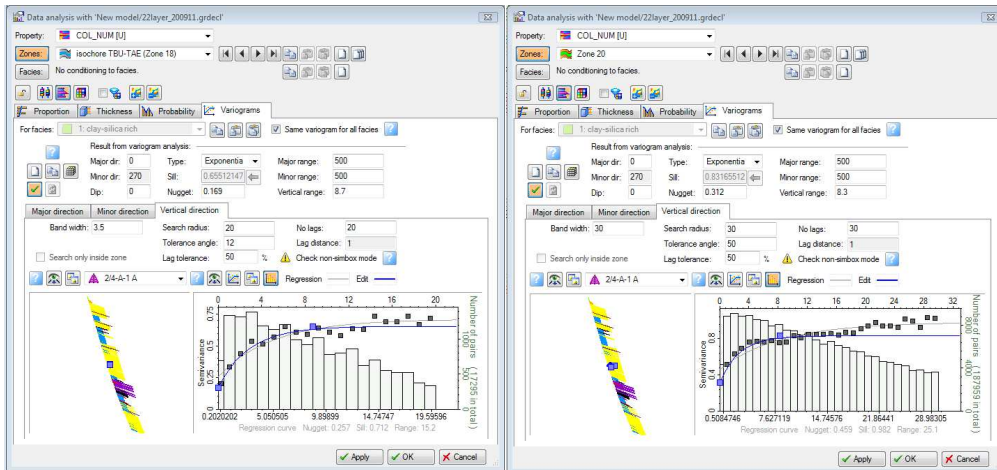
Layer EL2 (left) and Layer EL3 (right)



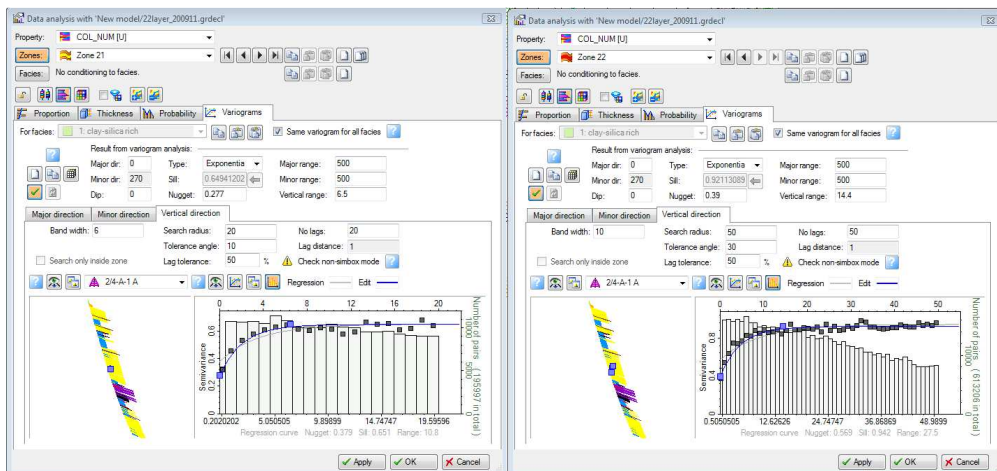
Layer TAA (left) and Layer TAB (right)



Layer TAC (left) and Layer TAD-TAE (right)



Layer TAE-TBU (left) and Layer TBU (right)



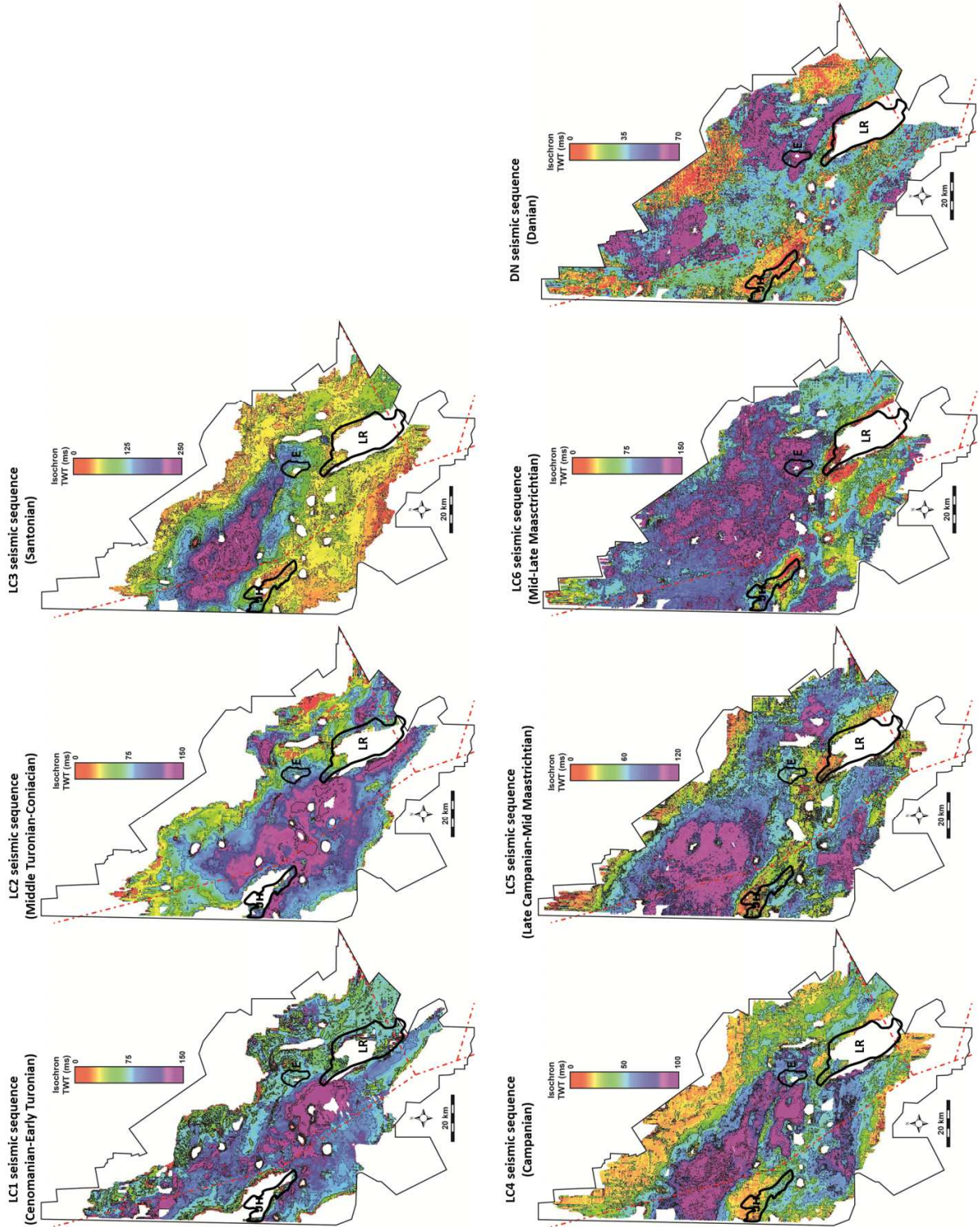
Layer TBL (left) and Layer TCU (right)

Table of Parameters from Vertical Variogram Analysis for Cell Size Purpose

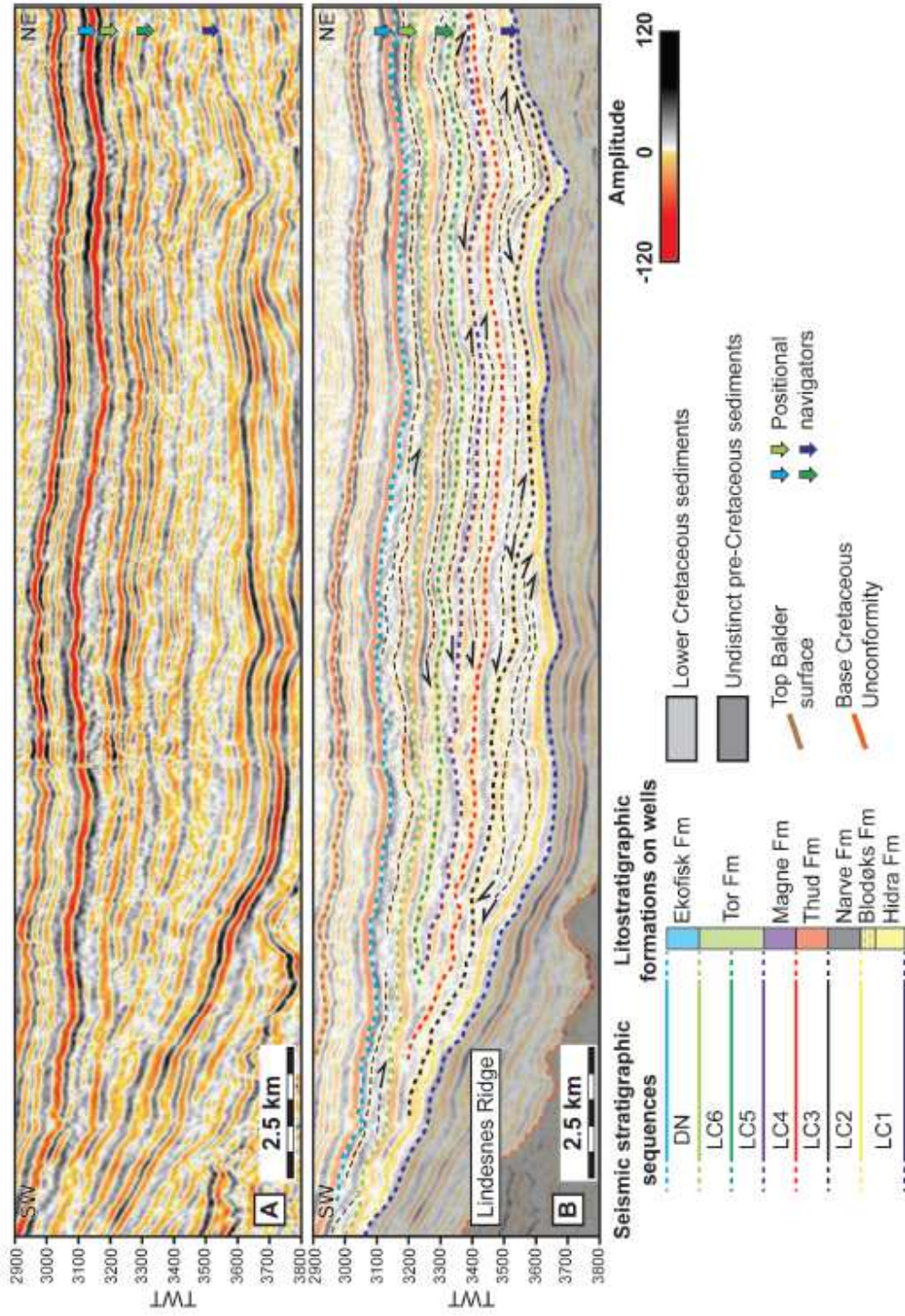
Interval	Zone	Lag Distance	Vertical range (ft)
Dense Zone	6 (EM2)	0.8	5.6
	8 (EM4)	0.6	6.2
	12 (EEU)	0.8	6.7
	13 (EEM)	1	3.8
	14 (EEL)	1.3	4.9
	19 (TBU)	1	17.2

Interval	Zone	Lag Distance	Vertical range (ft)
Main Zone	1 (EA1U)	1	6.3
	1 (EA1M)	0.7	2.6
	1 (EA1L)	0.9	3.3
	2 (EA2)	0.7	5.9
	3 (EA3U)	0.9	9.3
	3 (EA3M)	0.5	3.9
	4 (EA3L)	0.8	5.9
	5 (EM1)	0.8	7.7
	7 (EM3)	0.8	7.3
	9 (EL1)	0.8	8.5
	10 (EL2)	0.6	4.4
	11 (EL3)	0.6	5.2
	15 (TAA)	0.8	8.1
	16 (TAB)	0.5	10.1
	17 (TAC)	0.7	8.2
	18 (TAD)	1	12.3
	18 (TAE)	1	8.7
	20 (TBM)	1	8.3
	21 (TBL)	1	6.5
	22 (TCU)	1	14.4

Appendix 3.1 Isochron map



Appendix 3.2 Seismic Line



Reflection configuration and termination of seismic line showing direction of sedimentation.
 A) Uninterpreted B) Interpreted (Gennaro, 2011)

Appendix 4.1 Wells with data cleaning and handling; and Sensitivity result

Wells with Data Cleaning and Handling

No	Well	Log	Remark
1	2/4-M-13	POIS	Some interval is cut and normalization is from P5
2	2/4-M-17	POIS	Normalization is from P5
3	2/4-A-5	RHOB	Normalization at P5 and P95
4	2/4-C-11	RHOB	Normalization at P5 and P95
5	2/4-C-11 A	RHOB	Normalization at P5 and P95
6	2/4-M-22	RHOB	Normalization at P5 and P95
7	2/4-X-13 AT2	RHOB	Normalization at P5 and P95
8	2/4-W-4 AT2	GR-RHOB-POIS-YMOD	Smoothing by 10 times
9	2/4-X-17 T2	GR-RHOB-POIS-YMOD	Smoothing by 7 times
10	2/4-X-20	GR-RHOB-POIS-YMOD	Smoothing by 5 times
11	2/4-X-3	GR-RHOB-POIS-YMOD	Smoothing by 5 times
12	2/4-X-31	GR	Smoothing by 5 times

6 simplified facies for reference in GR, RHOB, YMOD, POIS, smothing and sampling rate sensitivity

P50	GR	RHOB	YMOD	POIS	Weight	Frac. Weight
Facies_1	6.7	2.49	5.5	0.25	1253	0.12
Facies_2	5.9	2.37	4.4	0.25	1488	0.15
Facies_3	6.8	2.23	3.1	0.24	1772	0.17
Facies_4	15.7	2.28	2.7	0.22	950	0.09
Facies_5	8.9	2.1	2.1	0.22	870	0.09
Facies_6	5.9	2.1	2	0.22	3878	0.38
					10211	1.00

GR Sensitivity

Type	Facies Match	Well				
		A6	B19A	K22	K4	X32
GR P50	1	0.00	0.00	0.01	0.00	0.02
	2	0.03	0.06	0.04	0.05	0.05
	3	0.07	0.01	0.01	0.04	0.03
	4	0.01	0.02	0.02	0.01	0.03
	5	0.02	0.01	0.00	0.00	0.01
	6	0.02	0.06	0.04	0.04	0.05
	Total Mis-match	0.17	0.16	0.12	0.16	0.19
	Min	0.00				
	Average	0.03				
	Max	0.07				

Type	Facies Match	Well				
		A6	B19A	K22	K4	X32
GR P50-P5	1	0.00	0.00	0.00	0.00	0.03
	2	0.03	0.05	0.04	0.02	0.02
	3	0.07	0.02	0.02	0.06	0.06
	4	0.01	0.02	0.01	0.02	0.07
	5	0.00	0.00	0.00	0.00	0.00
	6	0.07	0.05	0.03	0.04	0.02
	Total Mis-match	0.19	0.15	0.11	0.15	0.19
	Min	0.00				
	Average	0.03				
	Max	0.07				

Type	Facies Match	Well				
		A6	B19A	K22	K4	X32
GR P50-P5-P95	1	0.01	0.00	0.01	0.00	0.03
	2	0.03	0.04	0.03	0.04	0.03
	3	0.04	0.01	0.02	0.05	0.04
	4	0.02	0.06	0.06	0.05	0.05
	5	0.03	0.01	0.00	0.00	0.01
	6	0.06	0.07	0.04	0.08	0.02
	Total Mis-match	0.20	0.18	0.15	0.22	0.18
	Min	0.00				
	Average	0.03				
	Max	0.08				

RHOB Sensitivity

Type	Facies Match	Well				
		A6	B19A	K22	K4	X32
RHOB P50	1	0.01	0.00	0.01	0.01	0.03
	2	0.04	0.04	0.03	0.04	0.03
	3	0.11	0.06	0.06	0.09	0.10
	4	0.01	0.11	0.01	0.05	0.07
	5	0.00	0.01	0.01	0.00	0.07
	6	0.07	0.10	0.07	0.07	0.01
	Total Mis-match	0.24	0.32	0.17	0.26	0.32
	Min	0.00				
	Average	0.04				
	Max	0.11				

Type	Facies Match	Well				
		A6	B19A	K22	K4	X32
RHOB P50-P5	1	0.02	0.00	0.00	0.00	0.01
	2	0.04	0.04	0.04	0.03	0.02
	3	0.10	0.03	0.08	0.11	0.12
	4	0.01	0.02	0.05	0.02	0.08
	5	0.00	0.09	0.01	0.01	0.07
	6	0.02	0.03	0.07	0.02	0.03
	Total Mis-match	0.20	0.19	0.25	0.19	0.34
	Min	0.00				
	Average	0.04				
	Max	0.12				

Type	Facies Match	Well				
		A6	B19A	K22	K4	X32
RHOB P50-P5-P95	1	0.02	0.00	0.00	0.00	0.01
	2	0.04	0.04	0.04	0.04	0.02
	3	0.10	0.03	0.08	0.11	0.12
	4	0.01	0.02	0.05	0.02	0.08
	5	0.00	0.09	0.01	0.01	0.07
	6	0.02	0.03	0.07	0.01	0.02
	Total Mis-match	0.20	0.20	0.25	0.19	0.33
	Min	0.00				
	Average	0.04				
	Max	0.12				

YMOD Sensitivity

Type	Facies Match	Well				
		A6	B19A	K22	K4	X32
YMOD P50	1	0.01	0.00	0.00	0.01	0.01
	2	0.03	0.05	0.04	0.03	0.03
	3	0.03	0.02	0.03	0.04	0.08
	4	0.01	0.07	0.03	0.03	0.00
	5	0.01	0.00	0.01	0.00	0.00
	6	0.01	0.02	0.01	0.03	0.00
	Total Mis-match	0.10	0.16	0.12	0.13	0.13
Min	0.00					
Average	0.02					
Max	0.08					

Type	Facies Match	Well				
		A6	B19A	K22	K4	X32
YMOD P50-P5	1	0.01	0.00	0.00	0.01	0.01
	2	0.03	0.02	0.03	0.02	0.03
	3	0.07	0.02	0.05	0.08	0.09
	4	0.02	0.01	0.02	0.00	0.01
	5	0.01	0.00	0.01	0.00	0.01
	6	0.03	0.03	0.01	0.05	0.04
	Total Mis-match	0.16	0.10	0.11	0.16	0.18
Min	0.00					
Average	0.02					
Max	0.09					

Type	Facies Match	Well				
		A6	B19A	K22	K4	X32
YMOD P50-P5-P95	1	0.02	0.00	0.00	0.01	0.01
	2	0.03	0.03	0.03	0.03	0.02
	3	0.06	0.02	0.05	0.06	0.06
	4	0.01	0.06	0.07	0.05	0.00
	5	0.00	0.00	0.00	0.00	0.05
	6	0.04	0.01	0.01	0.03	0.05
	Total Mis-match	0.15	0.13	0.15	0.18	0.20
Min	0.00					
Average	0.03					
Max	0.07					

POIS Sensitivity

Type	Facies Match	Well				
		A6	B19A	K22	K4	X32
POIS P50	1	0.00	0.00	0.01	0.00	0.01
	2	0.03	0.01	0.01	0.02	0.02
	3	0.04	0.02	0.02	0.04	0.05
	4	0.01	0.07	0.02	0.04	0.03
	5	0.03	0.00	0.00	0.00	0.00
	6	0.04	0.04	0.04	0.05	0.02
	Total Mis-match	0.15	0.15	0.10	0.15	0.13
Min	0.00					
Average	0.02					
Max	0.07					

Type	Facies Match	Well				
		A6	B19A	K22	K4	X32
POIS P50-P5	1	0.00	0.00	0.00	0.00	0.00
	2	0.05	0.05	0.04	0.05	0.03
	3	0.02	0.02	0.03	0.05	0.06
	4	0.01	0.07	0.02	0.05	0.03
	5	0.01	0.00	0.00	0.00	0.01
	6	0.02	0.02	0.02	0.02	0.01
	Total Mis-match	0.10	0.17	0.10	0.17	0.14
Min	0.00					
Average	0.02					
Max	0.07					

Type	Facies Match	Well				
		A6	B19A	K22	K4	X32
POIS P50-P5-P95	1	0.00	0.00	0.00	0.00	0.00
	2	0.04	0.05	0.04	0.04	0.03
	3	0.06	0.06	0.09	0.06	0.08
	4	0.01	0.06	0.03	0.05	0.03
	5	0.03	0.00	0.00	0.00	0.01
	6	0.02	0.04	0.03	0.03	0.01
	Total Mis-match	0.16	0.20	0.18	0.18	0.15
Min	0.00					
Average	0.03					
Max	0.09					

Smoothing Sensitivity

Type	Facies Match	Well				
		A6	B19A	K22	K4	X32
SM 3 times	1	0.01	0.00	0.00	0.00	0.00
	2	0.04	0.03	0.04	0.03	0.02
	3	0.08	0.02	0.05	0.07	0.08
	4	0.01	0.01	0.01	0.01	0.03
	5	0.03	0.00	0.01	0.00	0.01
	6	0.01	0.02	0.02	0.02	0.00
	Total Mis-match	0.17	0.09	0.13	0.13	0.15
Min	0.00					
Average	0.02					
Max	0.08					

Type	Facies Match	Well				
		A6	B19A	K22	K4	X32
SM 5 times	1	0.02	0.00	0.01	0.00	0.03
	2	0.05	0.07	0.04	0.06	0.05
	3	0.08	0.05	0.07	0.09	0.08
	4	0.01	0.06	0.02	0.03	0.02
	5	0.00	0.00	0.01	0.00	0.01
	6	0.02	0.02	0.03	0.04	0.04
	Total Mis-match	0.19	0.21	0.17	0.22	0.23
Min	0.00					
Average	0.03					
Max	0.09					

Type	Facies Match	Well				
		A6	B19A	K22	K4	X32
SM 7 times	1	0.01	0.00	0.01	0.01	0.01
	2	0.04	0.06	0.03	0.04	0.03
	3	0.06	0.02	0.08	0.08	0.06
	4	0.01	0.05	0.05	0.04	0.03
	5	0.04	0.01	0.01	0.00	0.02
	6	0.04	0.02	0.02	0.03	0.07
	Total Mis-match	0.20	0.18	0.20	0.21	0.22
Min	0.00					
Average	0.03					
Max	0.08					

Sampling Rate Sensitivity

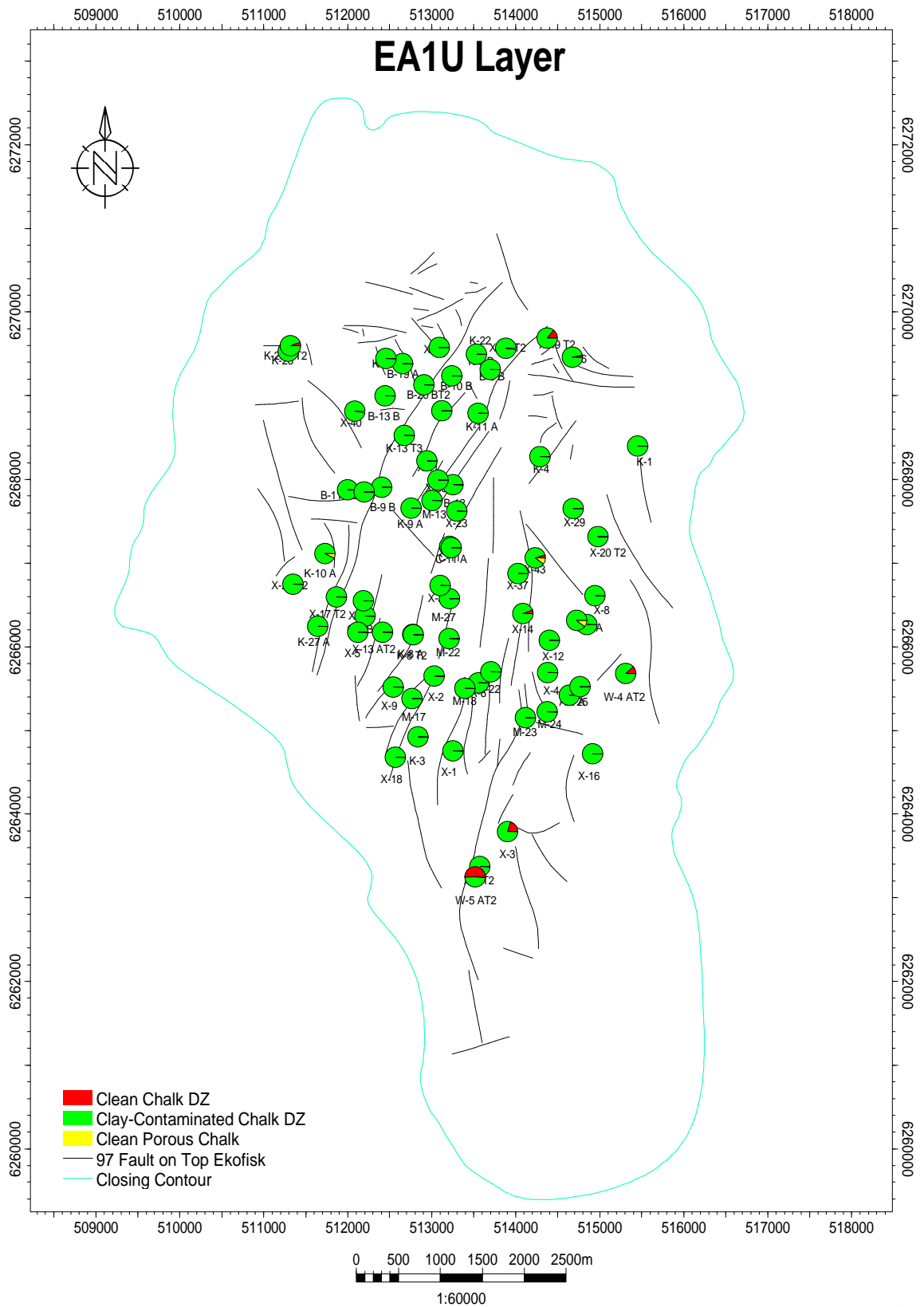
Type	Facies Match	Well				
		A6	B19A	K22	K4	X32
SR 1 ft	1	0.00	0.00	0.00	0.00	0.01
	2	0.03	0.04	0.04	0.03	0.02
	3	0.05	0.01	0.02	0.04	0.03
	4	0.01	0.02	0.02	0.01	0.01
	5	0.01	0.02	0.01	0.01	0.05
	6	0.03	0.04	0.04	0.06	0.07
	Total Mis-match	0.13	0.14	0.12	0.16	0.19
	Min	0.00				
	Average	0.02				
	Max	0.07				

Type	Facies Match	Well				
		A6	B19A	K22	K4	X32
SR 1.5 ft	1	0.01	0.00	0.00	0.01	0.03
	2	0.05	0.04	0.03	0.05	0.03
	3	0.08	0.03	0.05	0.10	0.08
	4	0.01	0.01	0.02	0.01	0.03
	5	0.03	0.05	0.01	0.01	0.02
	6	0.01	0.03	0.02	0.05	0.04
	Total Mis-match	0.19	0.16	0.14	0.22	0.22
	Min	0.00				
	Average	0.03				
	Max	0.10				

Type	Facies Match	Well				
		A6	B19A	K22	K4	X32
SR 2 ft	1	0.02	0.01	0.02	0.01	0.01
	2	0.02	0.03	0.02	0.03	0.02
	3	0.10	0.03	0.05	0.11	0.09
	4	0.02	0.01	0.02	0.01	0.03
	5	0.01	0.06	0.01	0.02	0.03
	6	0.04	0.03	0.04	0.04	0.01
	Total Mis-match	0.21	0.17	0.17	0.23	0.19
	Min	0.01				
	Average	0.03				
	Max	0.11				

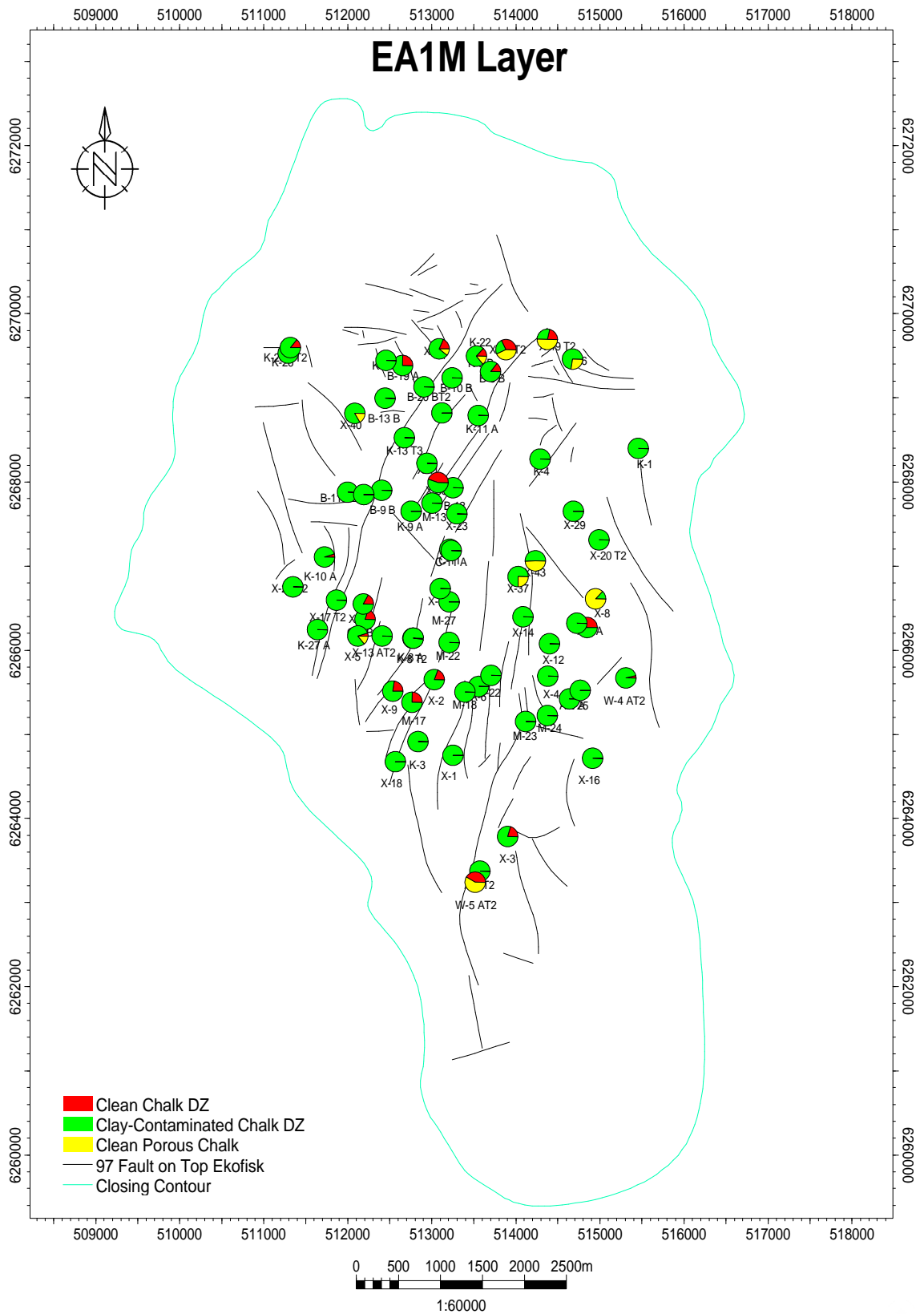
Appendix 4.2 Map of proportion of facies

Appendix 4.2.1 Map of facies proportion from 123 model (Well log)



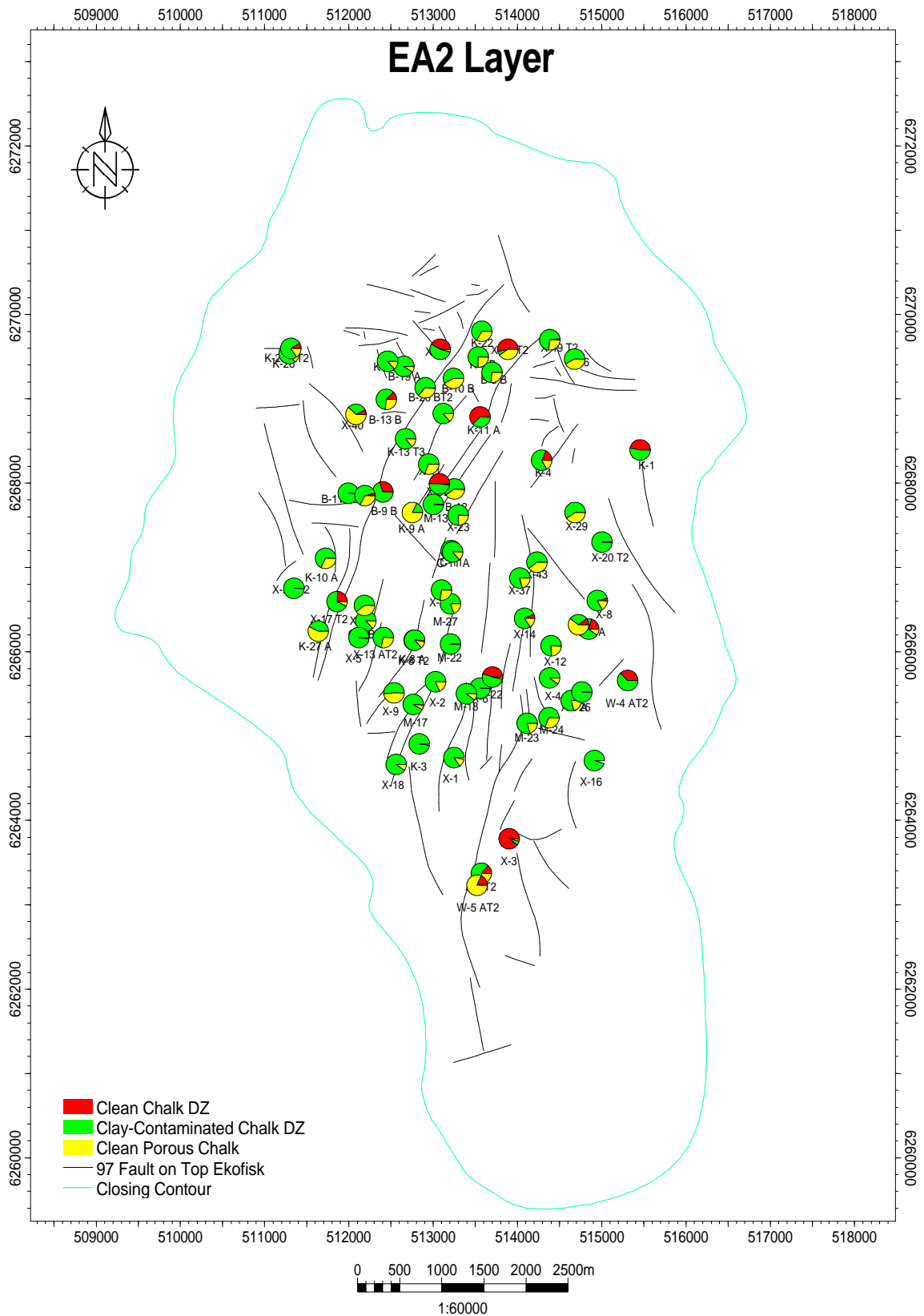
Project: total_ekofisk_well_201112_r1.pet (06/11/2012)





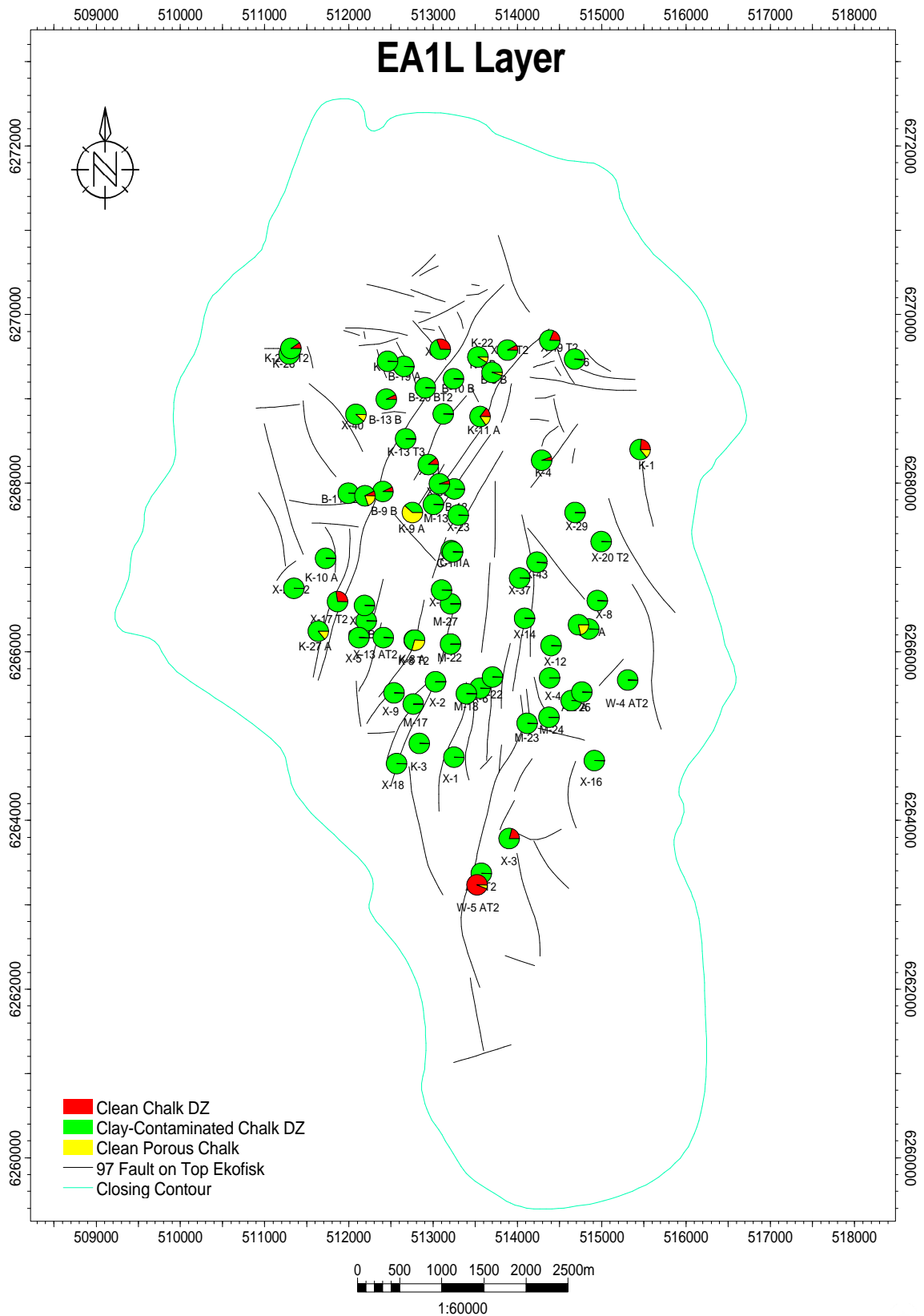
Project: total_ekofisk_well_201112_r1.pet (06/11/2012)





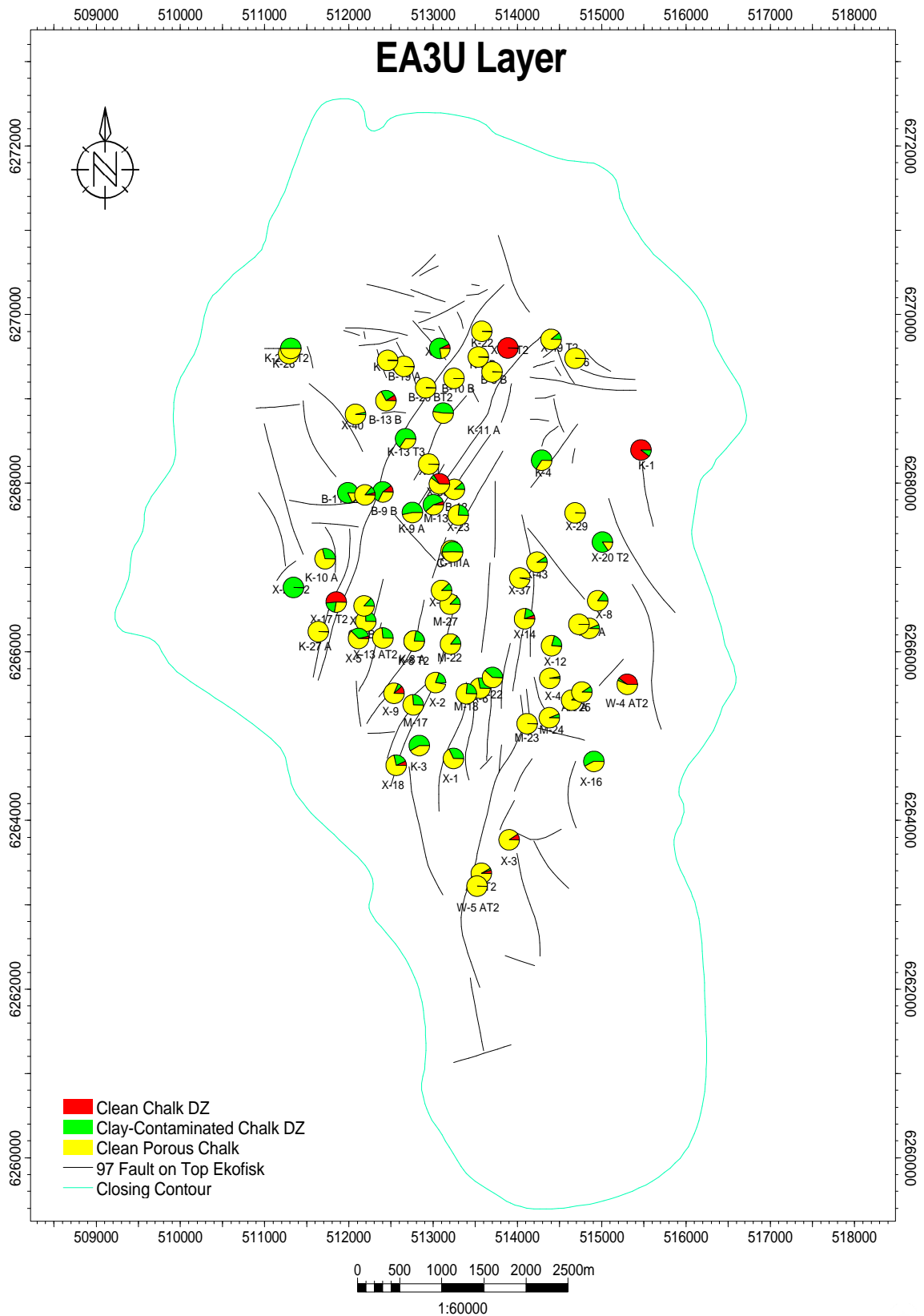
Project: total_ekofisk_well_201112_r1.pet (06/11/2012)





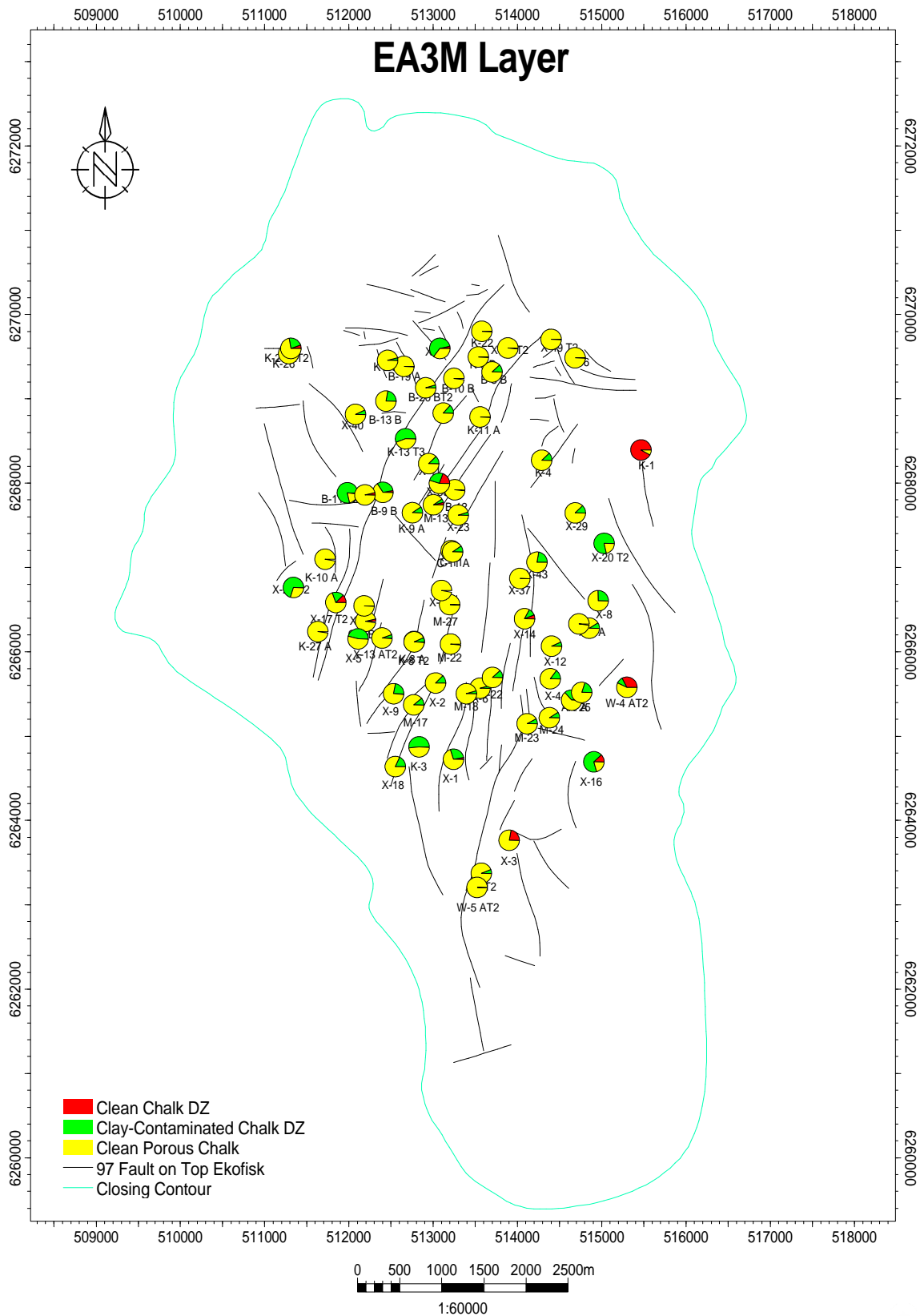
Project: total_ekofisk_well_201112_r1.pet (06/11/2012)





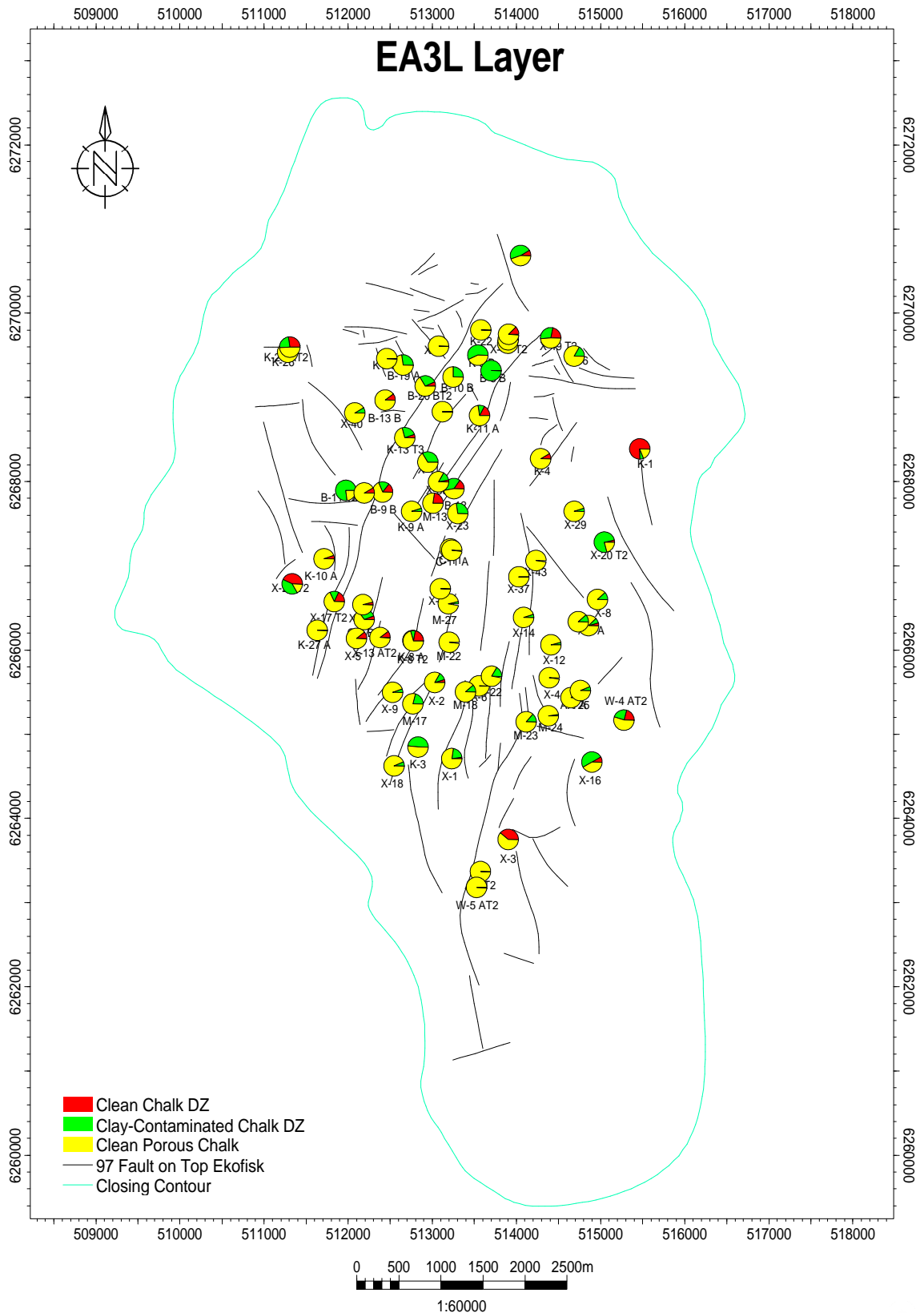
Project: total_ekofisk_well_201112_r1.pet (06/11/2012)





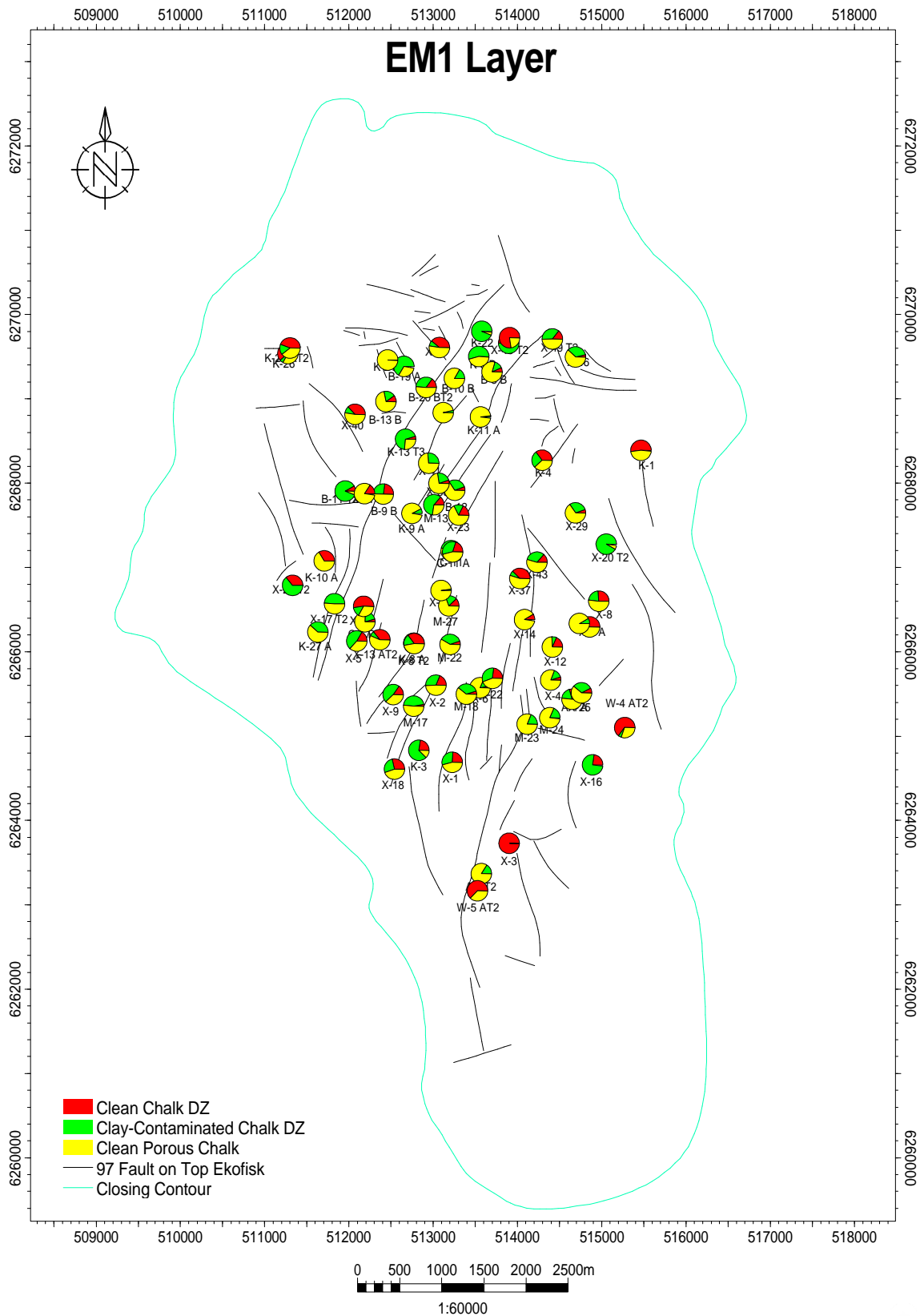
Project: total_ekofisk_well_201112_r1.pet (06/11/2012)





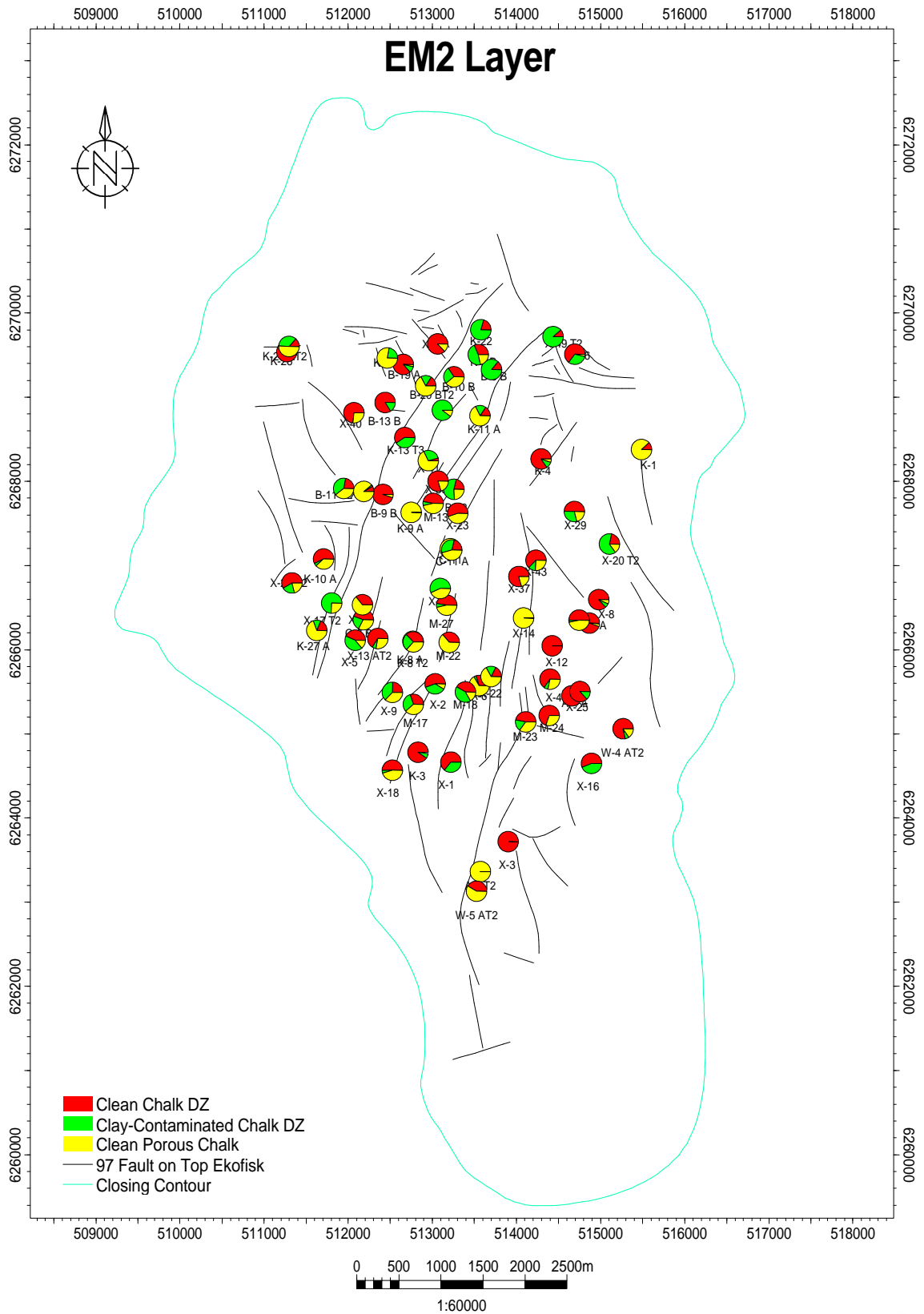
Project: total_ekofisk_well_201112_r1.pet (06/11/2012)





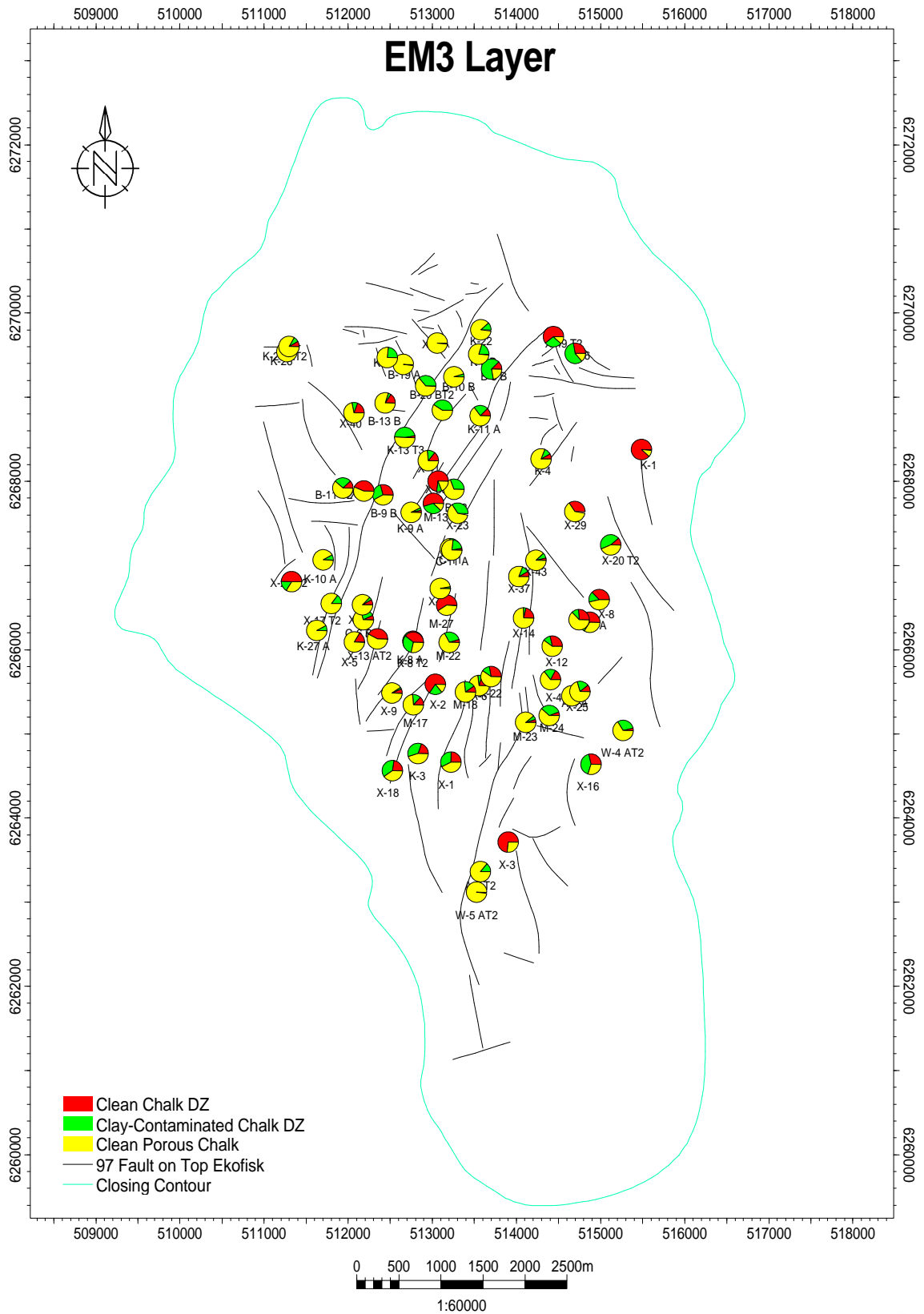
Project: total_ekofisk_well_201112_r1.pet (06/11/2012)





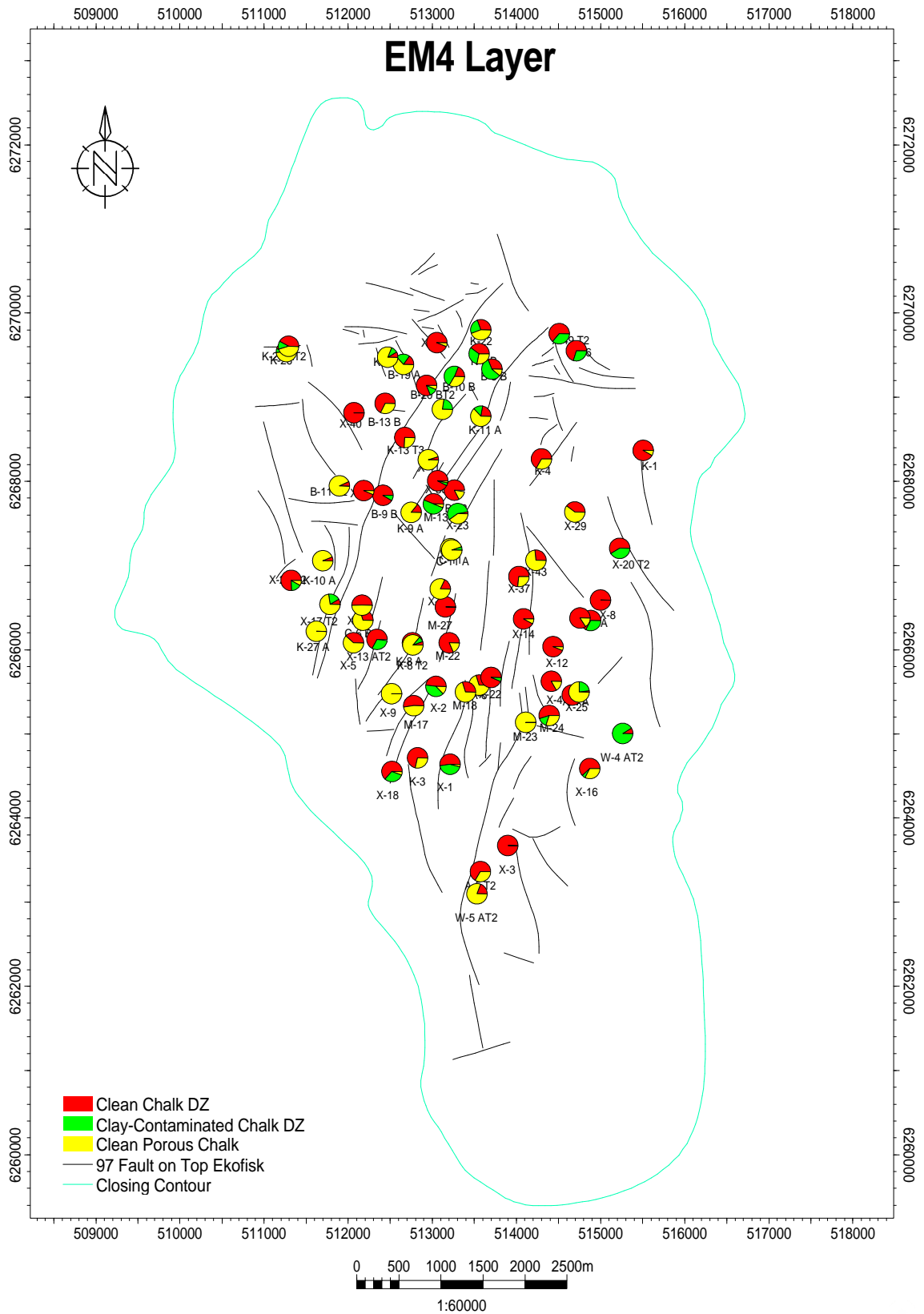
Project: total_ekofisk_well_201112_r1.pet (06/11/2012)





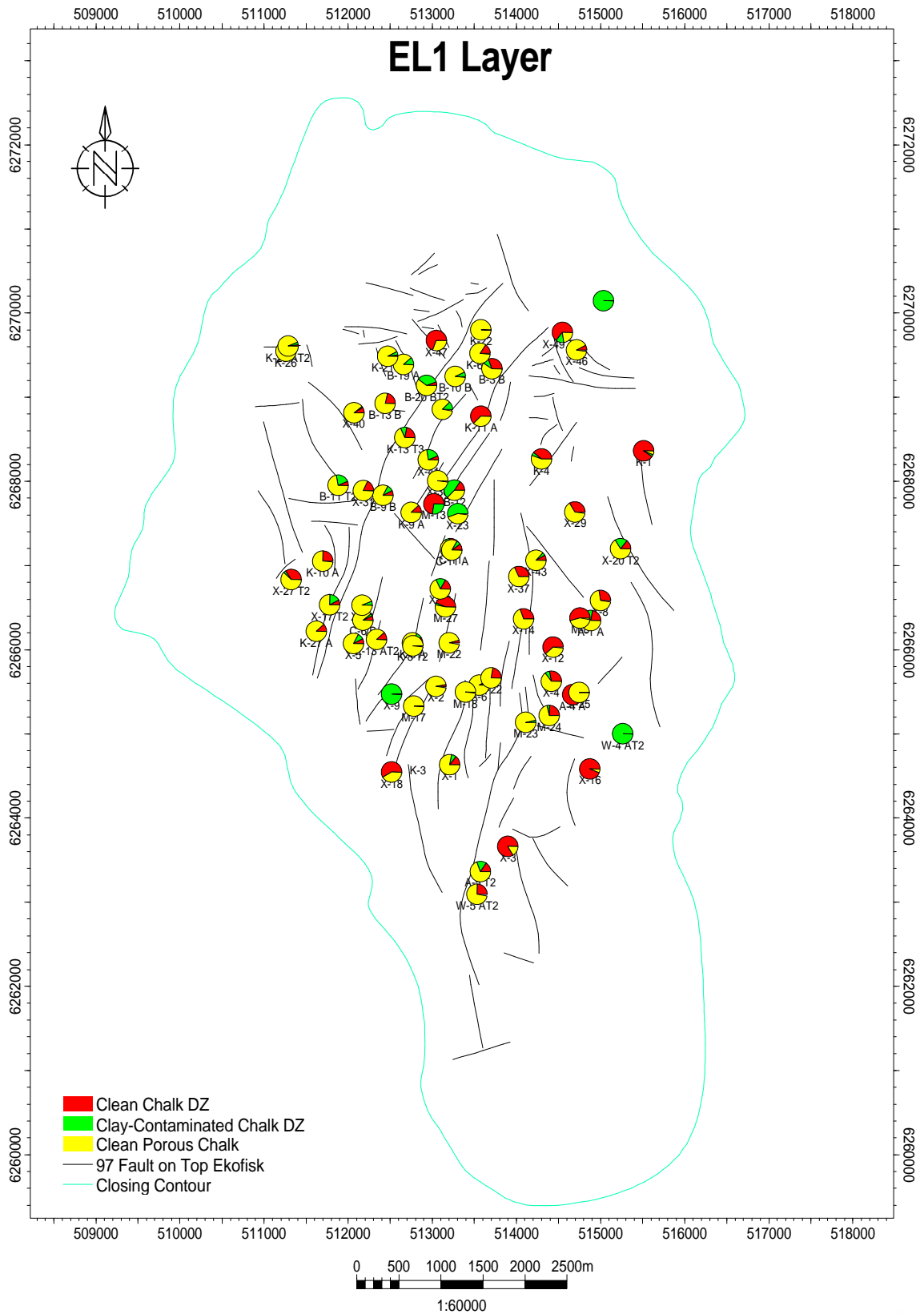
Project: total_ekofisk_well_201112_r1.pet (06/11/2012)





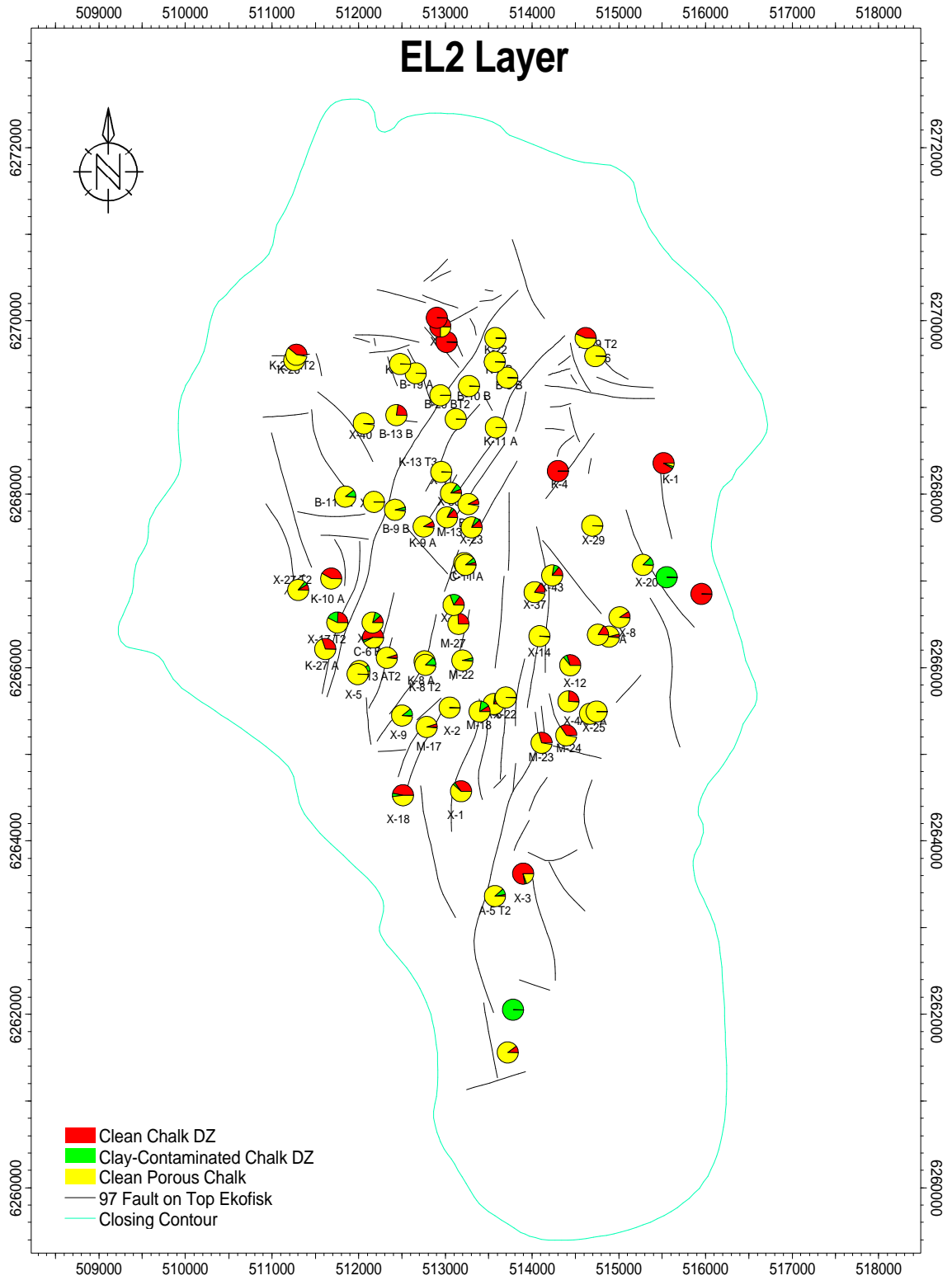
Project: total_ekofisk_well_201112_r1.pet (06/11/2012)





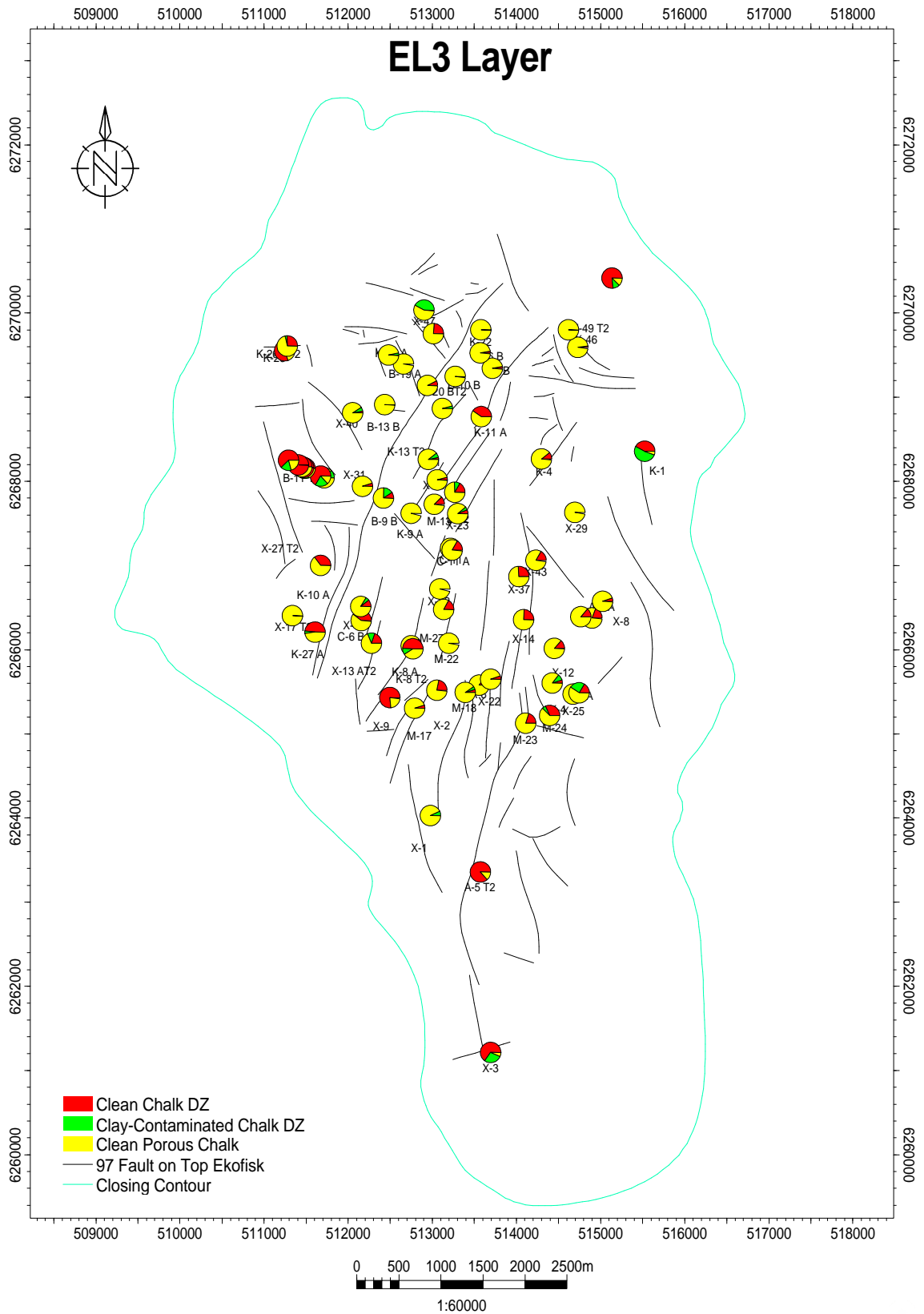
Project: total_ekofisk_well_201112_r1.pet (06/11/2012)





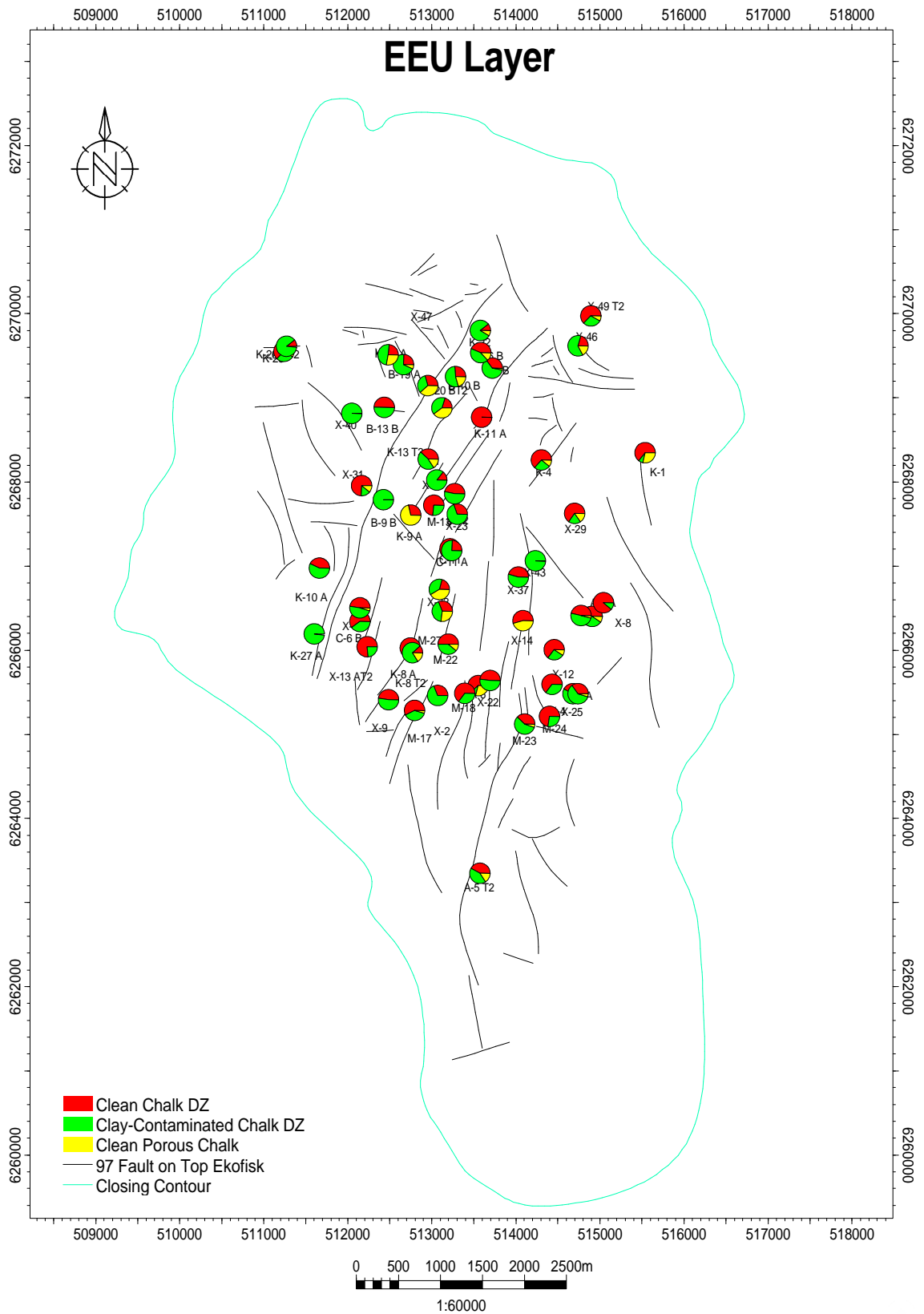
Project: total_ekofisk_well_201112_r1.pet (06/11/2012)





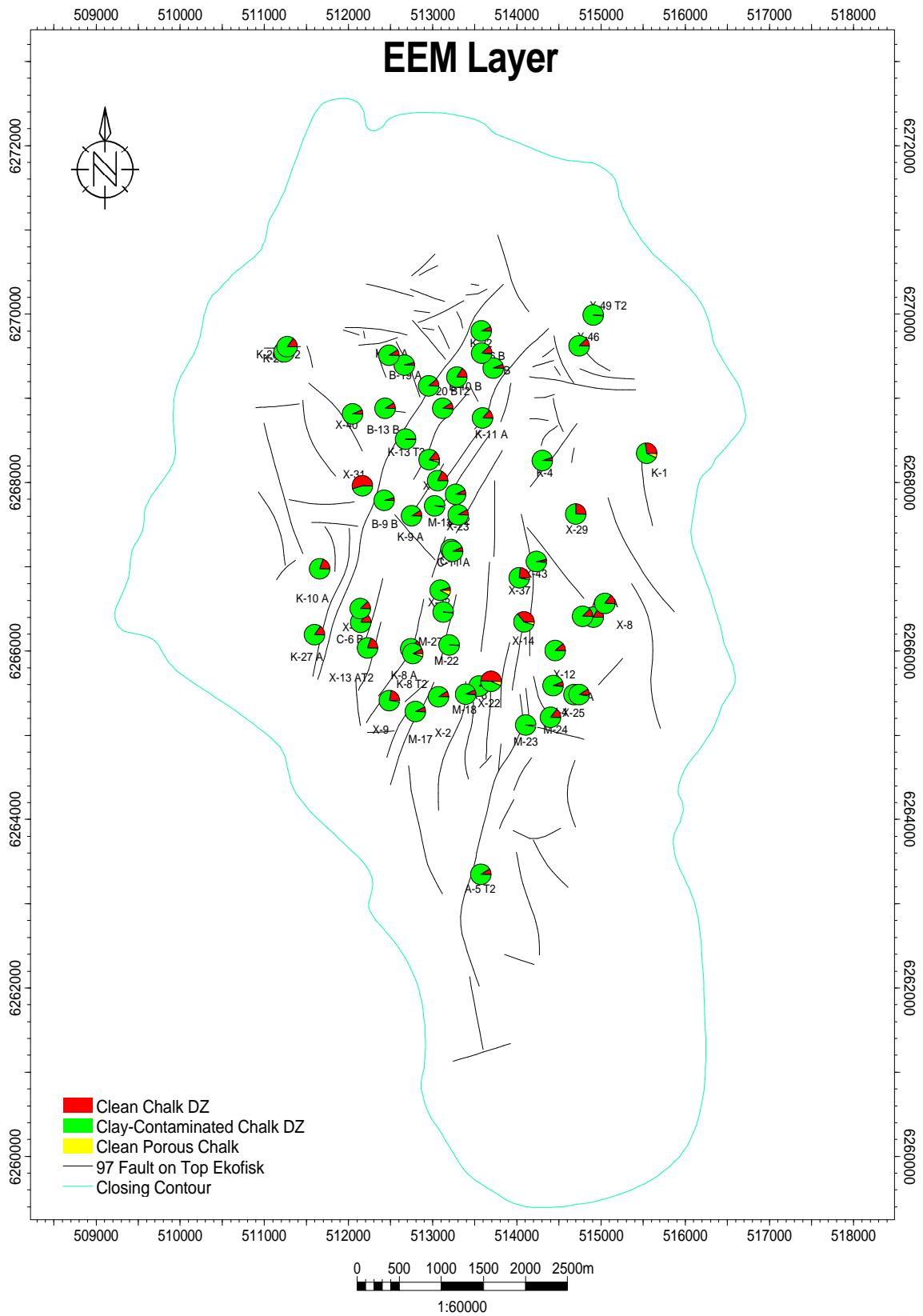
Project: total_ekofisk_well_201112_r1.pet (06/11/2012)





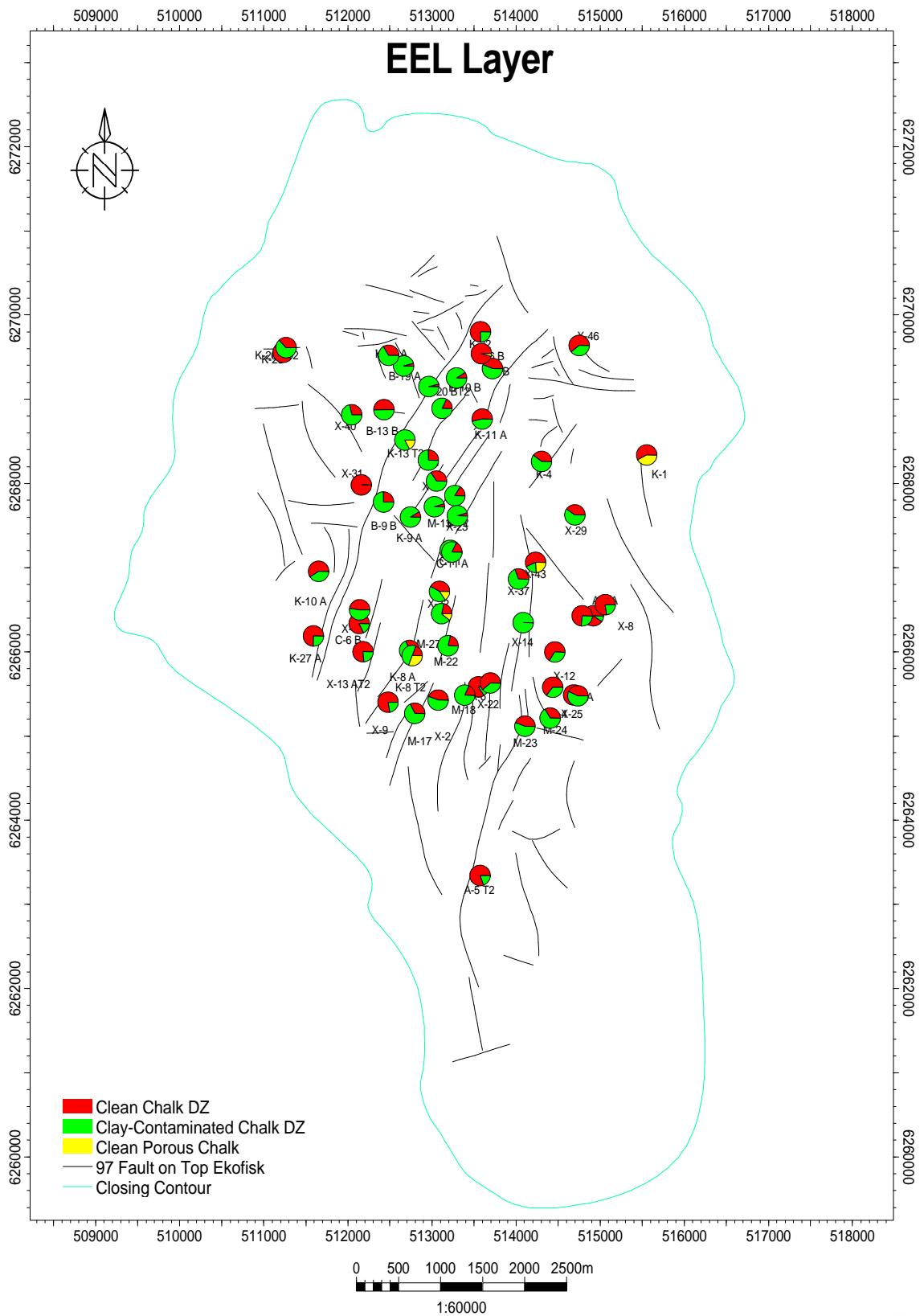
Project: total_ekofisk_well_201112_r1.pet (06/11/2012)





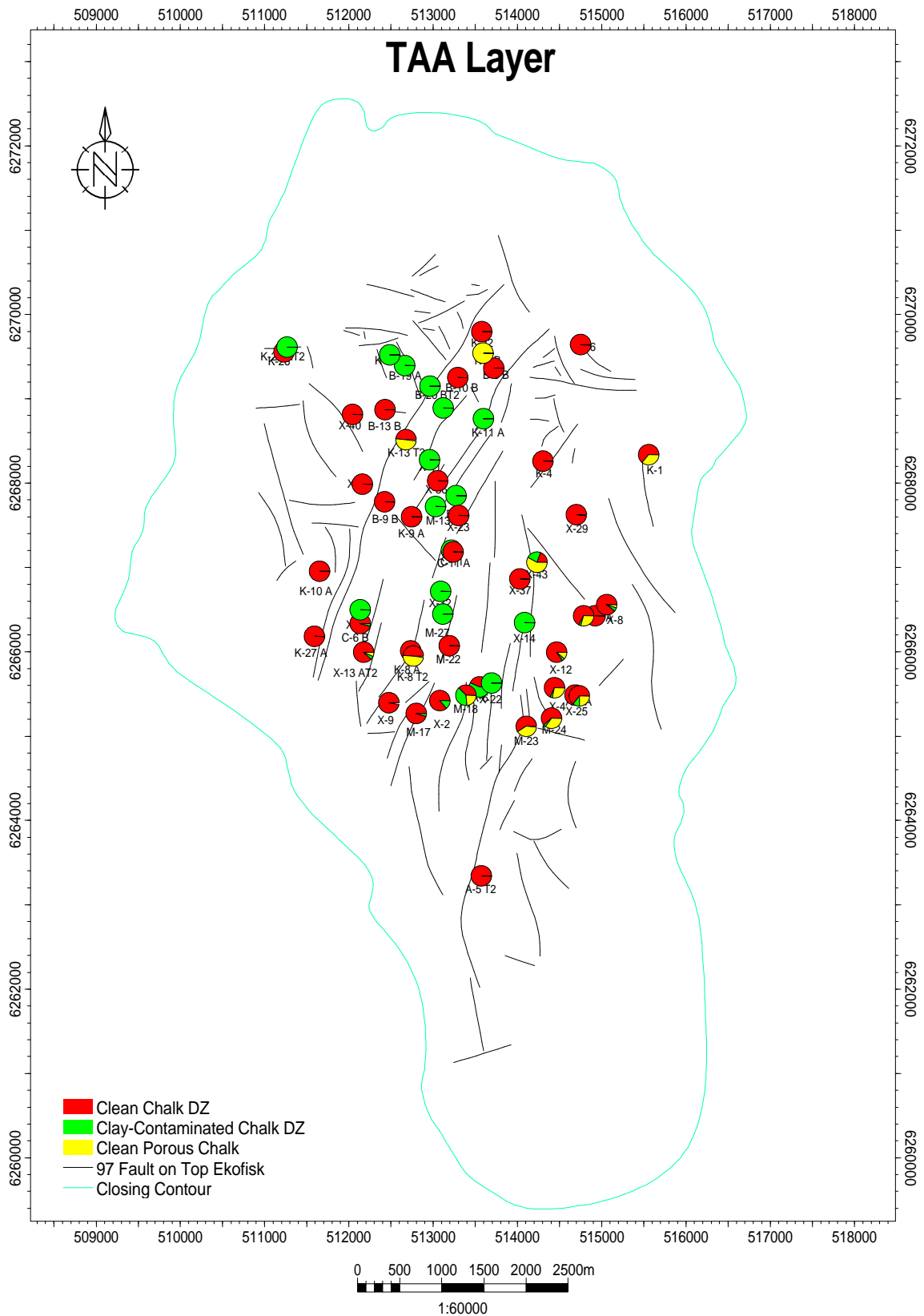
Project: total_ekofisk_well_201112_r1.pet (06/11/2012)





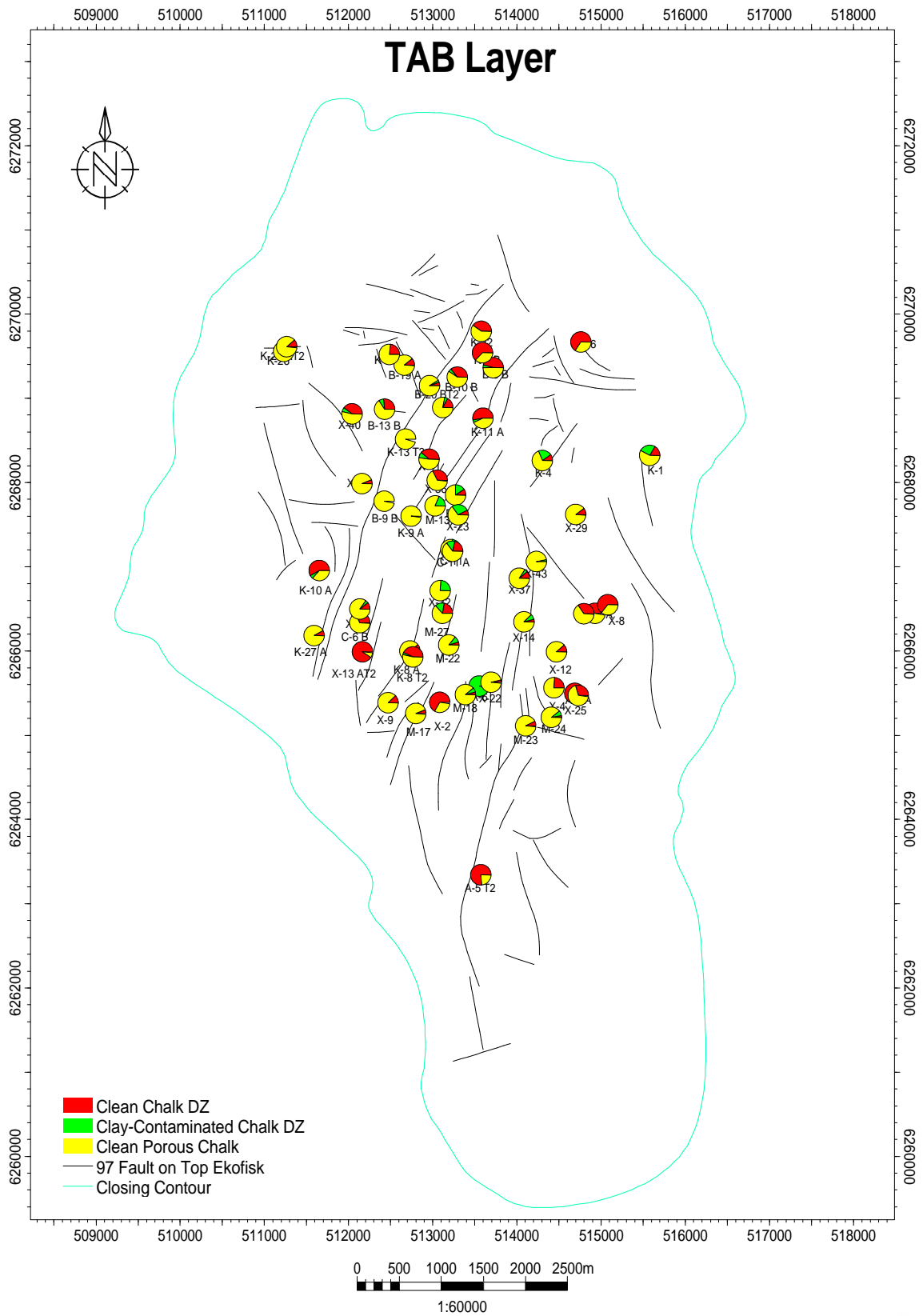
Project: total_ekofisk_well_201112_r1.pet (06/11/2012)





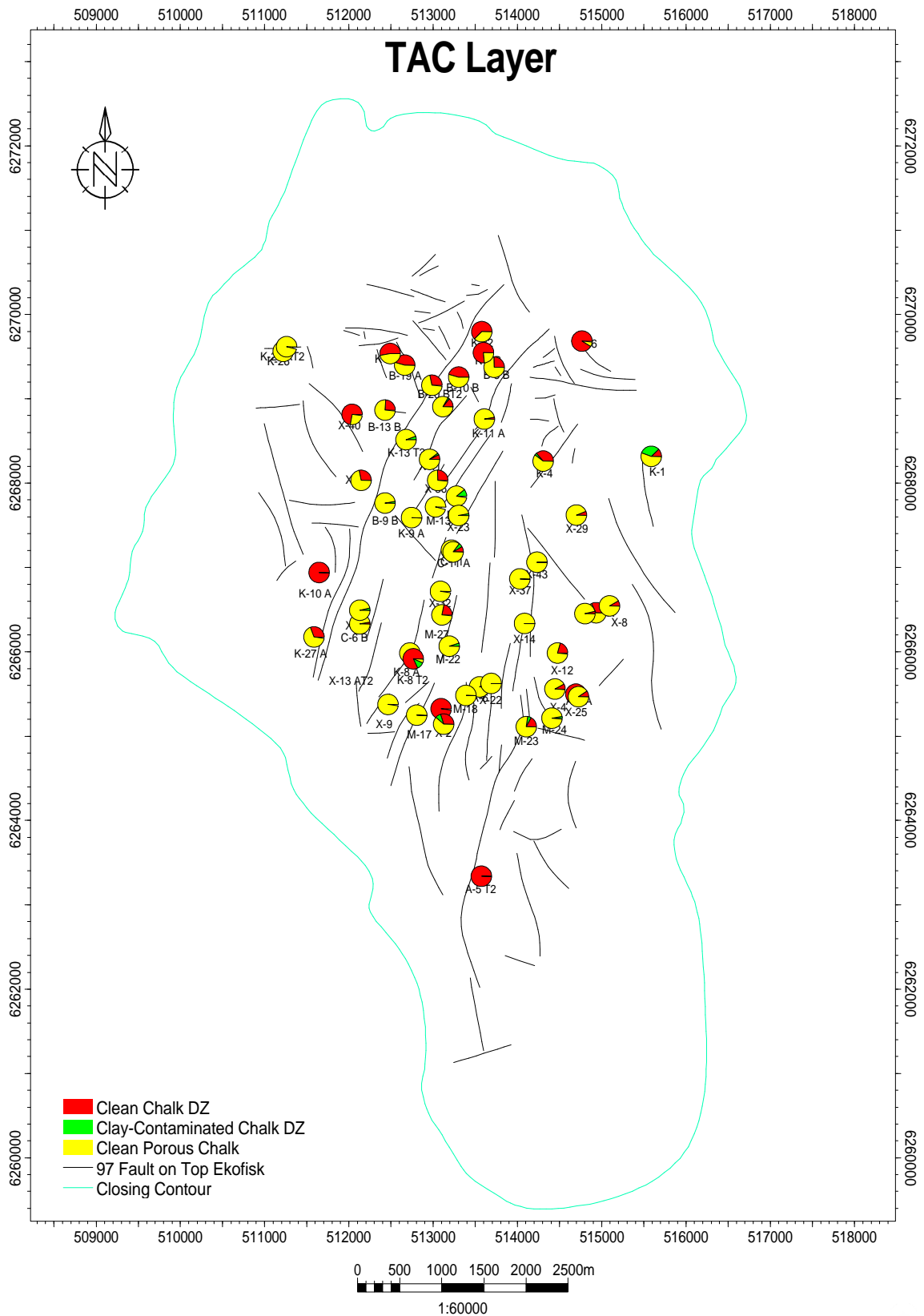
Project: total_ekofisk_well_201112_r1.pet (06/11/2012)





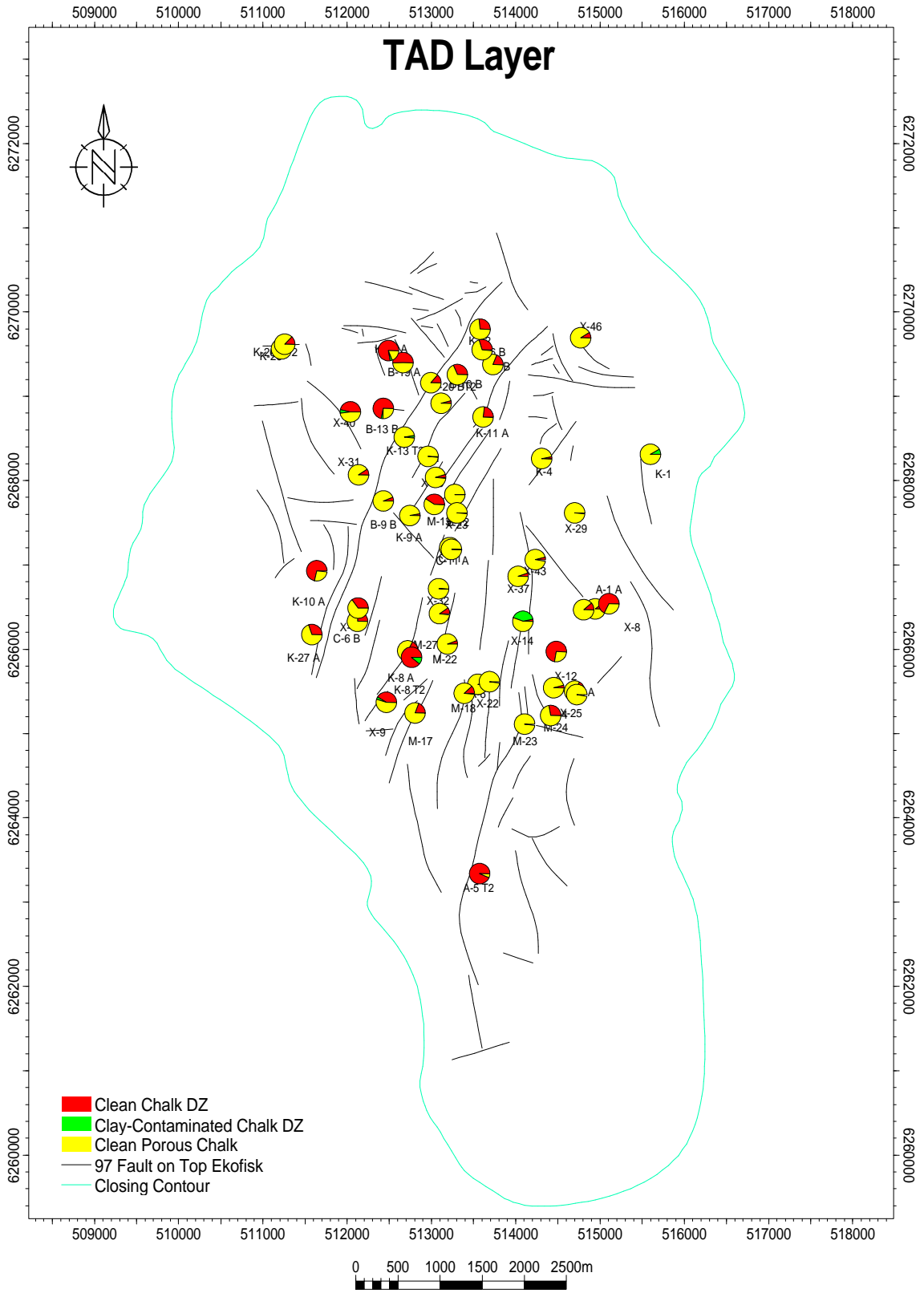
Project: total_ekofisk_well_201112_r1.pet (06/11/2012)





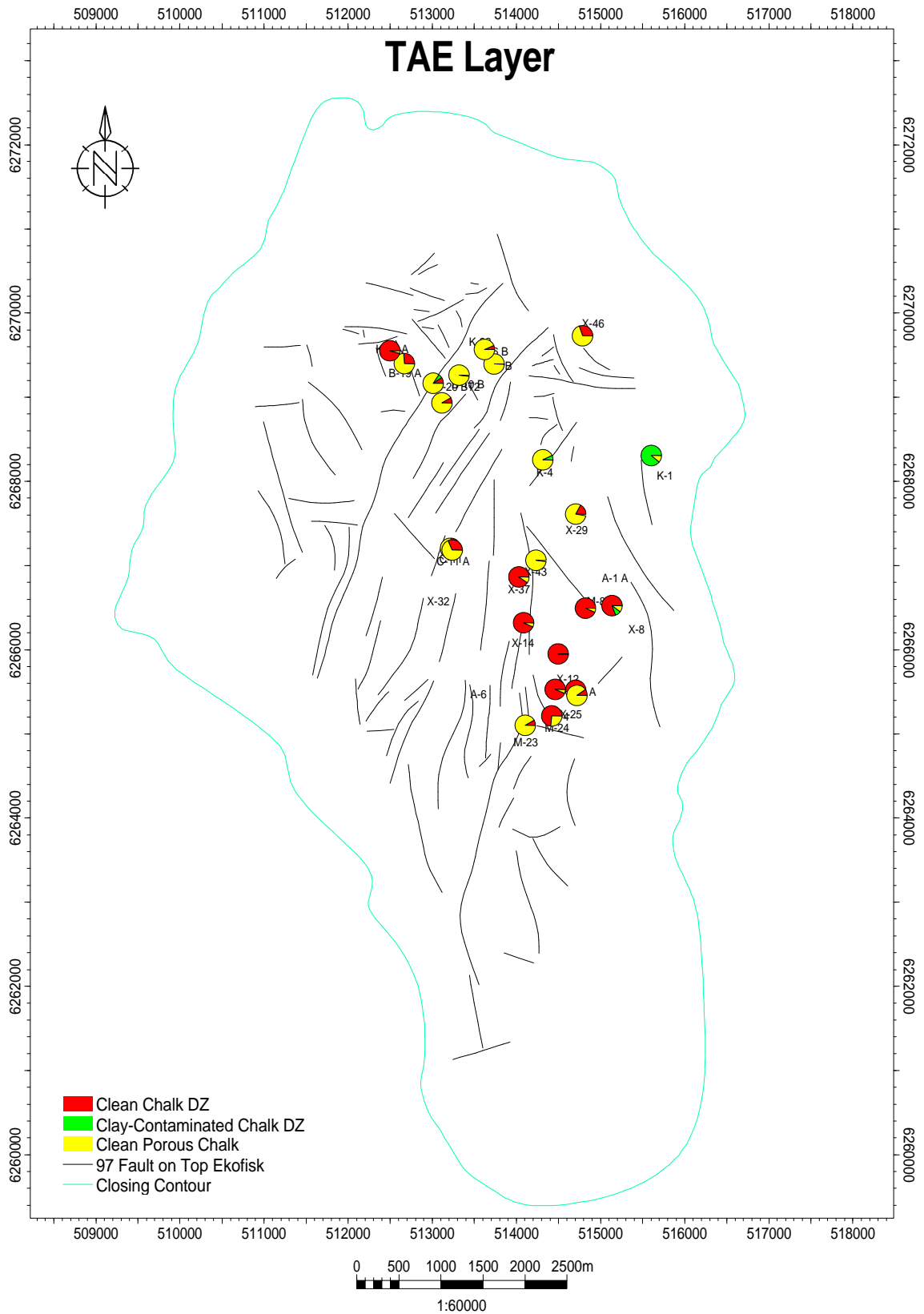
Project: total_ekofisk_well_201112_r1.pet (06/11/2012)





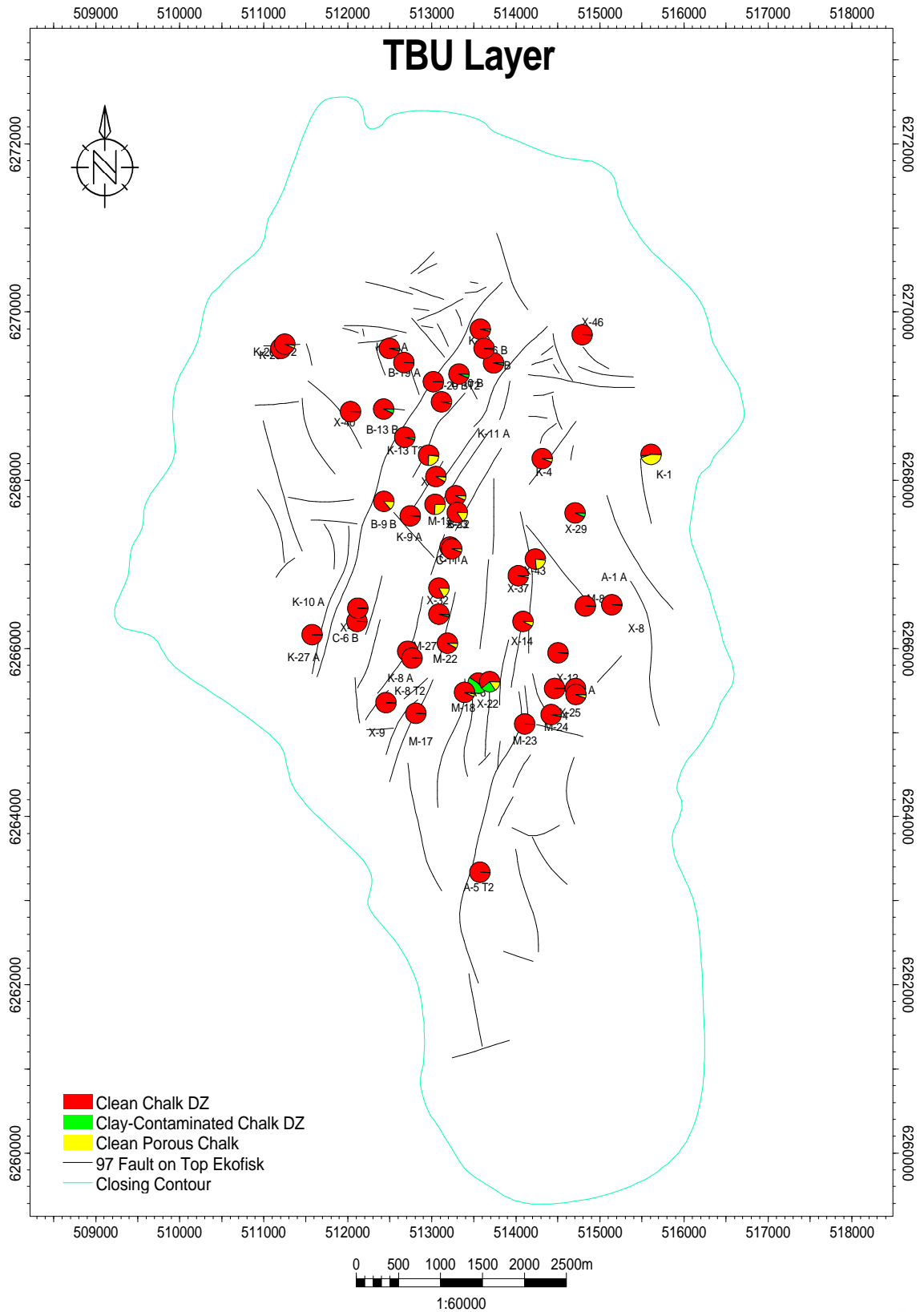
Project: total_ekofisk_well_201112_r1.pet (06/11/2012)





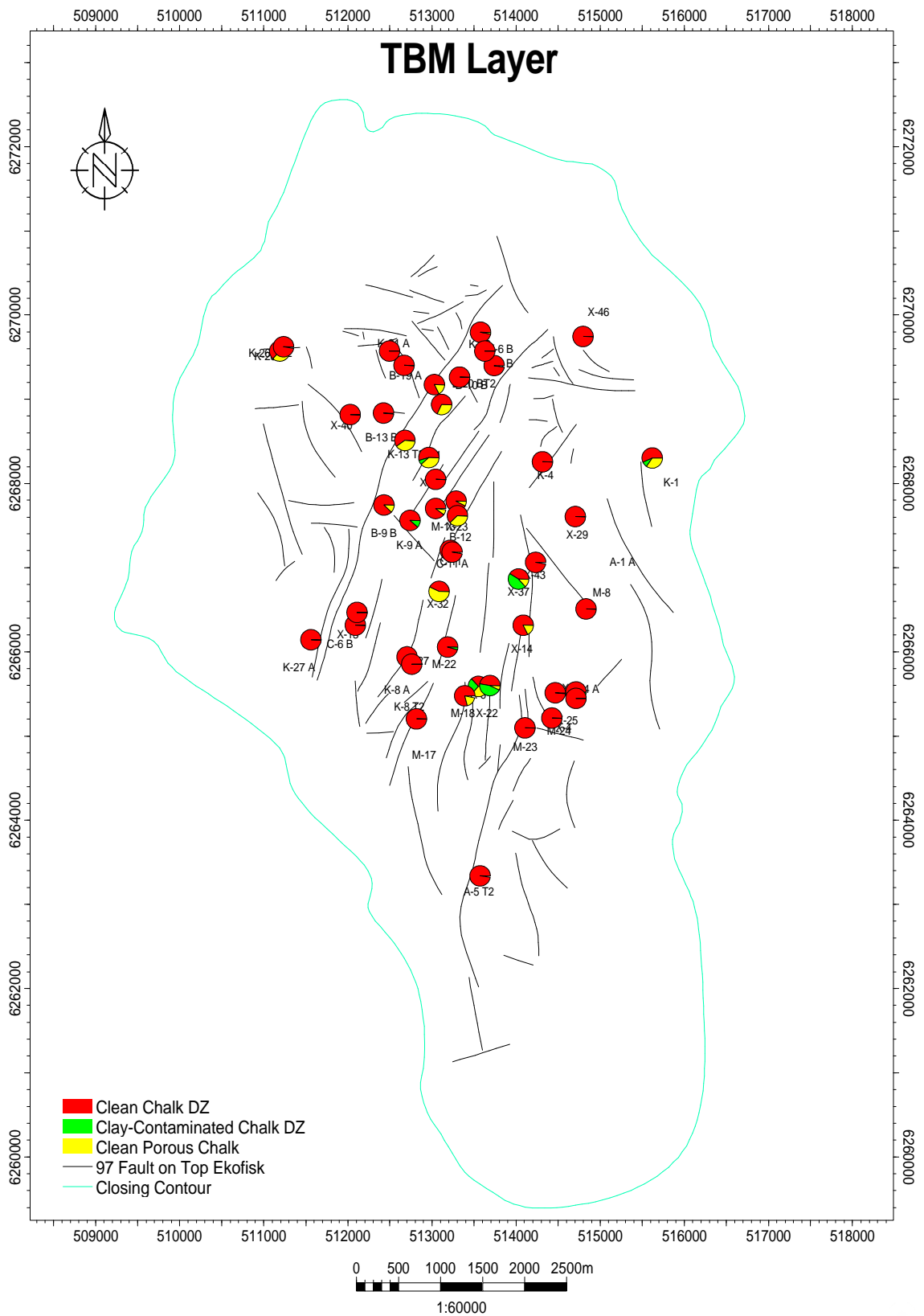
Project: total_ekofisk_well_201112_r1.pet (06/11/2012)





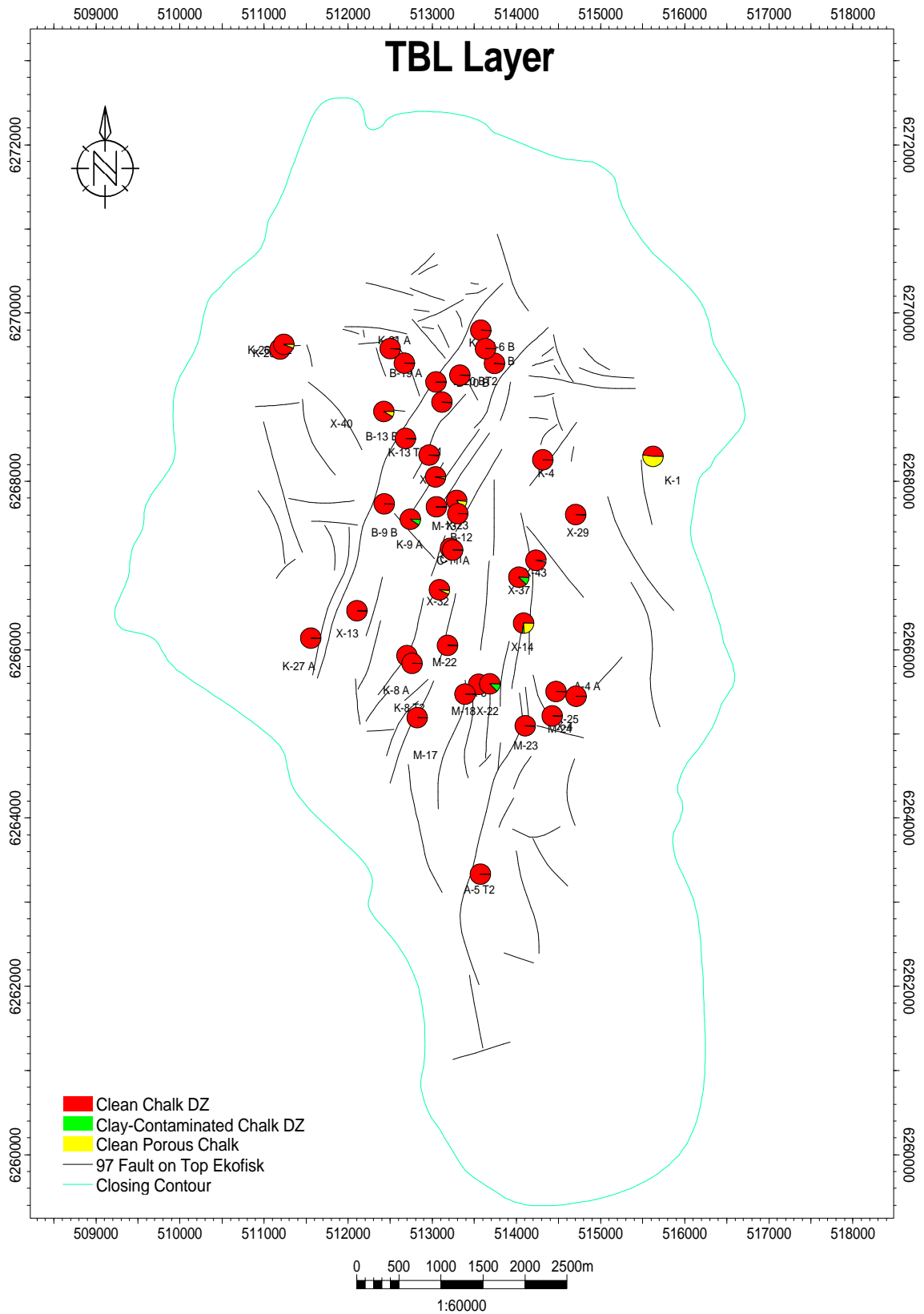
Project: total_ekofisk_well_201112_r1.pet (06/11/2012)





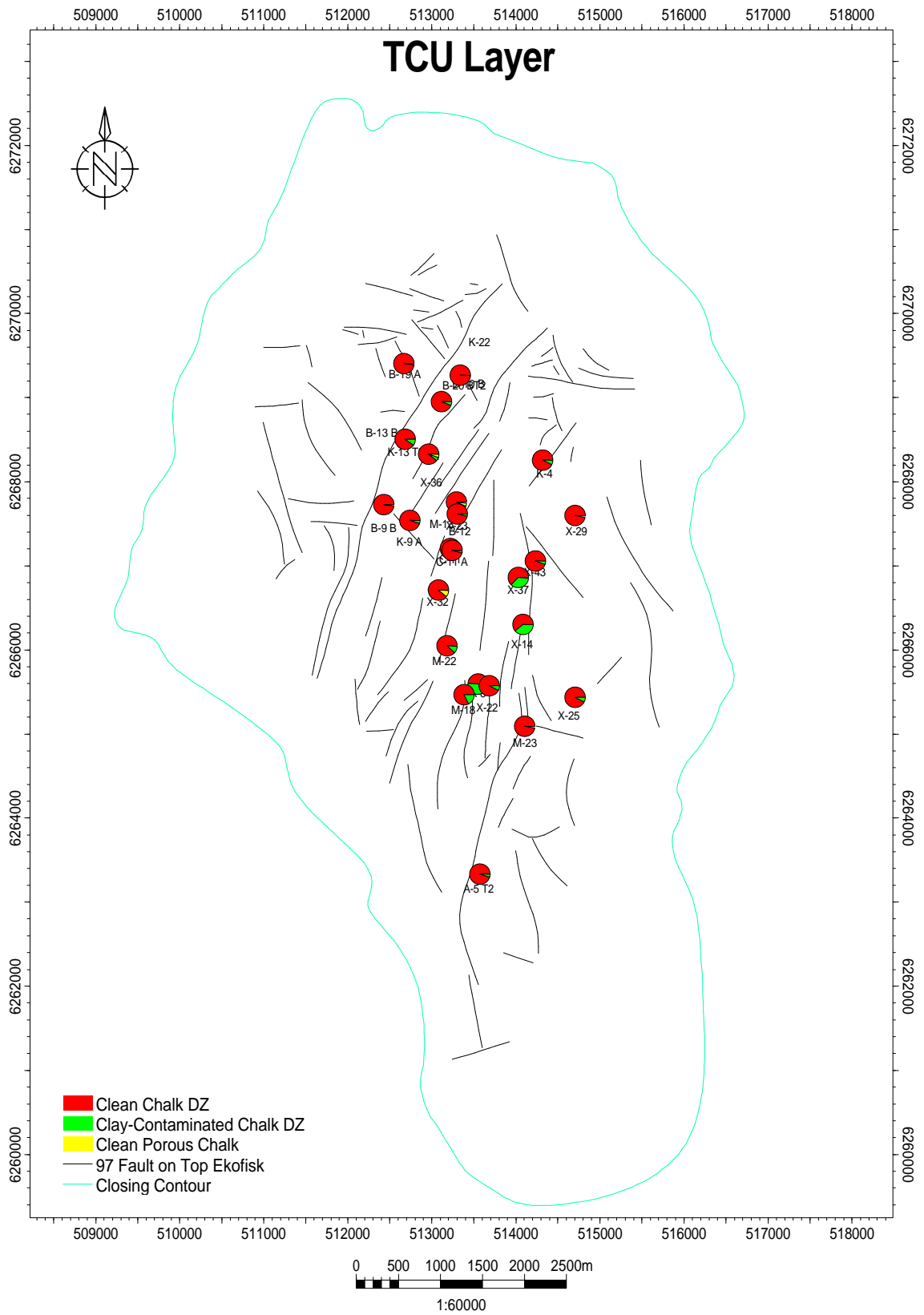
Project: total_ekofisk_well_201112_r1.pet (06/11/2012)





Project: total_ekofisk_well_201112_r1.pet (06/11/2012)

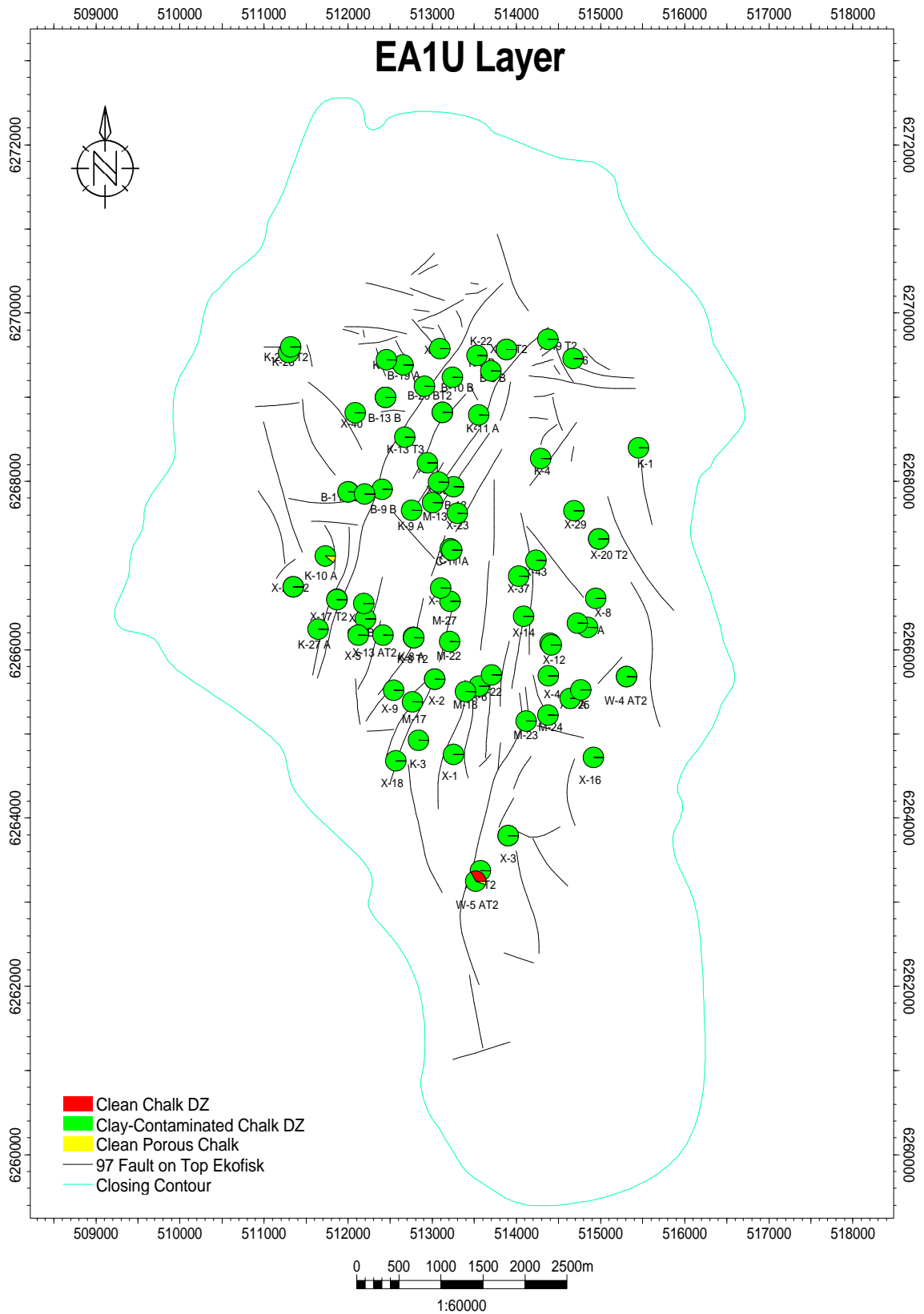




Project: total_ekofisk_well_201112_r1.pet (06/11/2012)

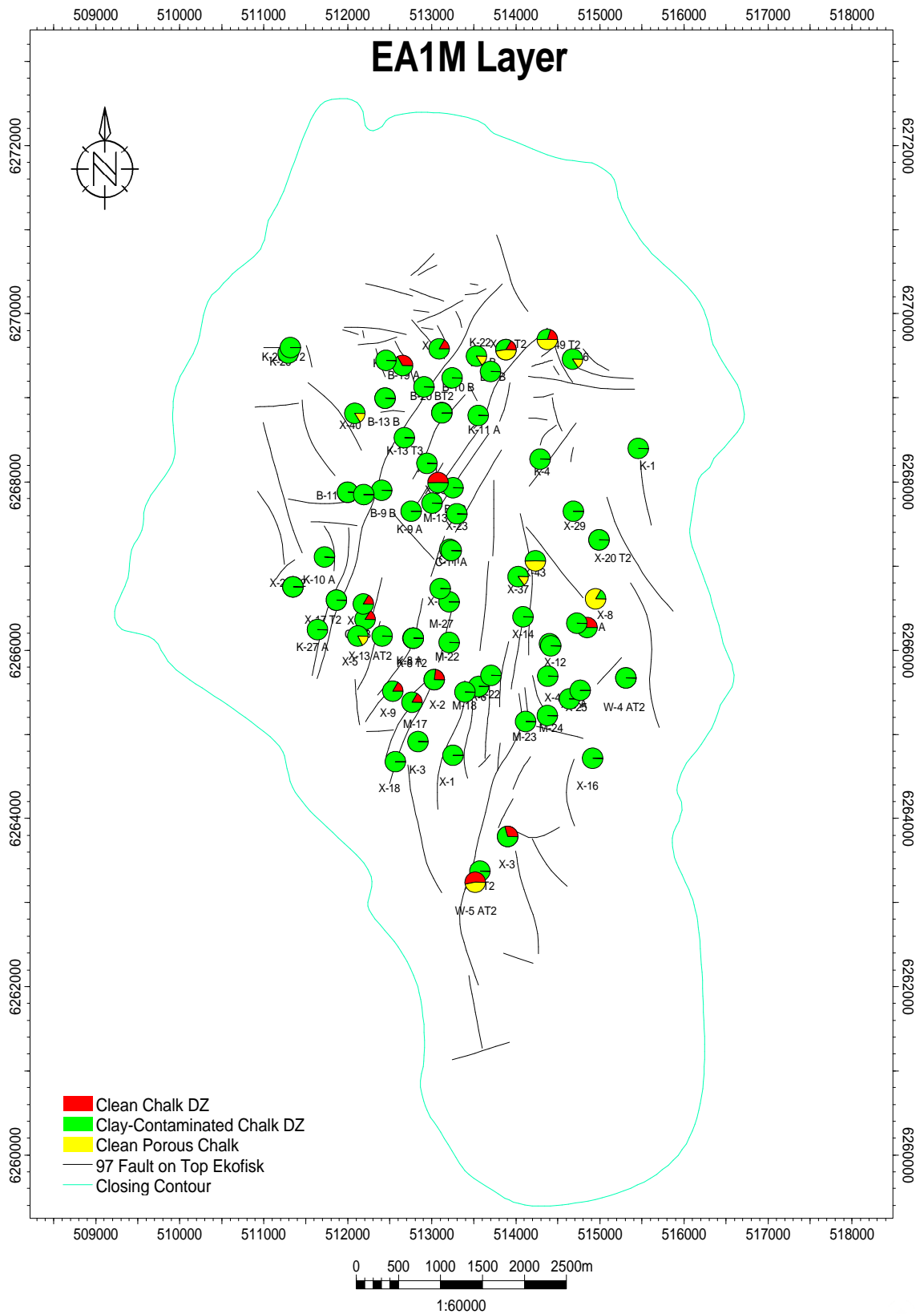


Appendix 4.2.2 Map of facies proportion from 123 model (Upscaled Well log)



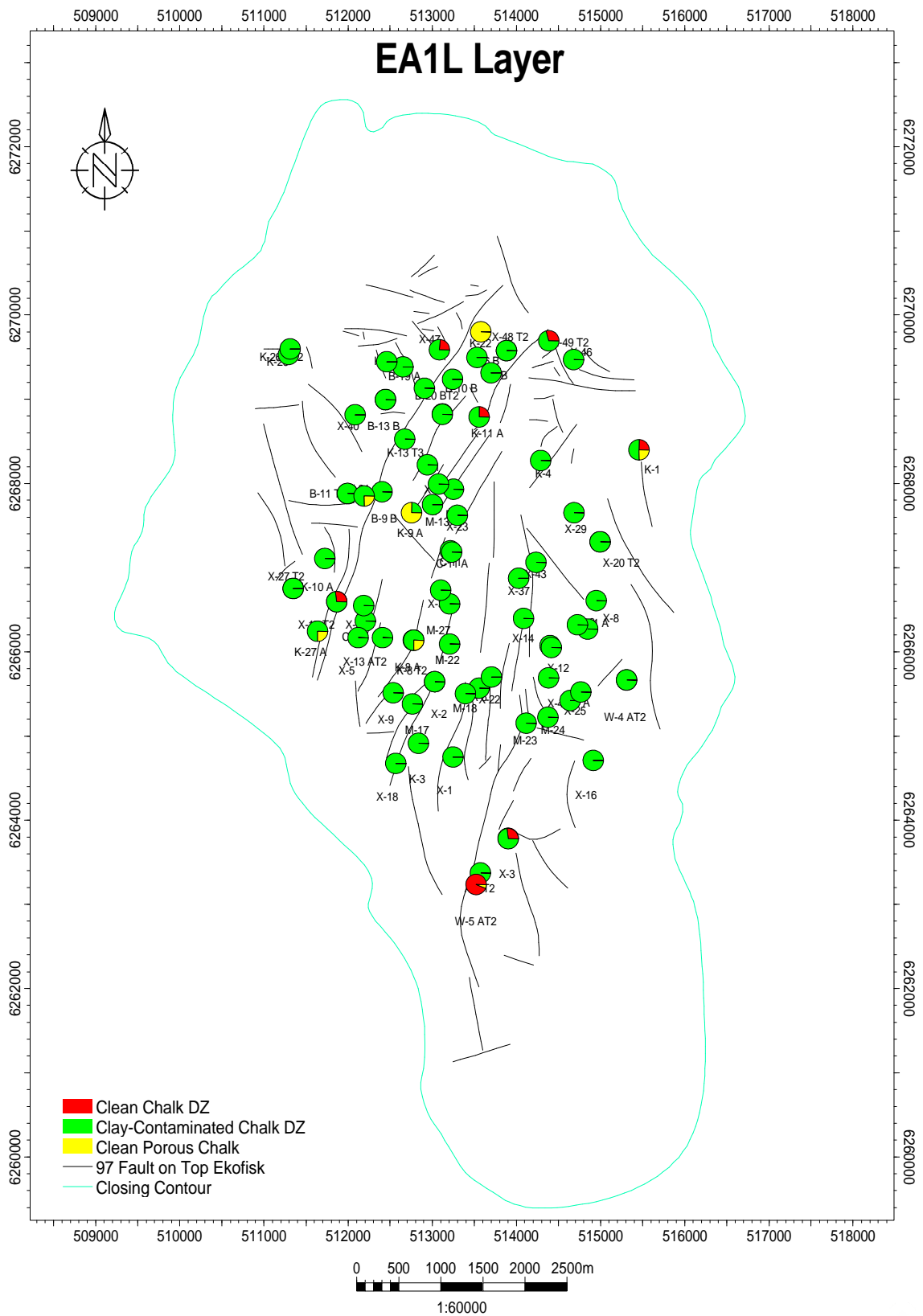
Project: total_ekofisk_well_201112_r1.pet (06/11/2012)





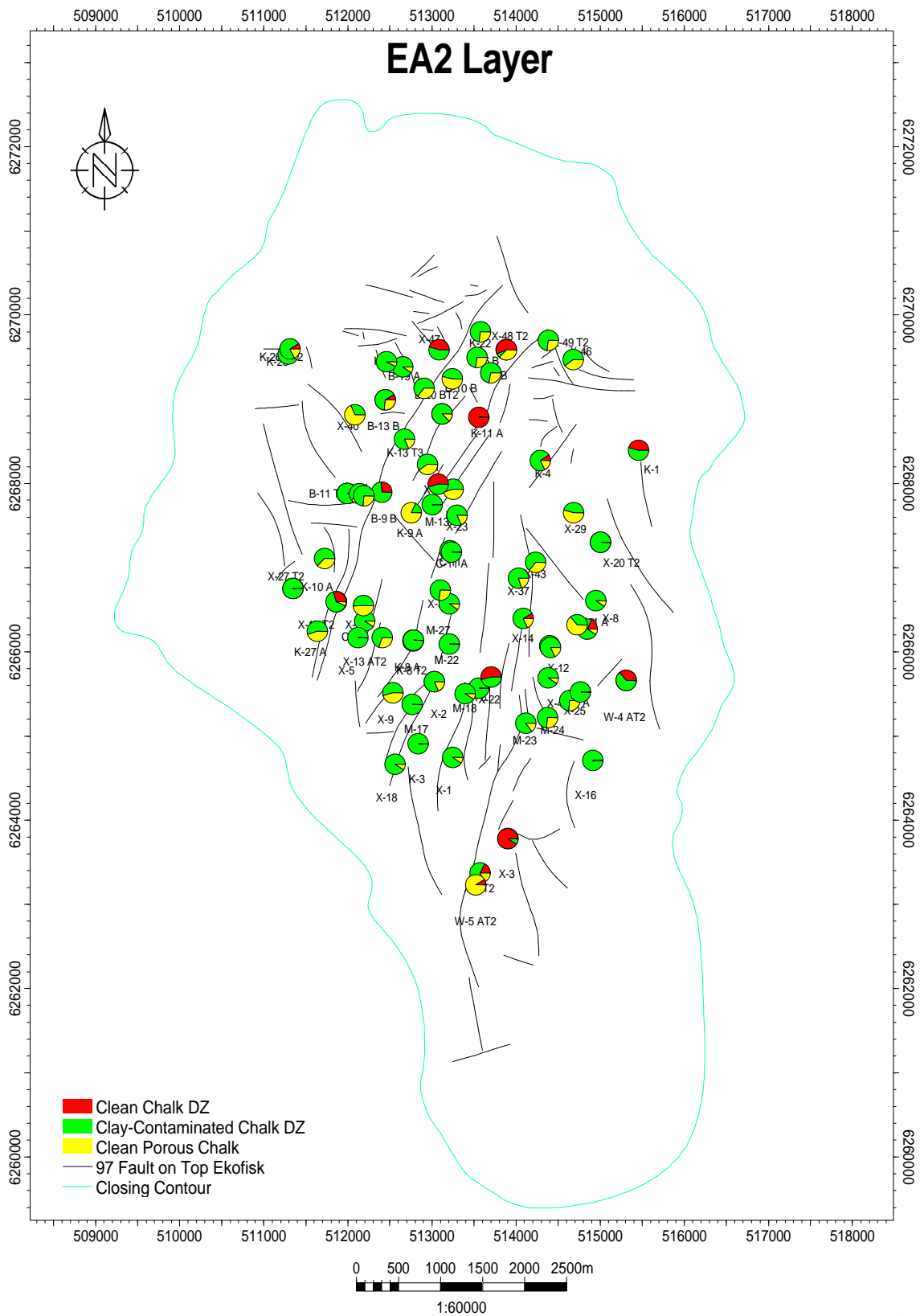
Project: total_ekofisk_well_201112_r1.pet (06/11/2012)





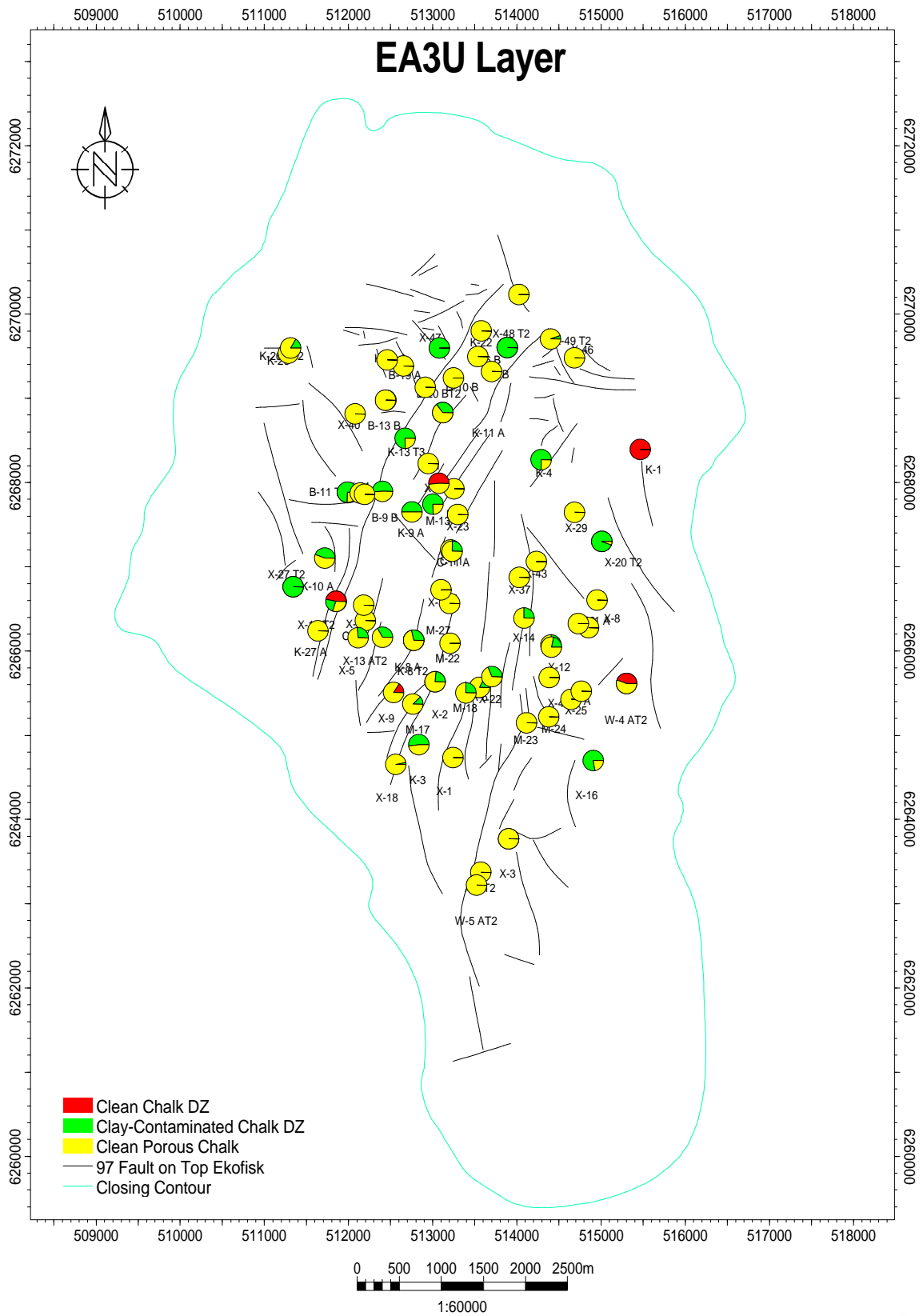
Project: total_ekofisk_well_201112_r1.pet (06/11/2012)





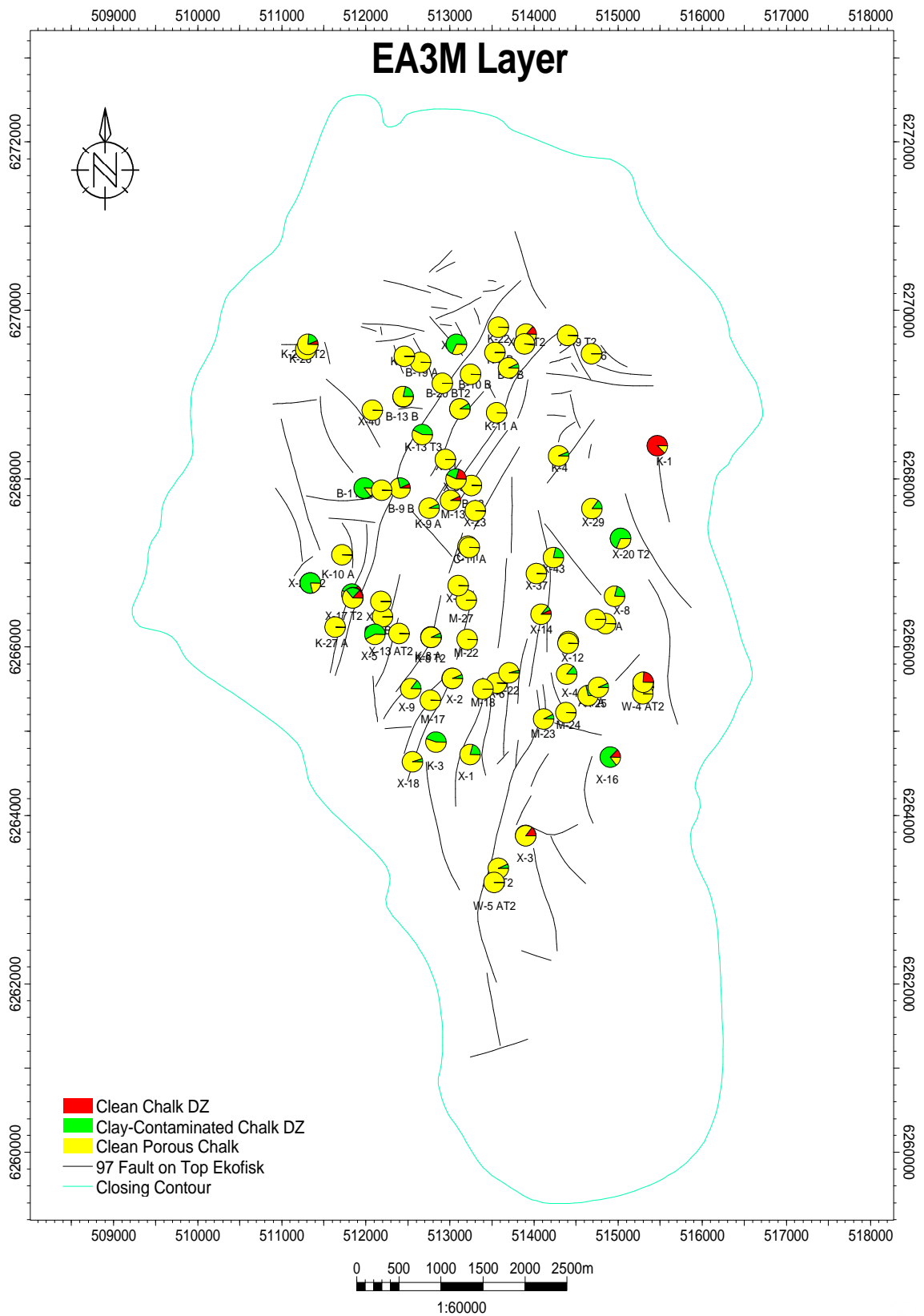
Project: total_ekofisk_well_201112_r1.pet (06/11/2012)





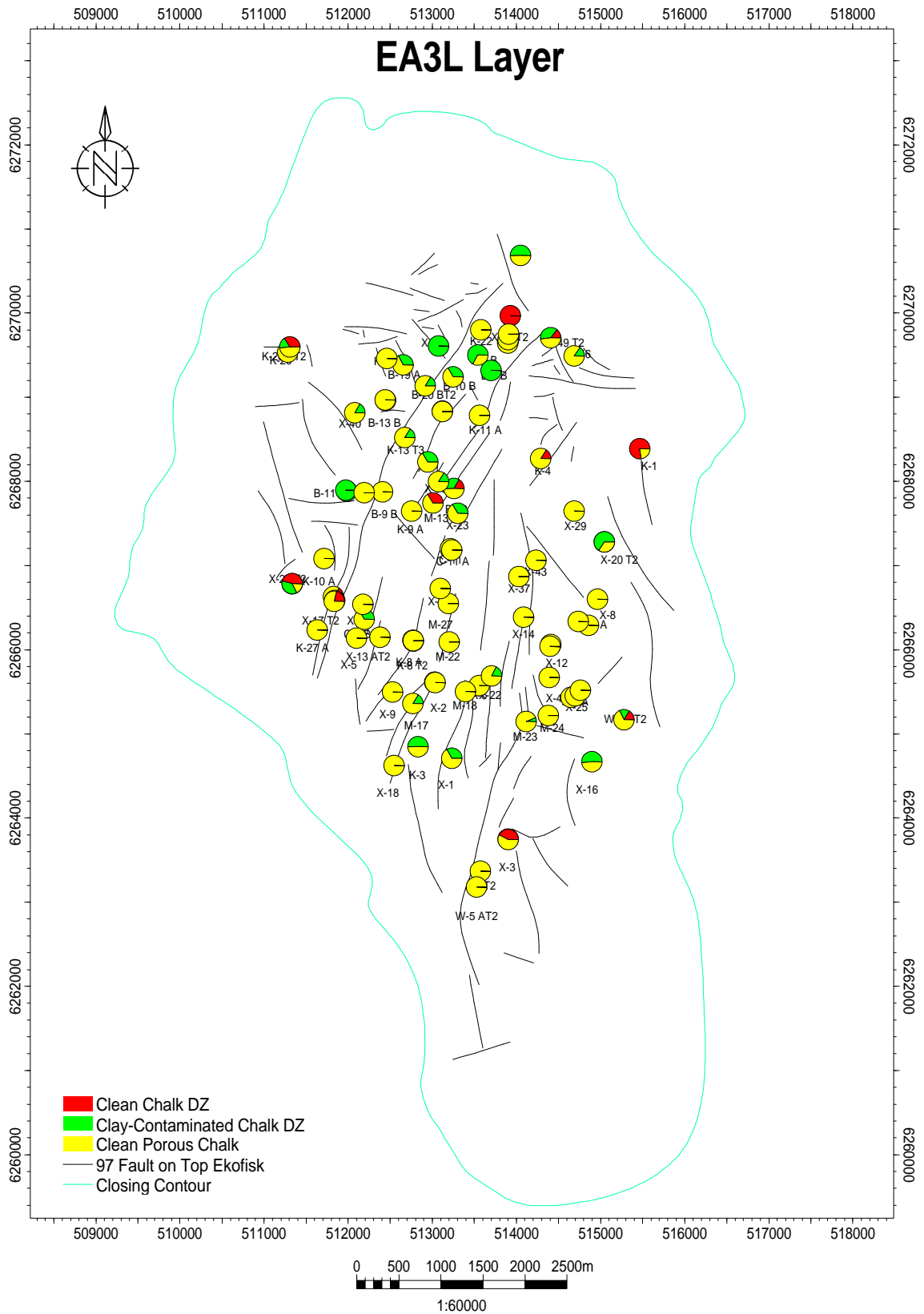
Project: total_ekofisk_well_201112_r1.pet (06/11/2012)





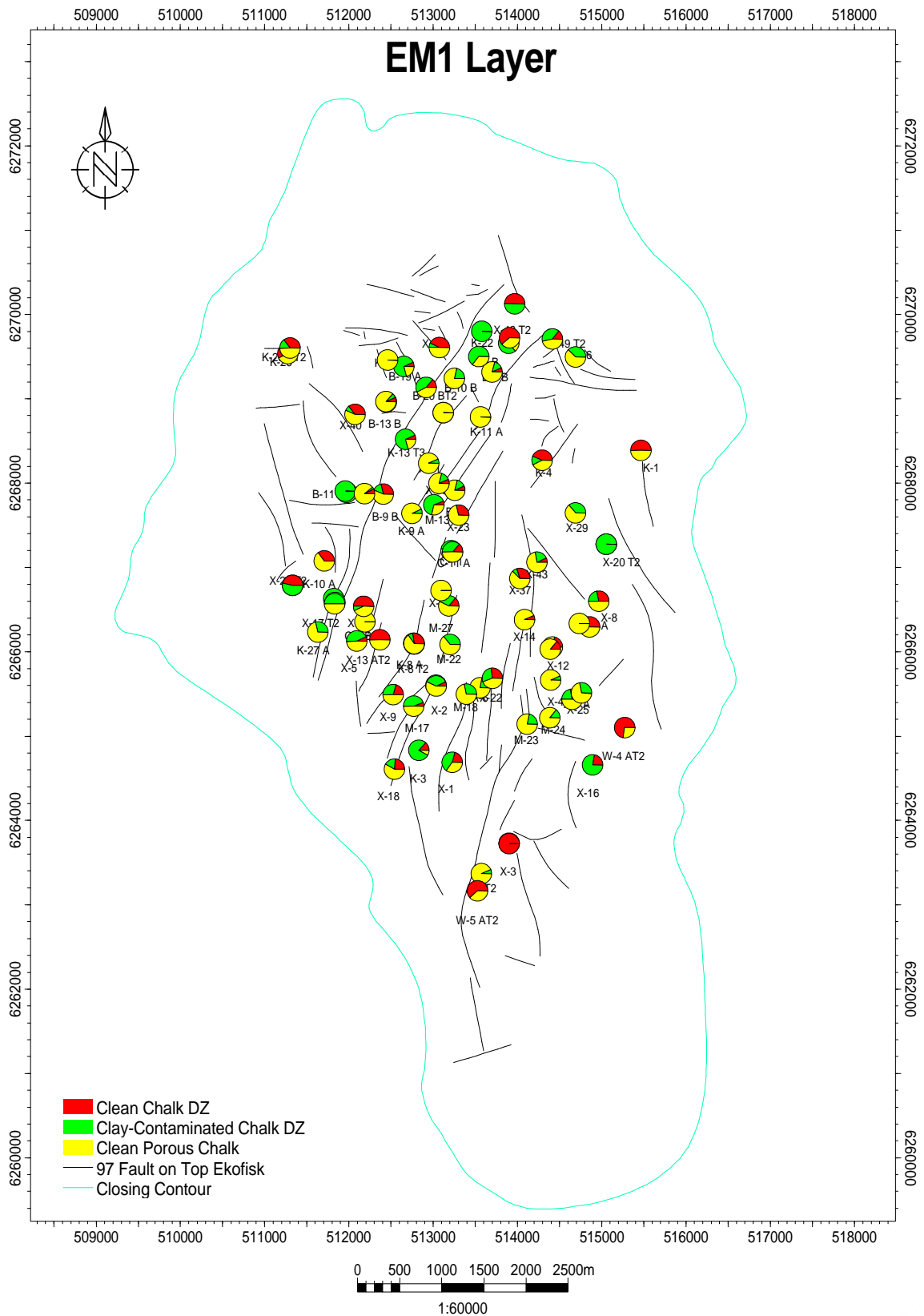
Project: total_ekofisk_well_201112_r1.pet (06/11/2012)





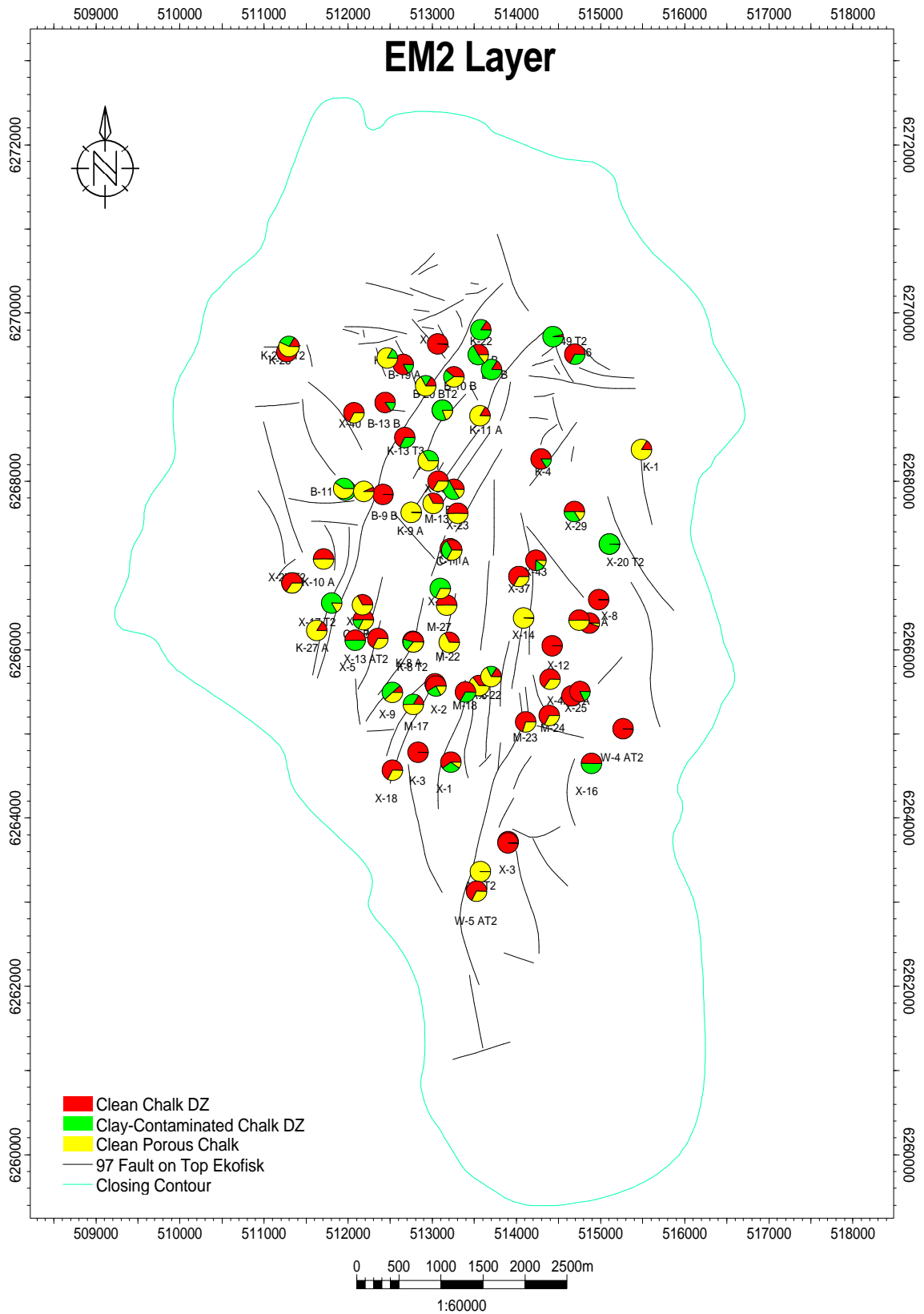
Project: total_ekofisk_well_201112_r1.pet (06/11/2012)





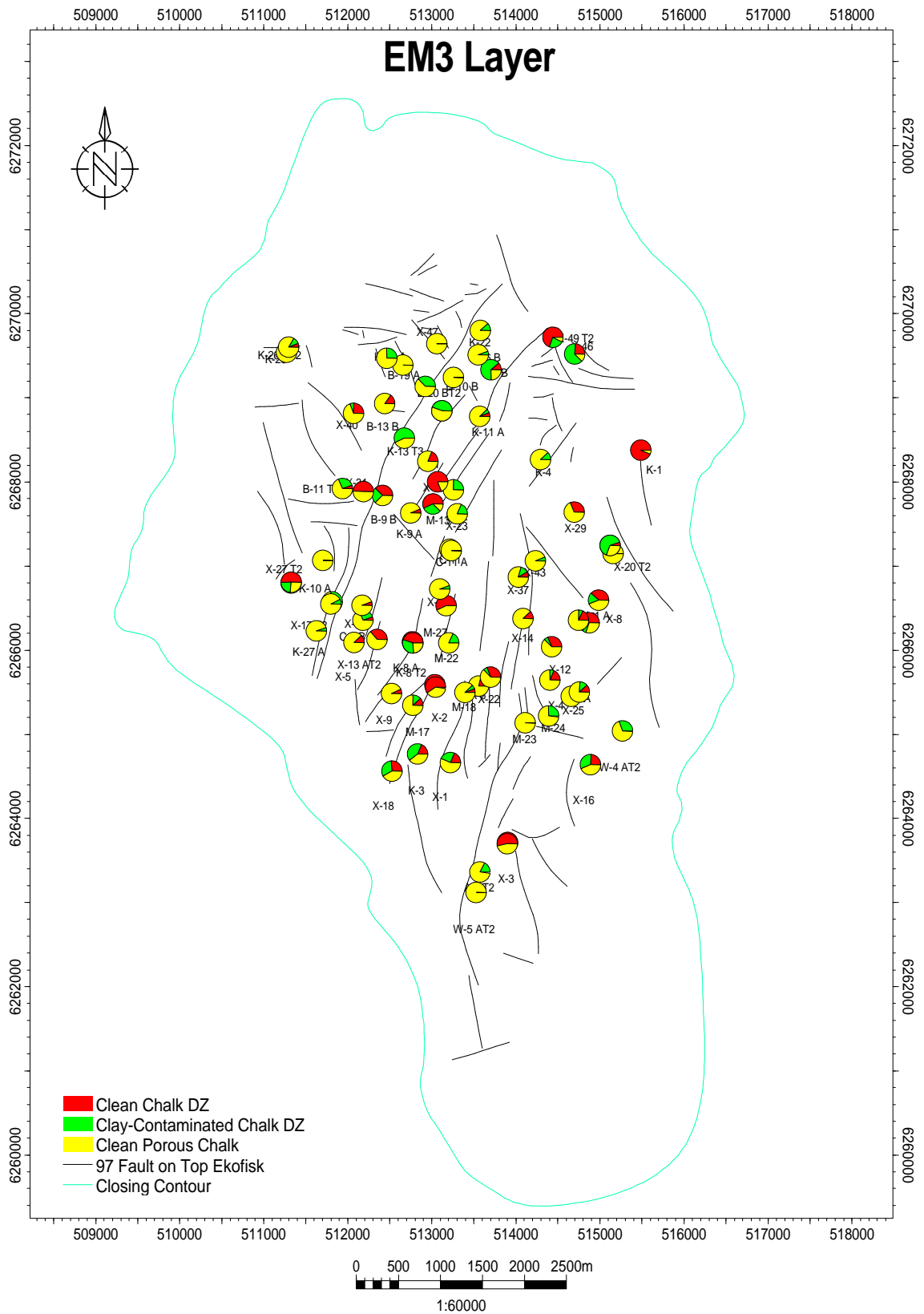
Project: total_ekofisk_well_201112_r1.pet (06/11/2012)





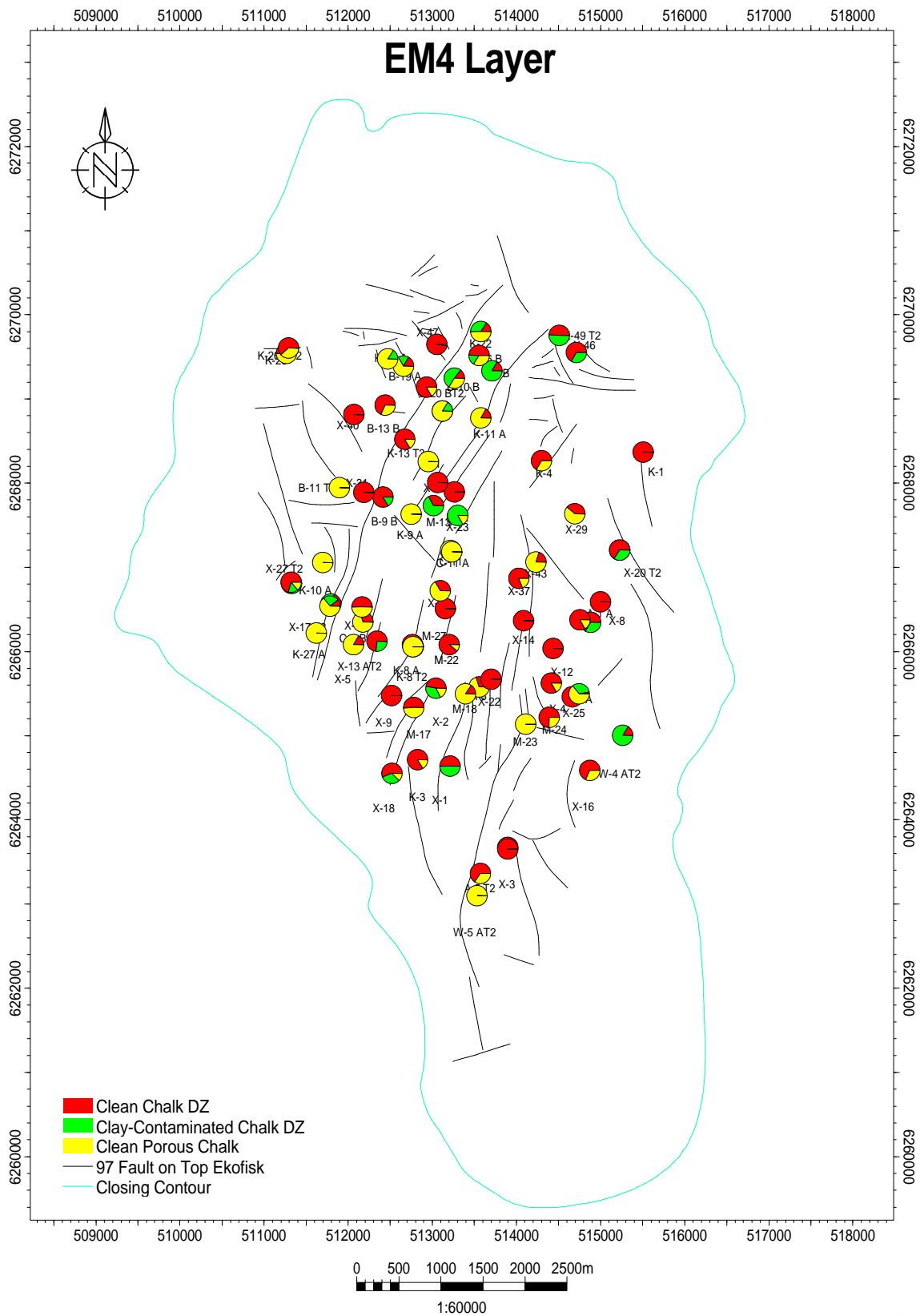
Project: total_ekofisk_well_201112_r1.pet (06/11/2012)





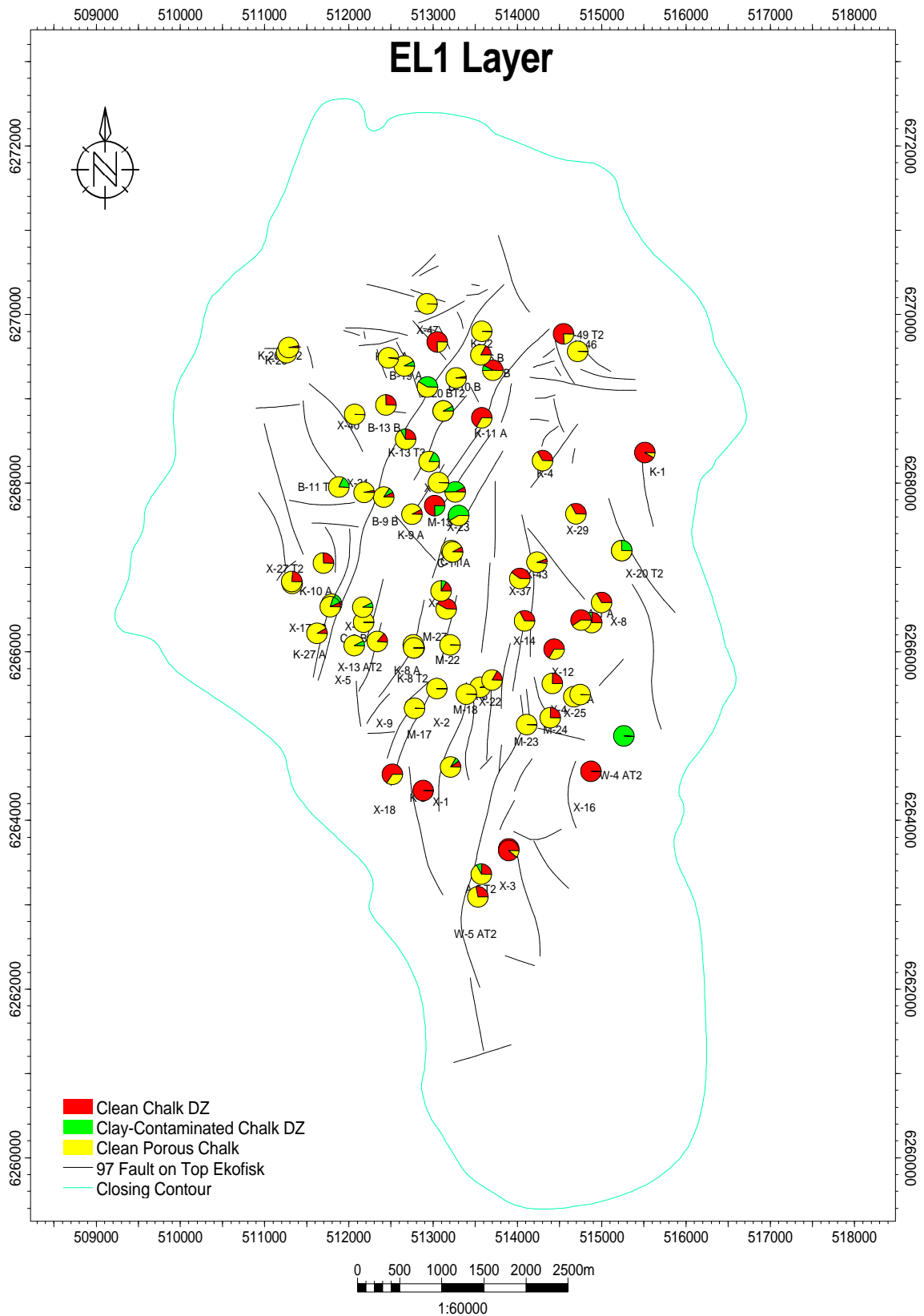
Project: total_ekofisk_well_201112_r1.pet (06/11/2012)





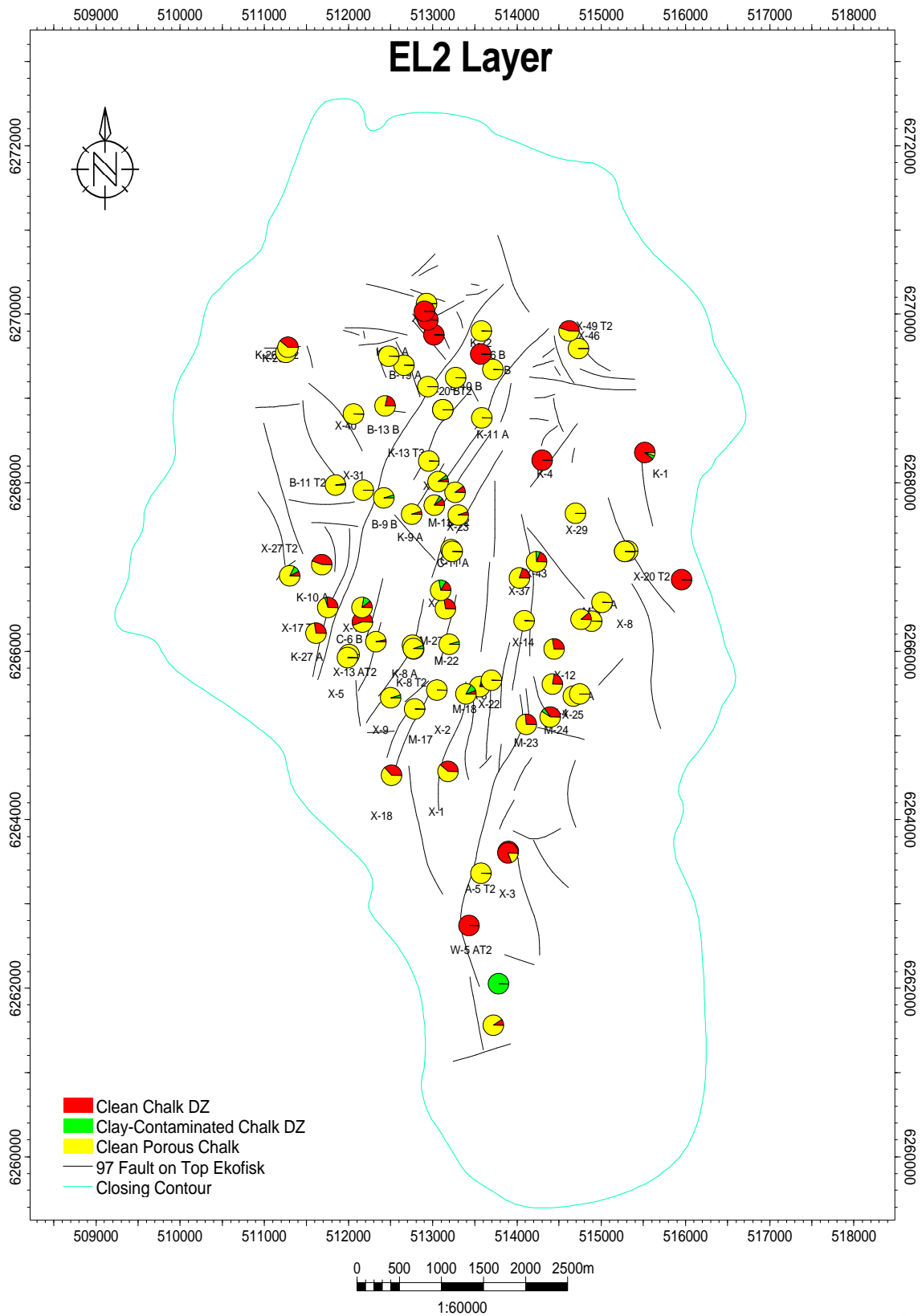
Project: total_ekofisk_well_201112_r1.pet (06/11/2012)





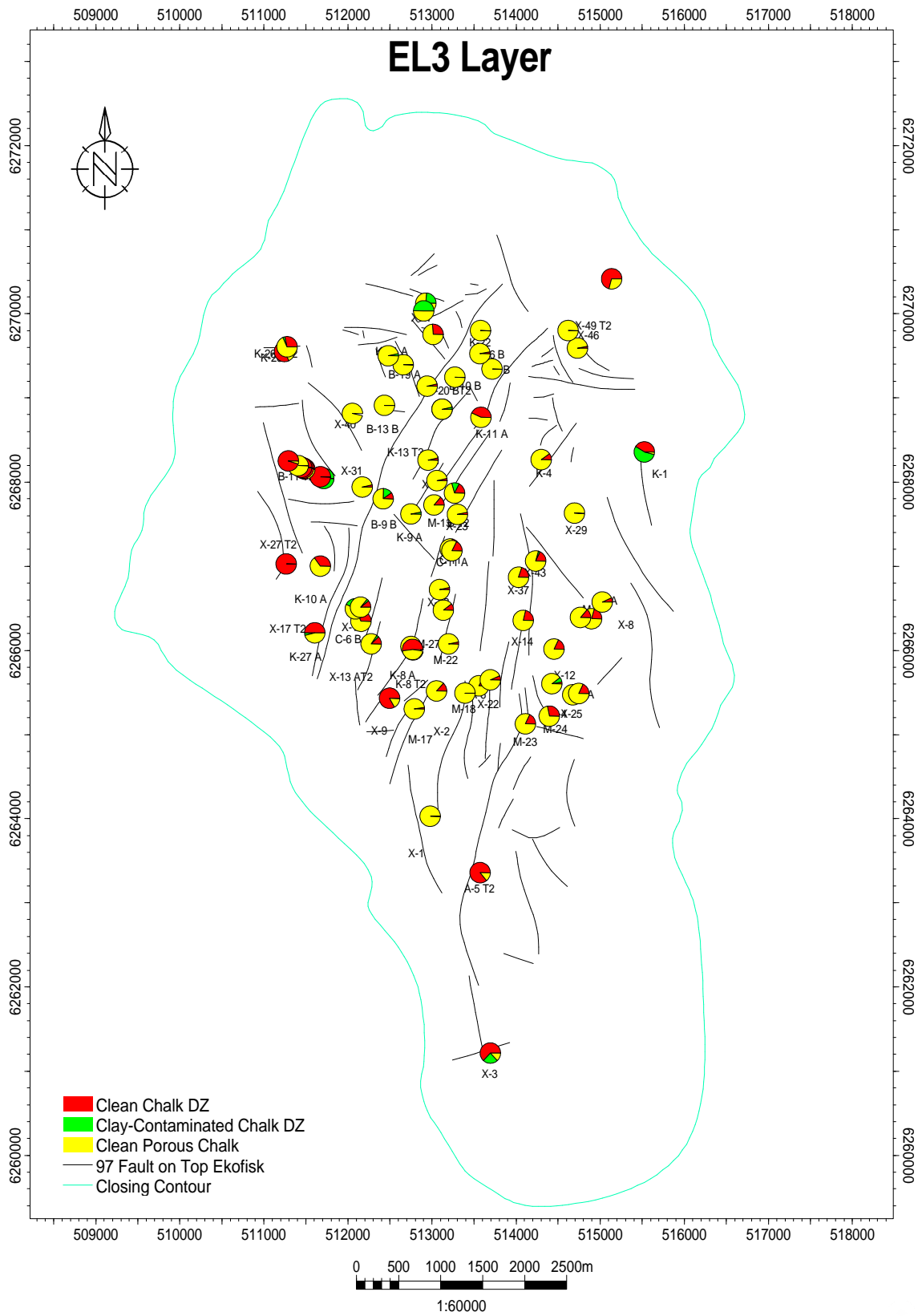
Project: total_ekofisk_well_201112_r1.pet (06/11/2012)

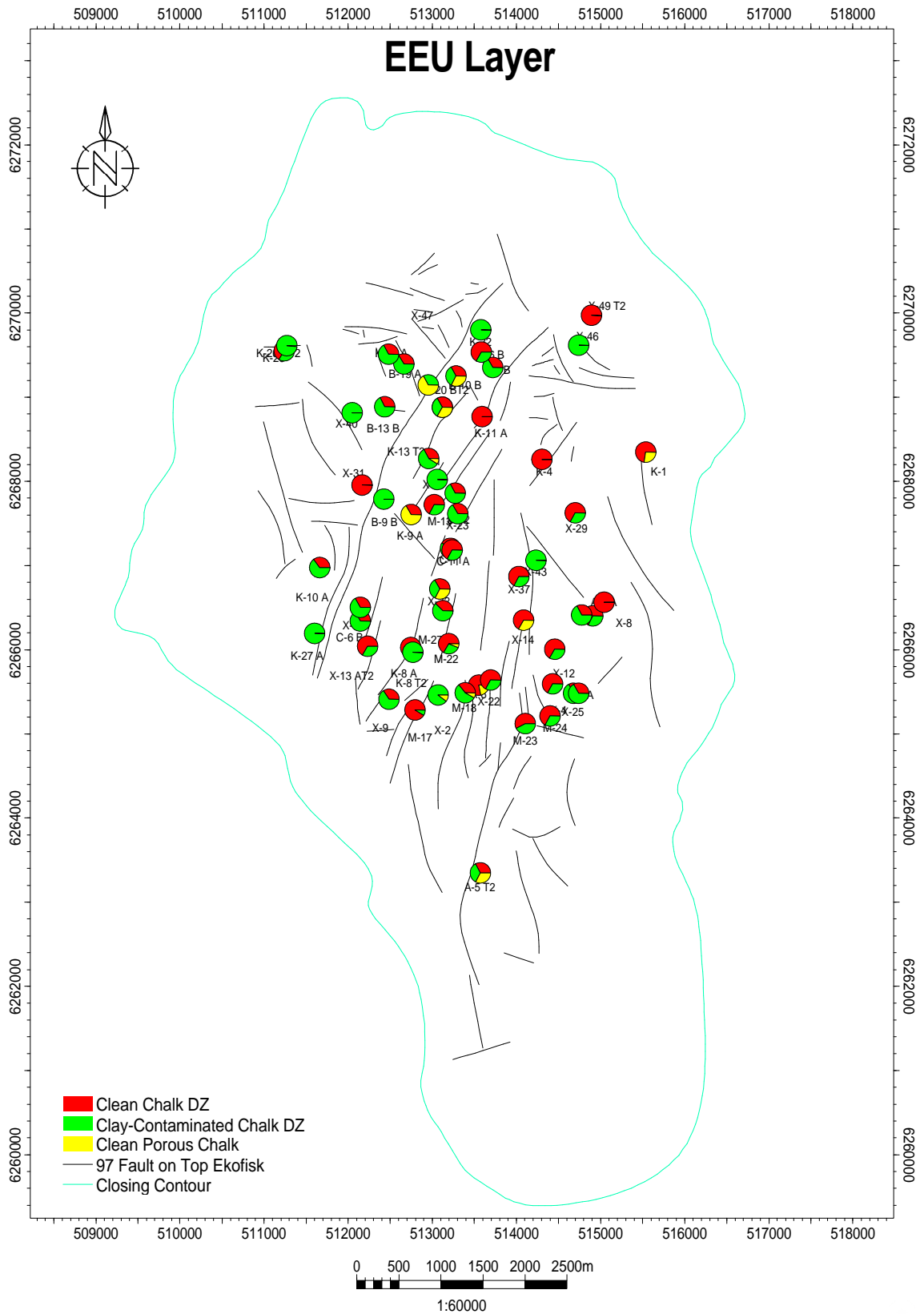




Project: total_ekofisk_well_201112_r1.pet (06/11/2012)

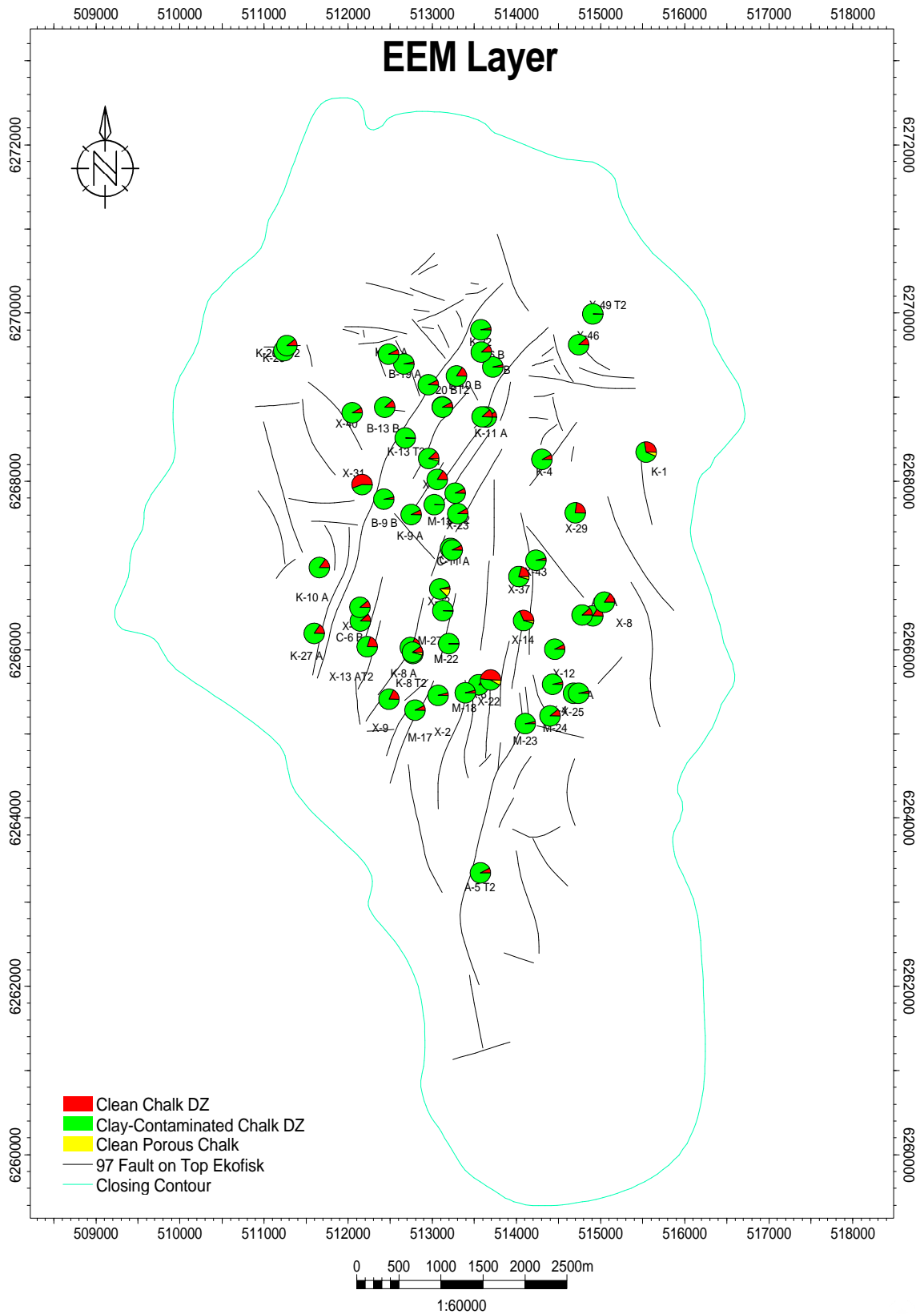






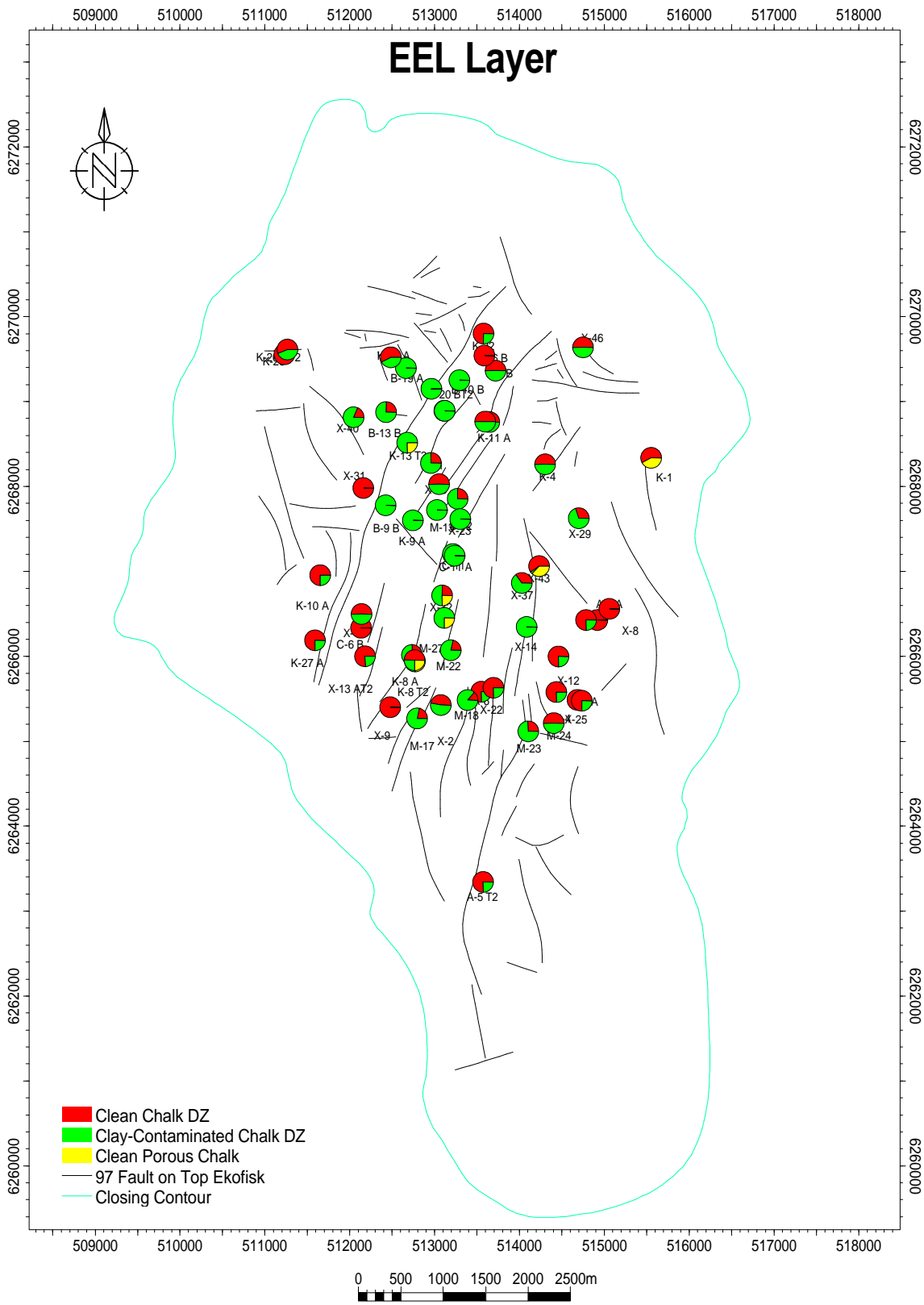
Project: total_ekofisk_well_201112_r1.pet (06/11/2012)





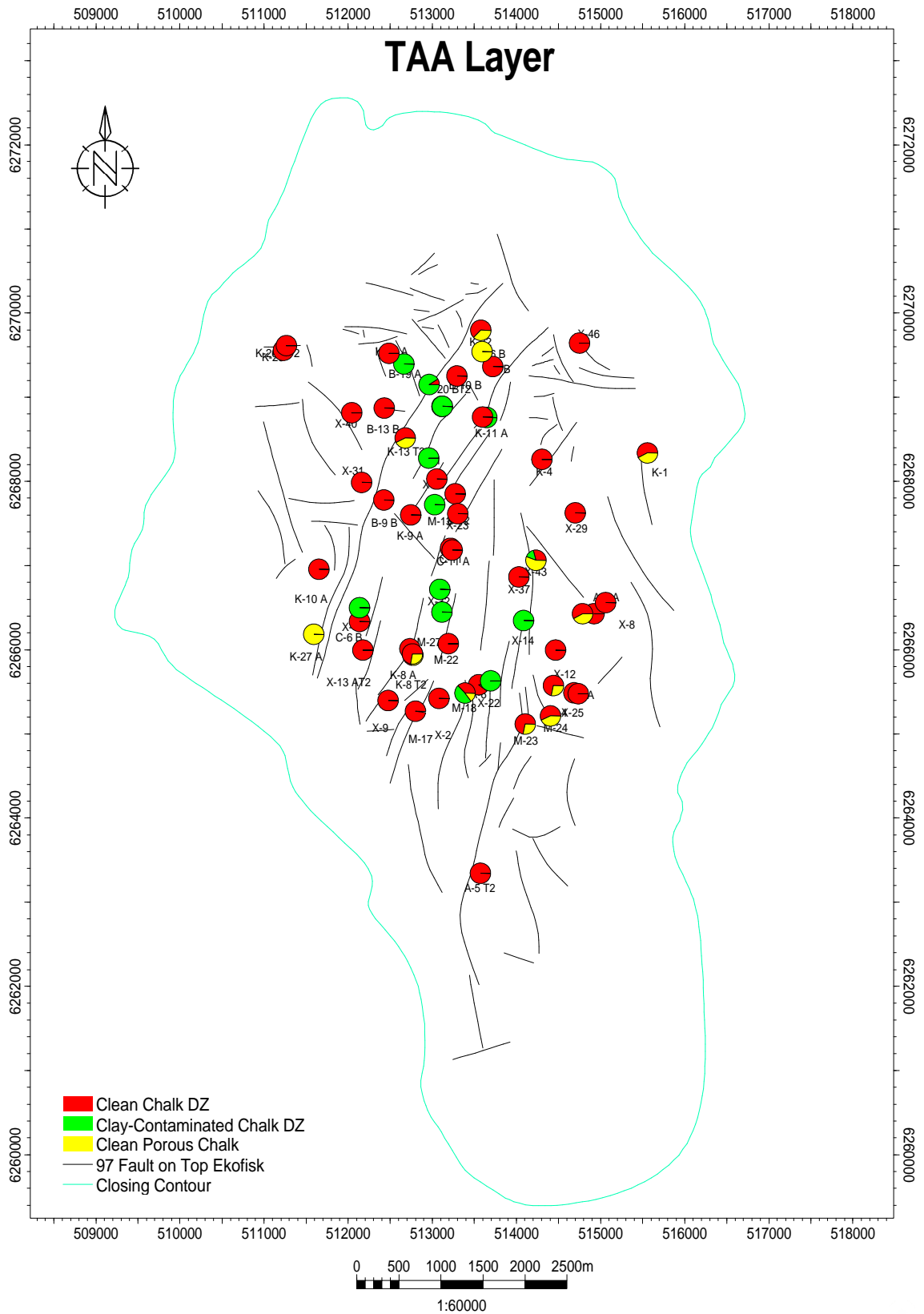
Project: total_ekofisk_well_201112_r1.pet (06/11/2012)

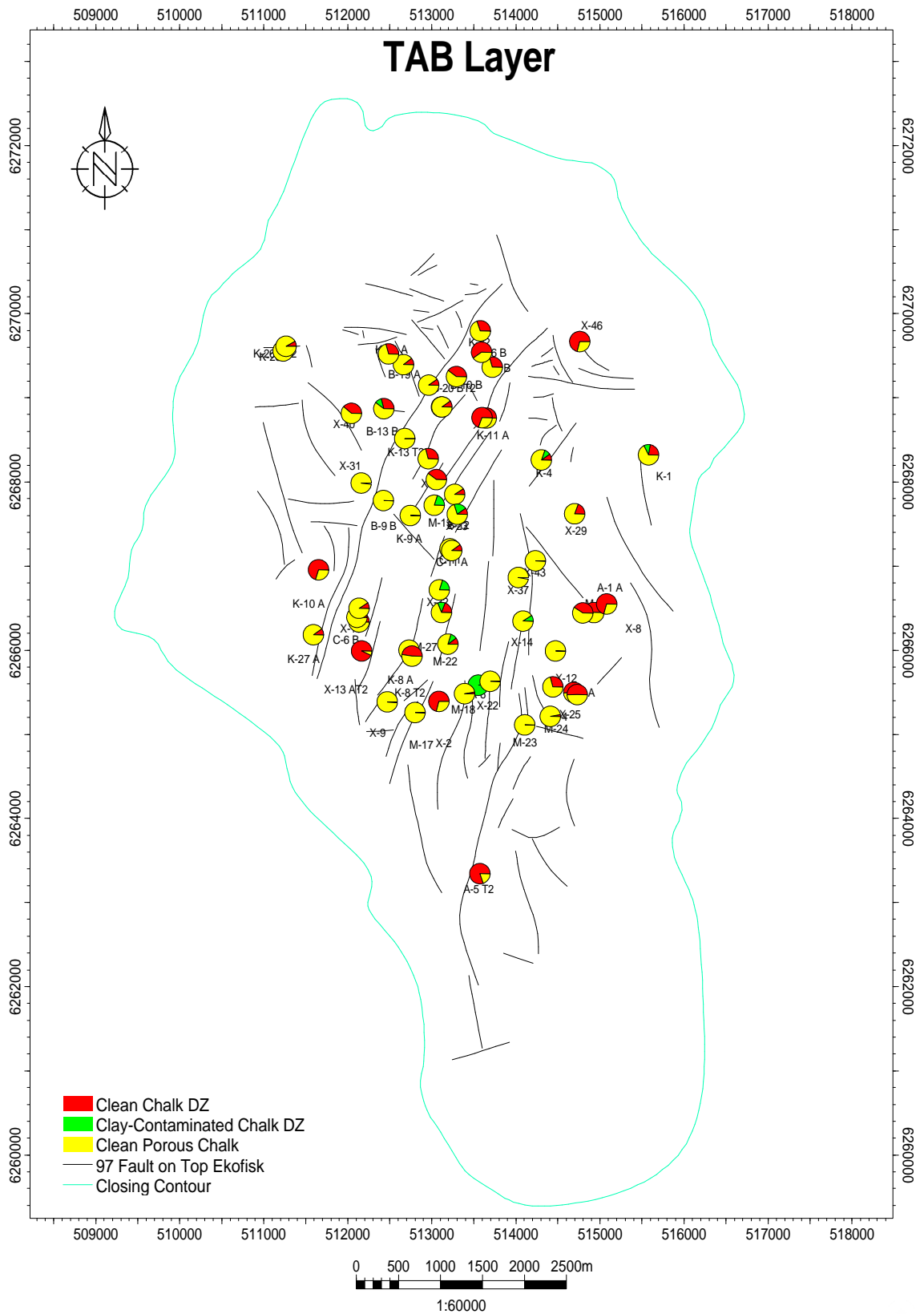




Project: total_ekofisk_well_201112_r1.pet (06/11/2012)

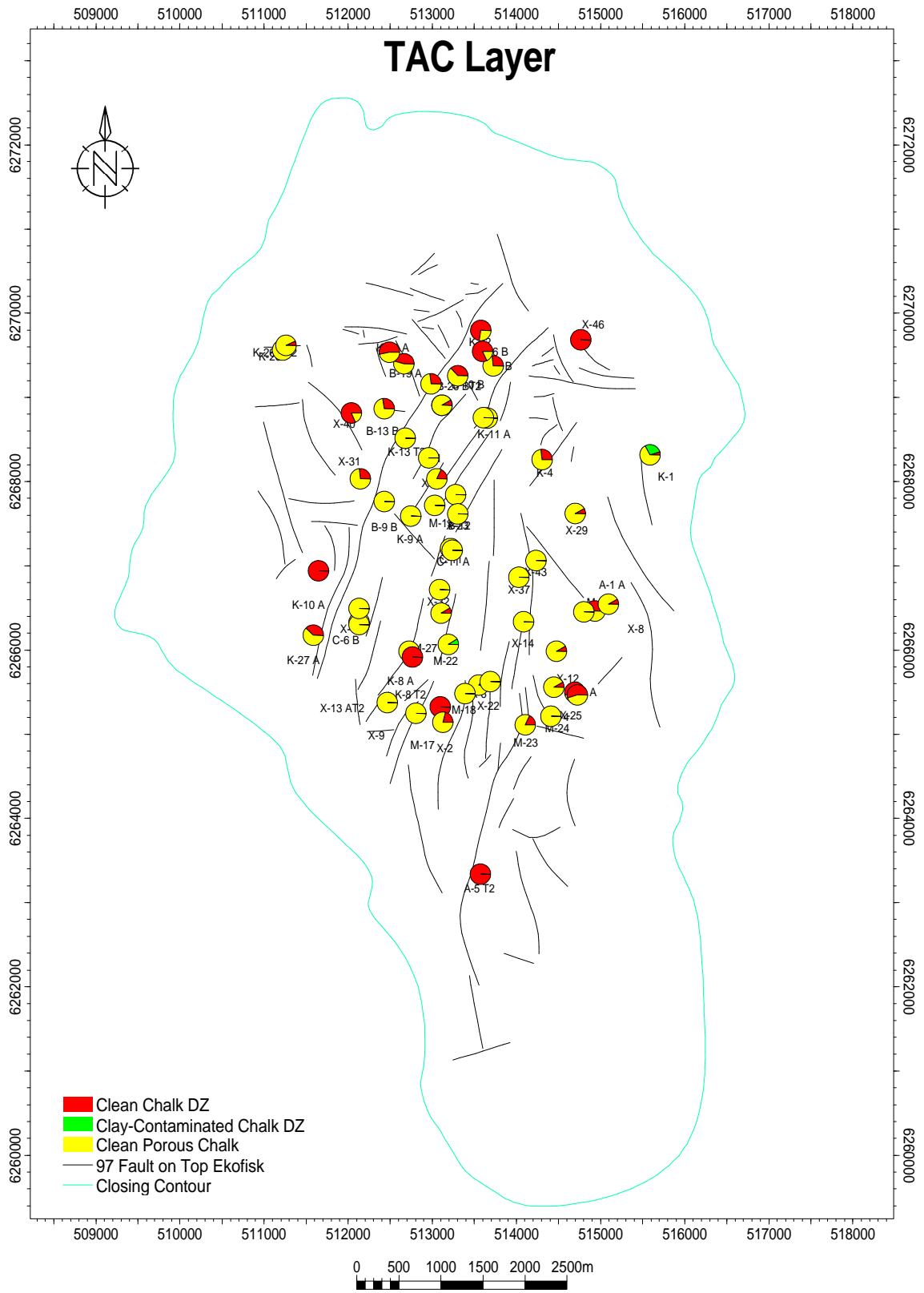






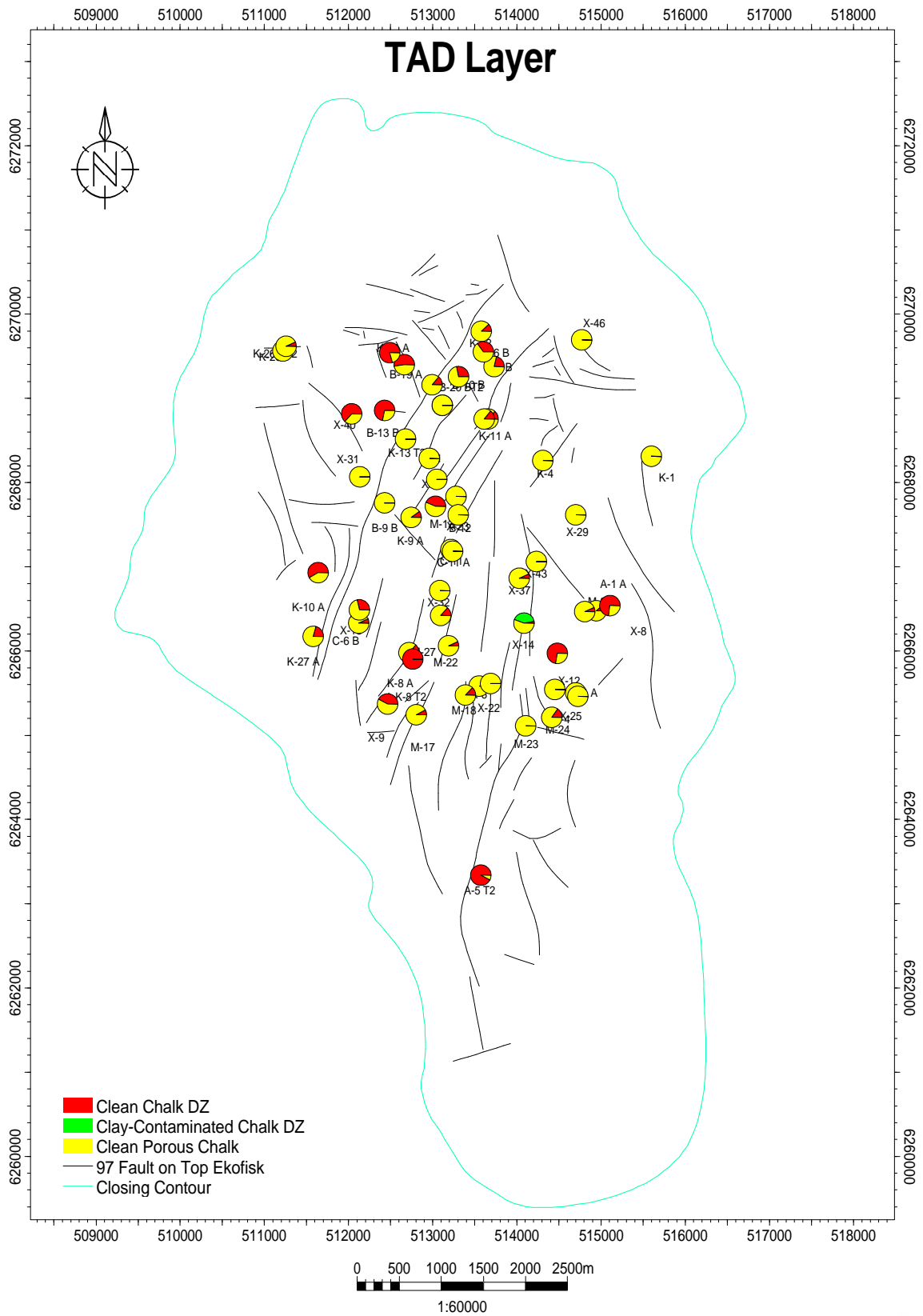
Project: total_ekofisk_well_201112_r1.pet (06/11/2012)





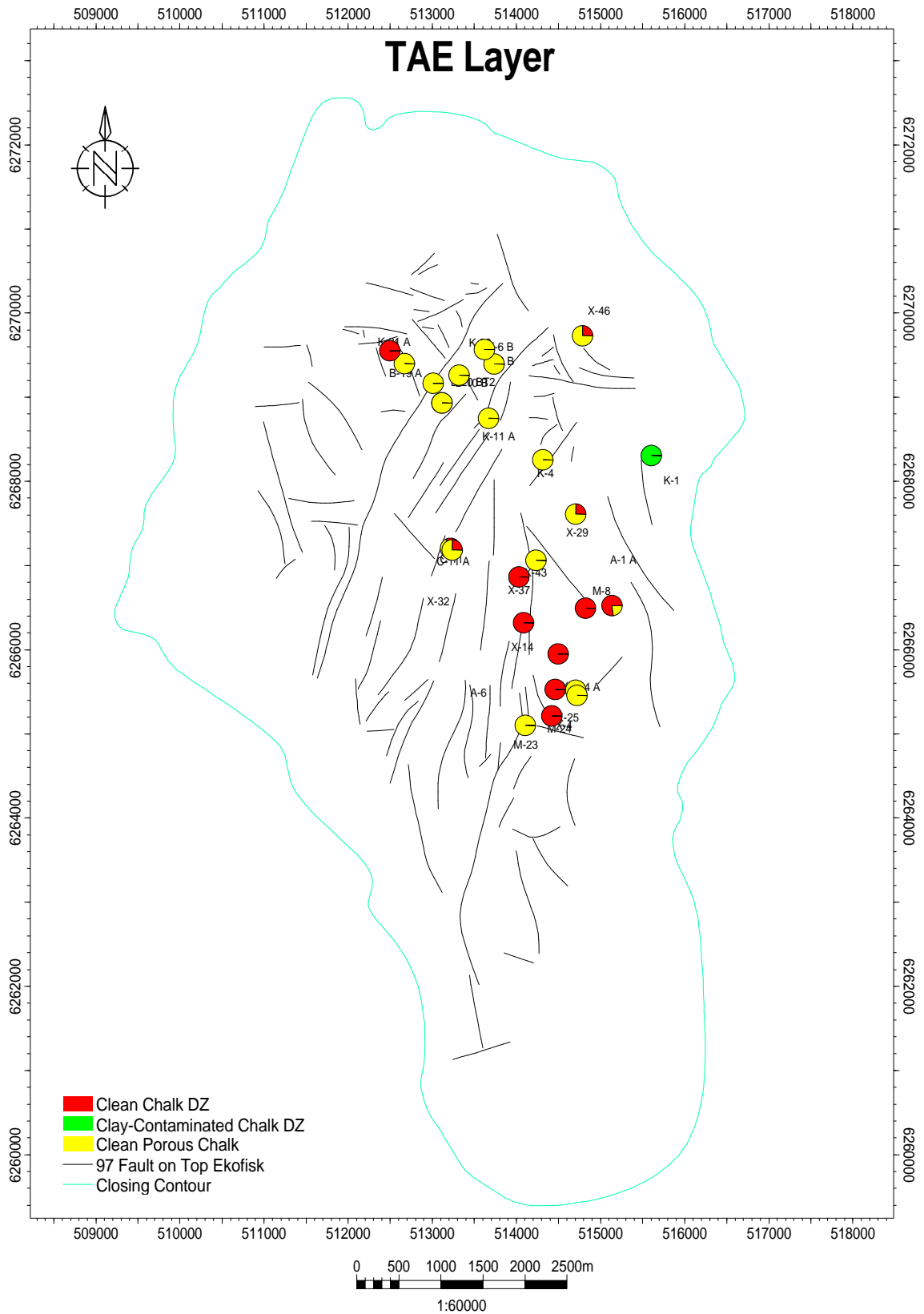
Project: total_ekofisk_well_201112_r1.pet (06/11/2012)





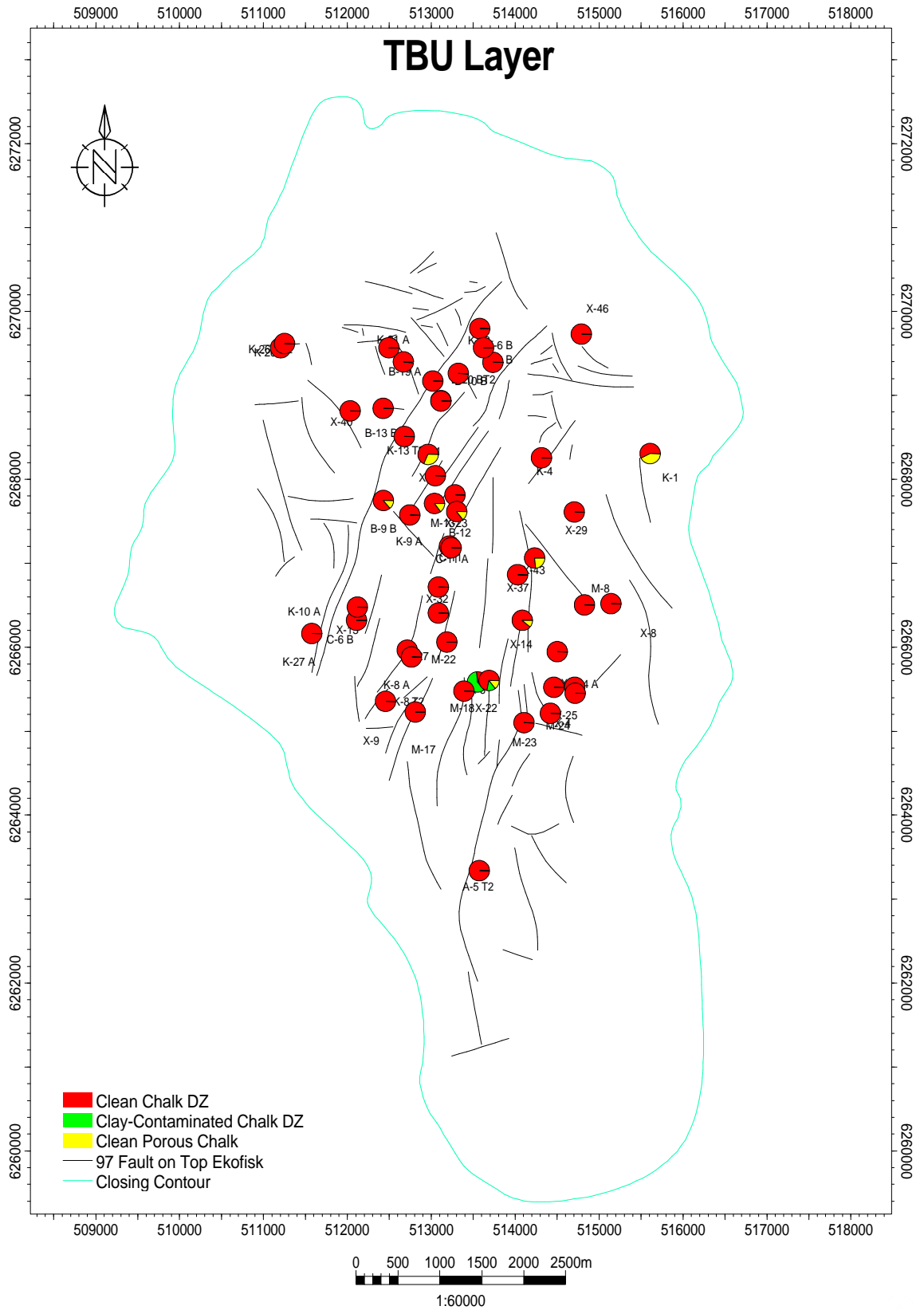
Project: total_ekofisk_well_201112_r1.pet (06/11/2012)





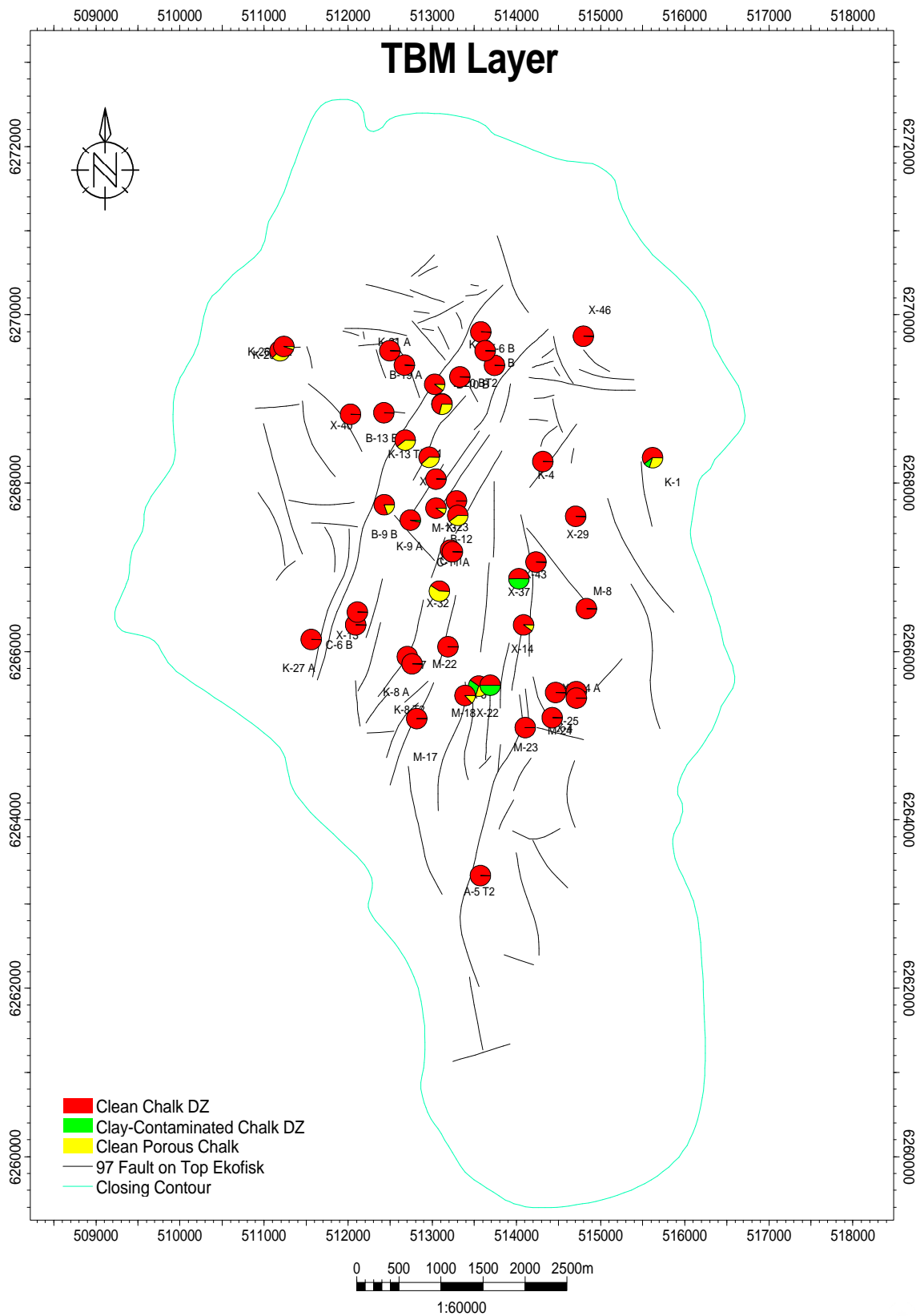
Project: total_ekofisk_well_201112_r1.pet (06/11/2012)





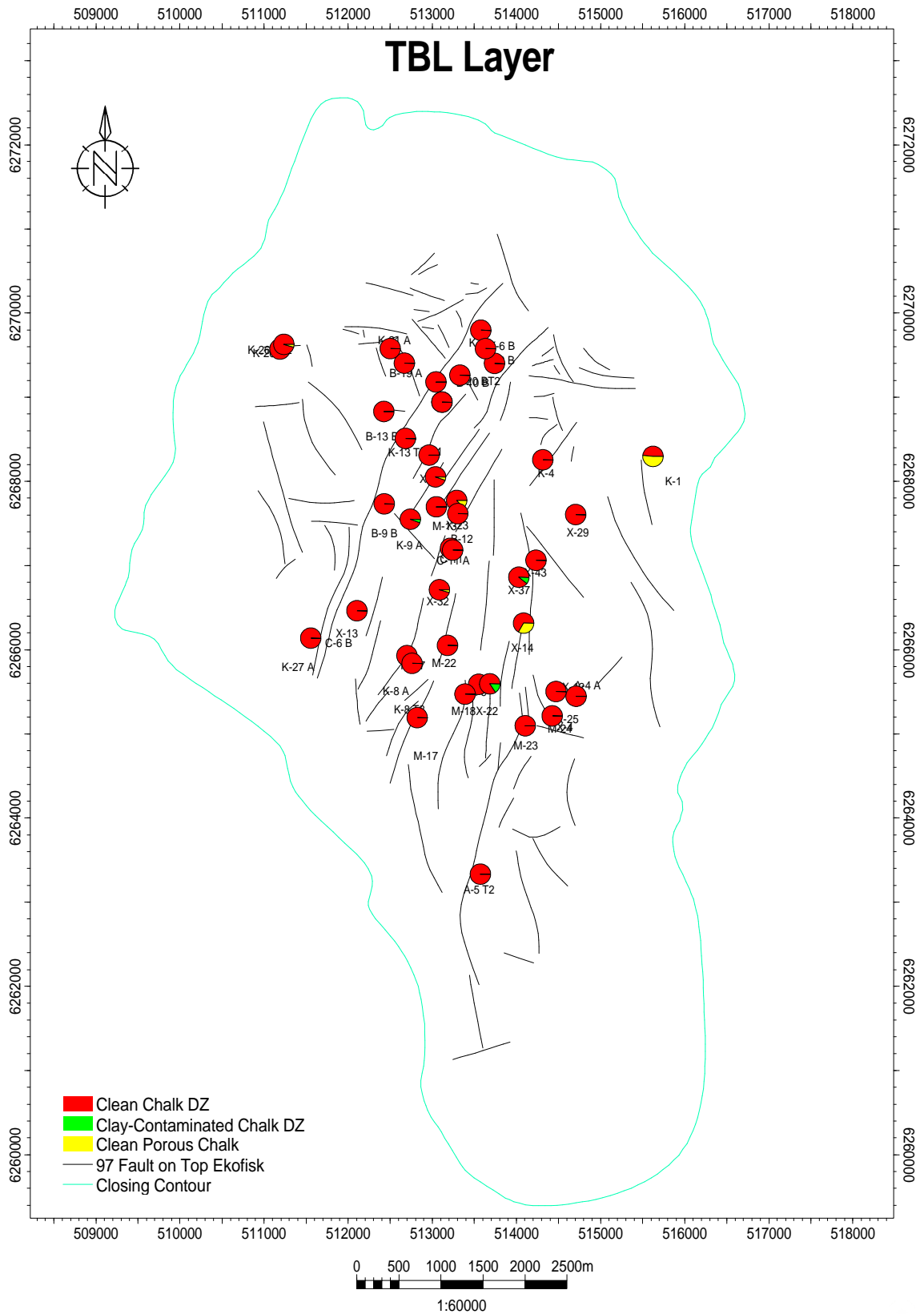
Project: total_ekofisk_well_201112_r1.pet (06/11/2012)





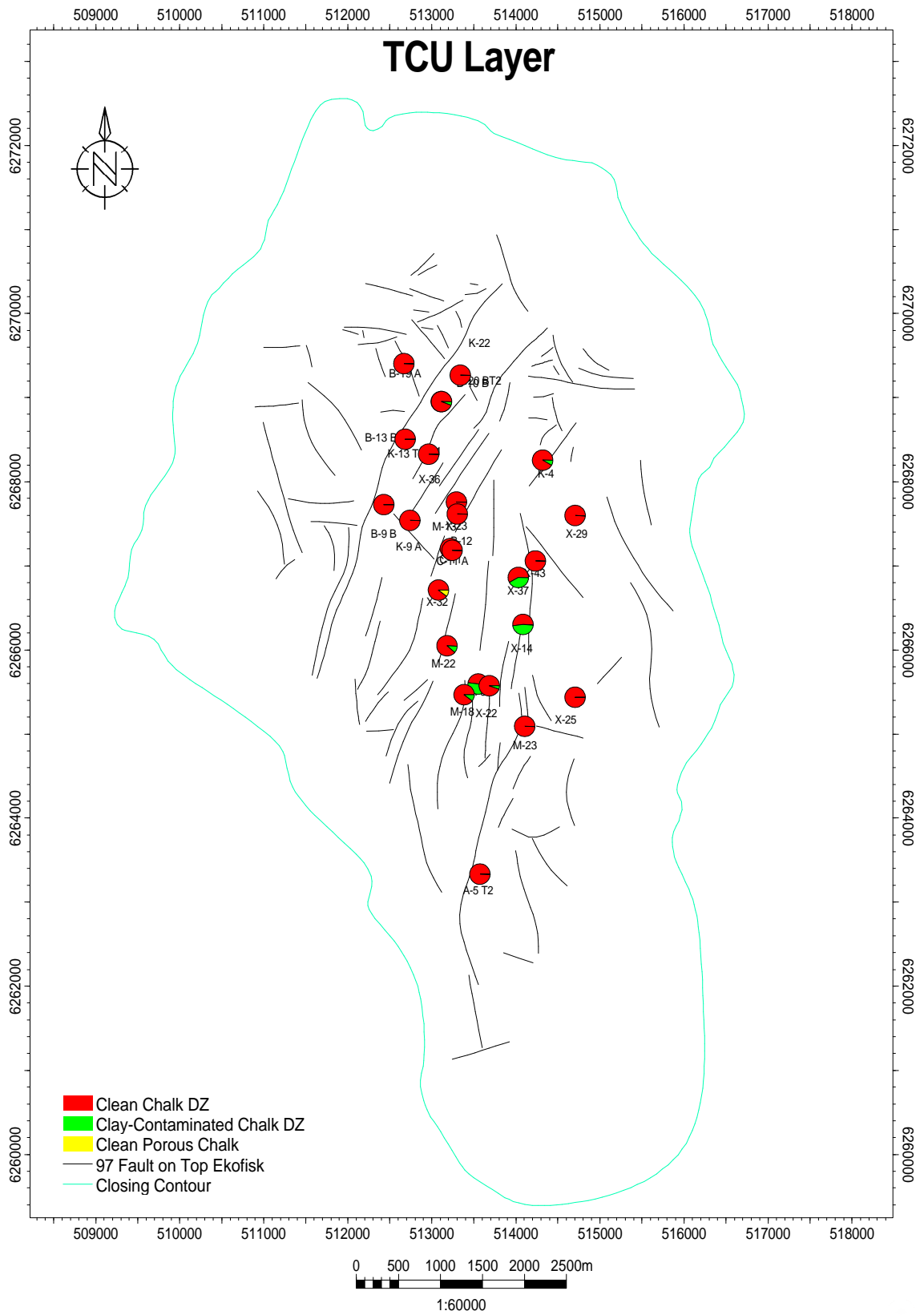
Project: total_ekofisk_well_201112_r1.pet (06/11/2012)





Project: total_ekofisk_well_201112_r1.pet (06/11/2012)

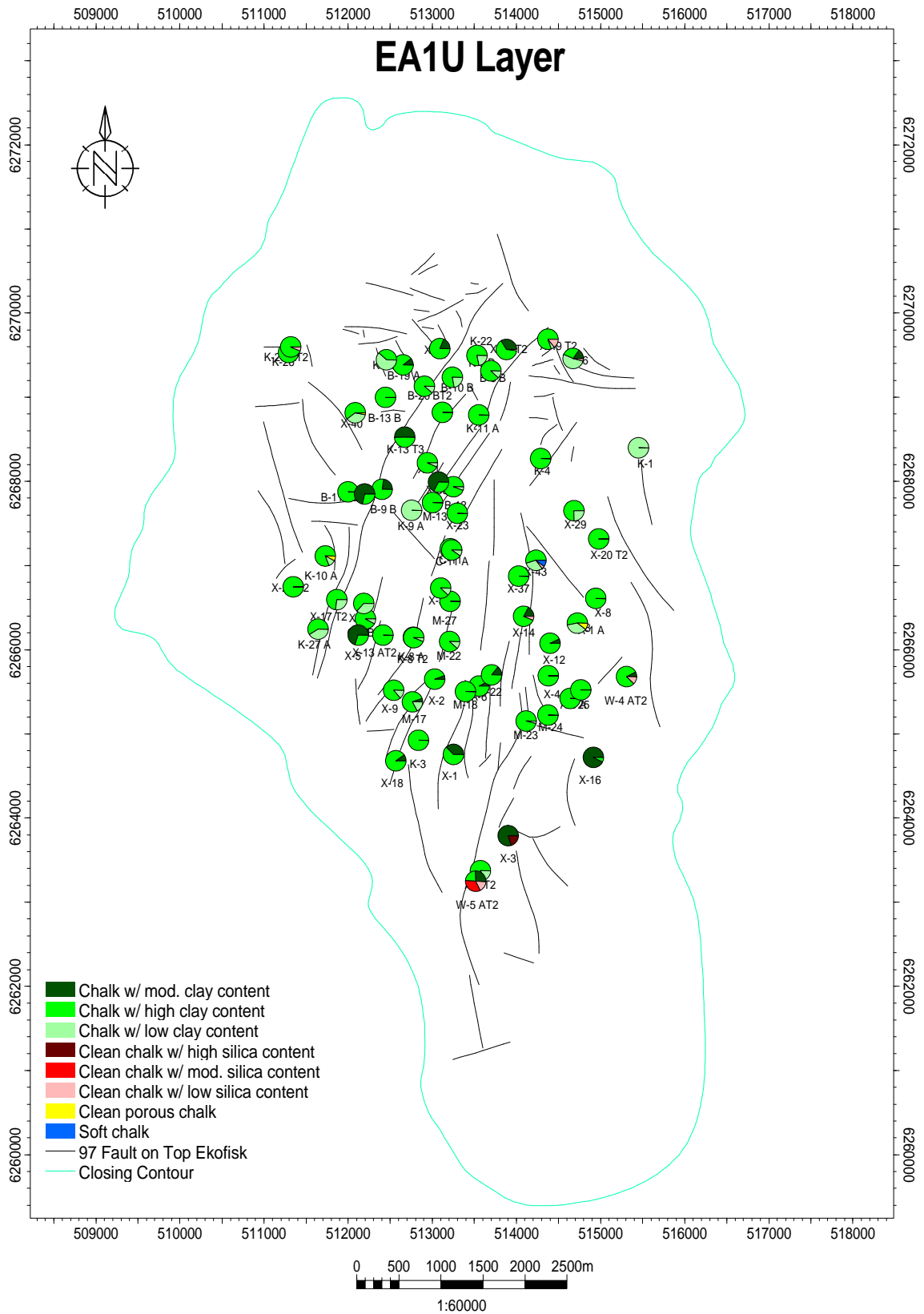




Project: total_ekofisk_well_201112_r1.pet (06/11/2012)

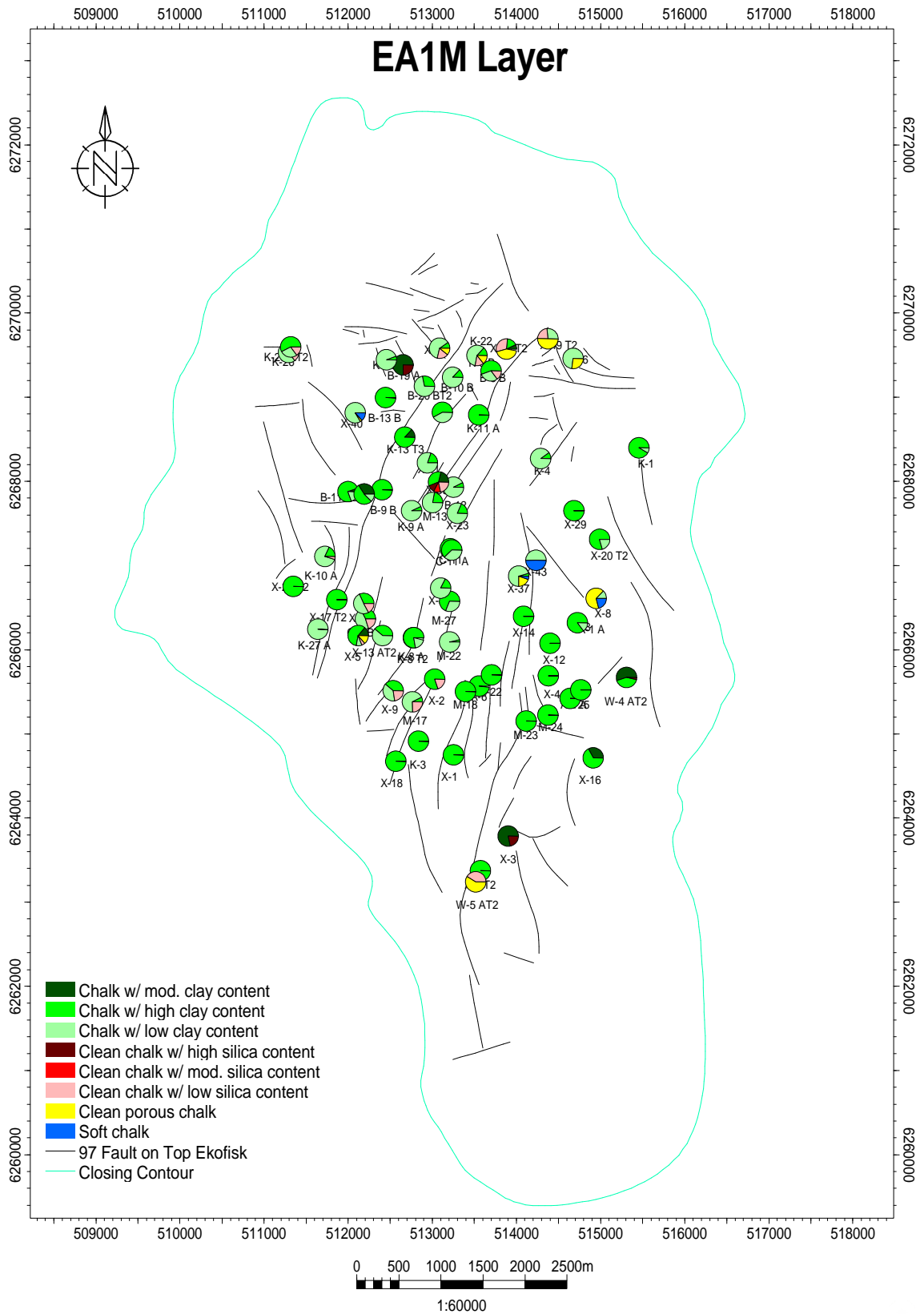


Appendix 4.2.3 Map of facies proportion from 1-8 model (Well log)



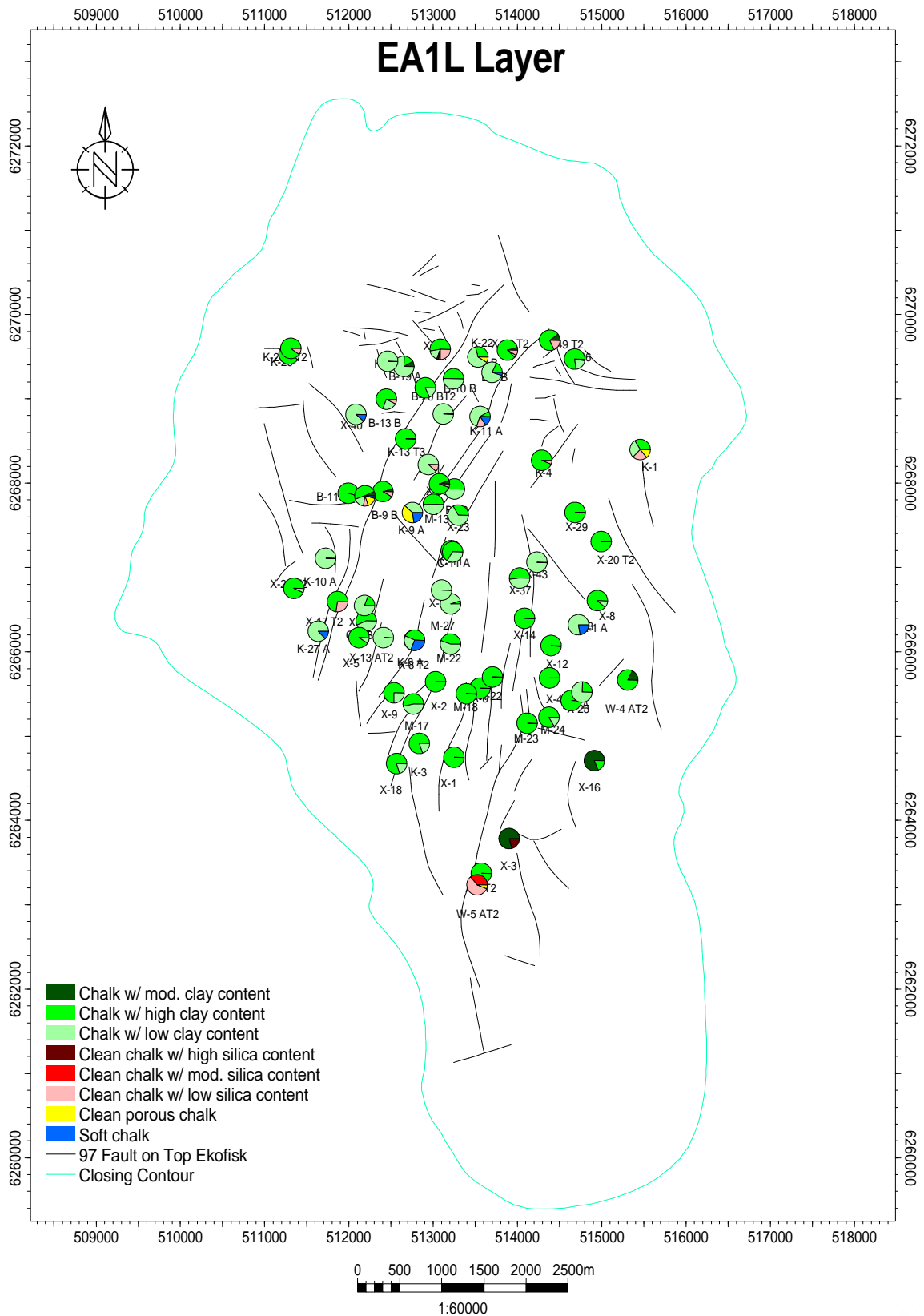
Project: total_ekofisk_well_201112_r1.pet (06/11/2012)





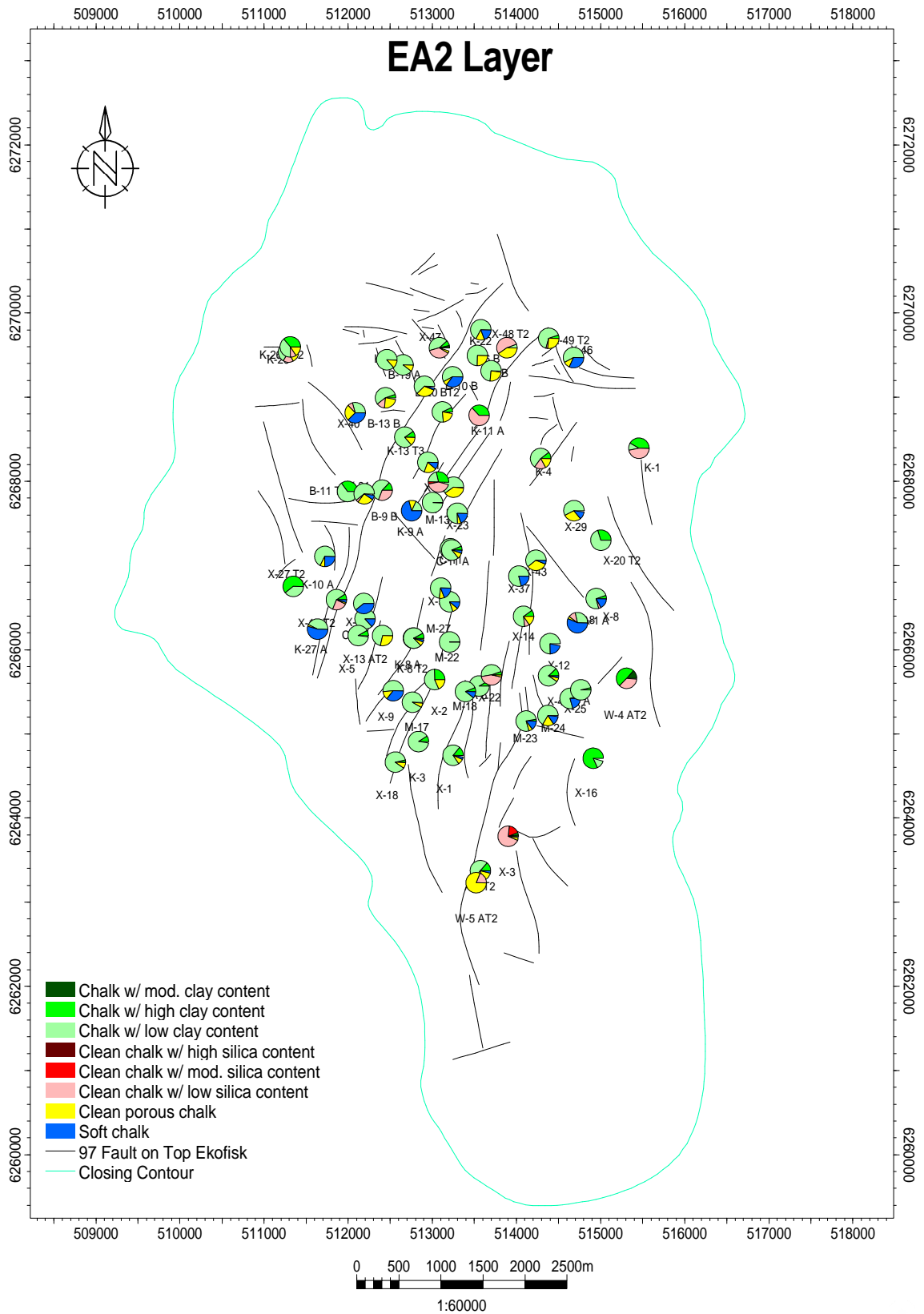
Project: total_ekofisk_well_201112_r1.pet (06/11/2012)





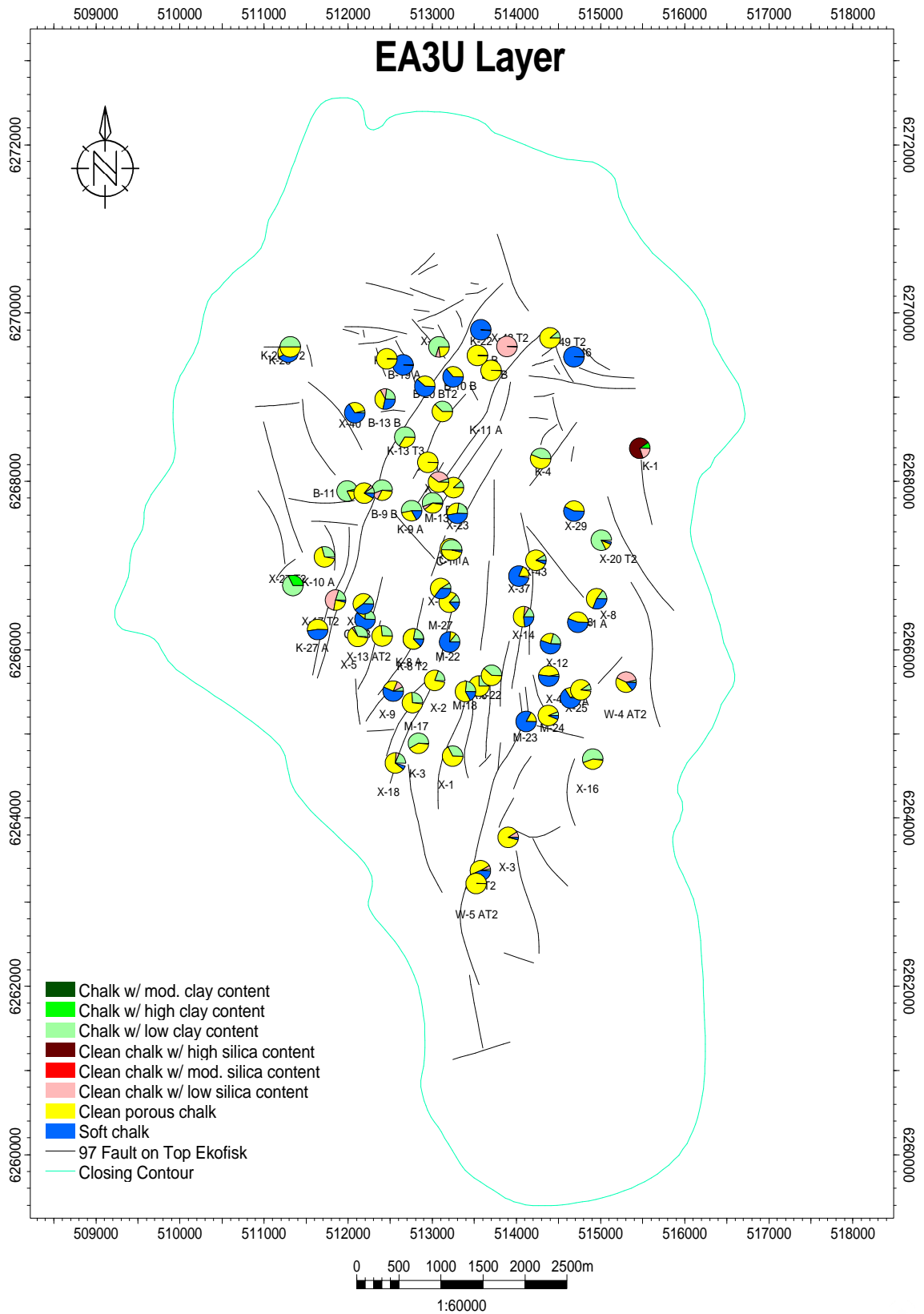
Project: total_ekofisk_well_201112_r1.pet (06/11/2012)





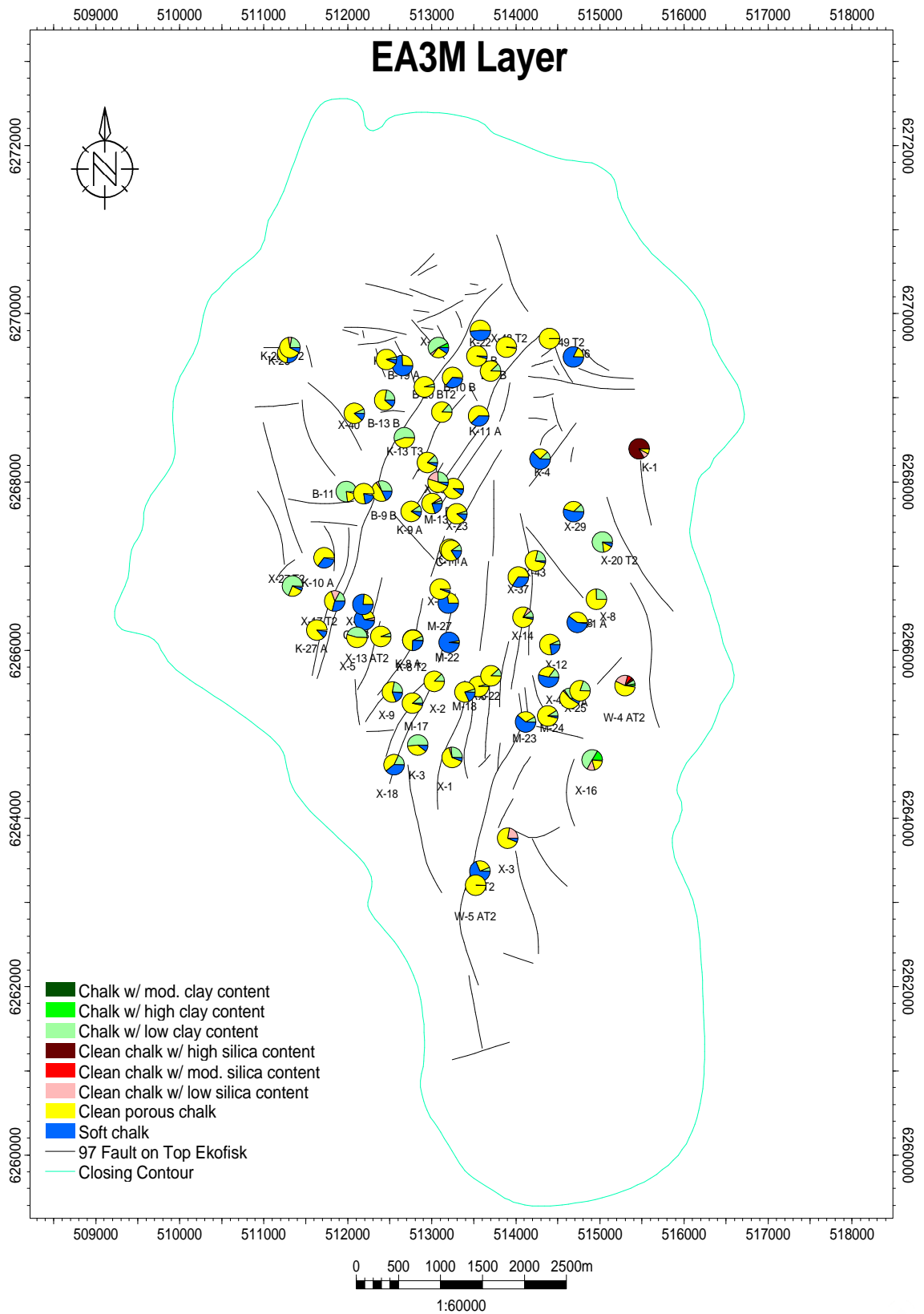
Project: total_ekofisk_well_201112_r1.pet (06/11/2012)





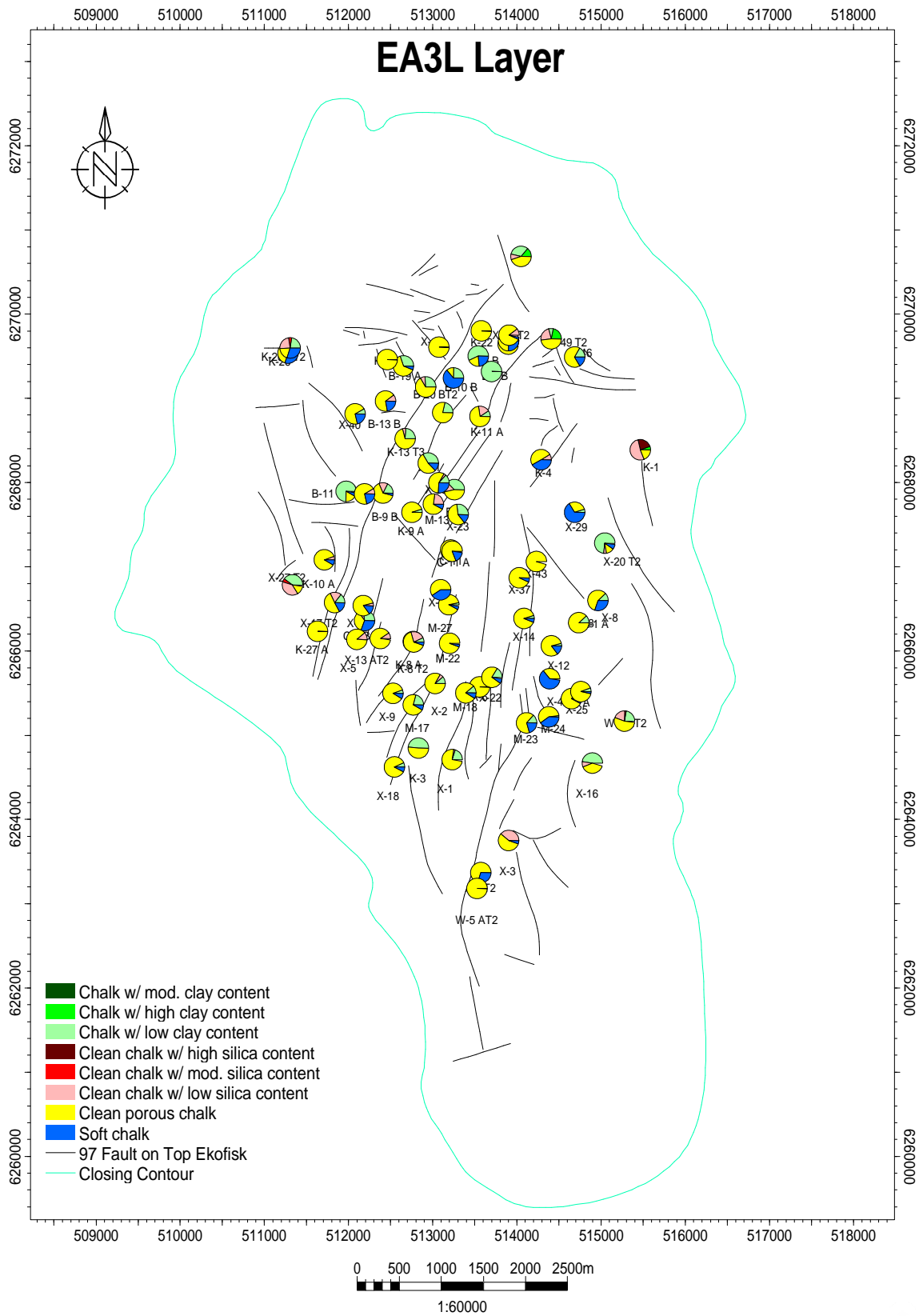
Project: total_ekofisk_well_201112_r1.pet (06/11/2012)





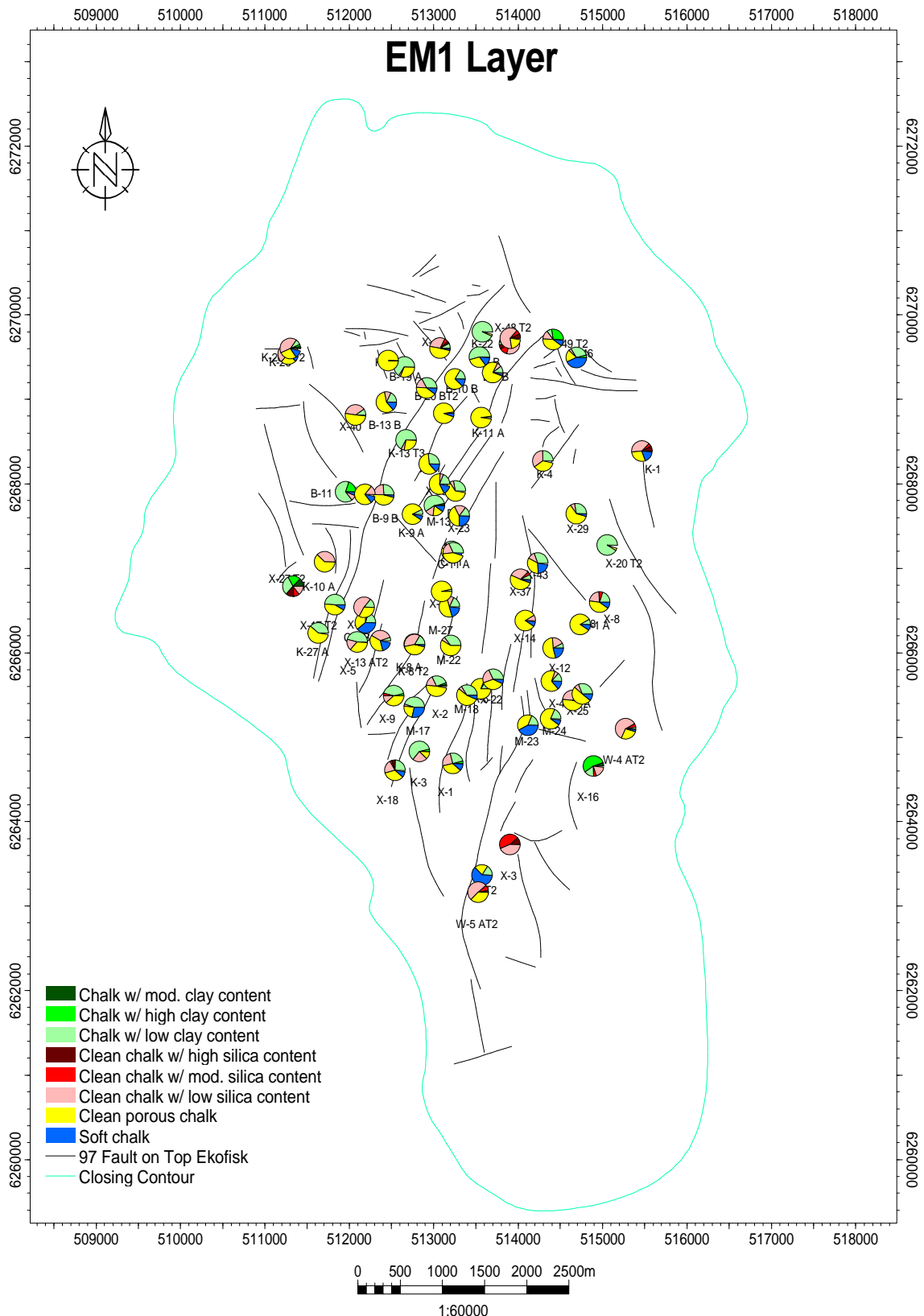
Project: total_ekofisk_well_201112_r1.pet (06/11/2012)





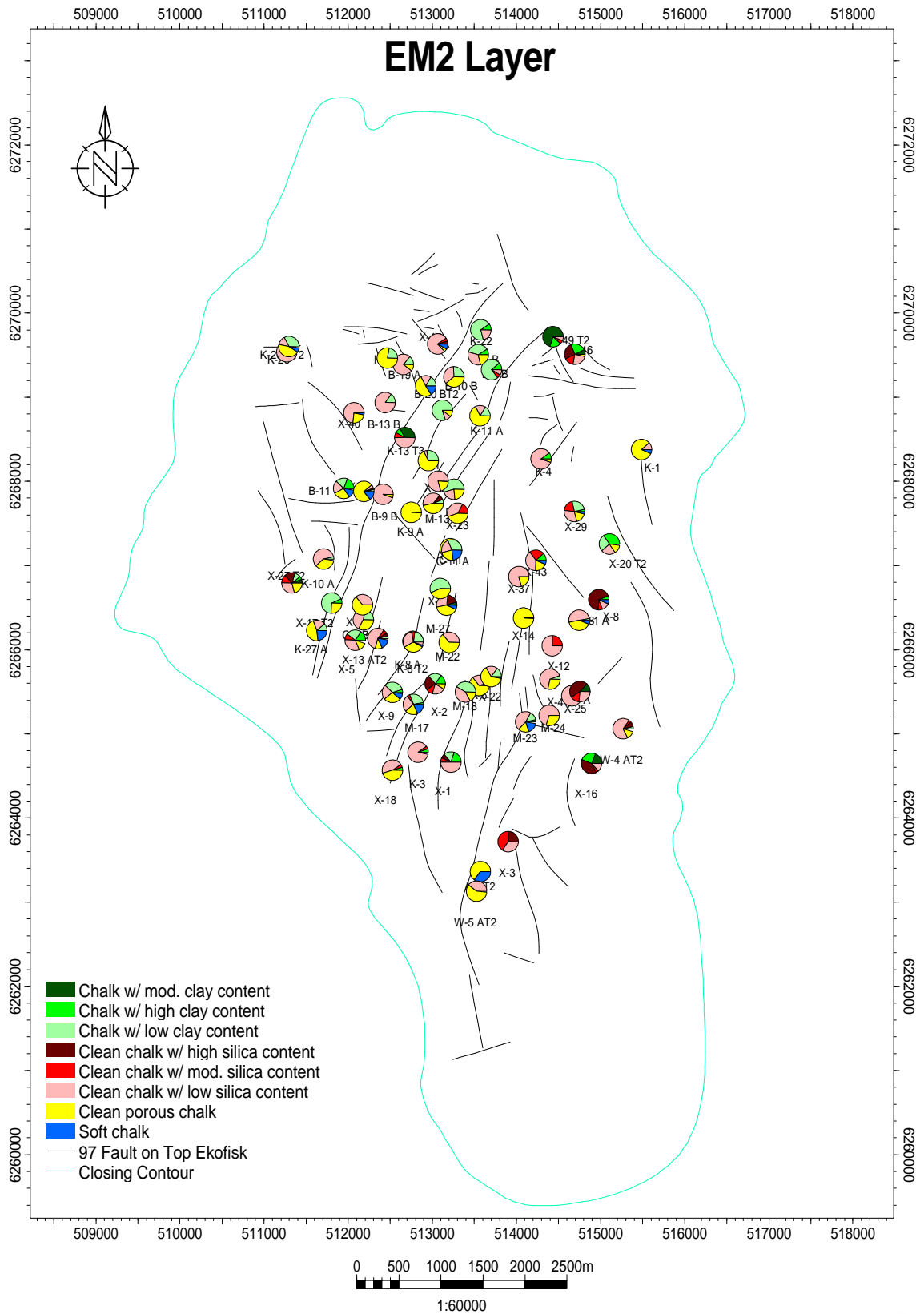
Project: total_ekofisk_well_201112_r1.pet (06/11/2012)





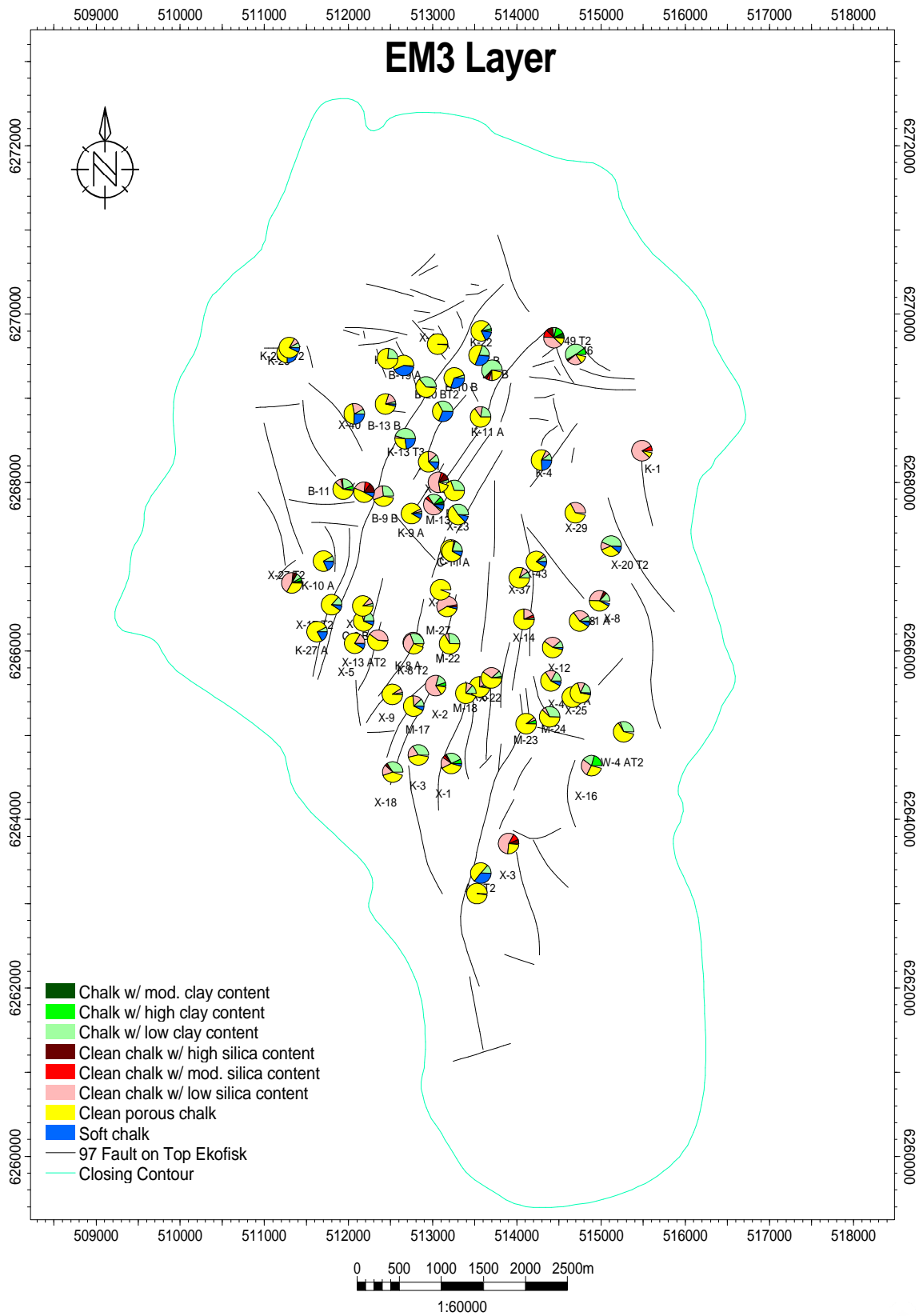
Project: total_ekofisk_well_201112_r1.pet (06/11/2012)





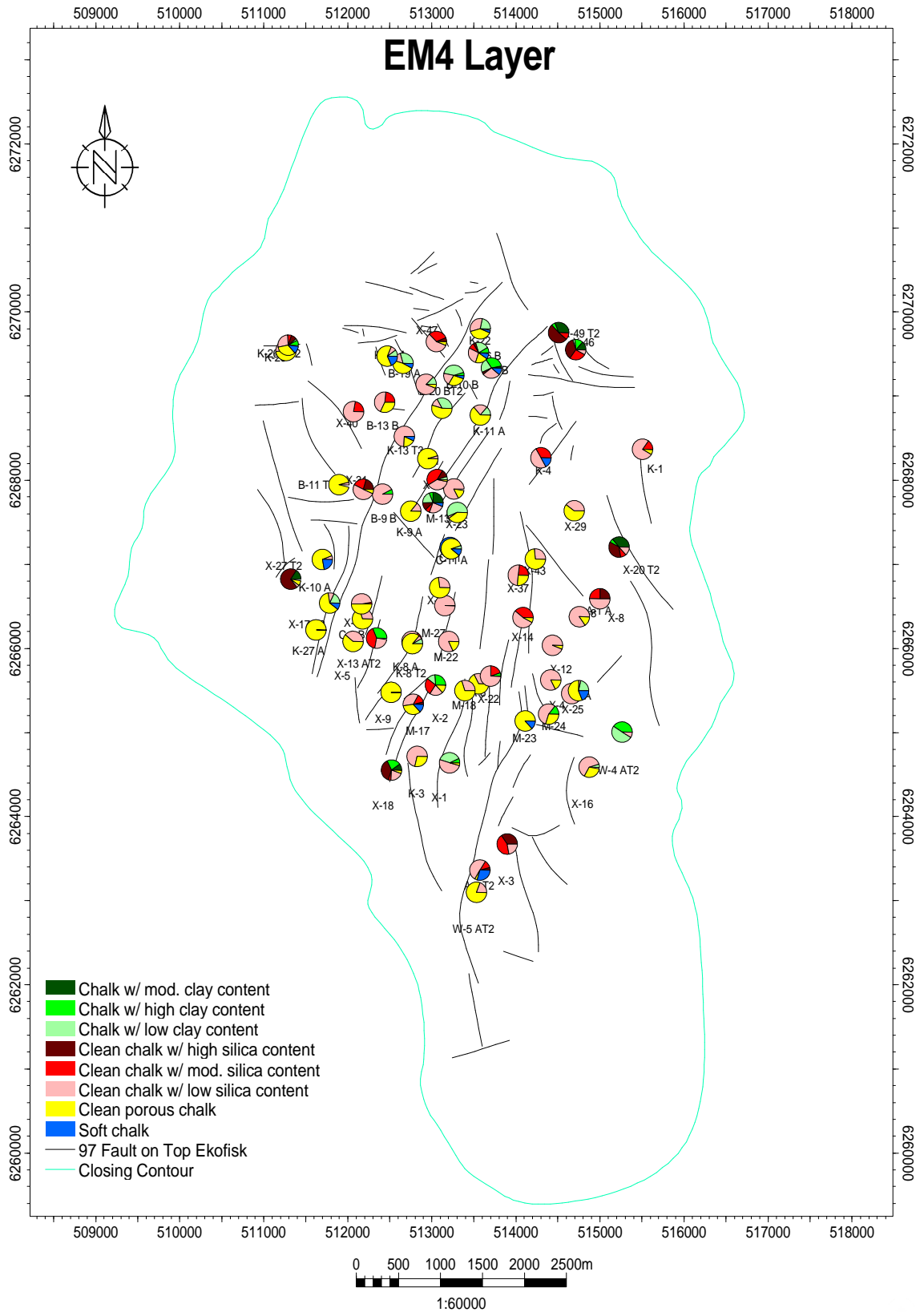
Project: total_ekofisk_well_201112_r1.pet (06/11/2012)





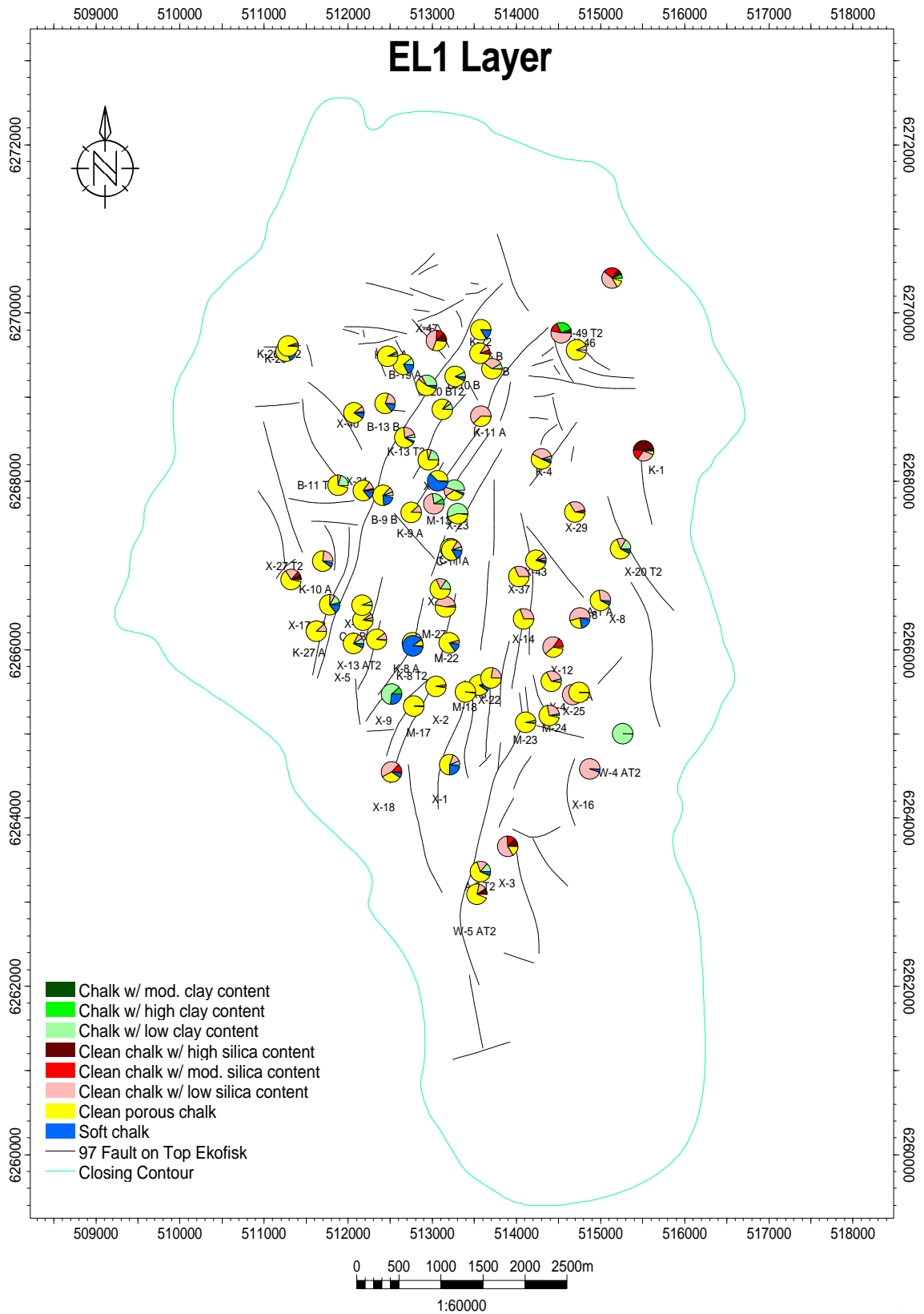
Project: total_ekofisk_well_201112_r1.pet (06/11/2012)

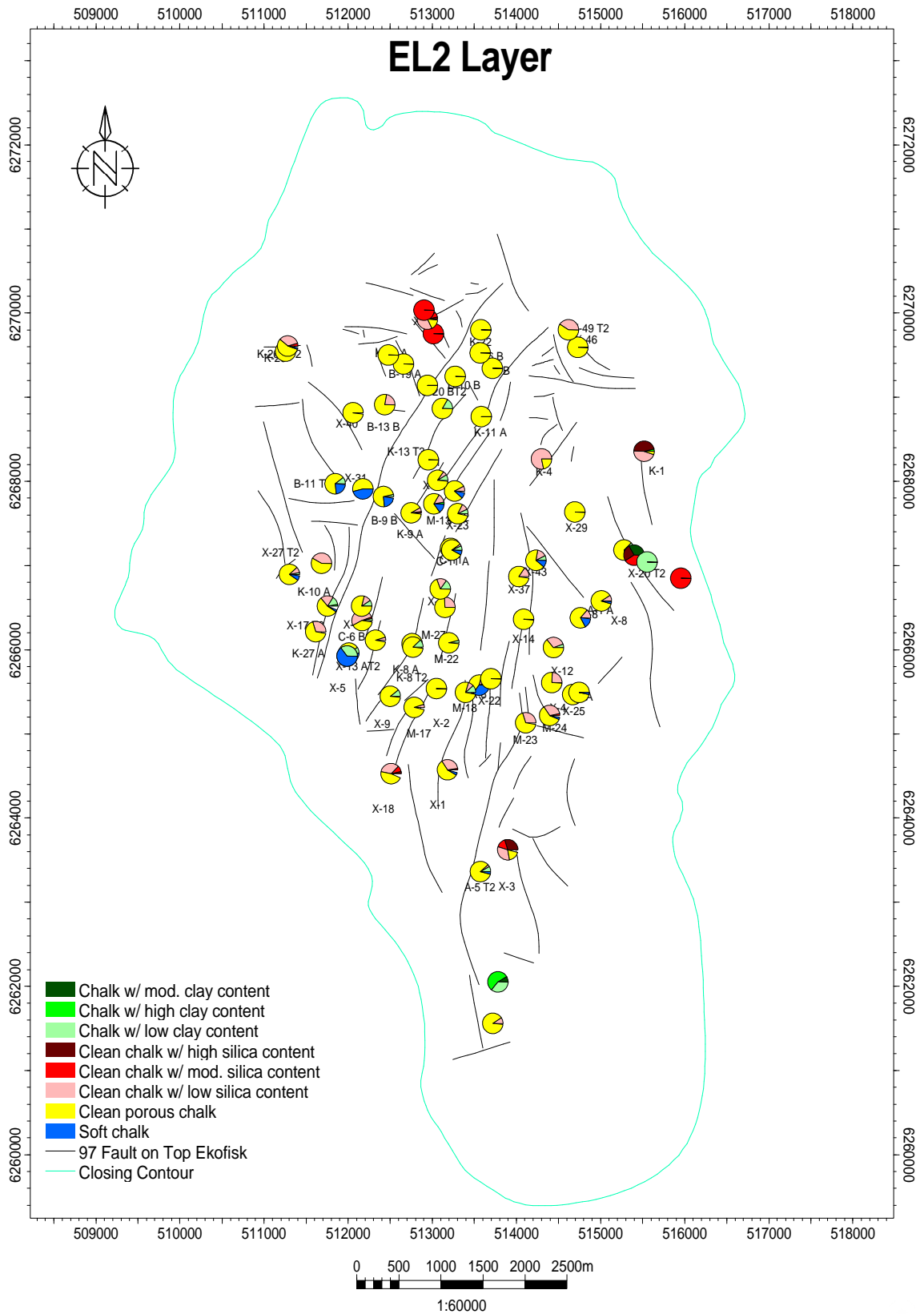




Project: total_ekofisk_well_201112_r1.pet (06/11/2012)

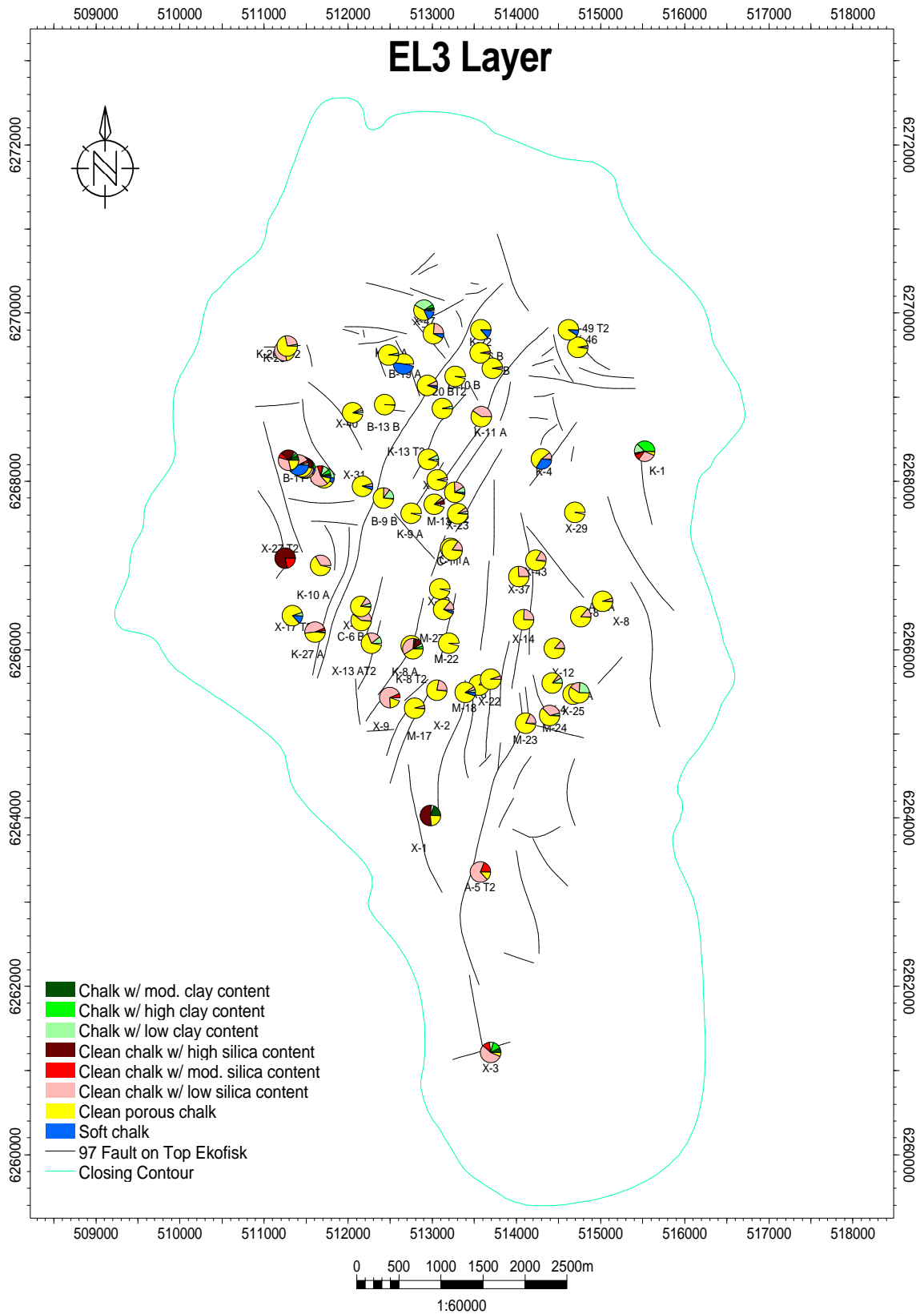






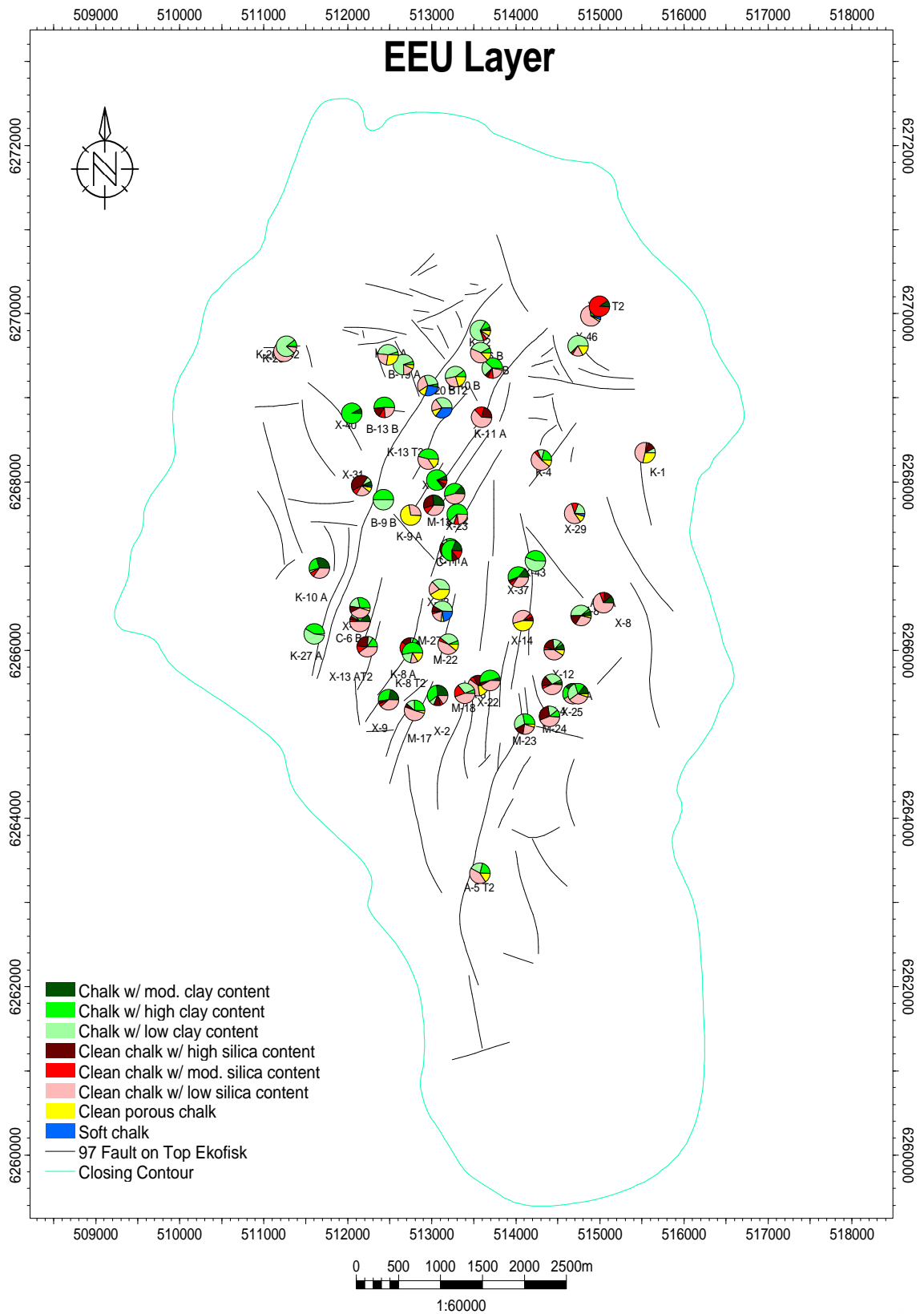
Project: total_ekofisk_well_201112_r1.pet (06/11/2012)





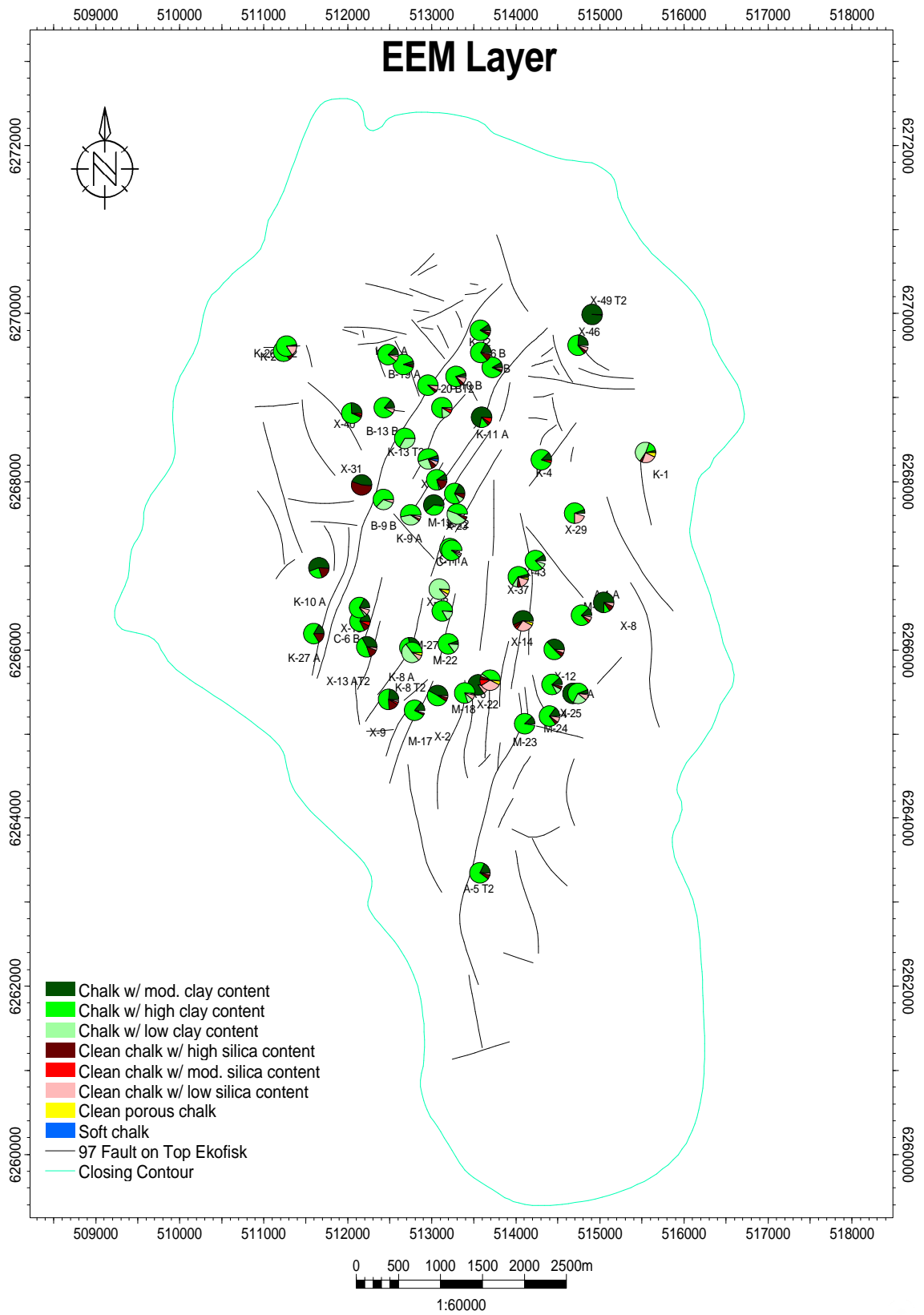
Project: total_ekofisk_well_201112_r1.pet (06/11/2012)





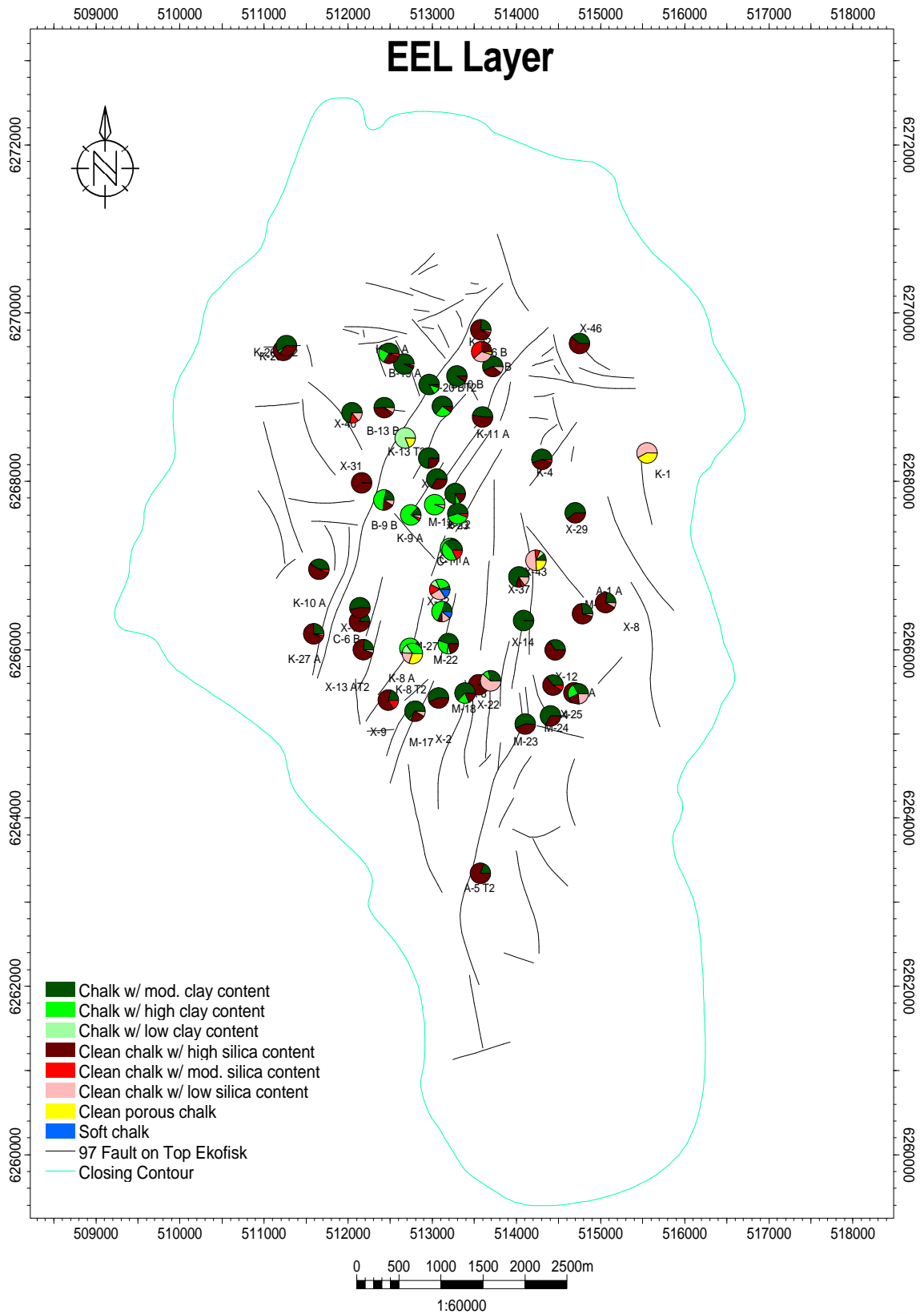
Project: total_ekofisk_well_201112_r1.pet (06/11/2012)





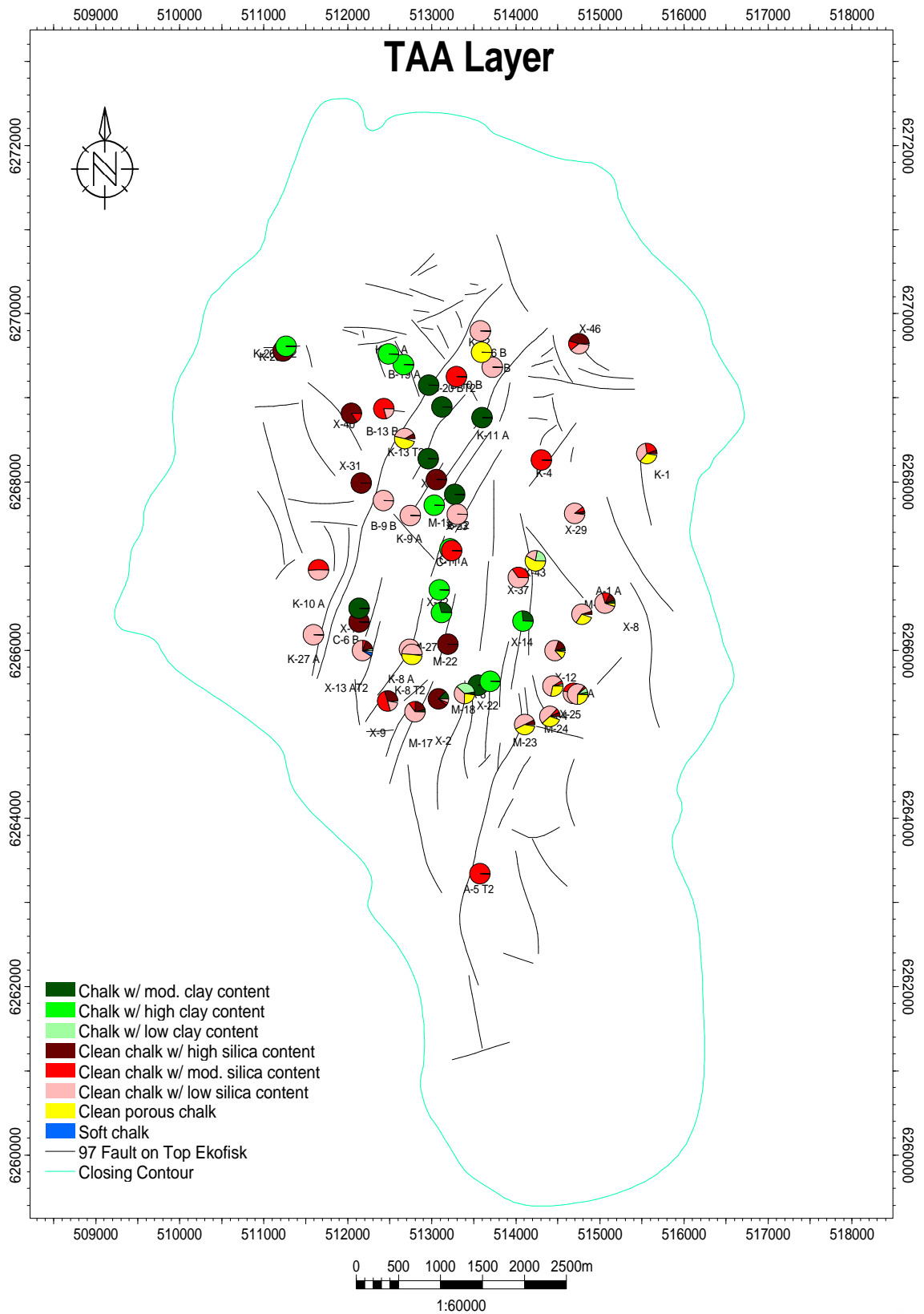
Project: total_ekofisk_well_201112_r1.pet (06/11/2012)





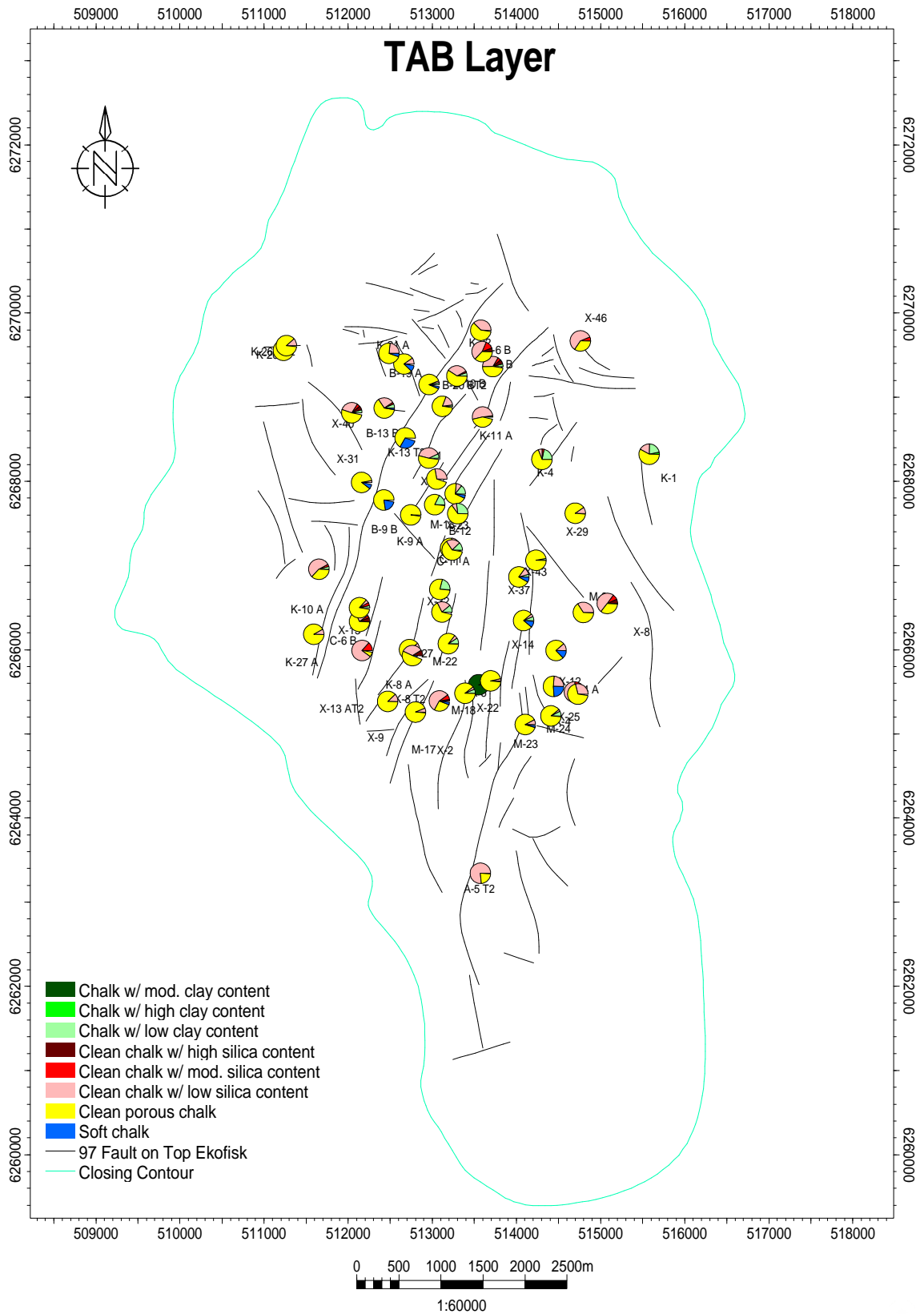
Project: total_ekofisk_well_201112_r1.pet (06/11/2012)





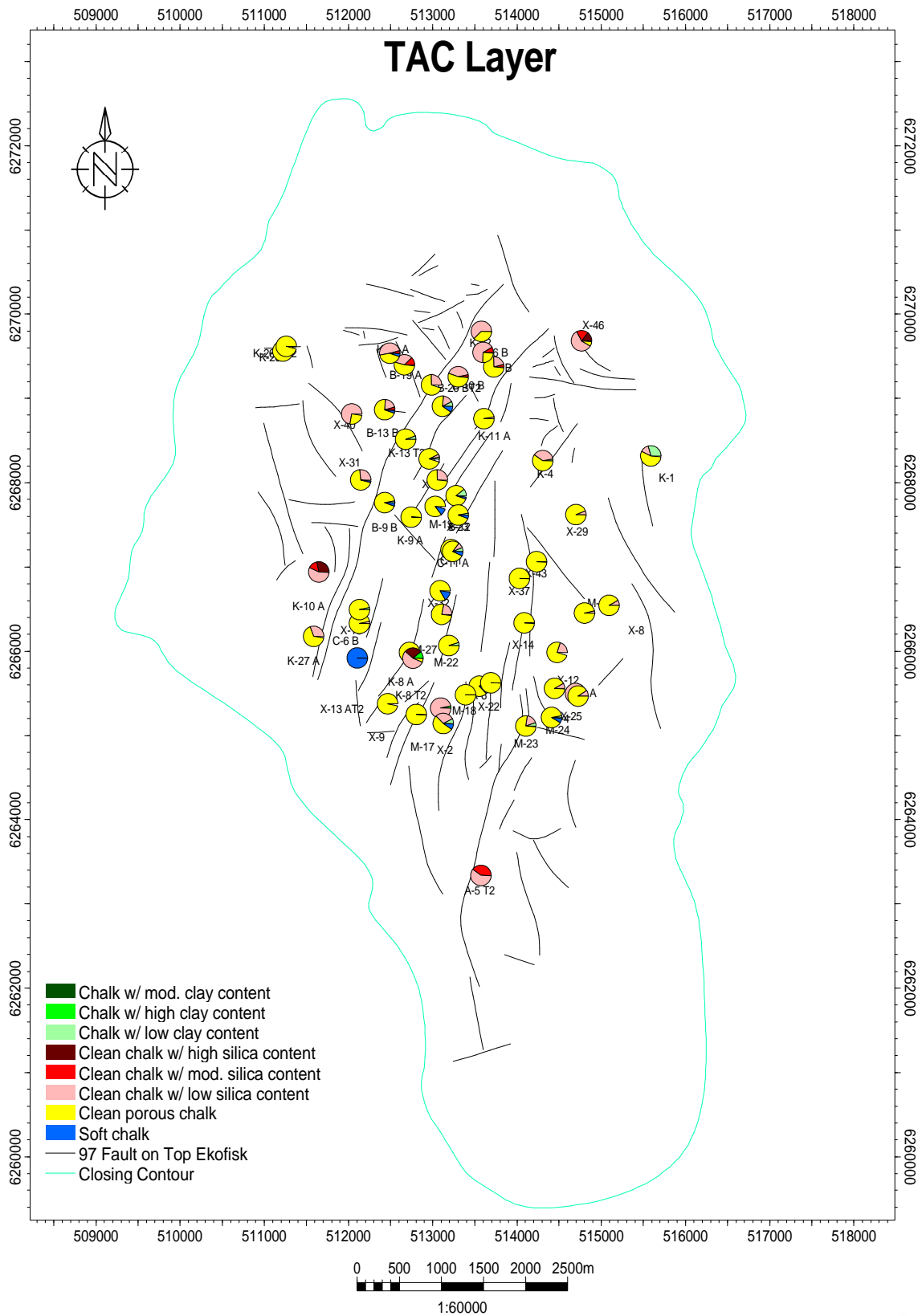
Project: total_ekofisk_well_201112_r1.pet (06/11/2012)





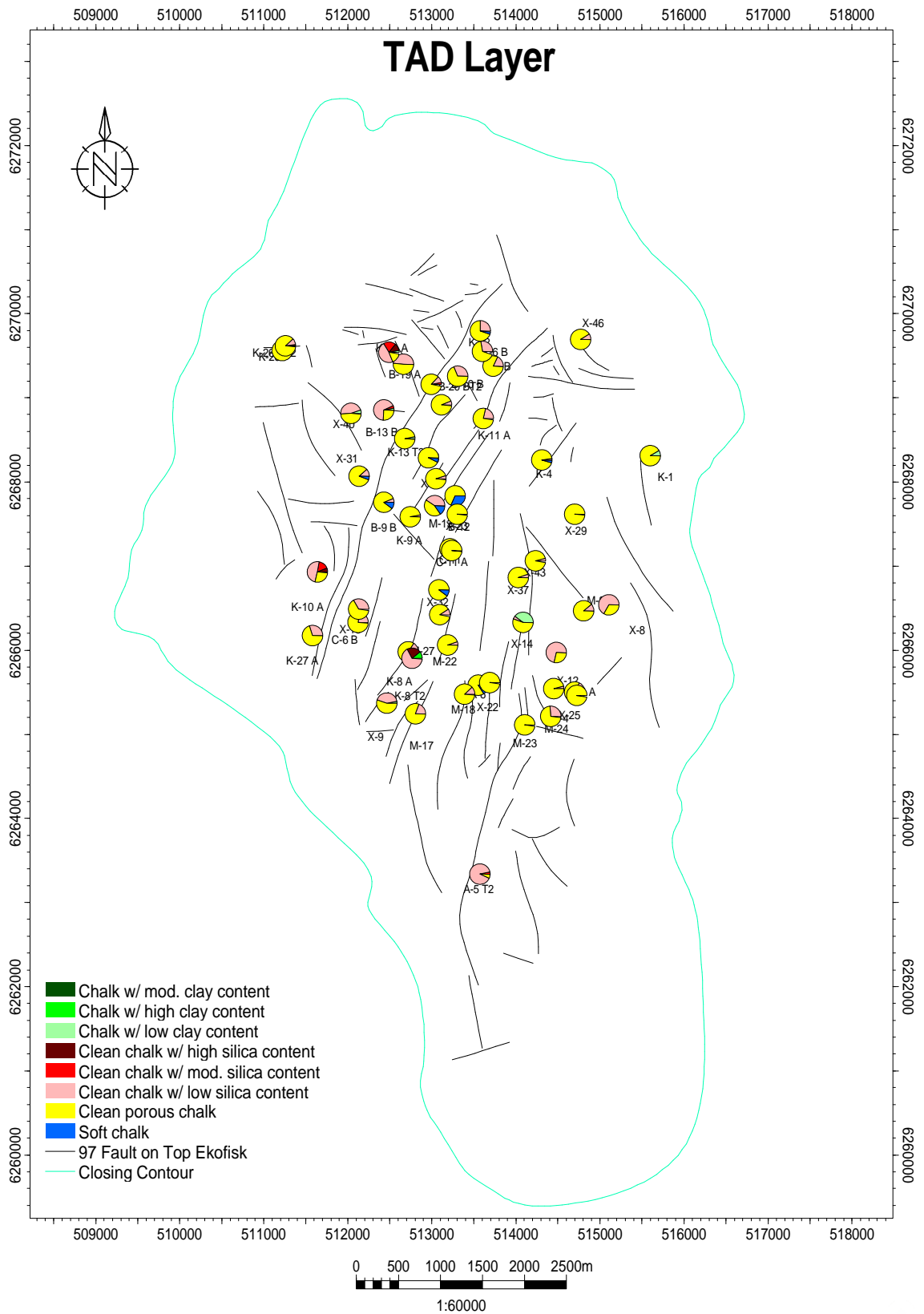
Project: total_ekofisk_well_201112_r1.pet (06/11/2012)





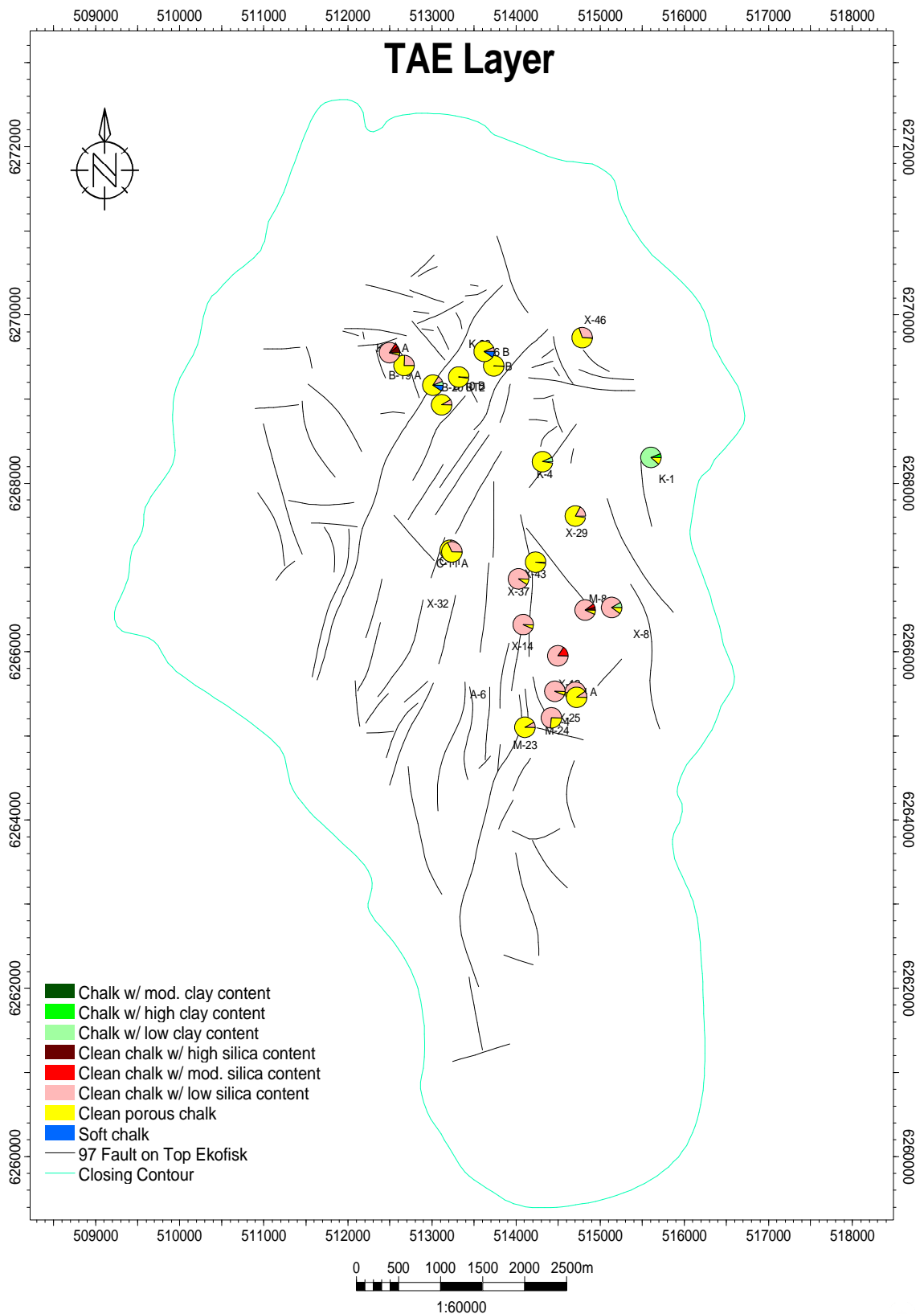
Project: total_ekofisk_well_201112_r1.pet (06/11/2012)





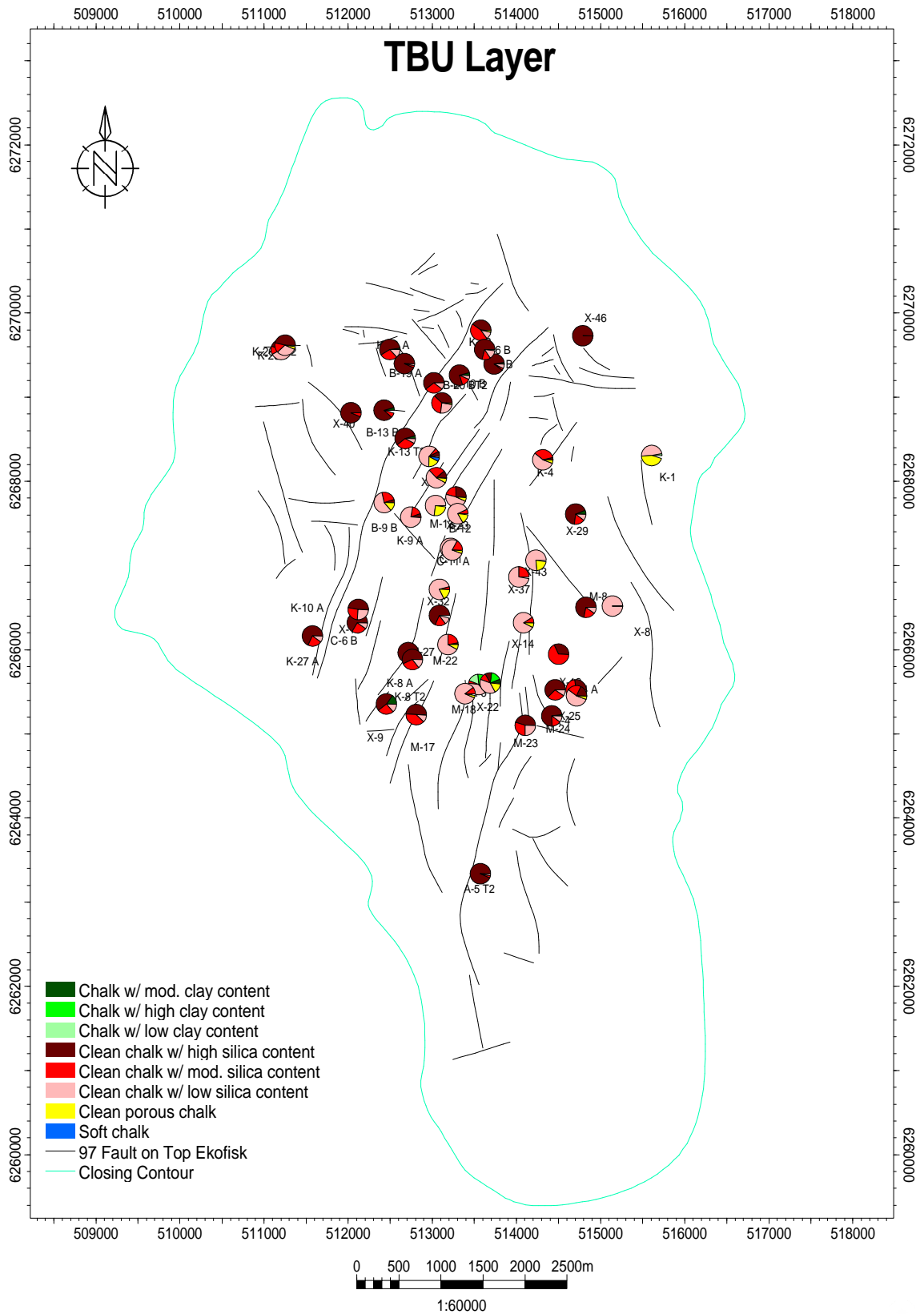
Project: total_ekofisk_well_201112_r1.pet (06/11/2012)





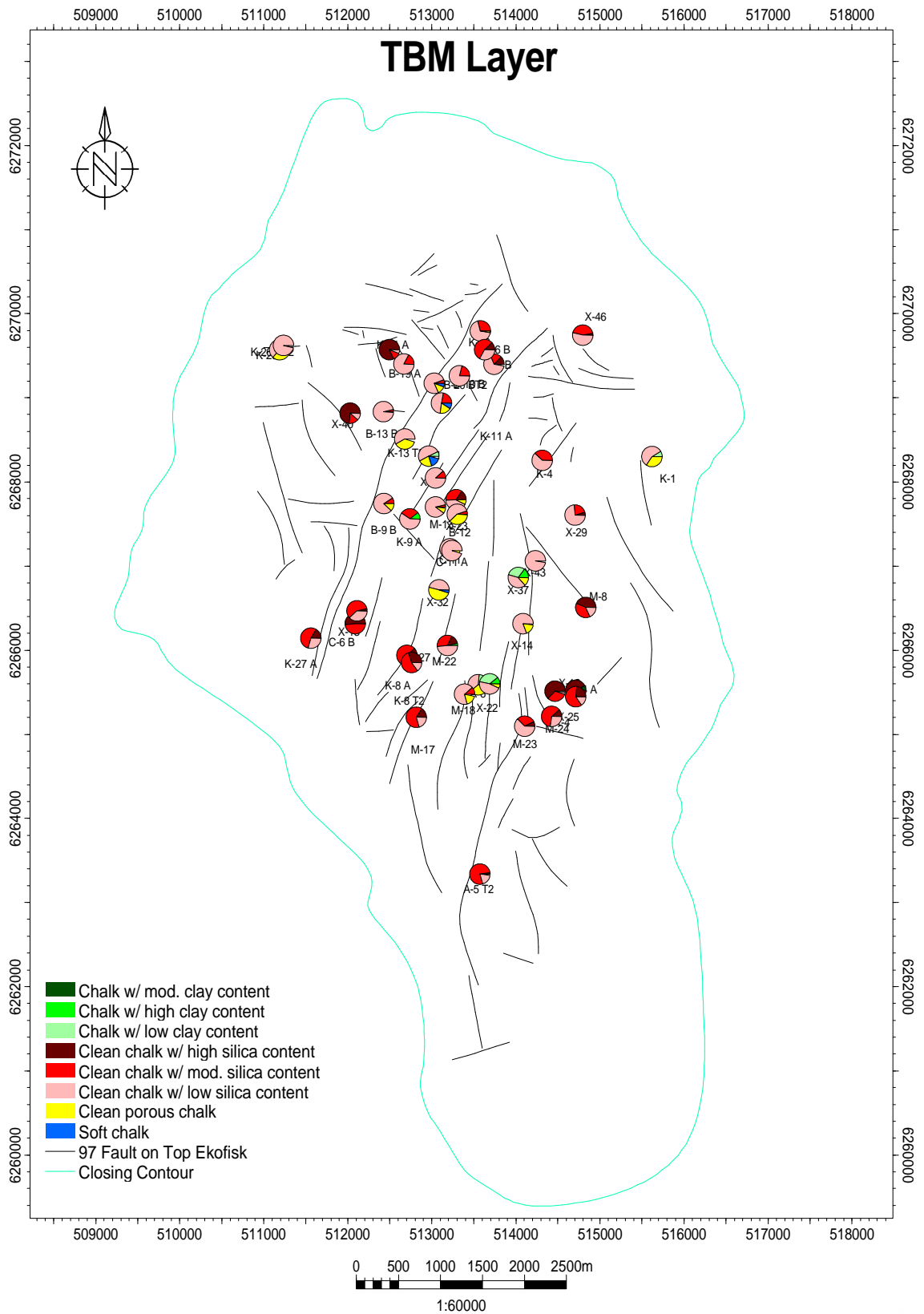
Project: total_ekofisk_well_201112_r1.pet (06/11/2012)





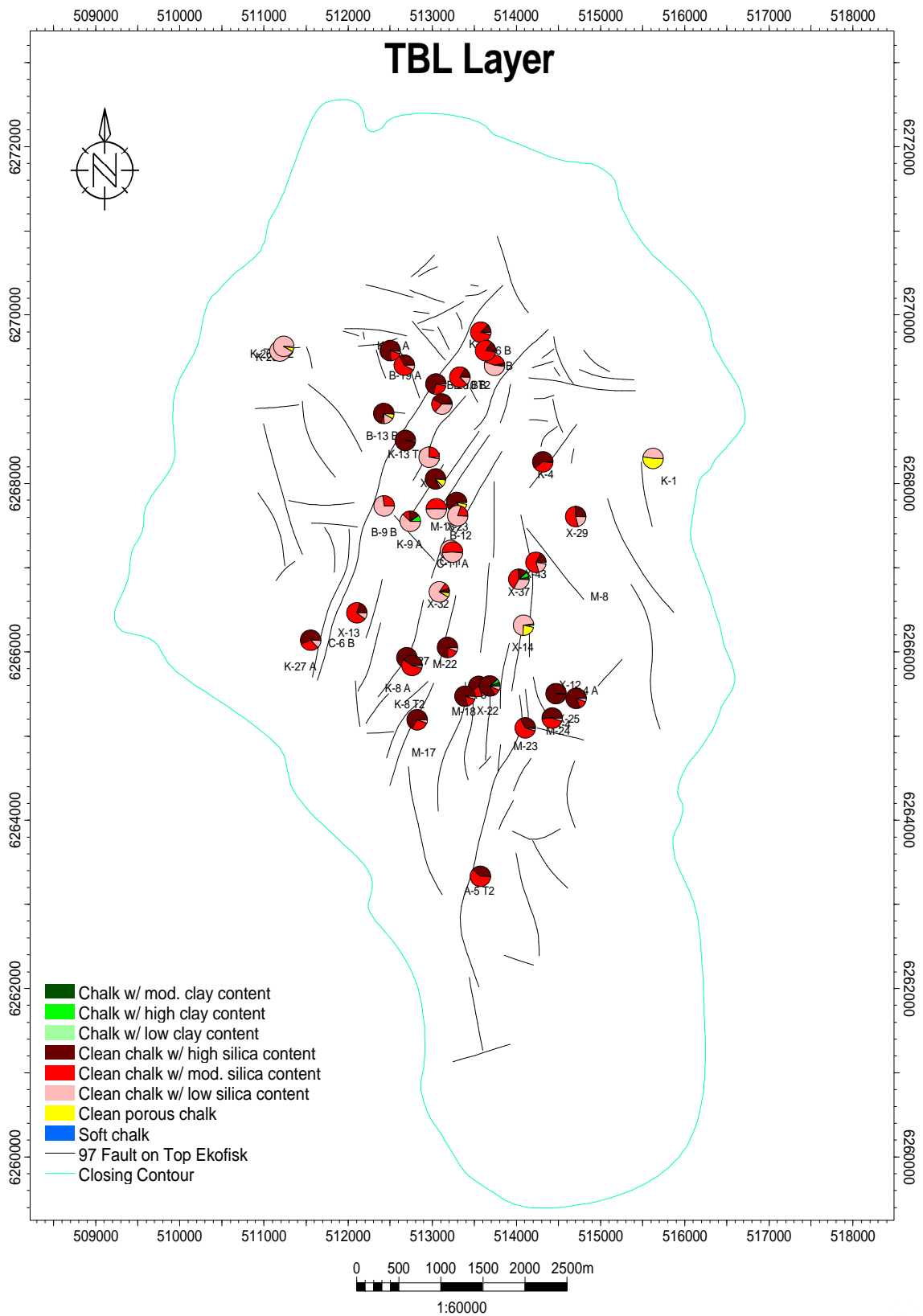
Project: total_ekofisk_well_201112_r1.pet (06/11/2012)





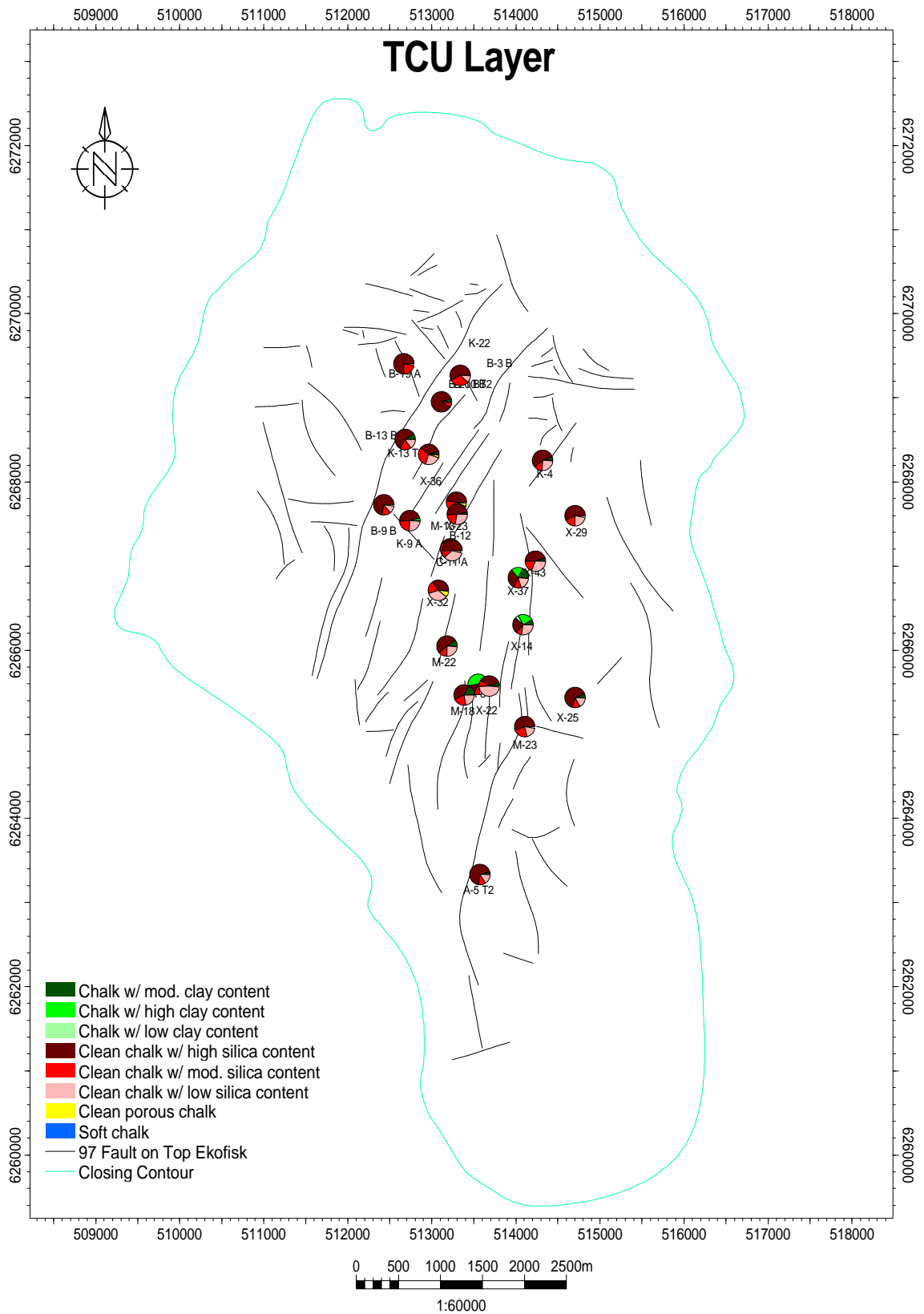
Project: total_ekofisk_well_201112_r1.pet (06/11/2012)





Project: total_ekofisk_well_201112_r1.pet (06/11/2012)

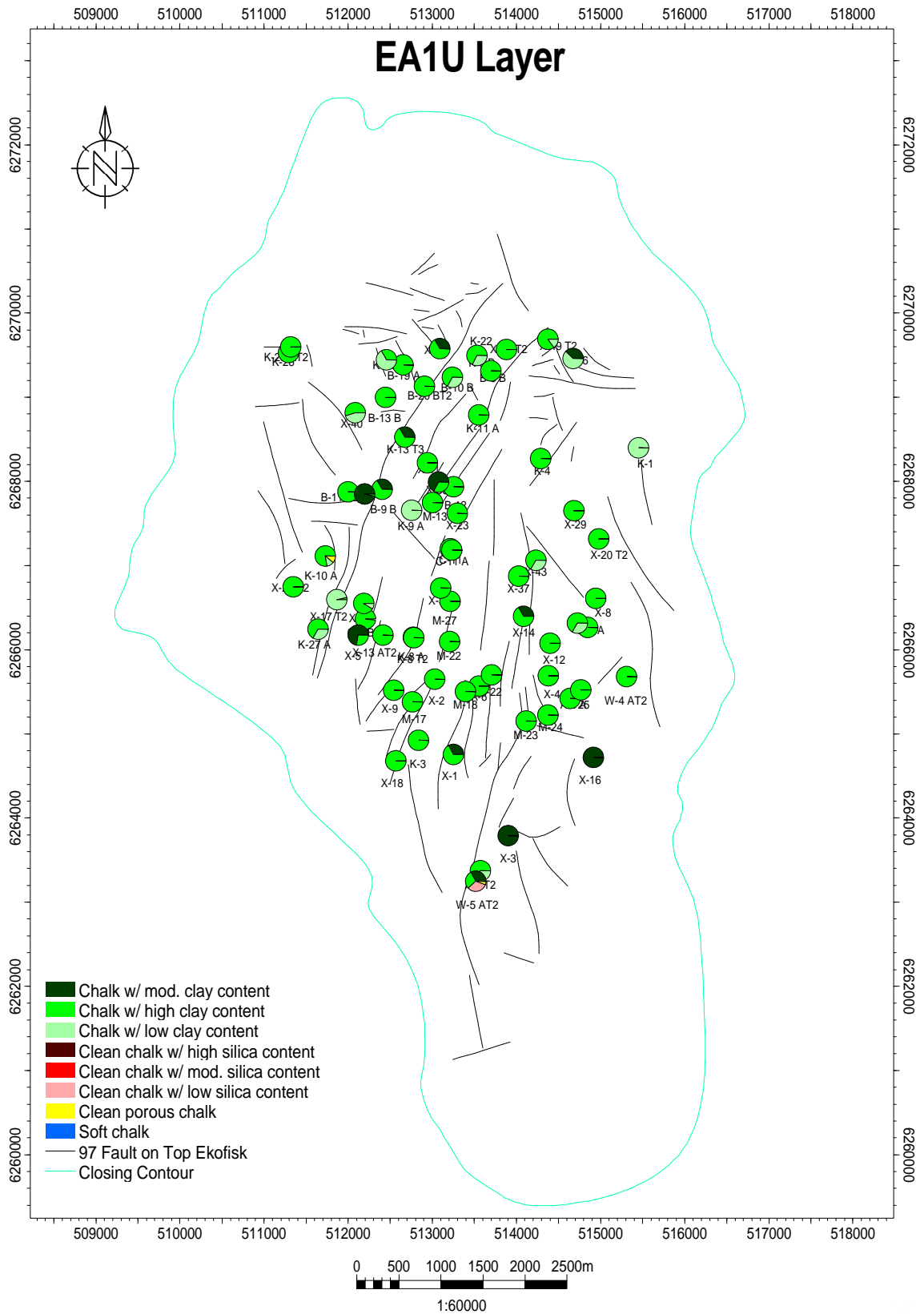




Project: total_ekofisk_well_201112_r1.pet (06/11/2012)

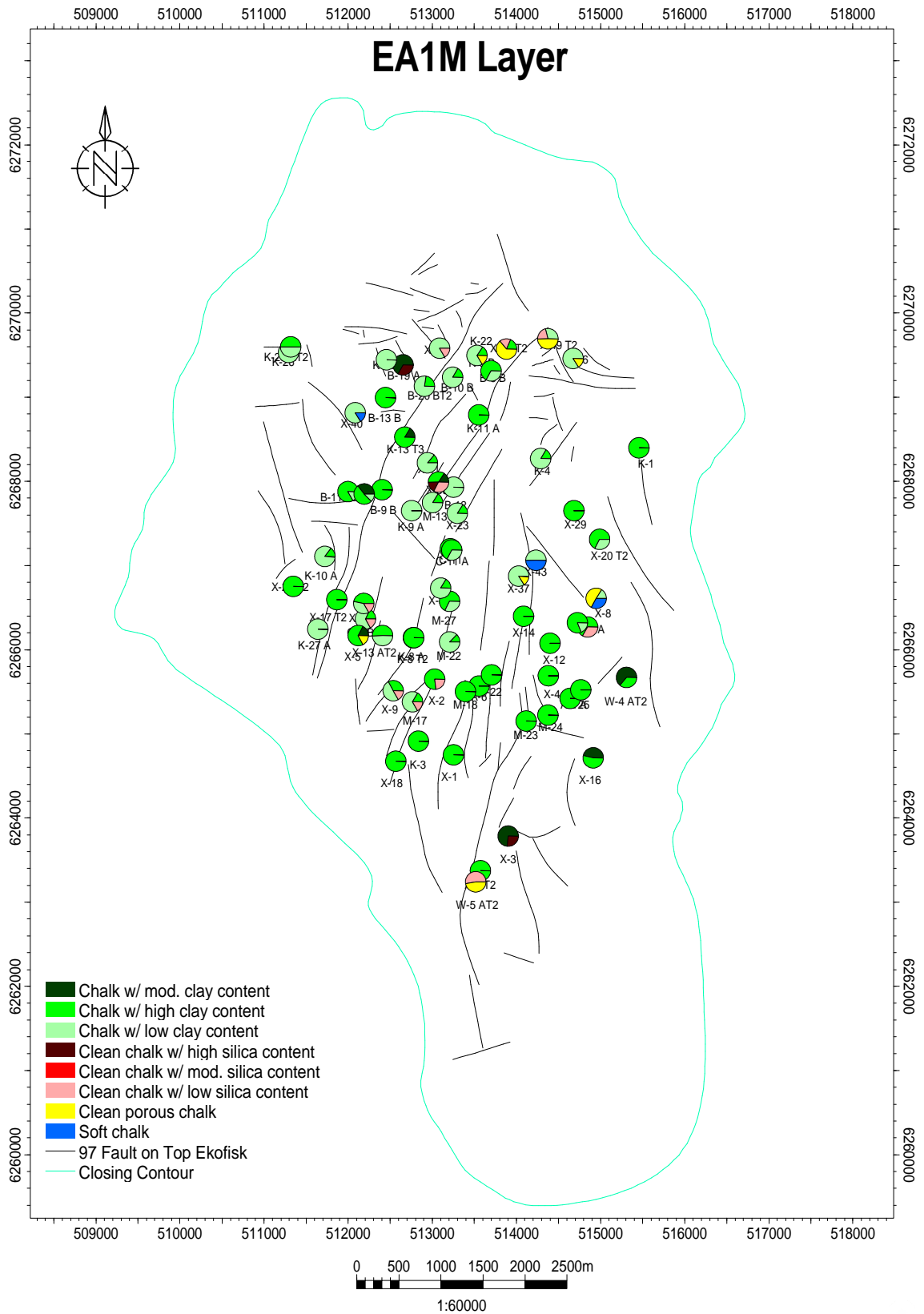


Appendix 4.2.4 Map of facies proportion from 1-8 model (Upscaled Well log)



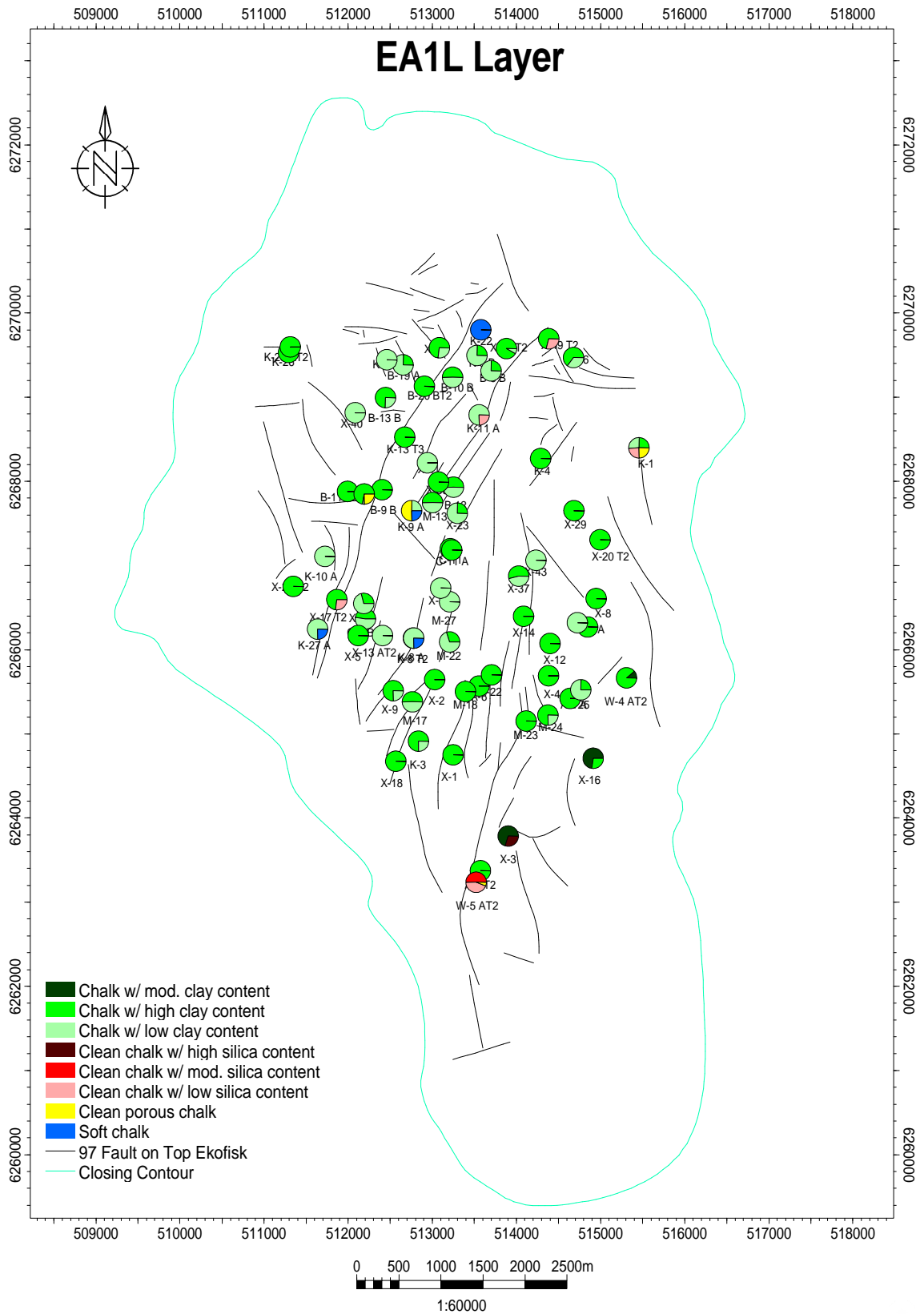
Project: total_ekofisk_well_201112_r1.pet (06/11/2012)





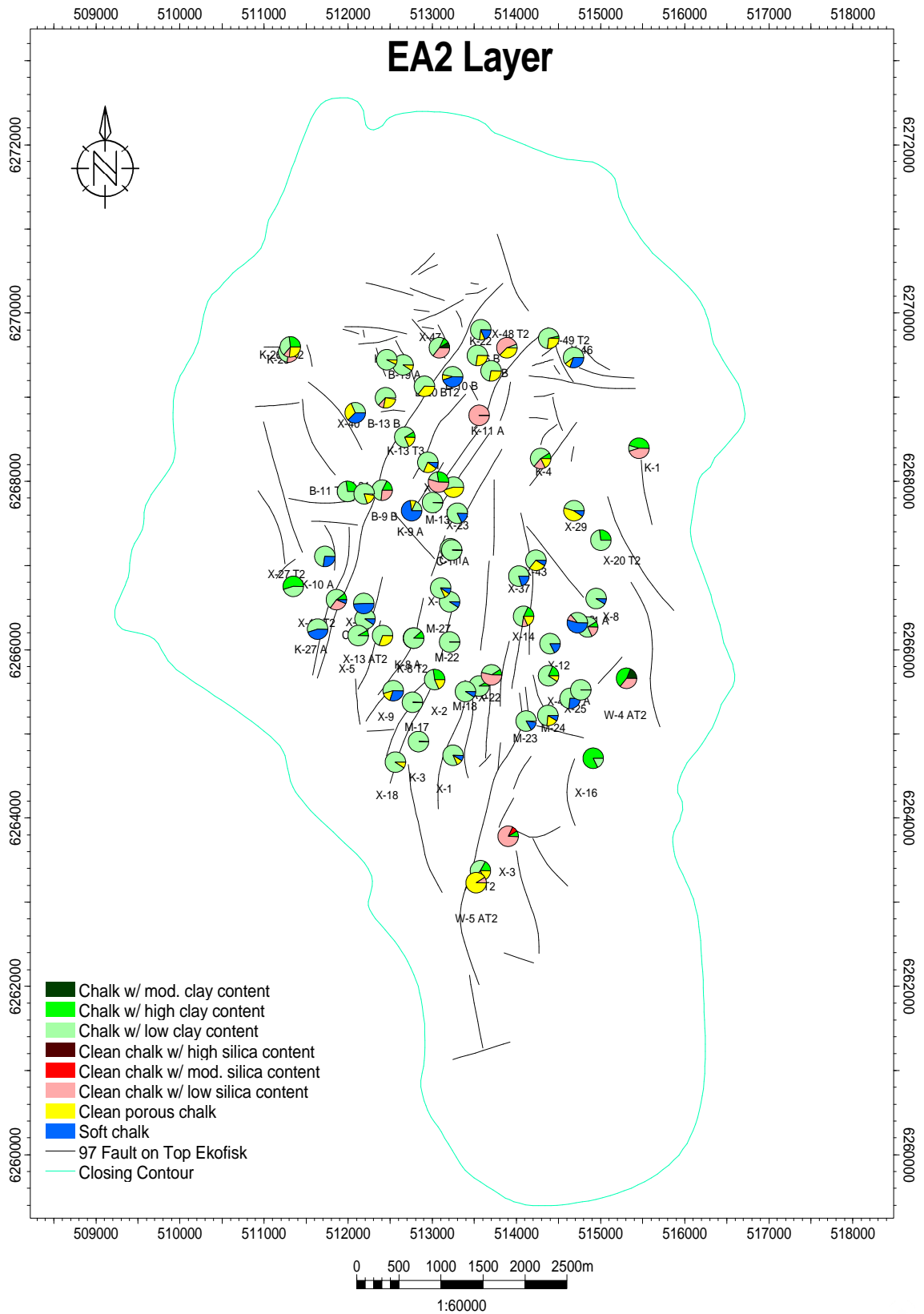
Project: total_ekofisk_well_201112_r1.pet (06/11/2012)





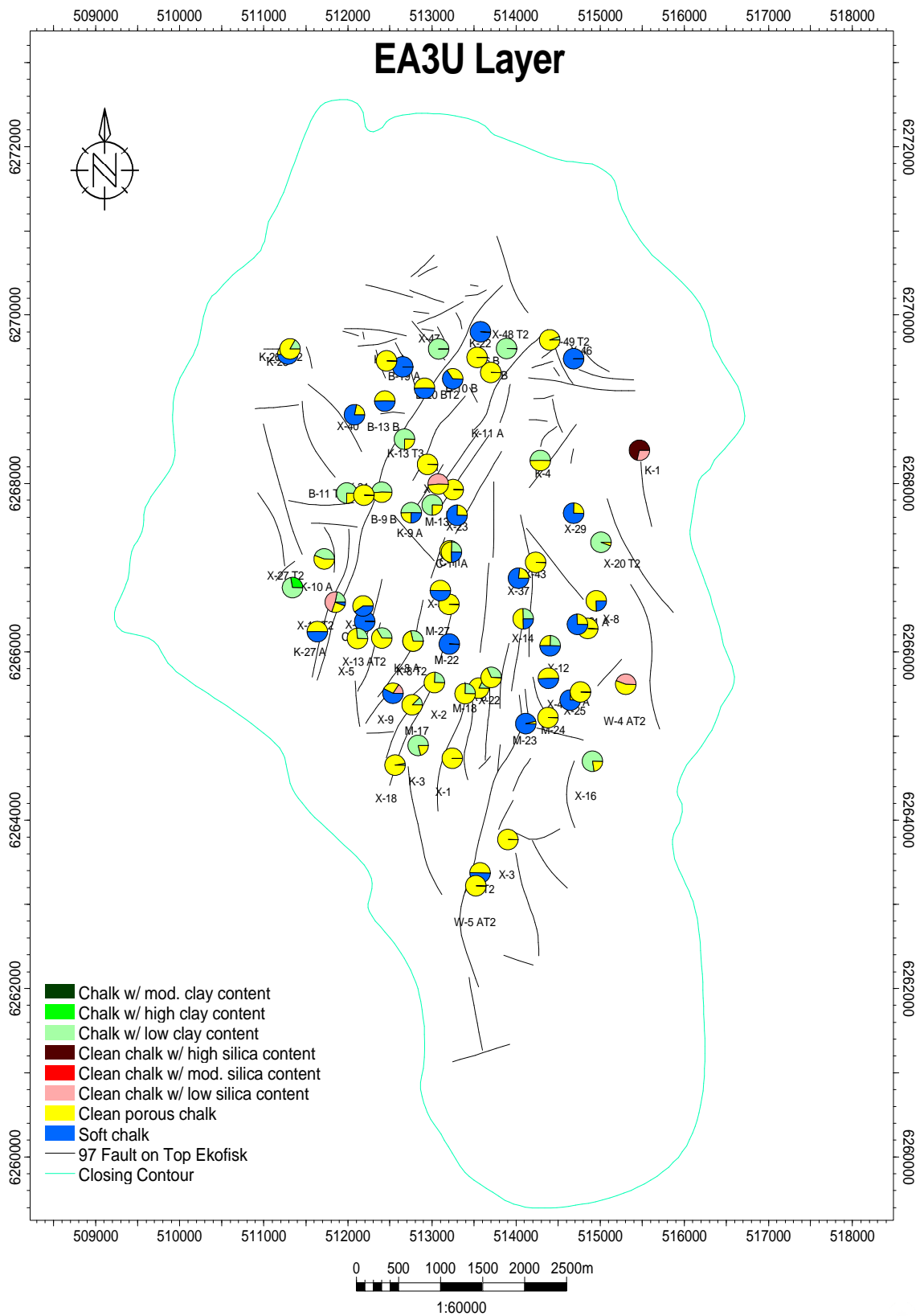
Project: total_ekofisk_well_201112_r1.pet (06/11/2012)





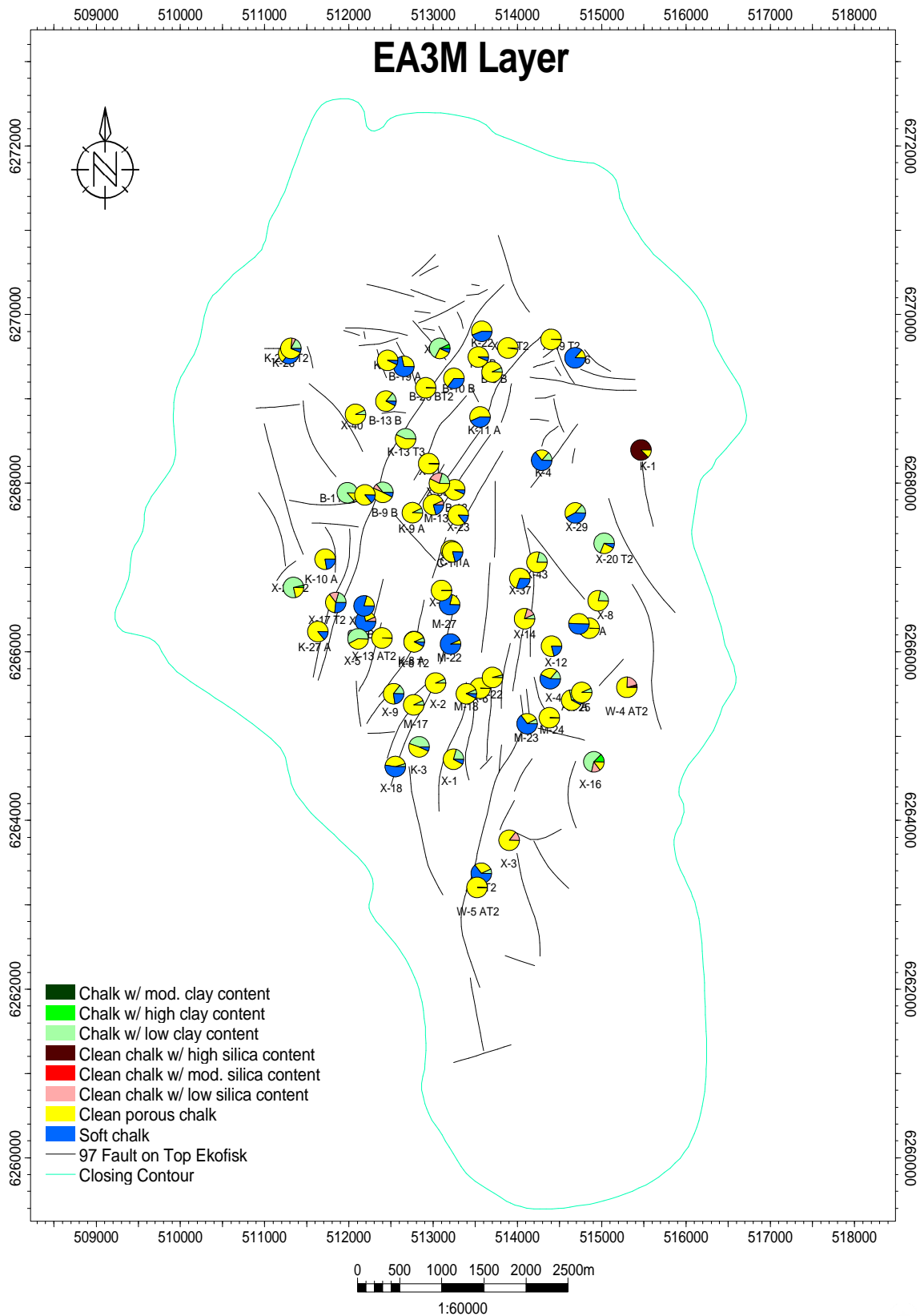
Project: total_ekofisk_well_201112_r1.pet (06/11/2012)





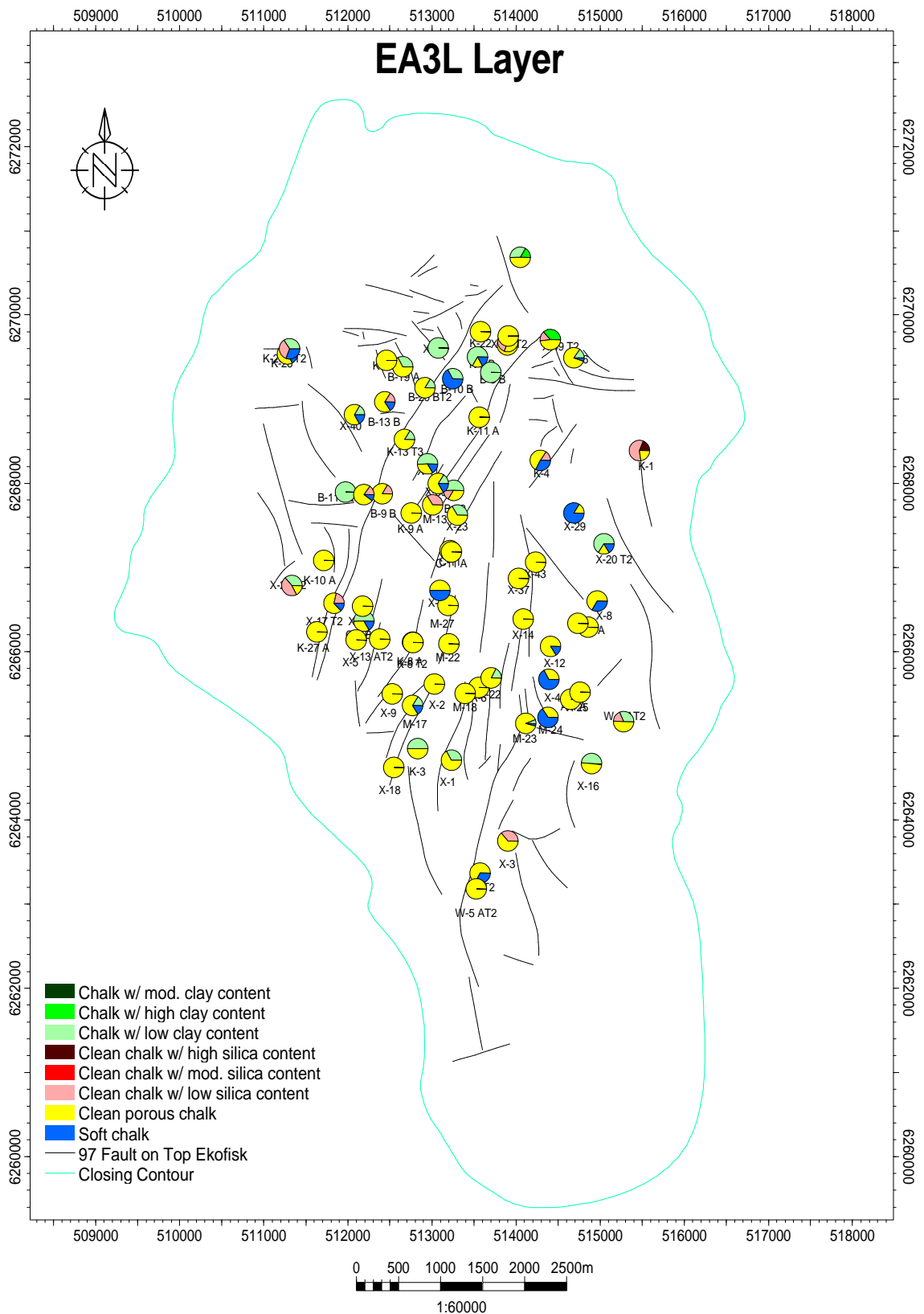
Project: total_ekofisk_well_201112_r1.pet (06/11/2012)





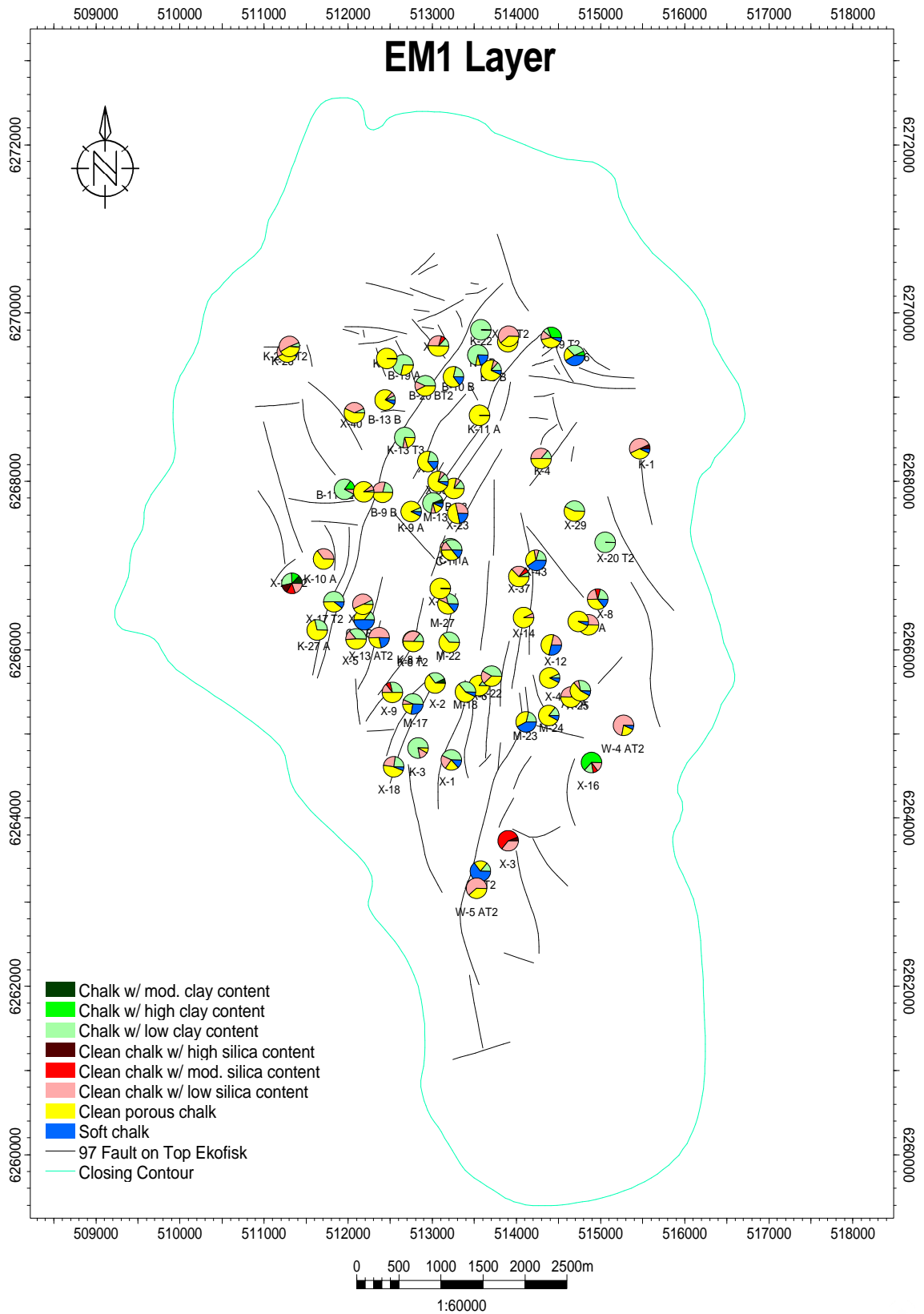
Project: total_ekofisk_well_201112_r1.pet (06/11/2012)





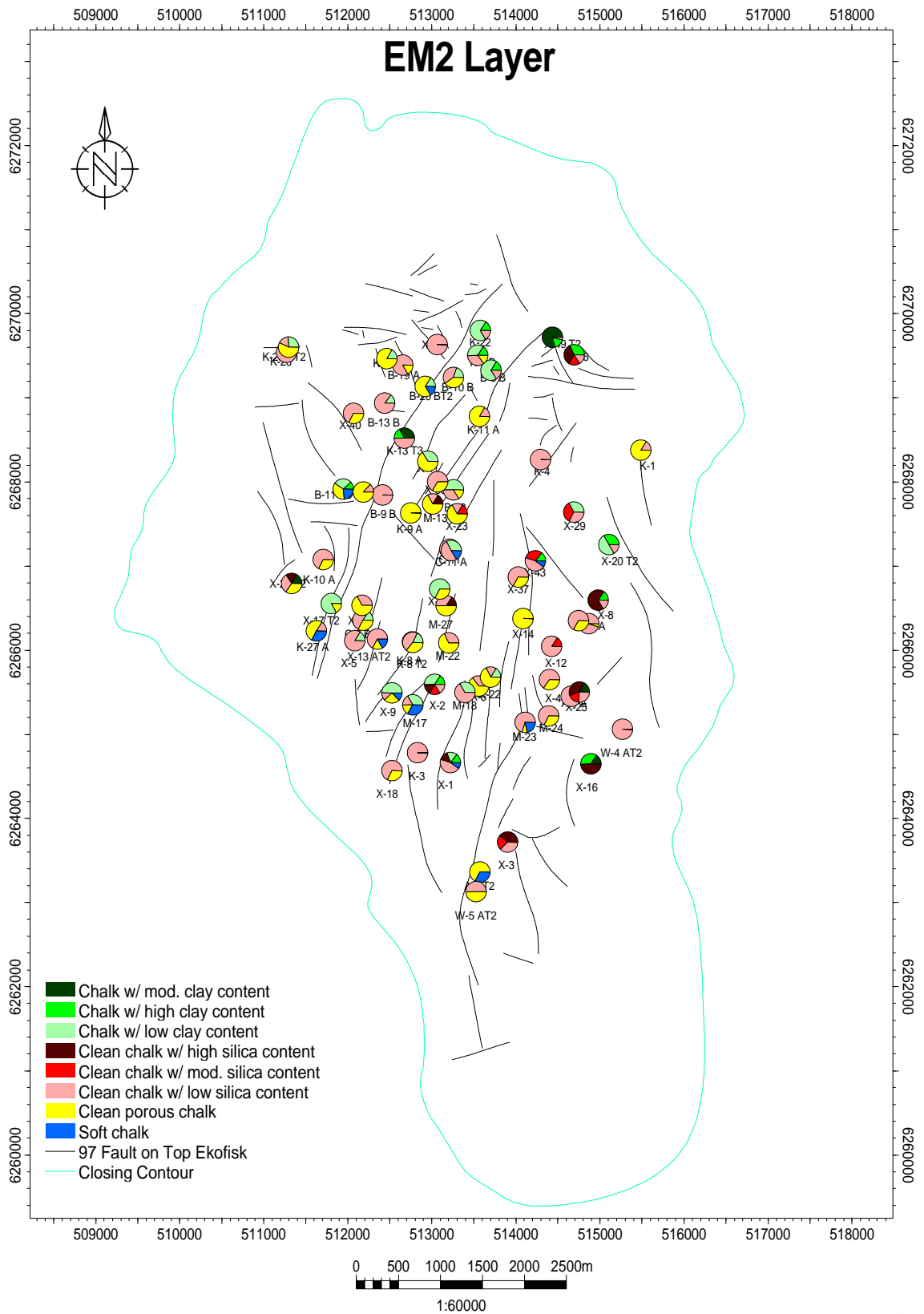
Project: total_ekofisk_well_201112_r1.pet (06/11/2012)





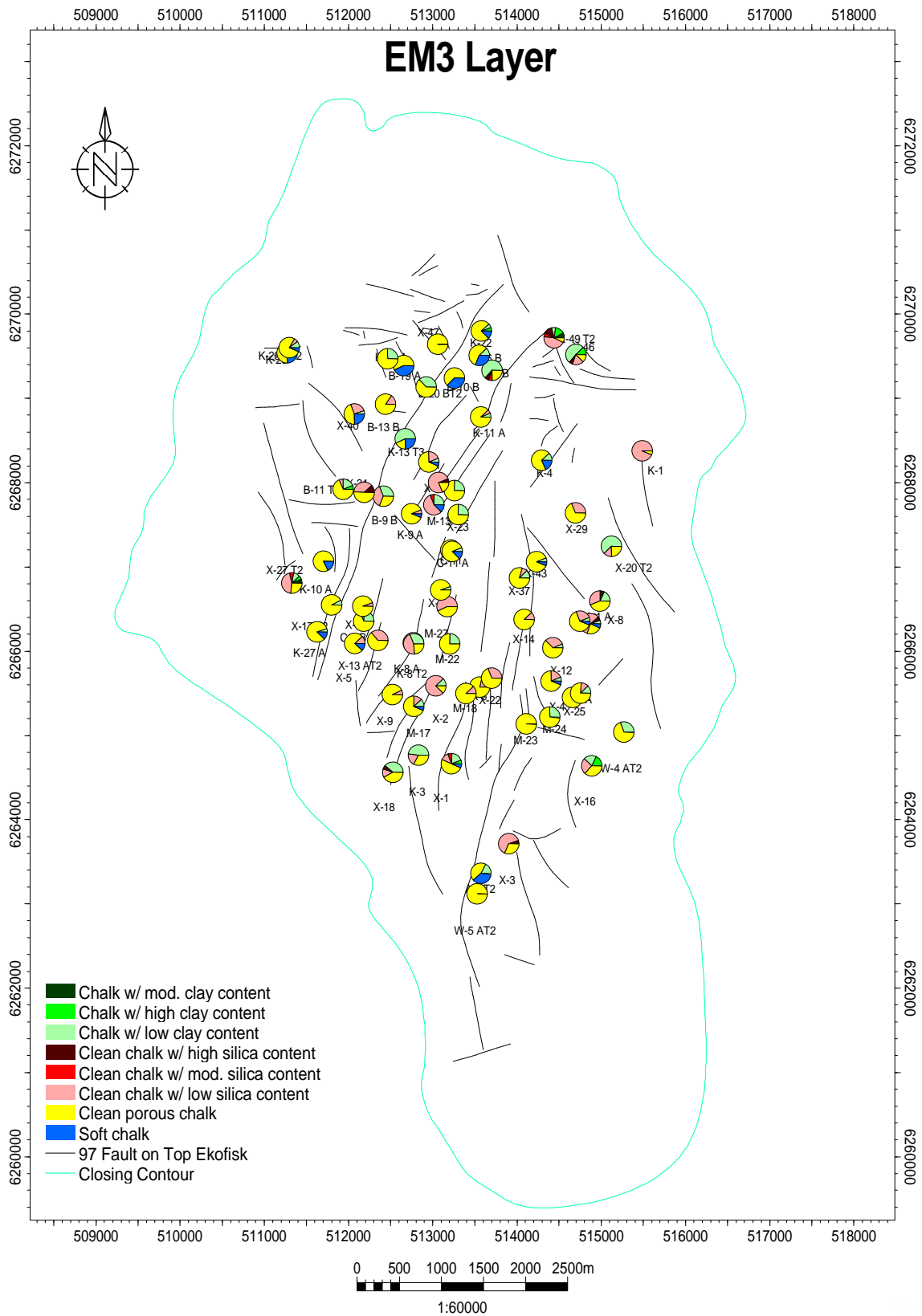
Project: total_ekofisk_well_201112_r1.pet (06/11/2012)





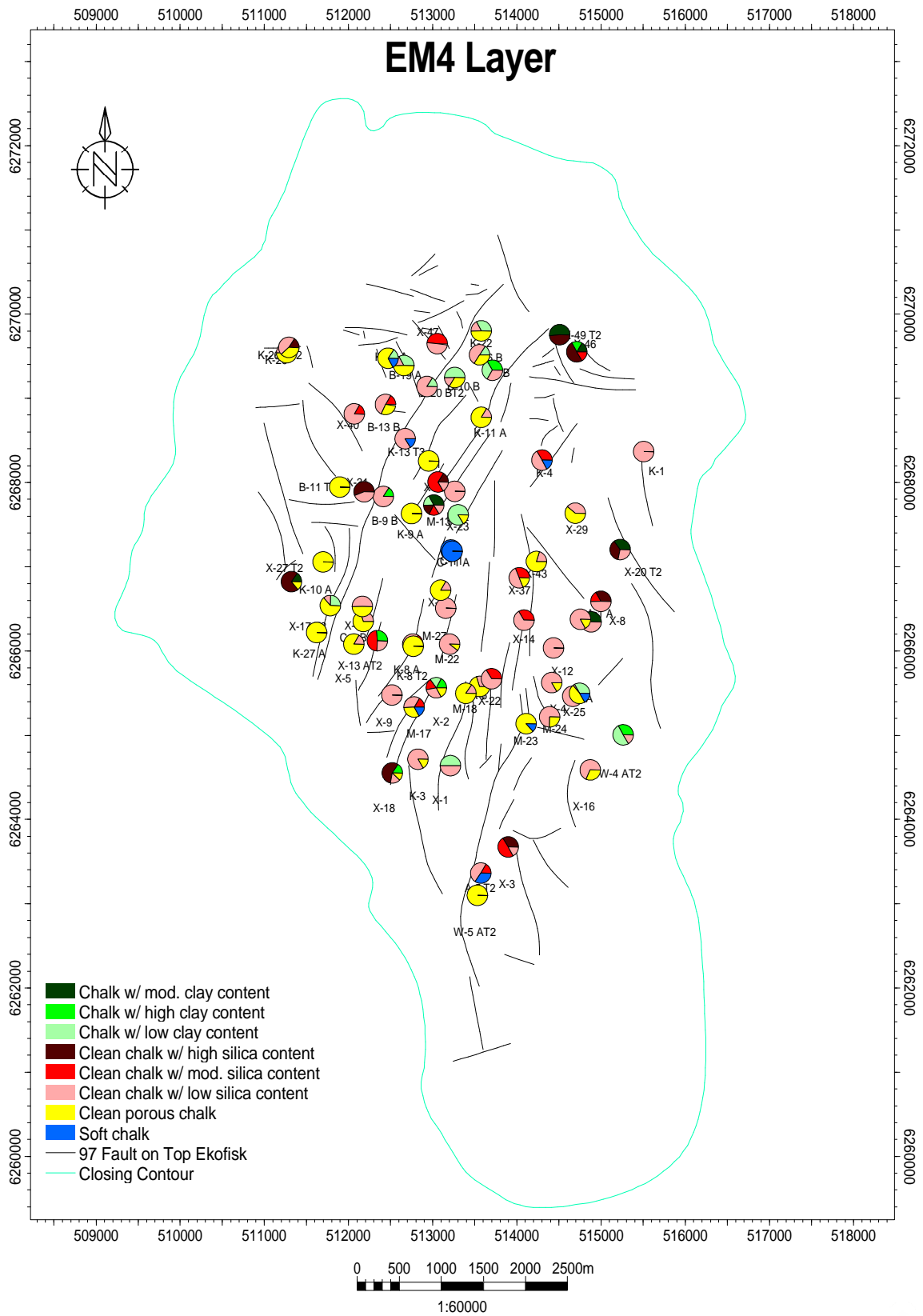
Project: total_ekofisk_well_201112_r1.pet (06/11/2012)





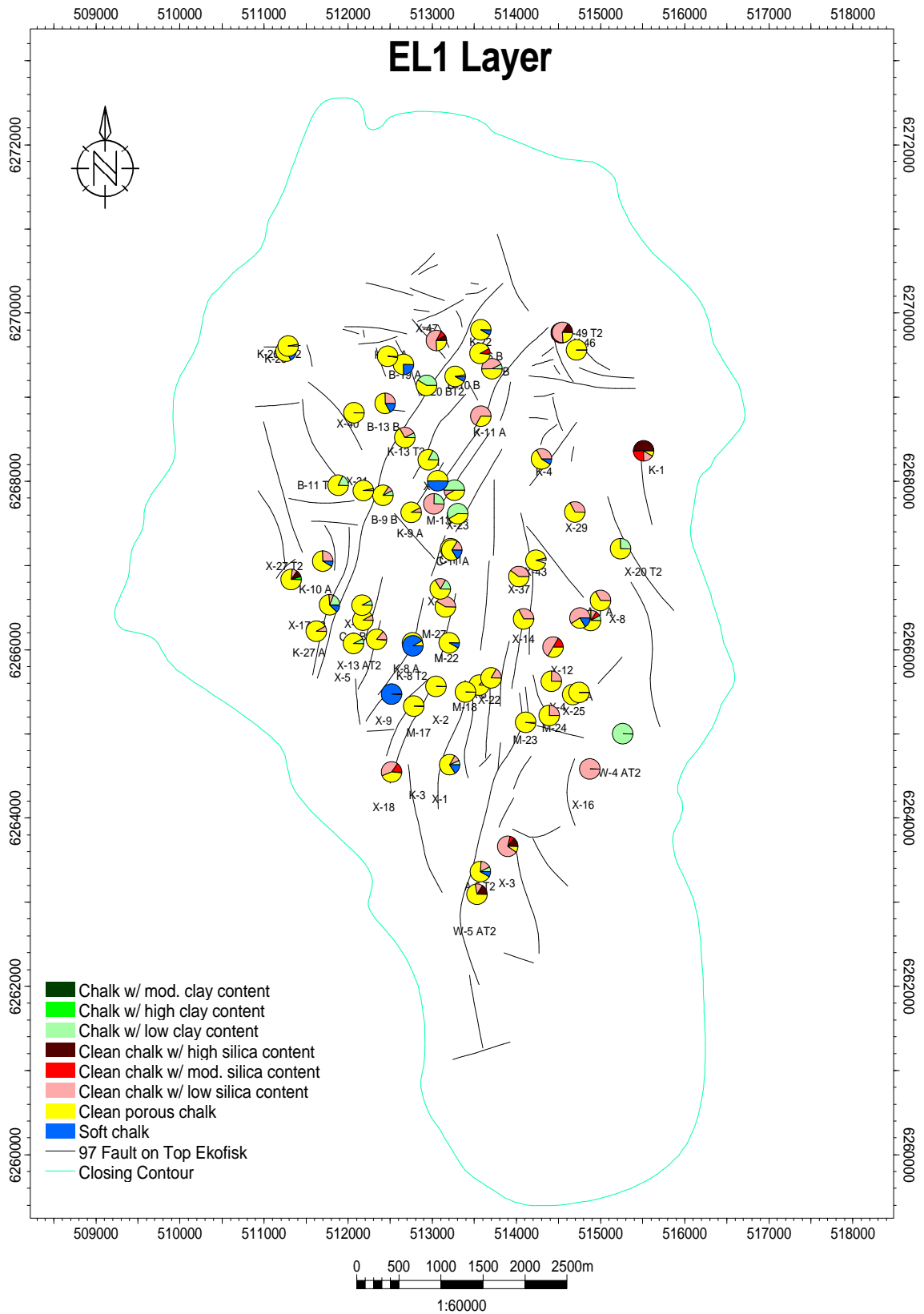
Project: total_ekofisk_well_201112_r1.pet (06/11/2012)

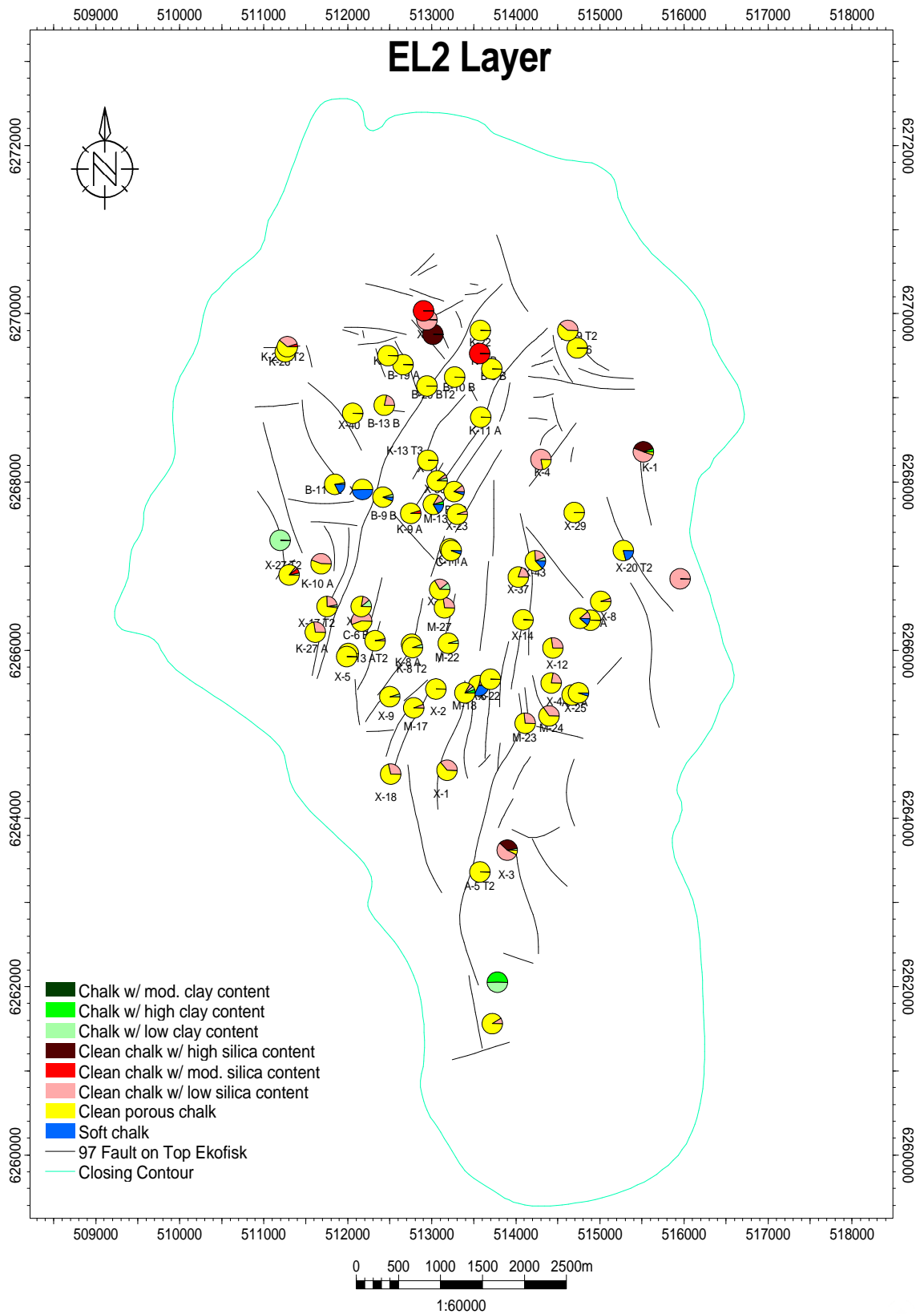




Project: total_ekofisk_well_201112_r1.pet (06/11/2012)

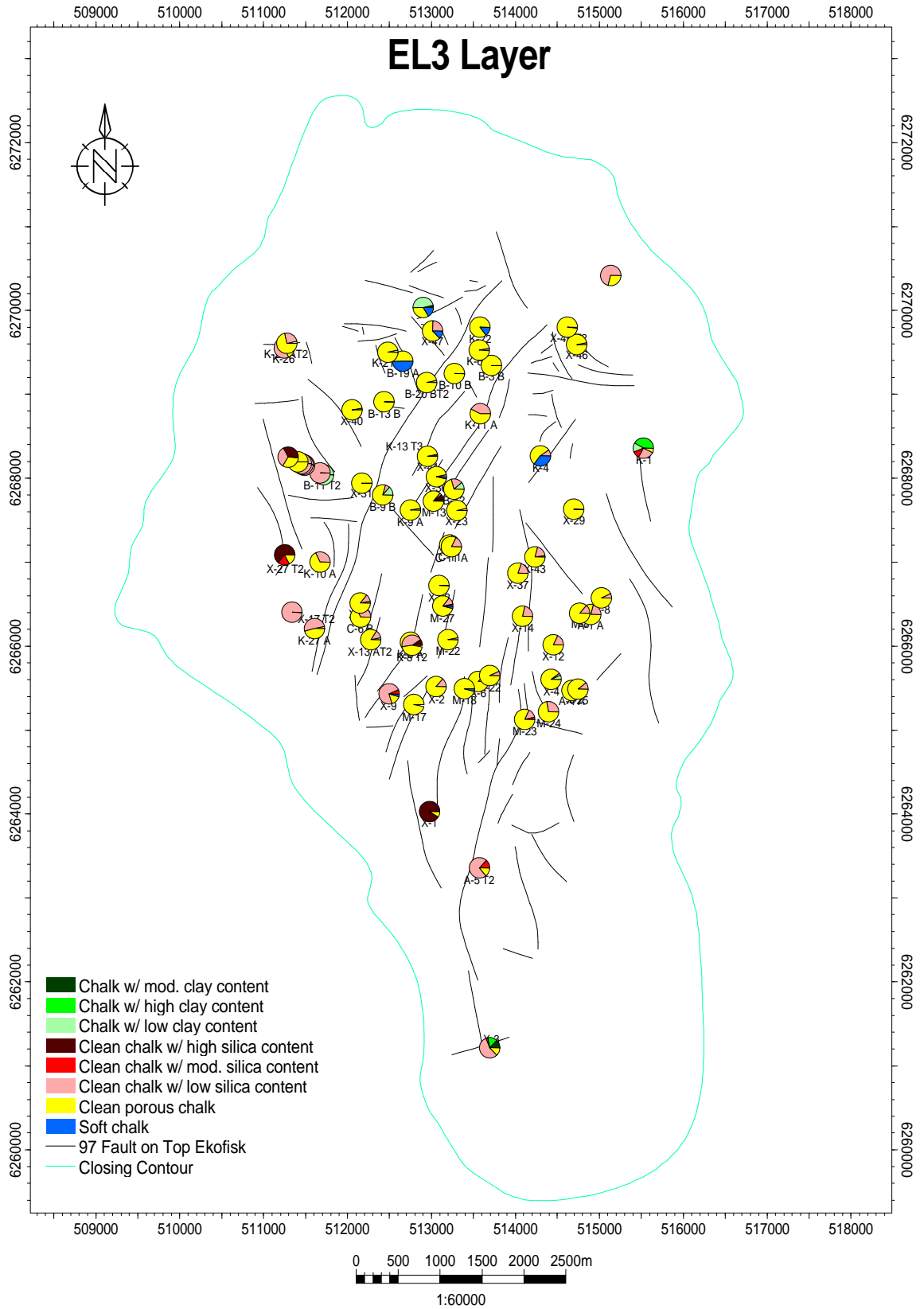






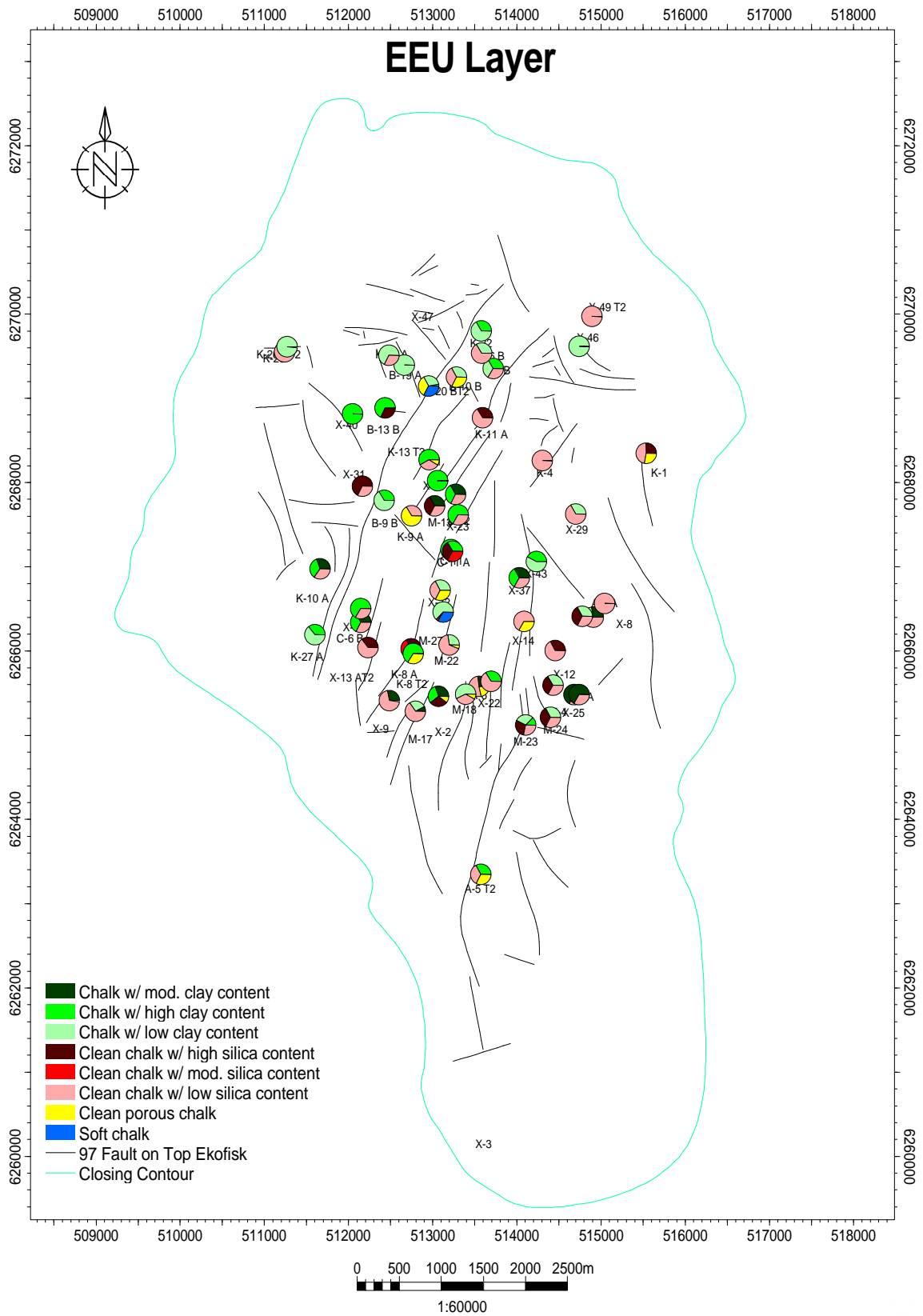
Project: total_ekofisk_well_201112_r1.pet (06/11/2012)





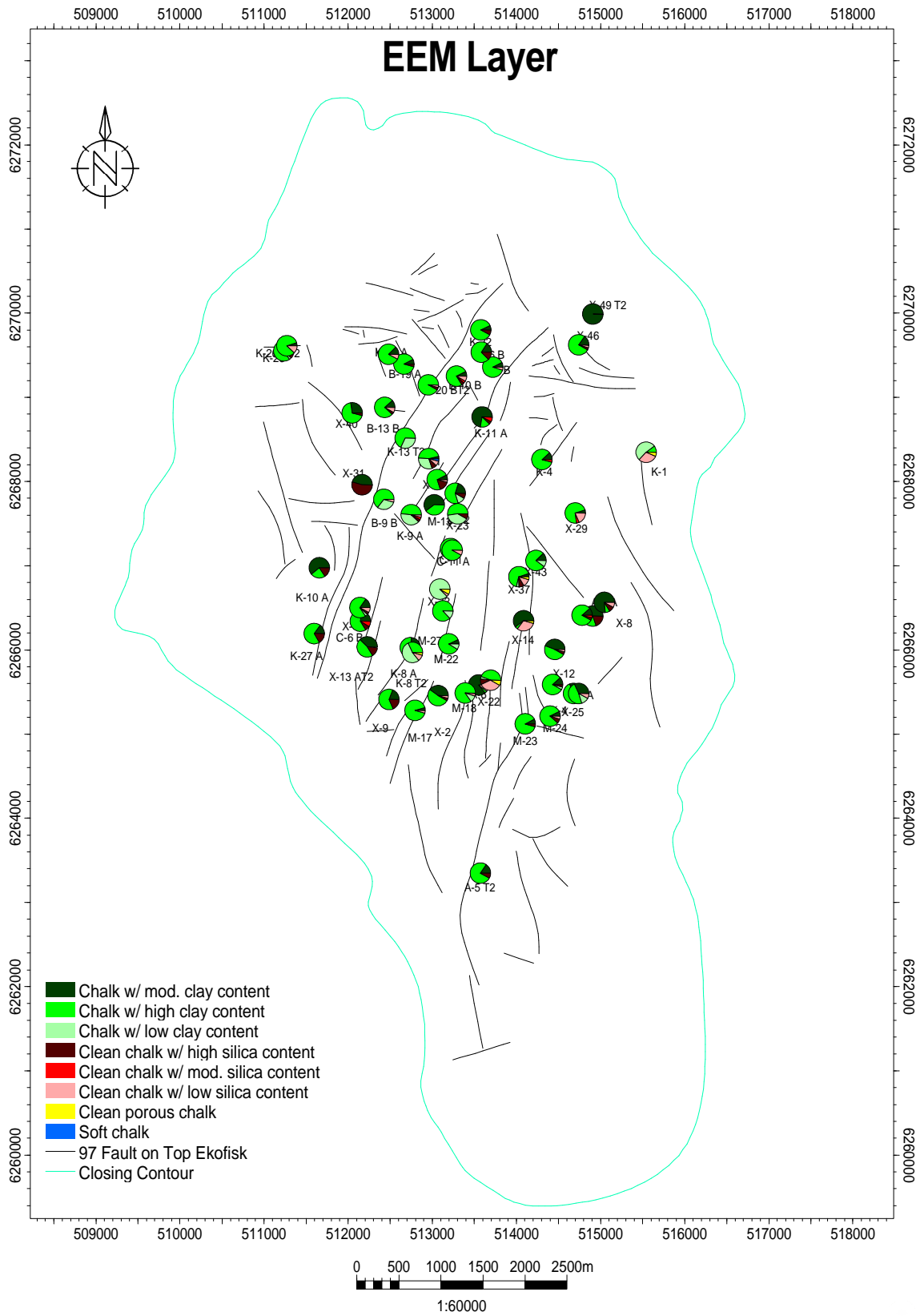
Project: total_ekofisk_well_201112_r1.pet (06/11/2012)





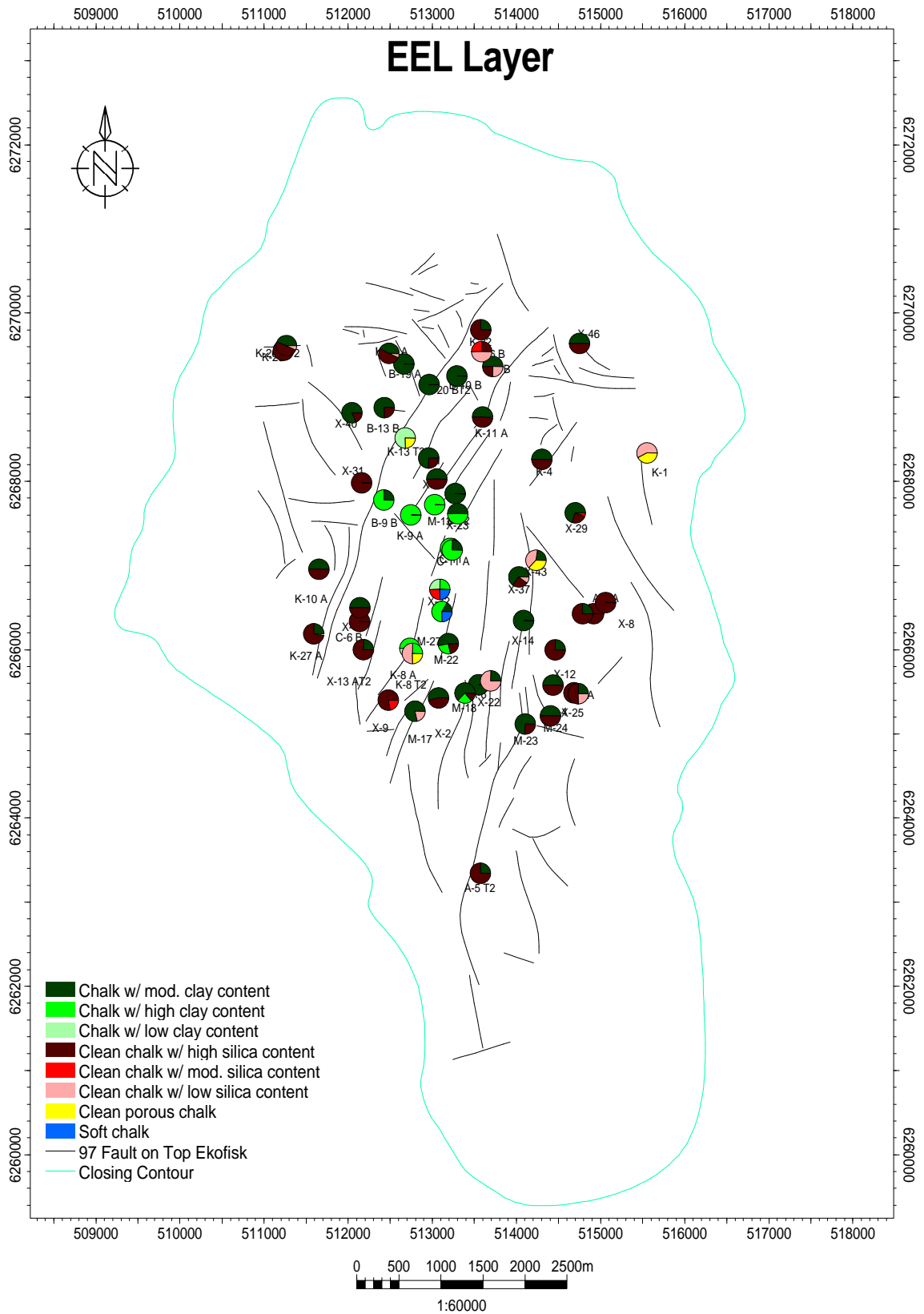
Project: total_ekofisk_well_201112_r1.pet (06/11/2012)





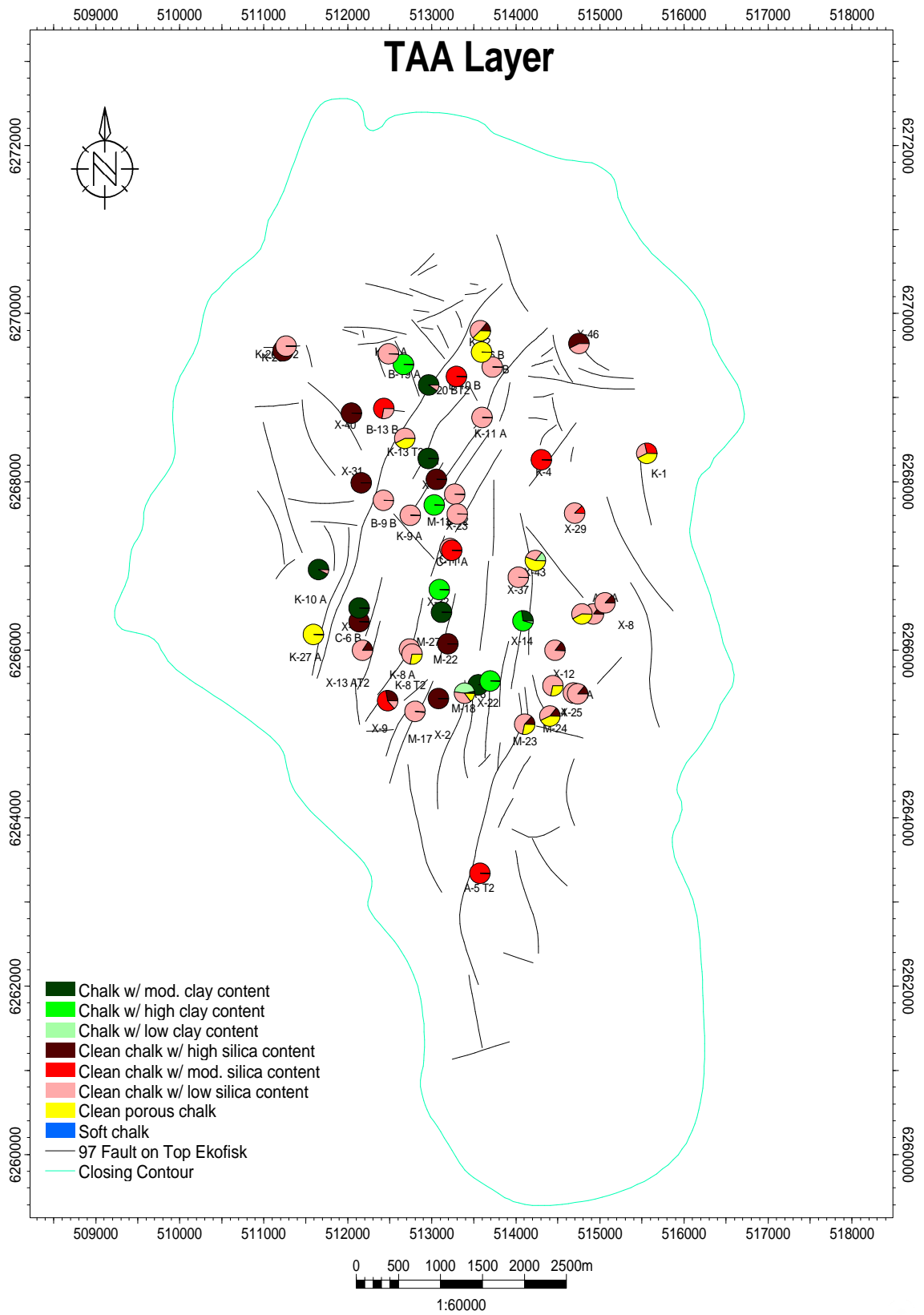
Project: total_ekofisk_well_201112_r1.pet (06/11/2012)





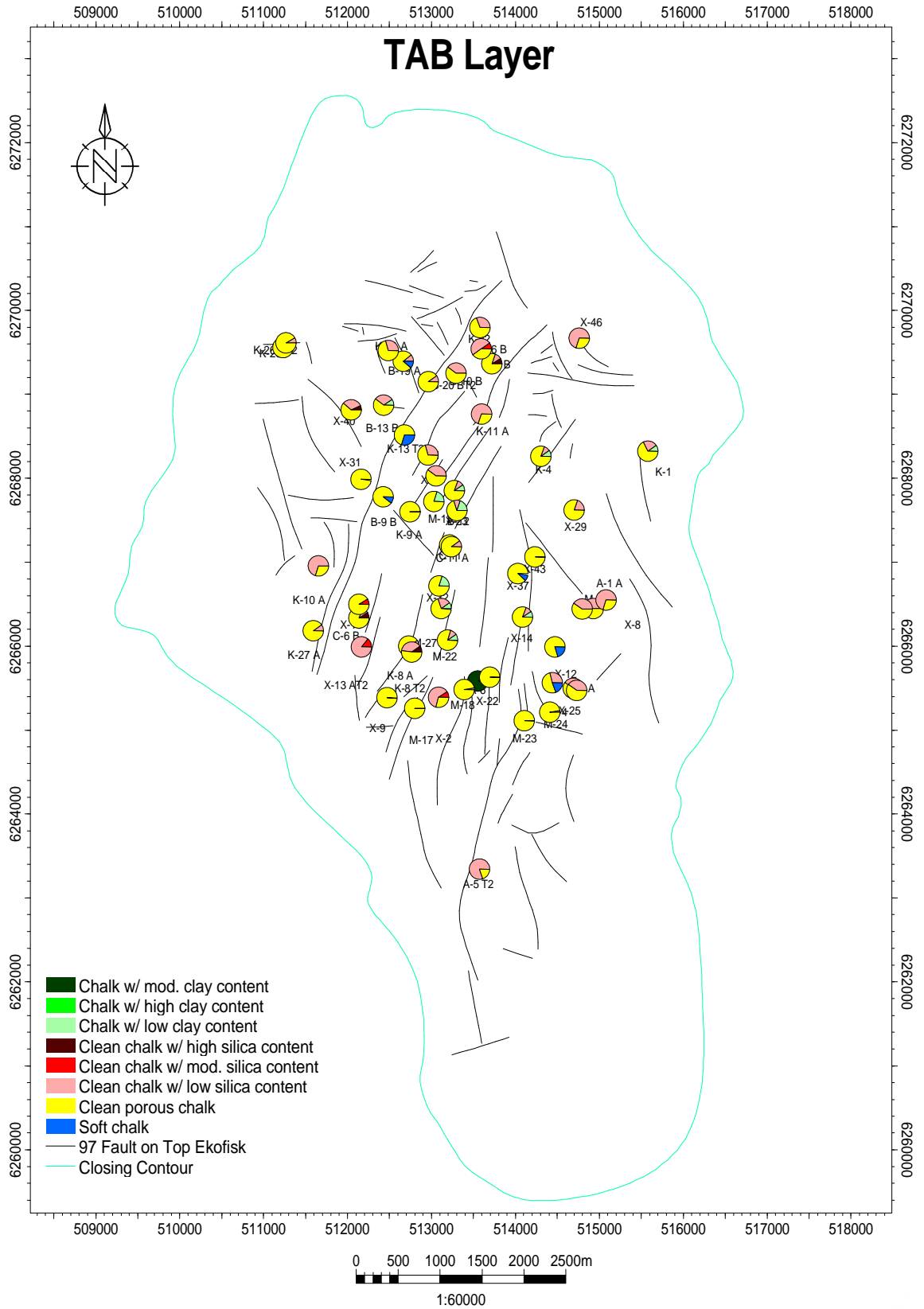
Project: total_ekofisk_well_201112_r1.pet (06/11/2012)





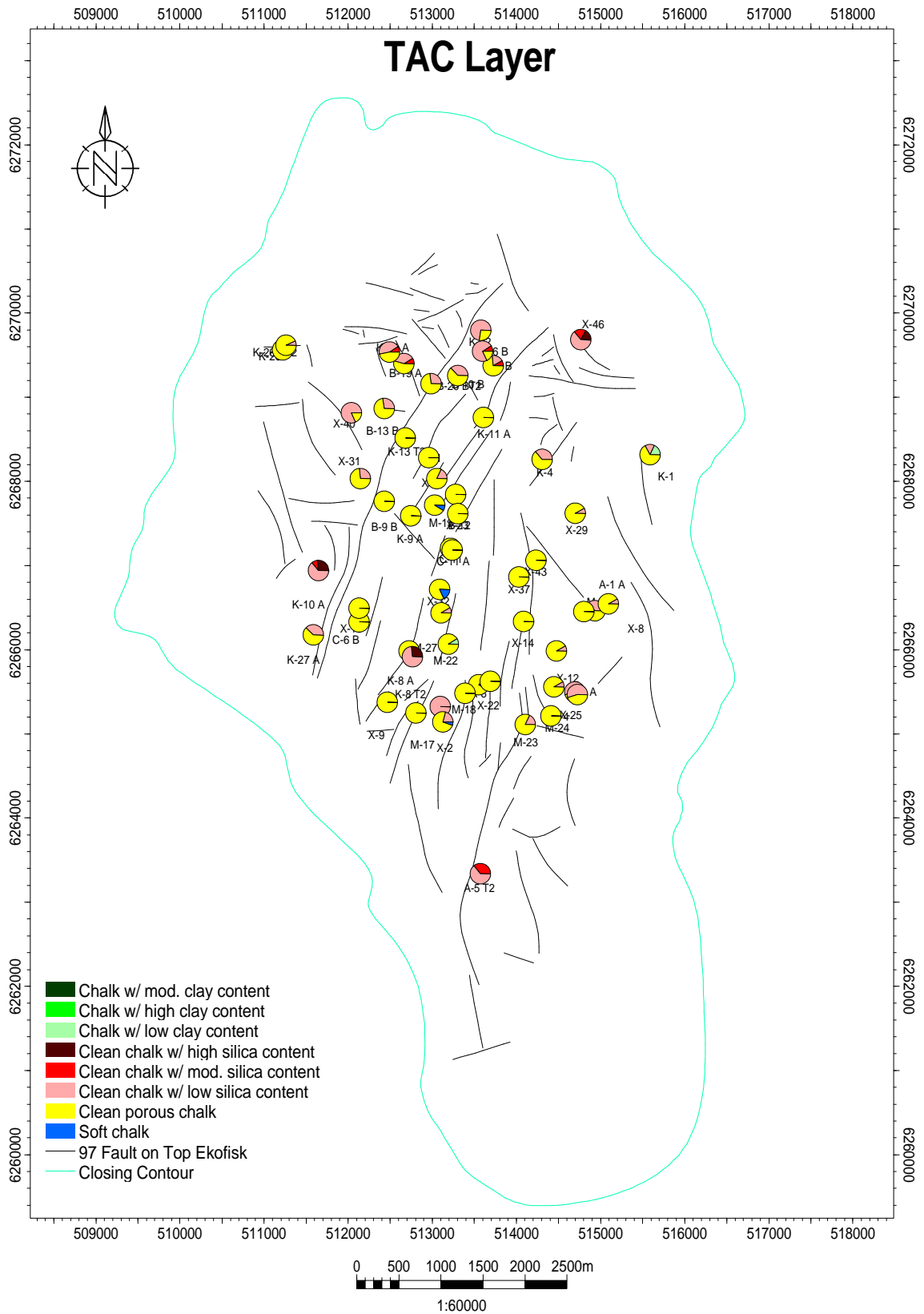
Project: total_ekofisk_well_201112_r1.pet (06/11/2012)





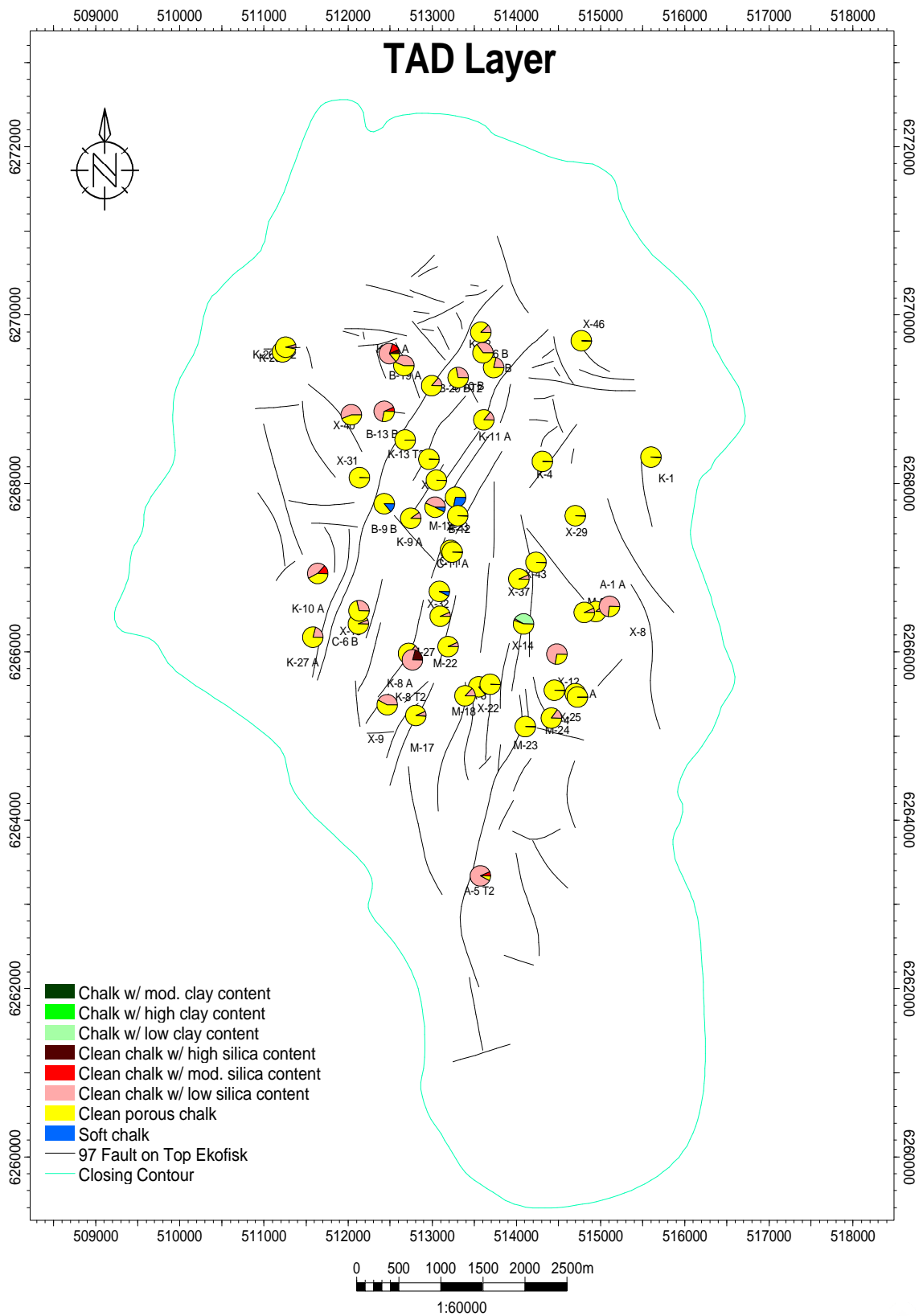
Project: total_ekofisk_well_201112_r1.pet (06/11/2012)





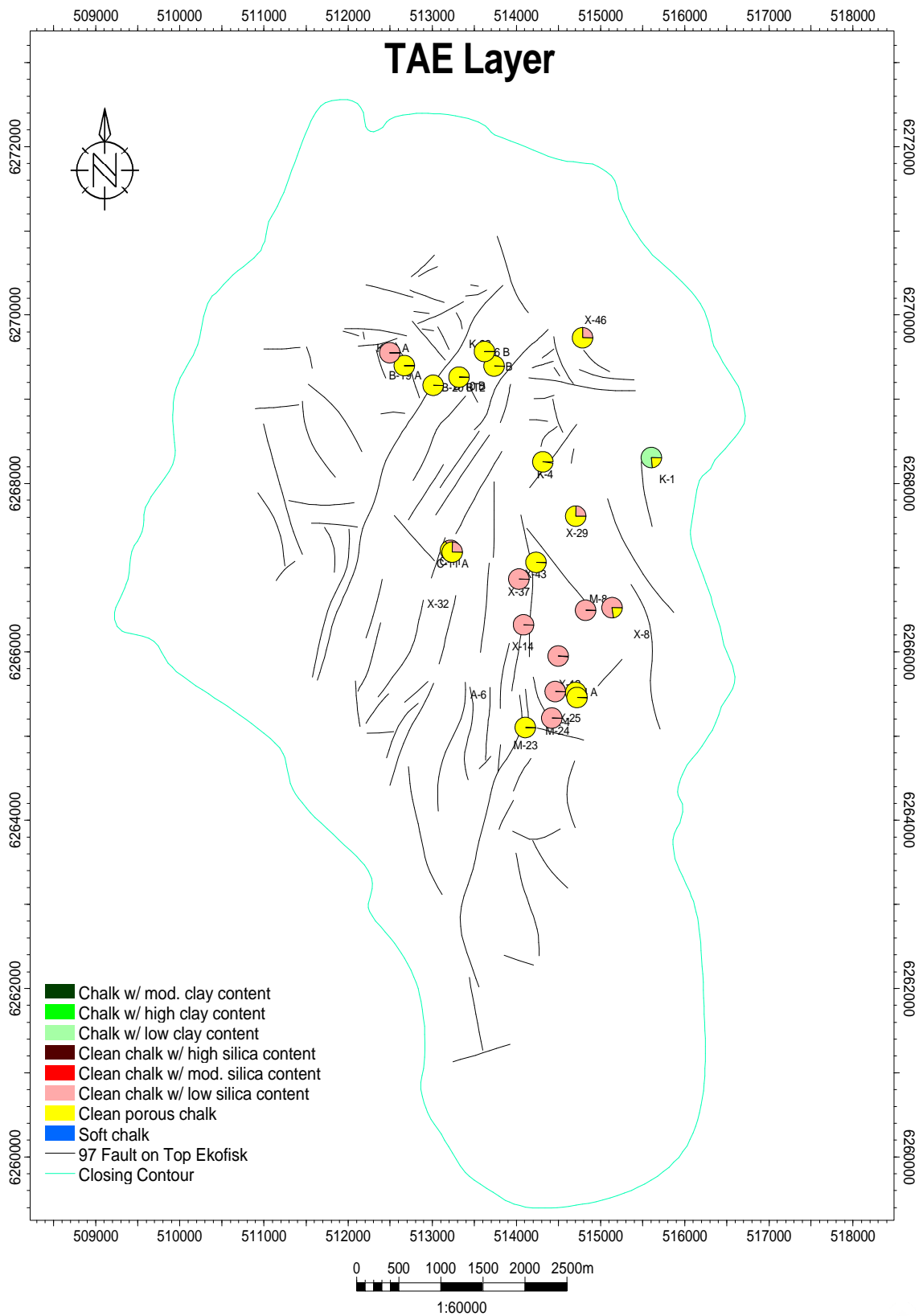
Project: total_ekofisk_well_201112_r1.pet (06/11/2012)





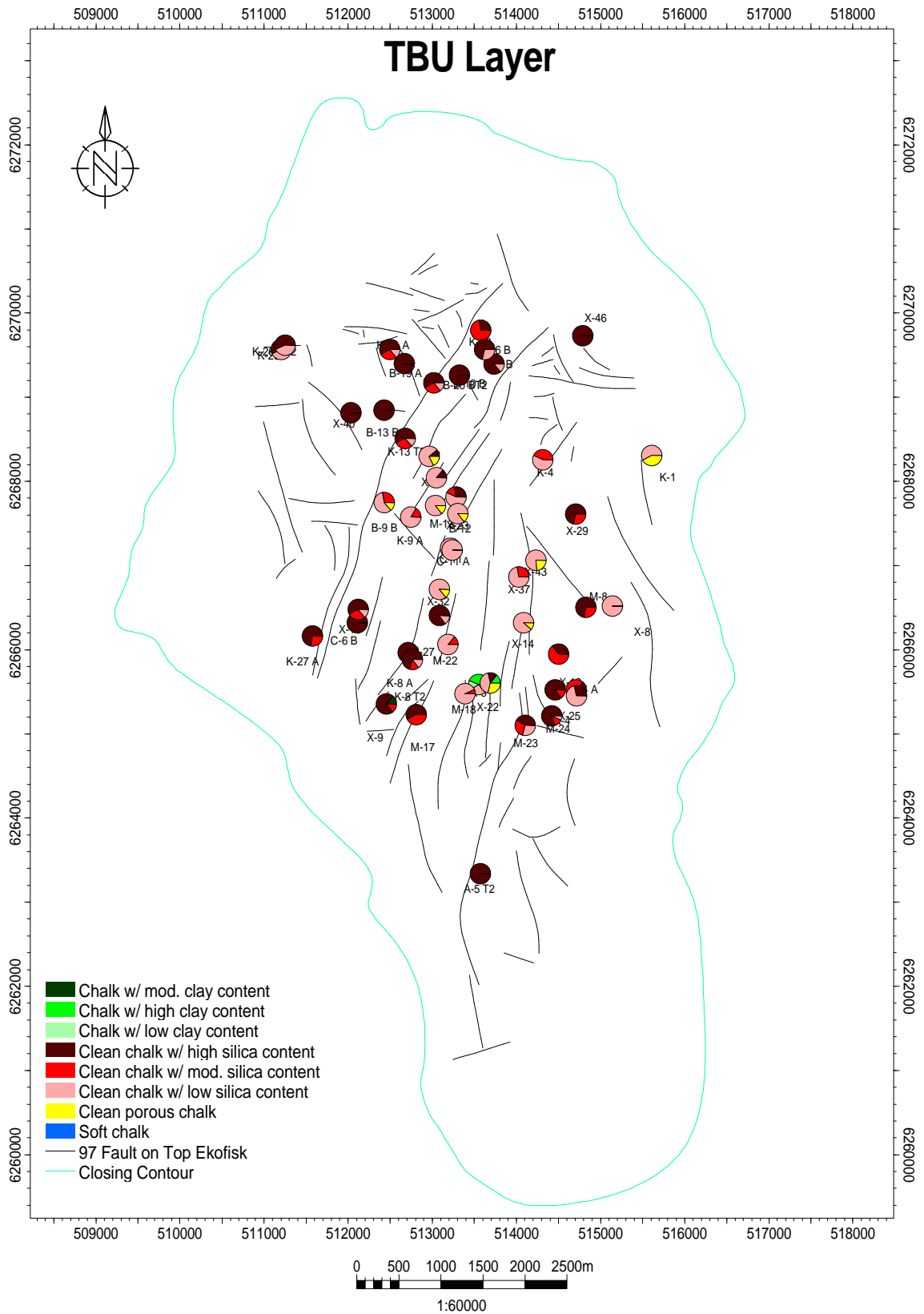
Project: total_ekofisk_well_201112_r1.pet (06/11/2012)





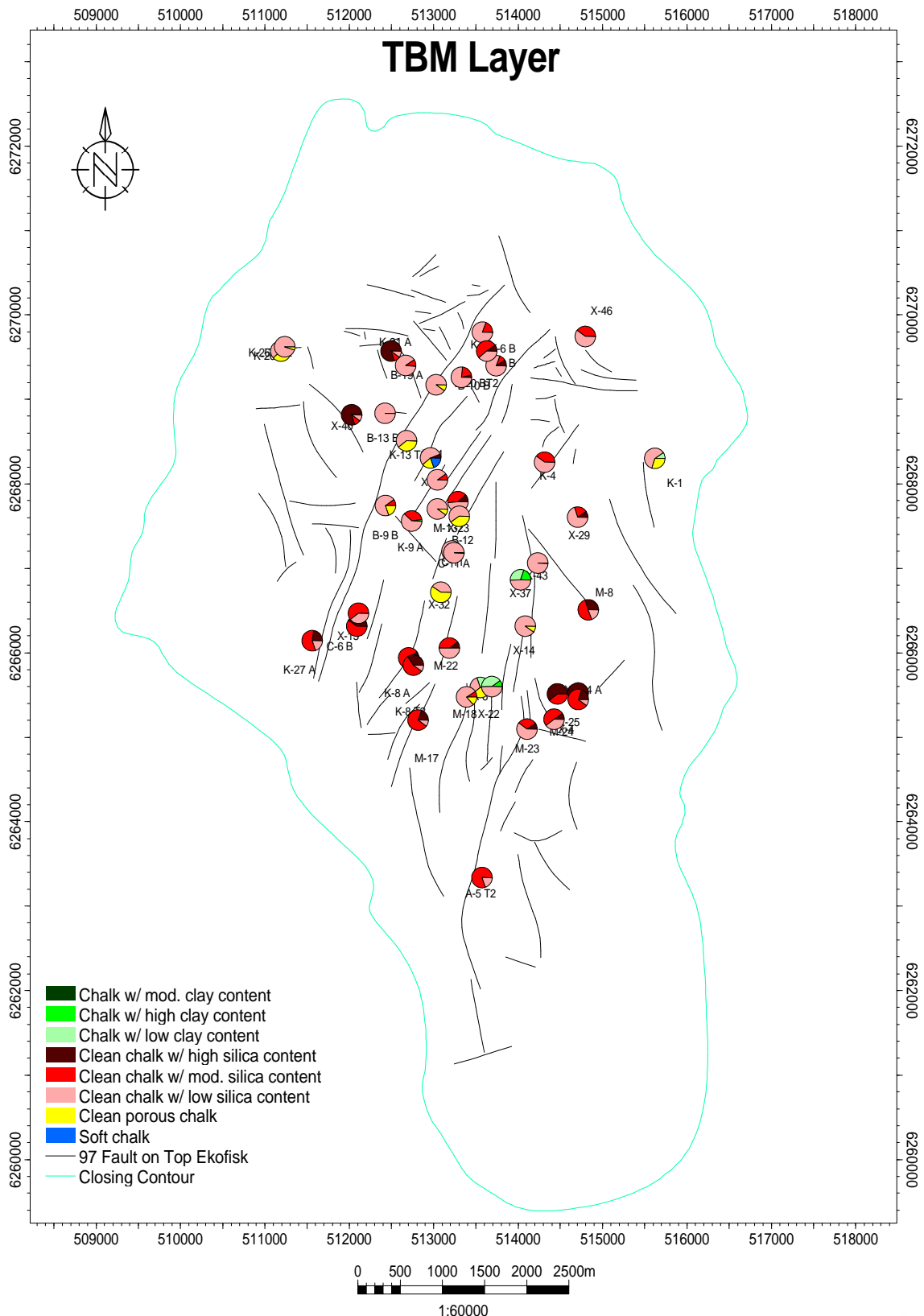
Project: total_ekofisk_well_201112_r1.pet (06/11/2012)





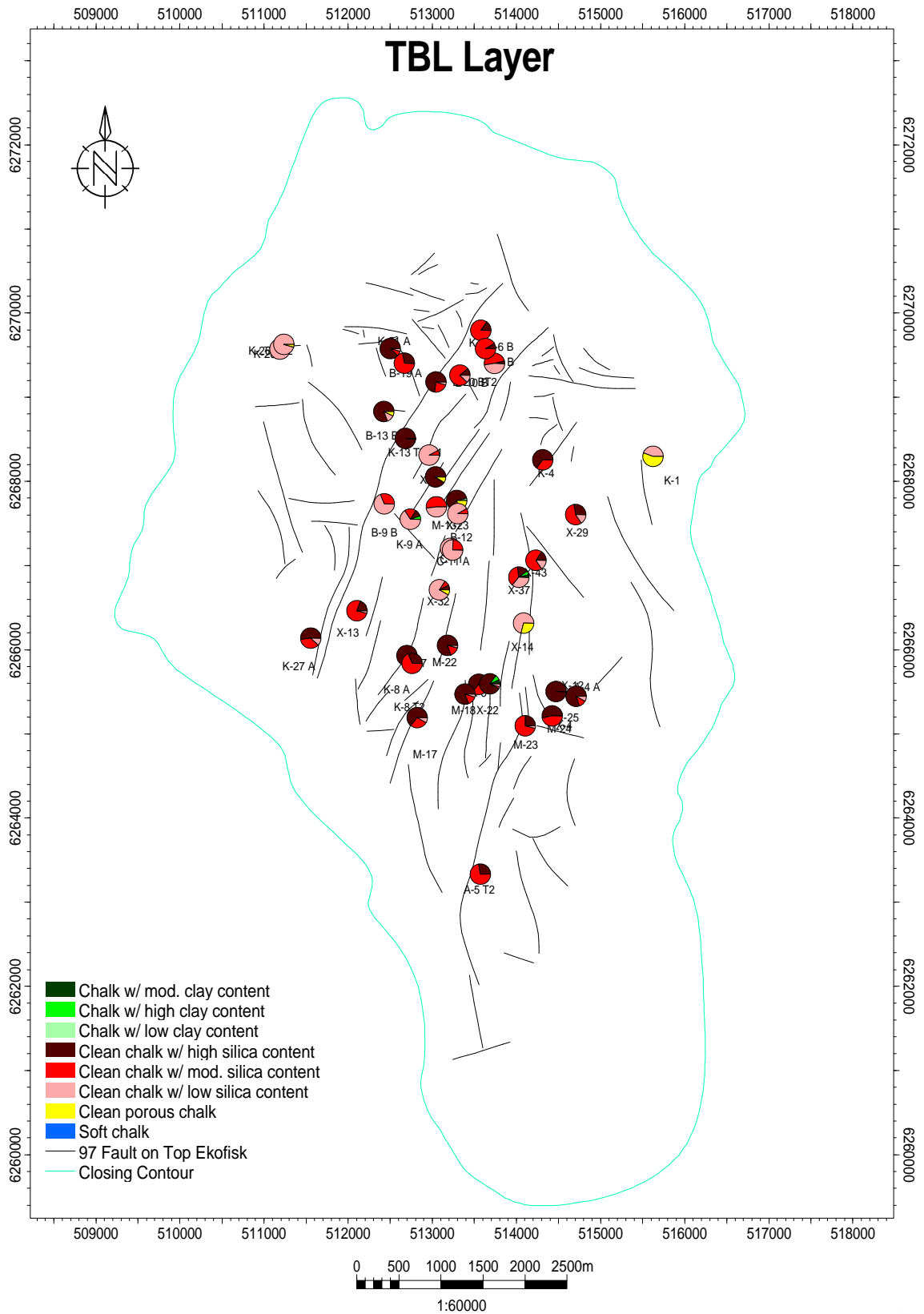
Project: total_ekofisk_well_201112_r1.pet (06/11/2012)





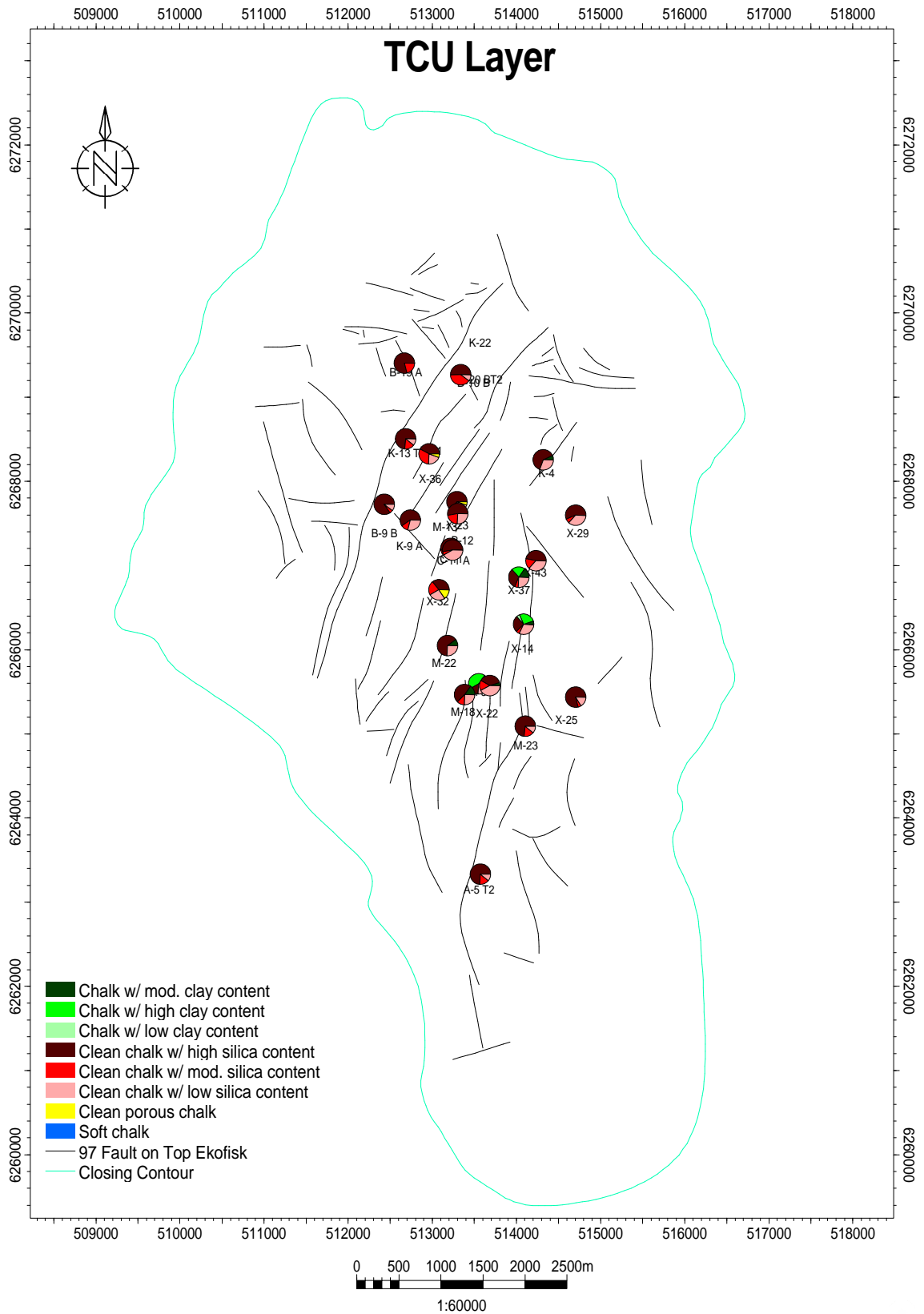
Project: total_ekofisk_well_201112_r1.pet (06/11/2012)





Project: total_ekofisk_well_201112_r1.pet (06/11/2012)



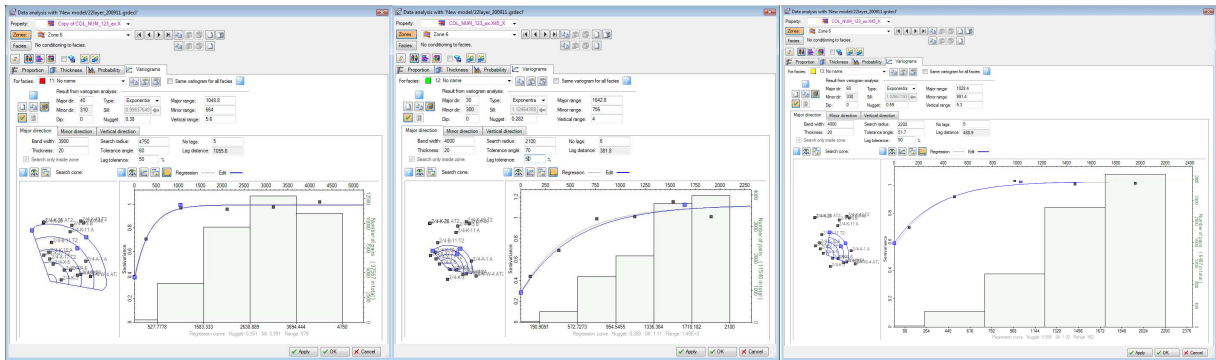


Project: total_ekofisk_well_201112_r1.pet (06/11/2012)

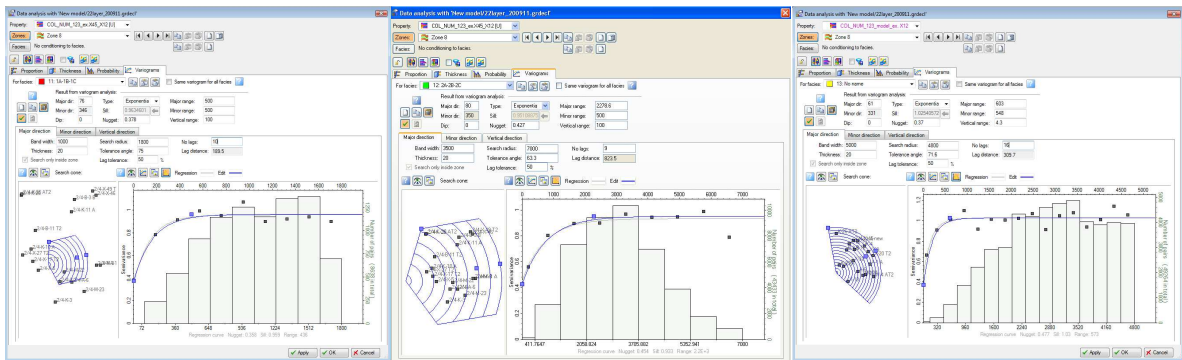


Appendix 4.3 Variogram analysis of 3 facies model

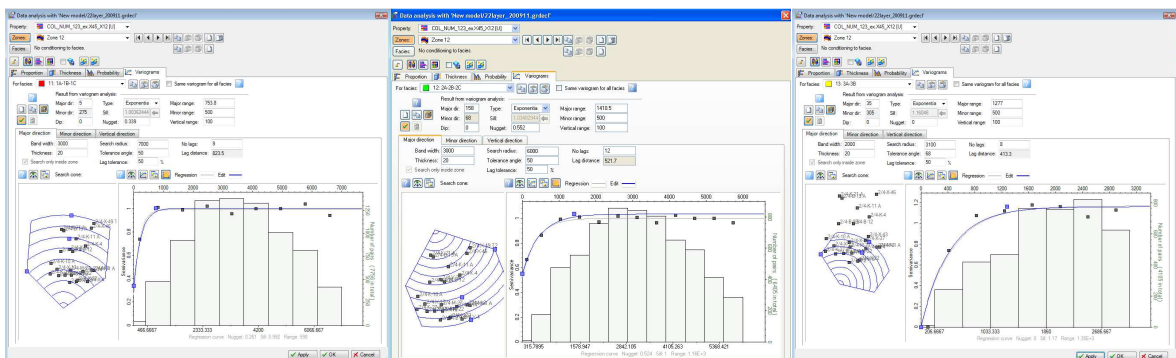
MAJOR DIRECTION



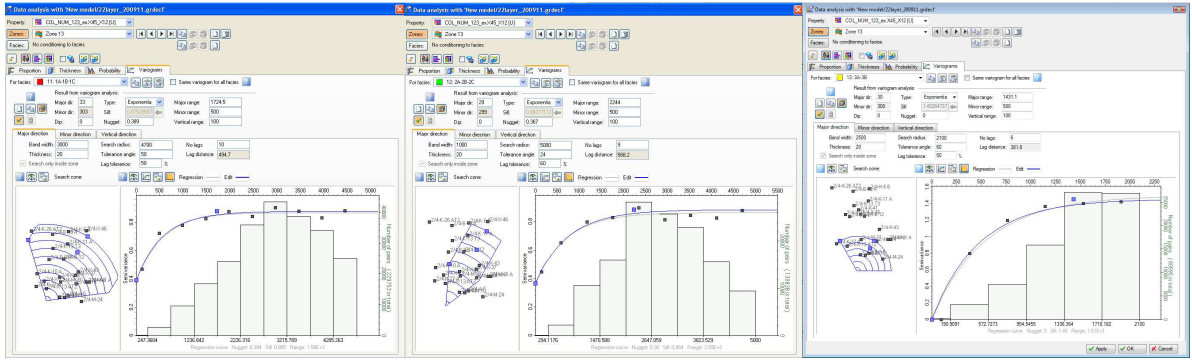
LAYER EM2 – Facies 1 (left) , Facies 2 (middle) and Facies 3 (right)



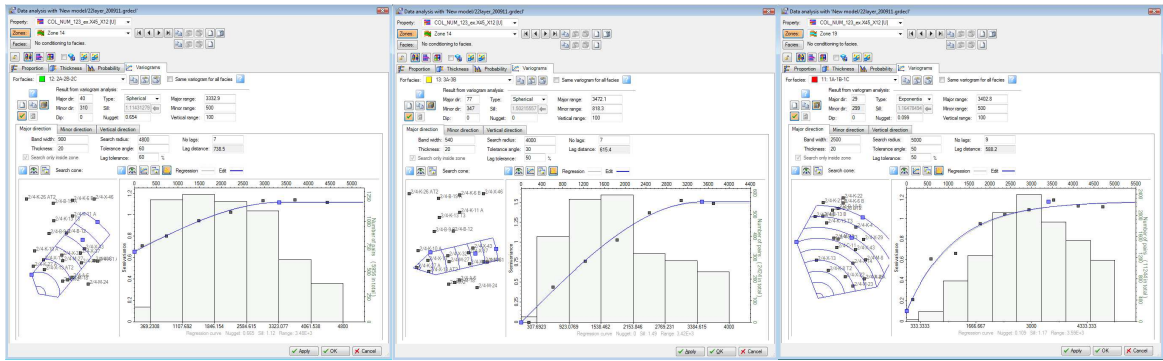
LAYER EM4 – Facies 1 (left) , Facies 2 (middle) and Facies 3 (right)



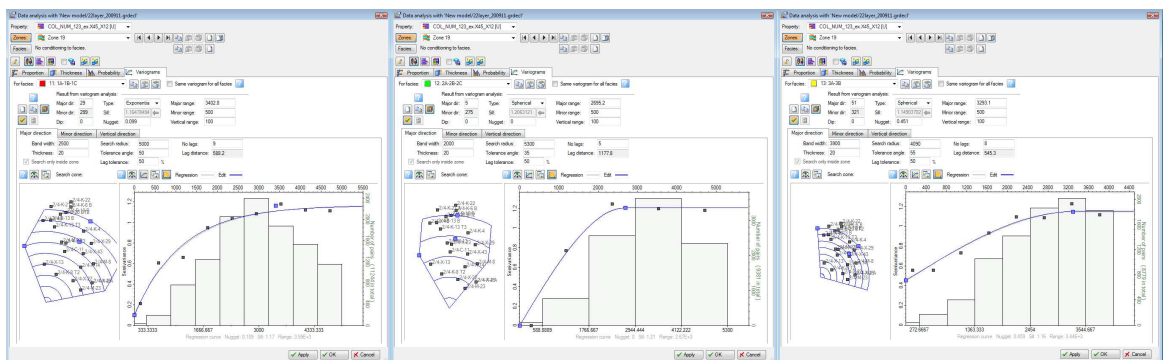
LAYER EEU – Facies 1 (left) , Facies 2 (middle) and Facies 3 (right)



LAYER EEM – Facies 1 (left) , Facies 2 (middle) and Facies 3 (right)

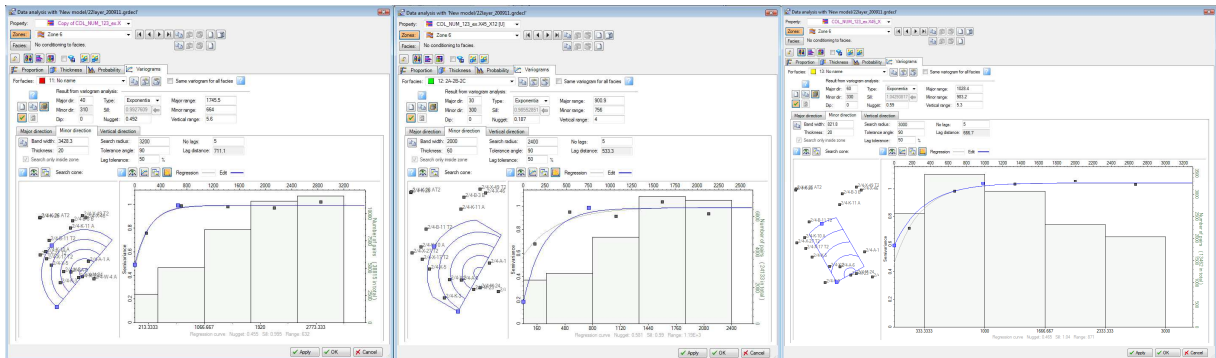


LAYER EEL – Facies 1 (left) , Facies 2 (middle) and Facies 3 (right)

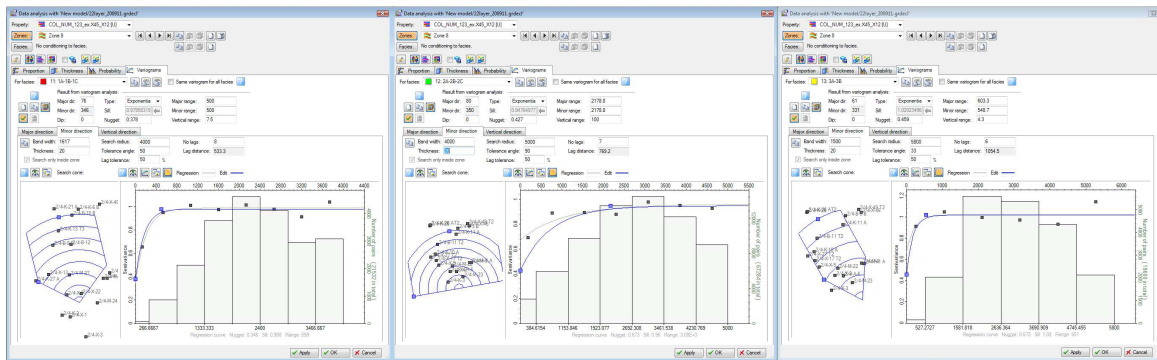


LAYER TBU – Facies 1 (left) , Facies 2 (middle) and Facies 3 (right)

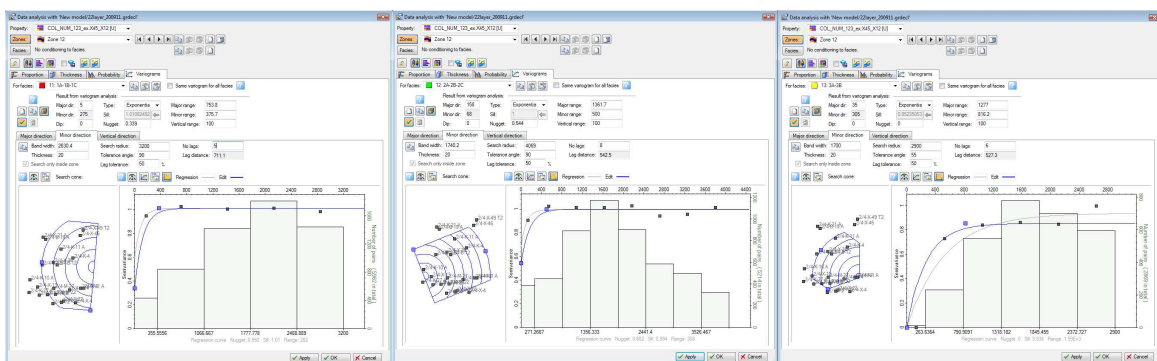
MINOR DIRECTION



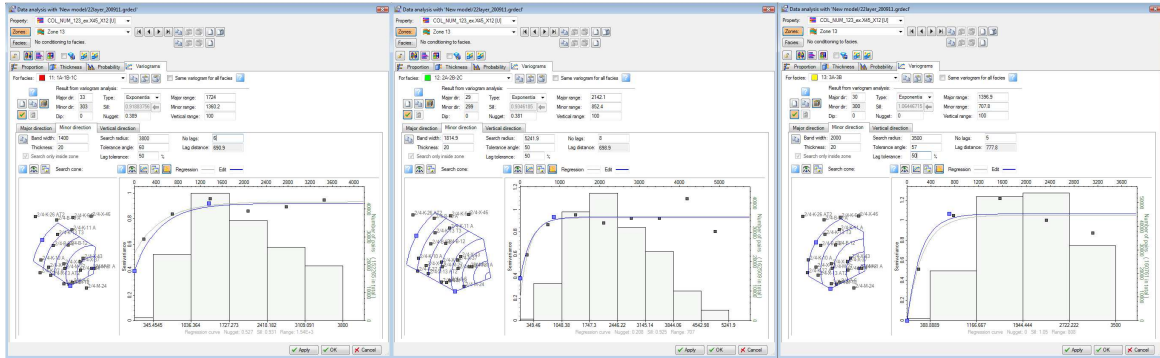
LAYER EM2 – Facies 1 (left) , Facies 2 (middle) and Facies 3 (right)



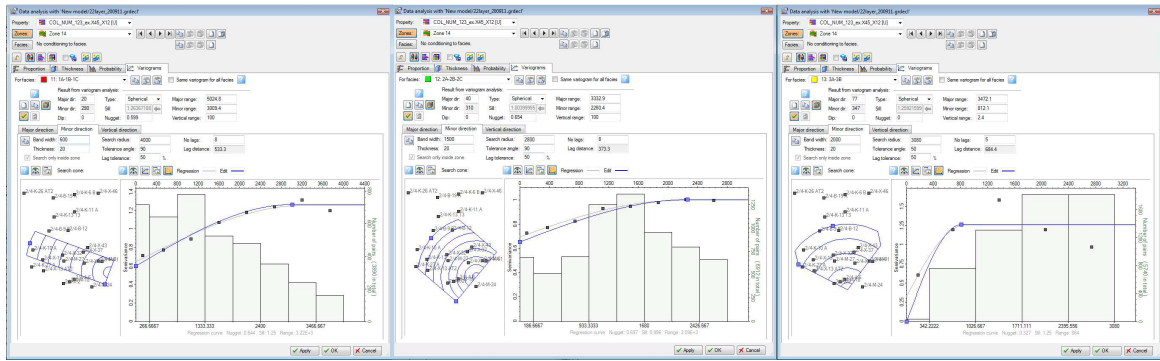
LAYER EM4 – Facies 1 (left) , Facies 2 (middle) and Facies 3 (right)



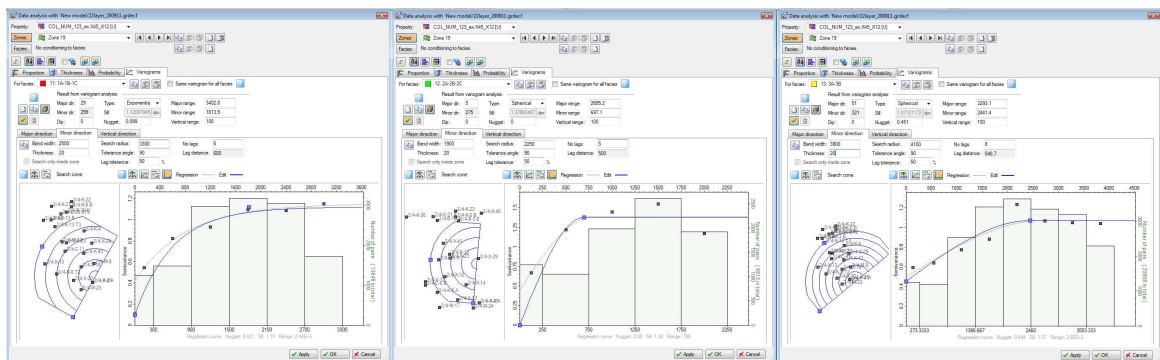
LAYER EEU – Facies 1 (left) , Facies 2 (middle) and Facies 3 (right)



LAYER EEM – Facies 1 (left) , Facies 2 (middle) and Facies 3 (right)

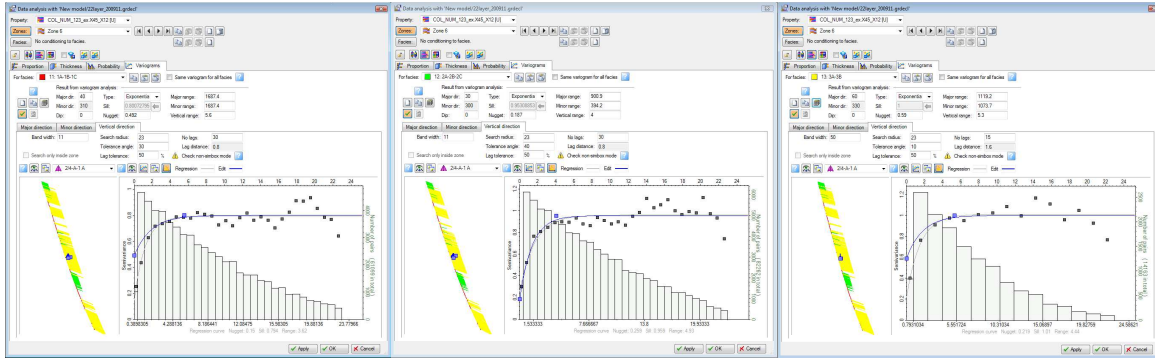


LAYER EEL – Facies 1 (left) , Facies 2 (middle) and Facies 3 (right)

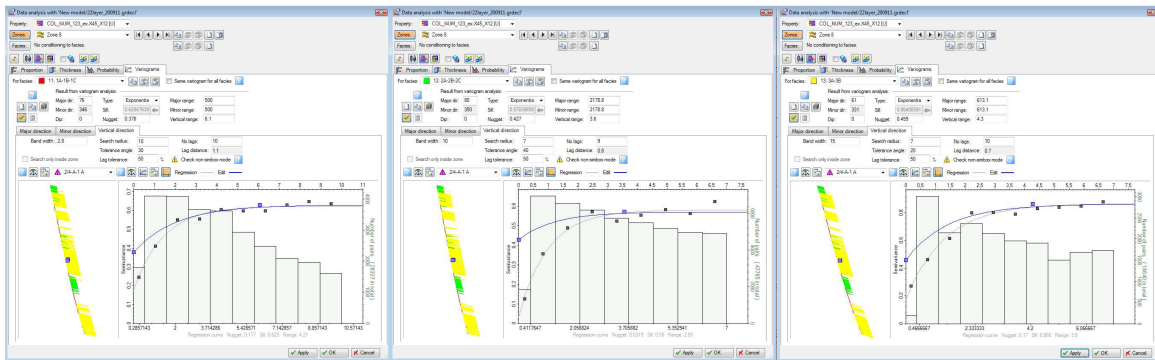


LAYER TBU – Facies 1 (left) , Facies 2 (middle) and Facies 3 (right)

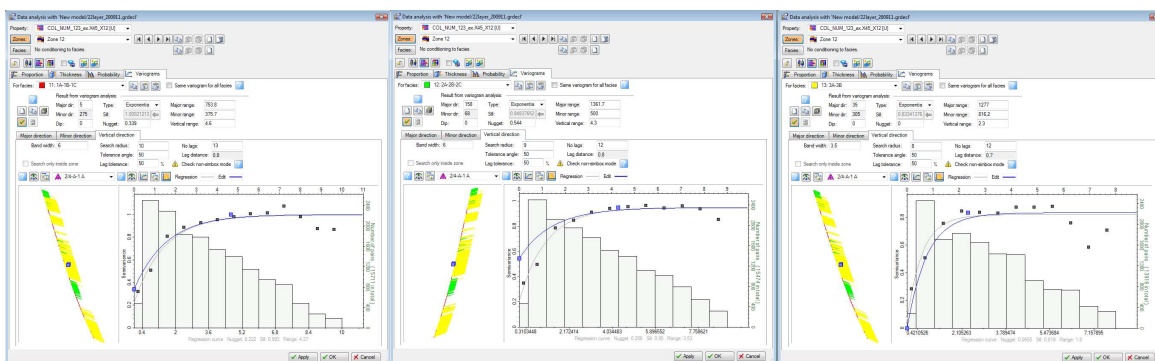
VERTICAL DIRECTION



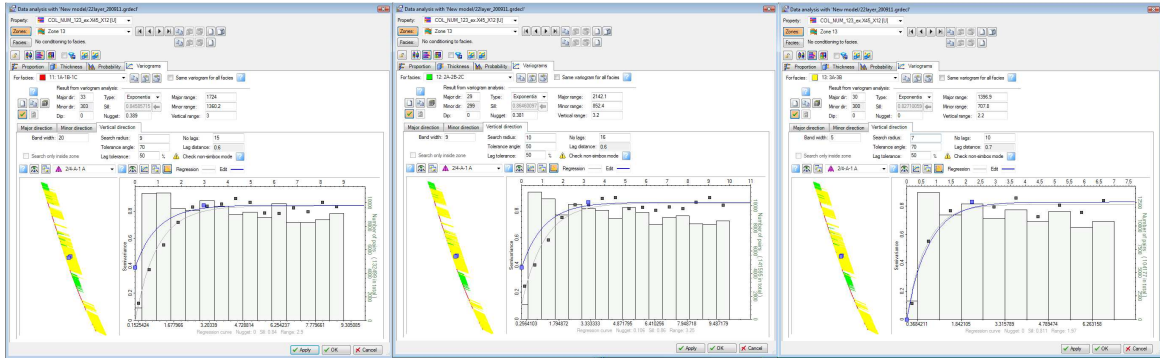
LAYER EM2 – Facies 1 (left) , Facies 2 (middle) and Facies 3 (right)



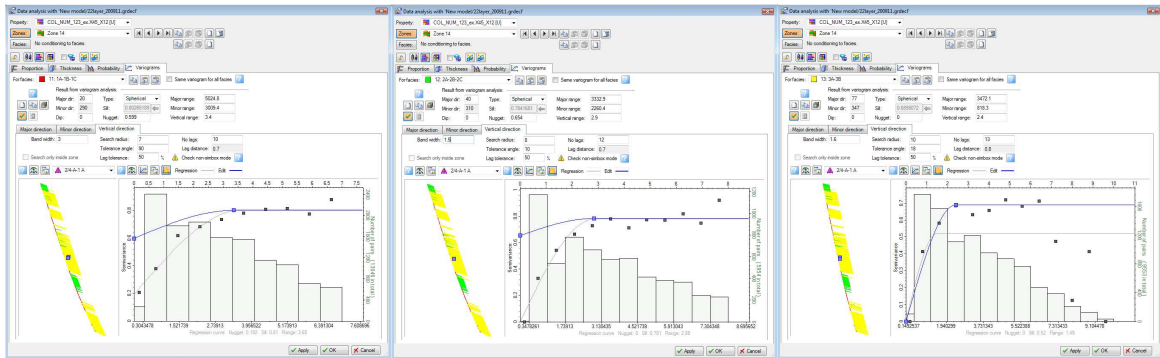
LAYER EM4 – Facies 1 (left) , Facies 2 (middle) and Facies 3 (right)



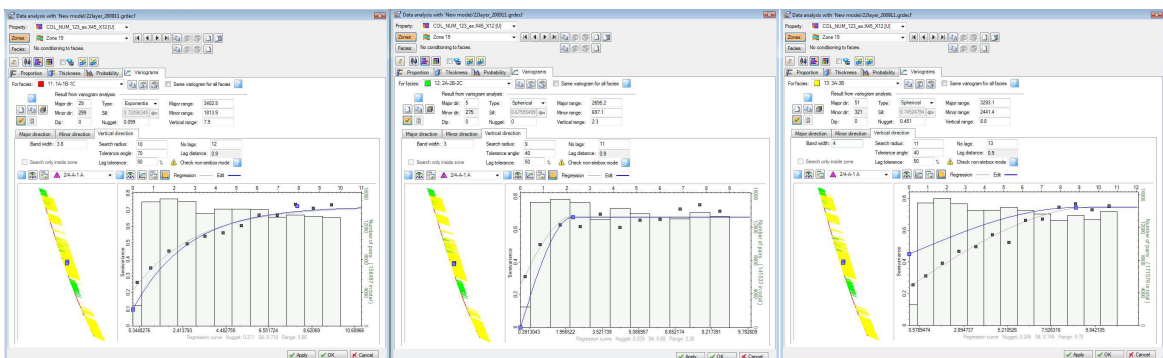
LAYER EEU – Facies 1 (left) , Facies 2 (middle) and Facies 3 (right)



LAYER EEM – Facies 1 (left) , Facies 2 (middle) and Facies 3 (right)



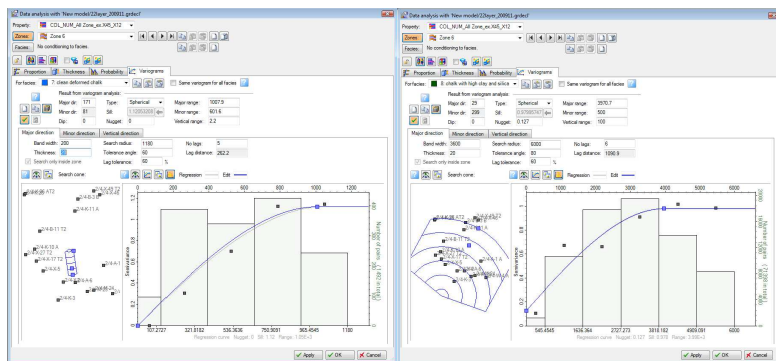
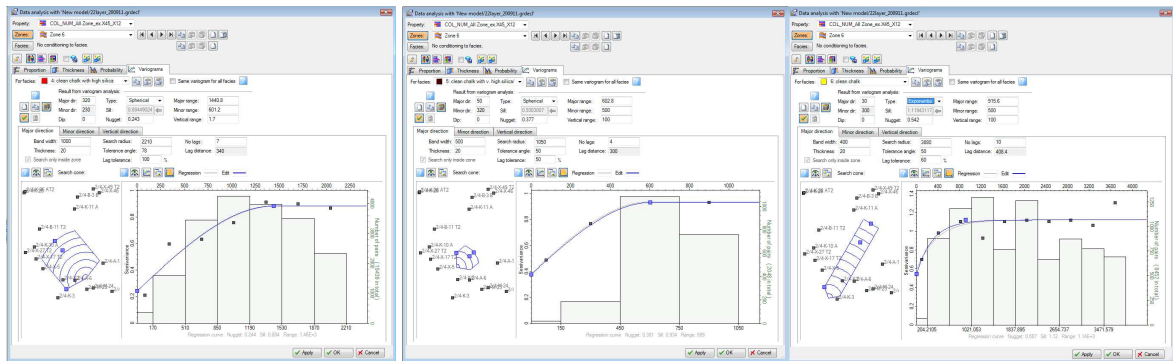
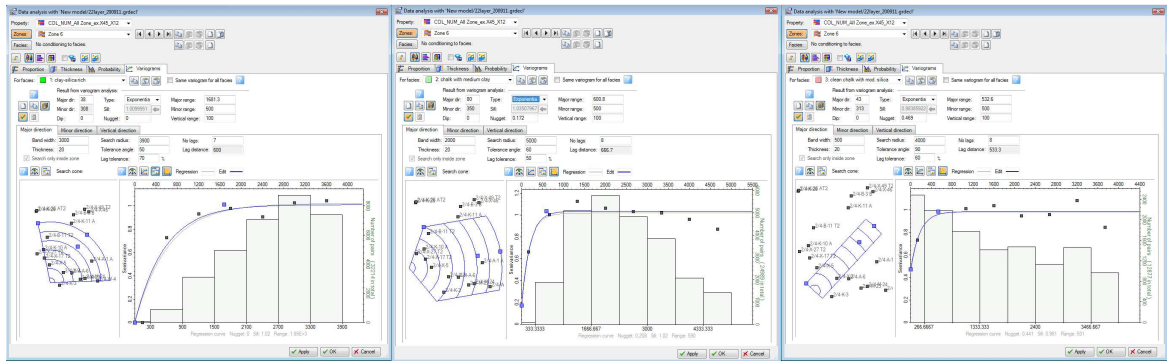
LAYER EEL – Facies 1 (left) , Facies 2 (middle) and Facies 3 (right)



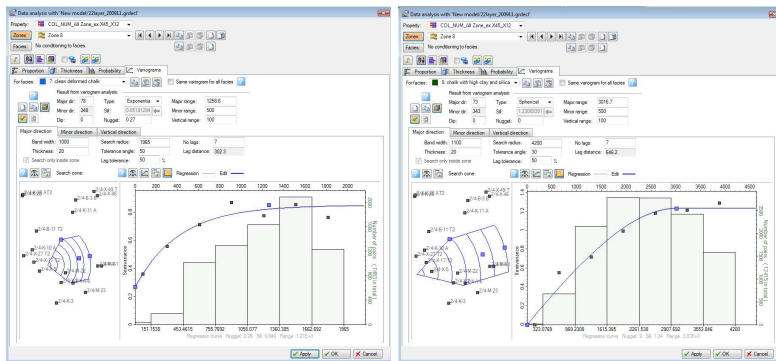
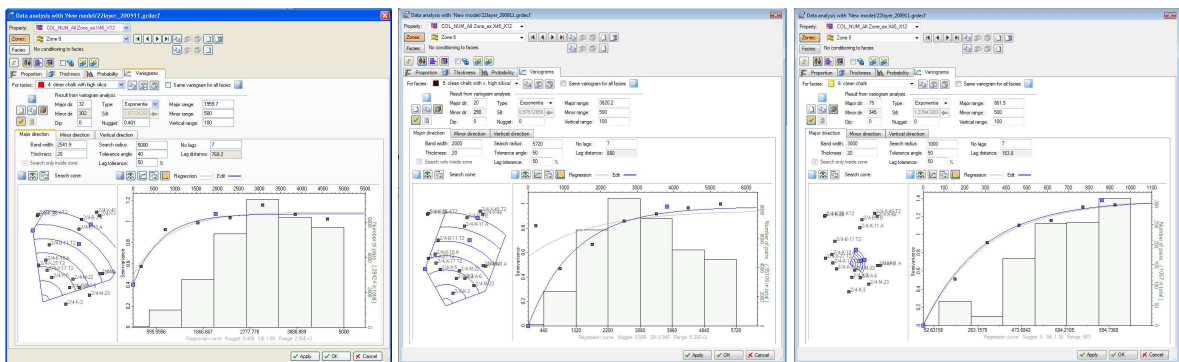
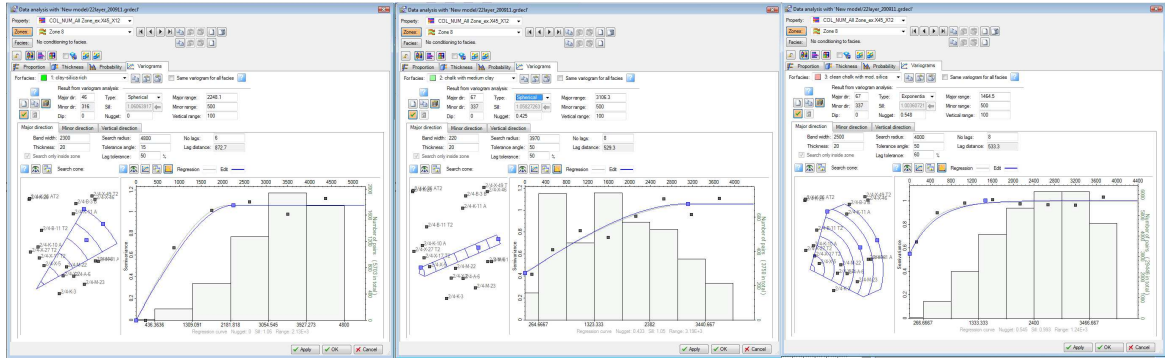
LAYER TBU – Facies 1 (left) , Facies 2 (middle) and Facies 3 (right)

Appendix 4.4 Variogram analysis of 8 facies model

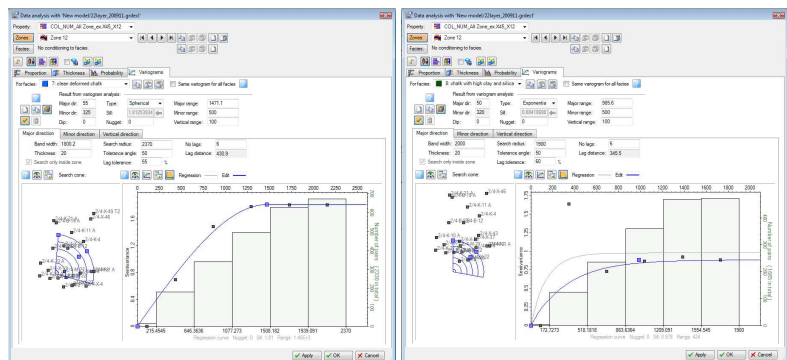
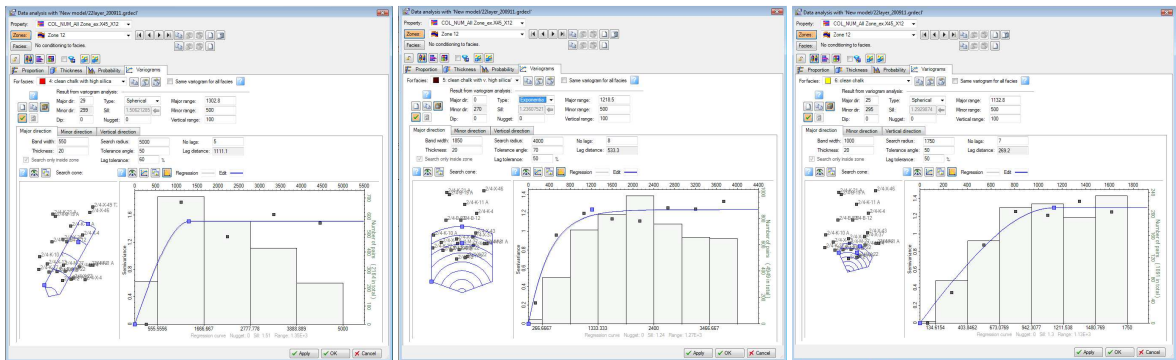
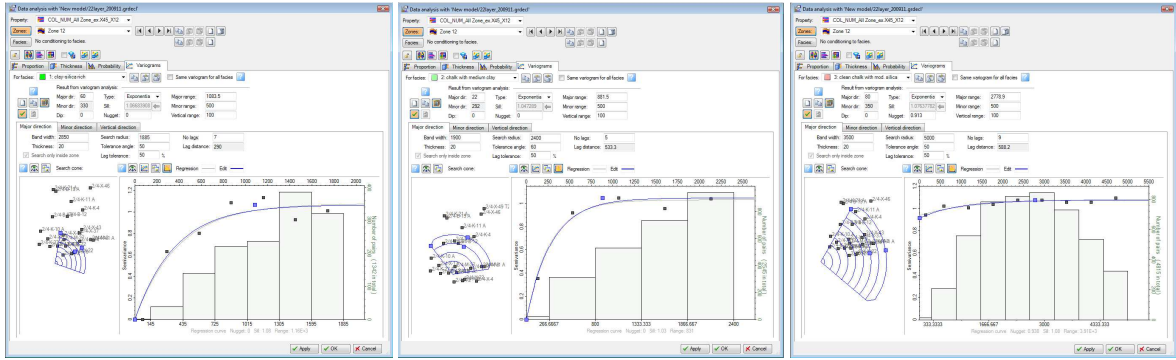
MAJOR DIRECTION



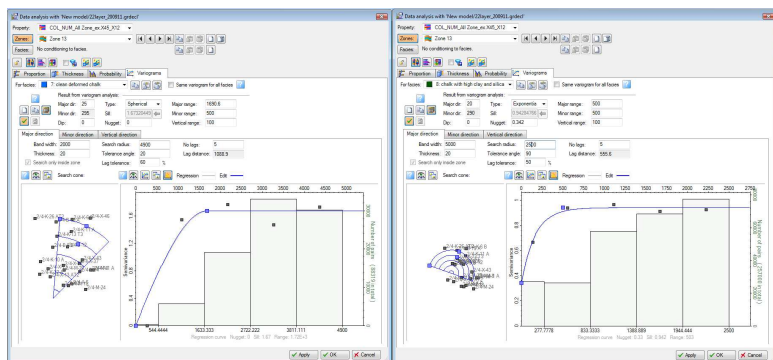
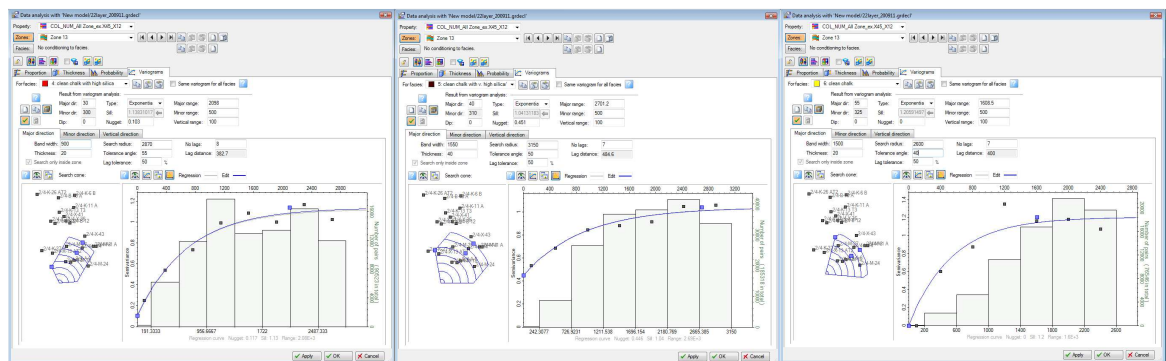
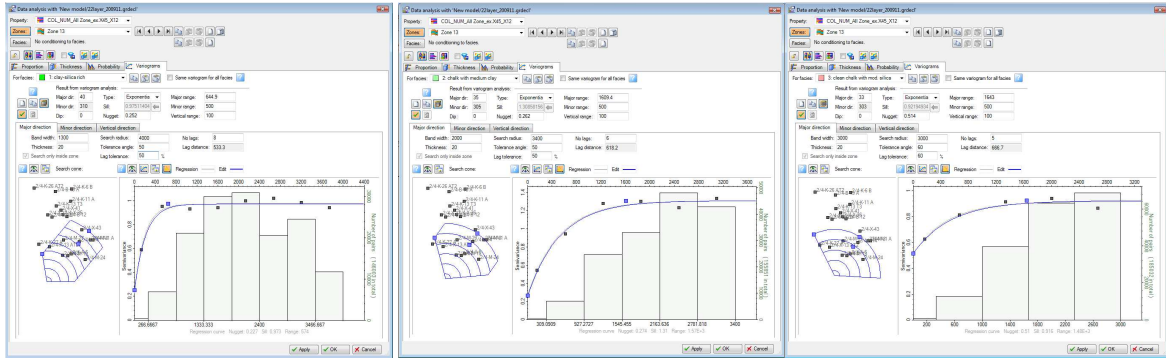
LAYER EM2 – Facies 1 to 8 is from left to right in the top to bottom



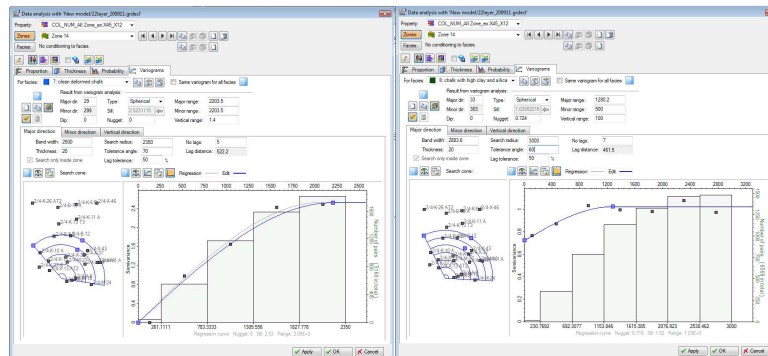
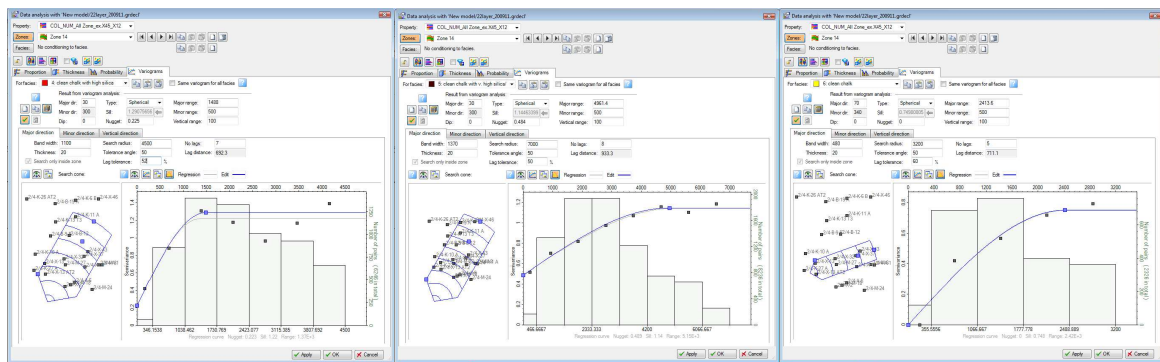
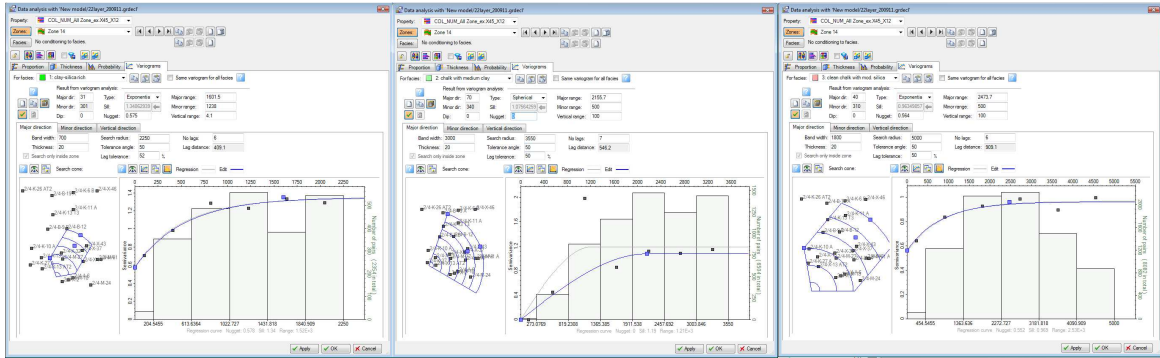
LAYER EM4 – Facies 1 to 8 is from left to right in the top to bottom



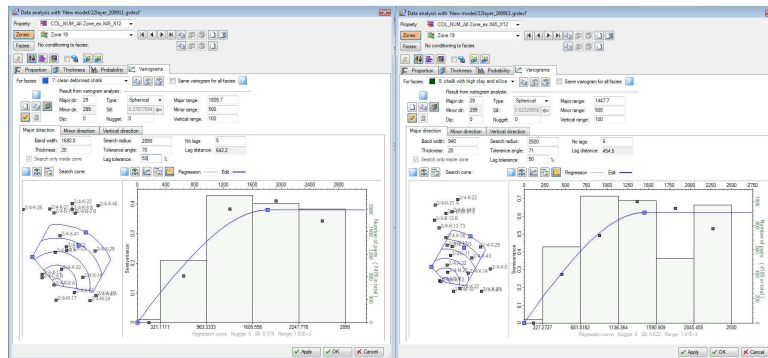
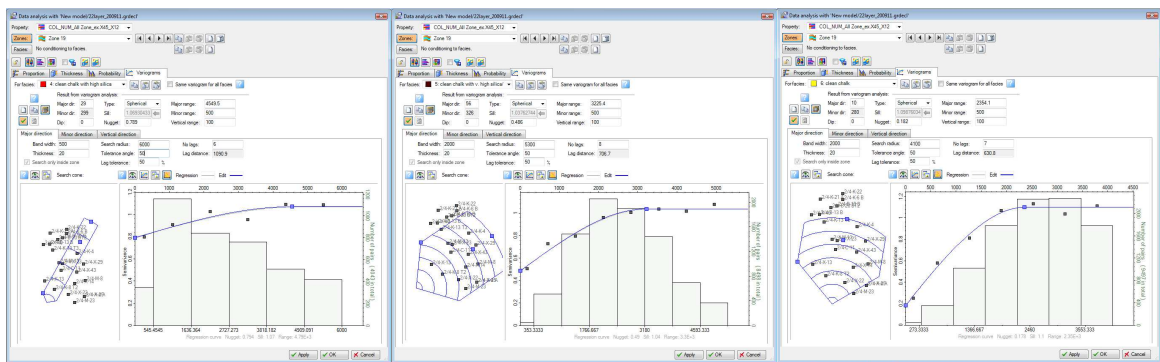
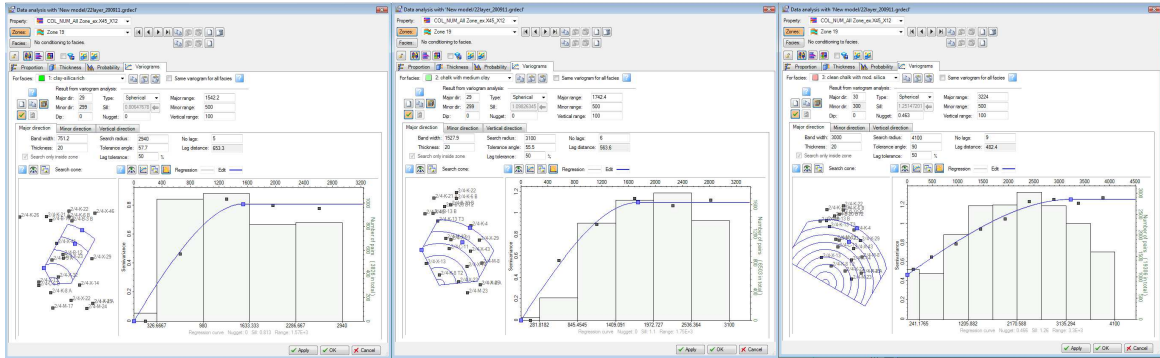
LAYER EEU – Facies 1 to 8 is from left to right in the top to bottom



LAYER EEM – Facies 1 to 8 is from left to right in the top to bottom

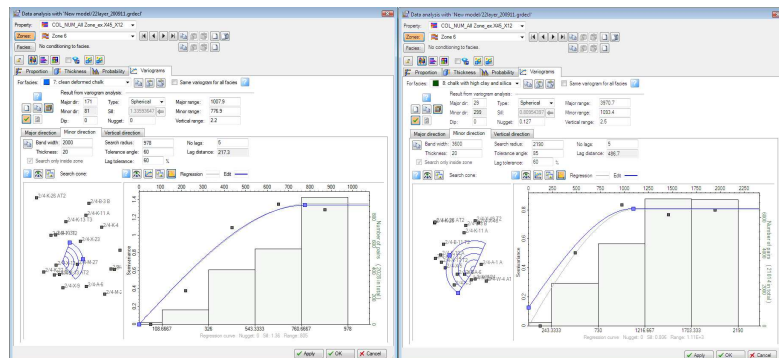
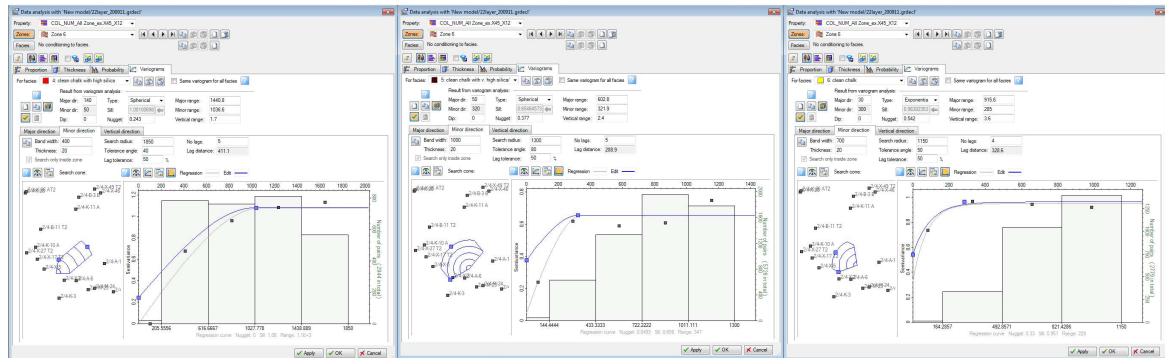
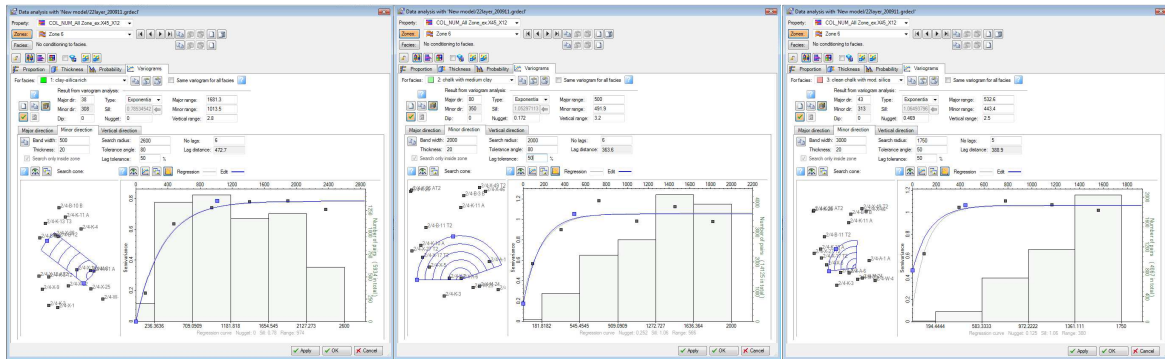


LAYER EEL – Facies 1 to 8 is from left to right in the top to bottom

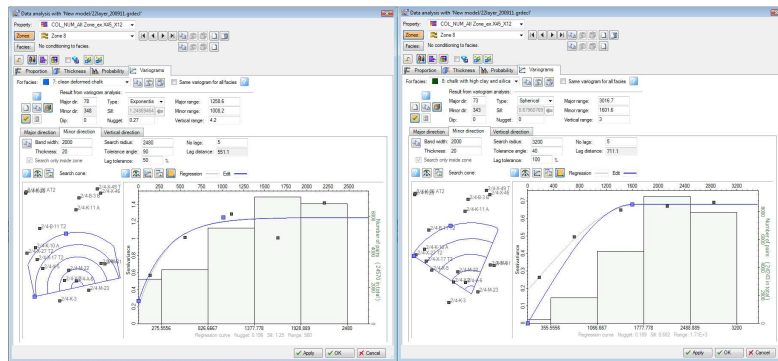
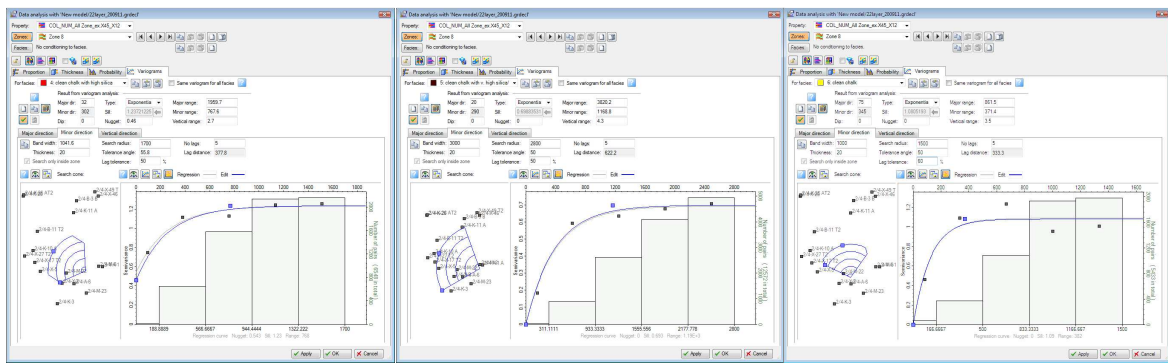
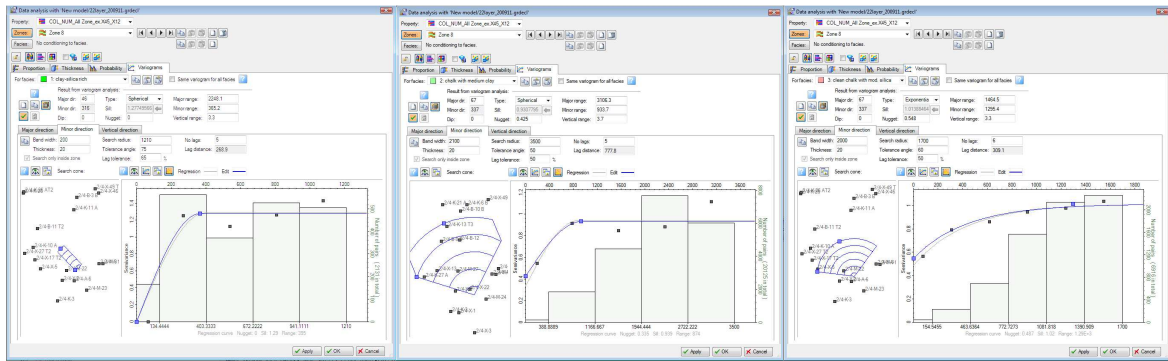


LAYER TBU – Facies 1 to 8 is from left to right in the top to bottom

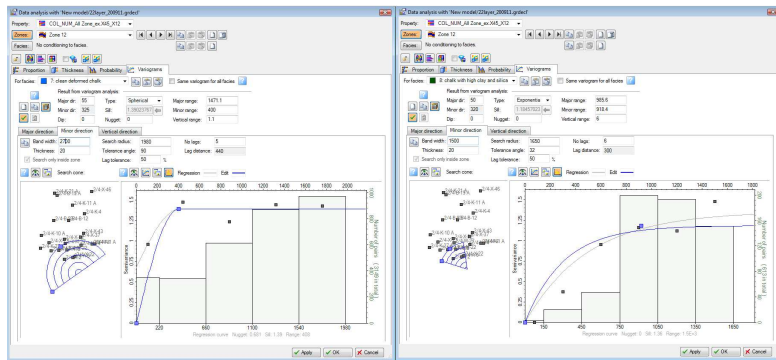
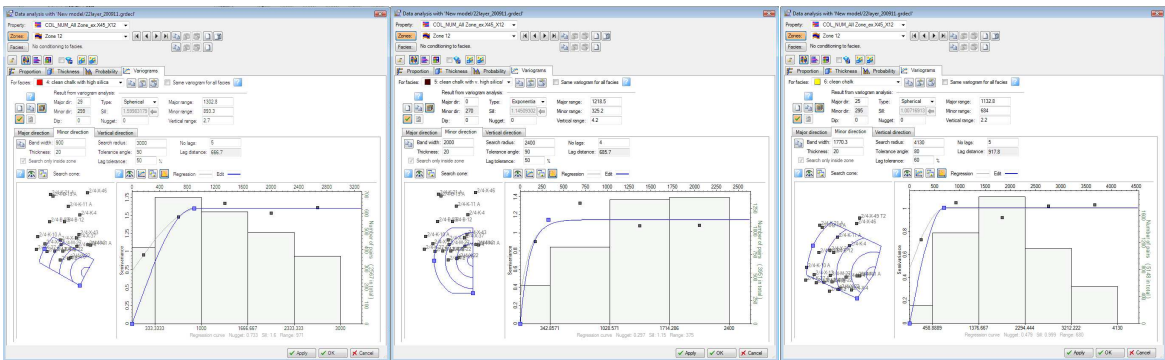
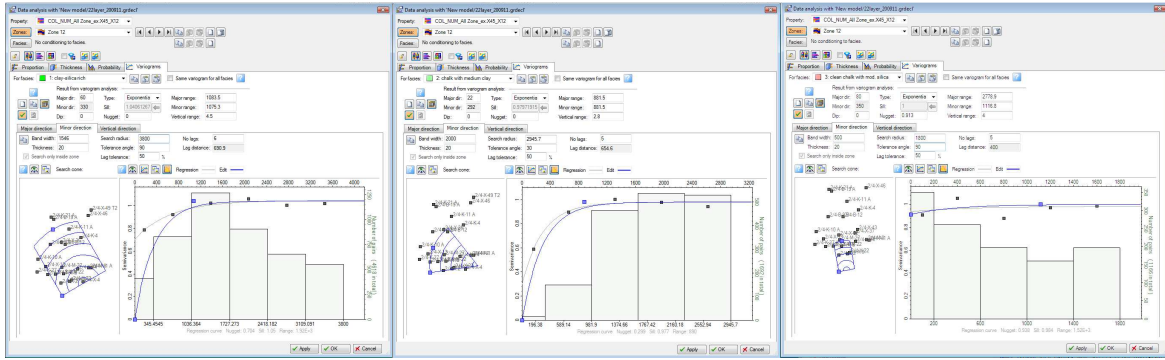
MINOR DIRECTION



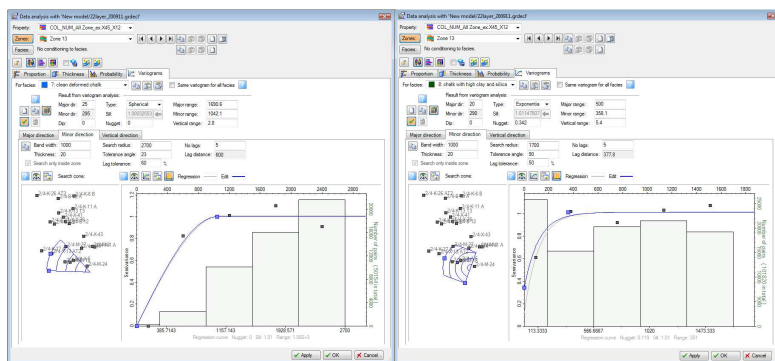
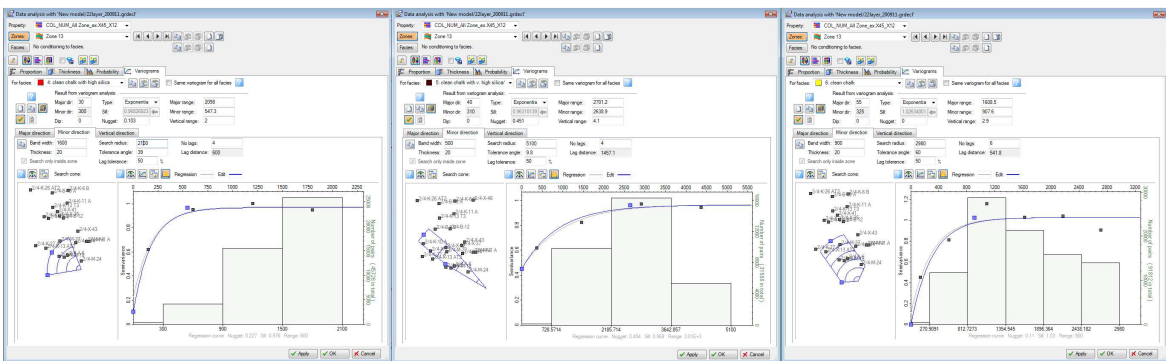
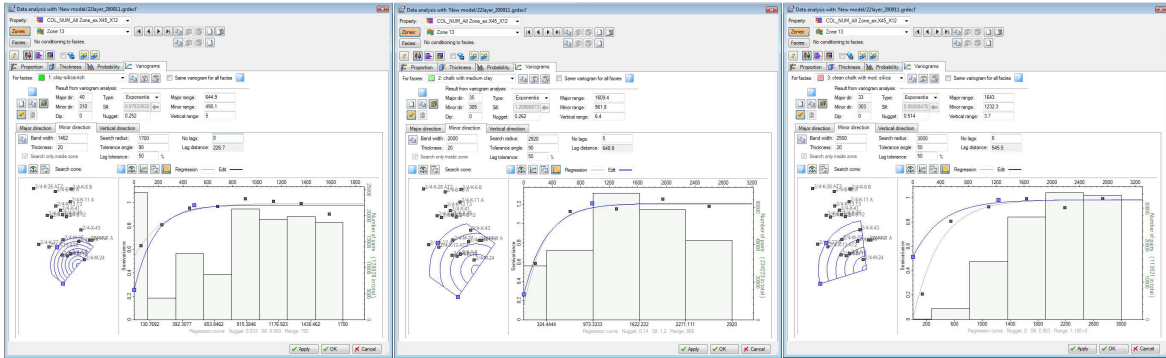
LAYER EM2 – Facies 1 to 8 is from left to right in the top to bottom



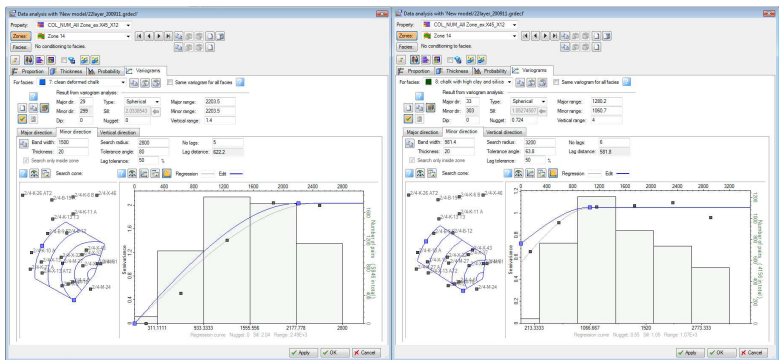
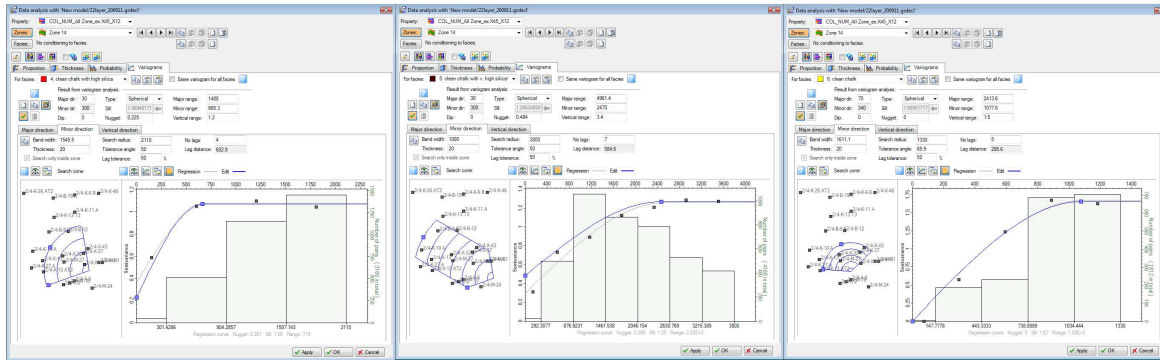
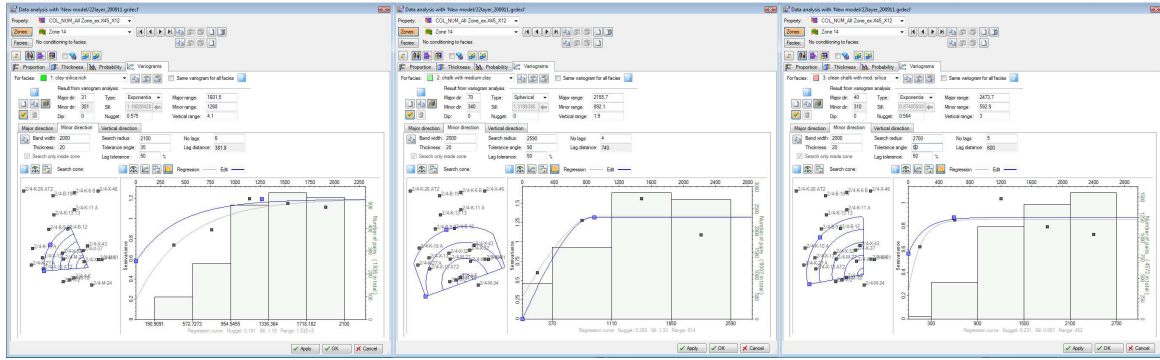
LAYER EM4 – Facies 1 to 8 is from left to right in the top to bottom



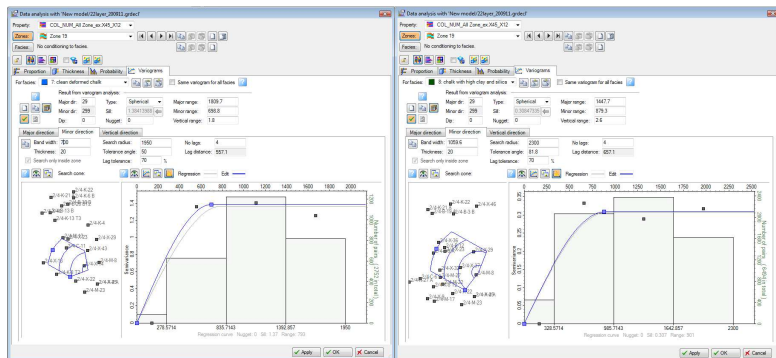
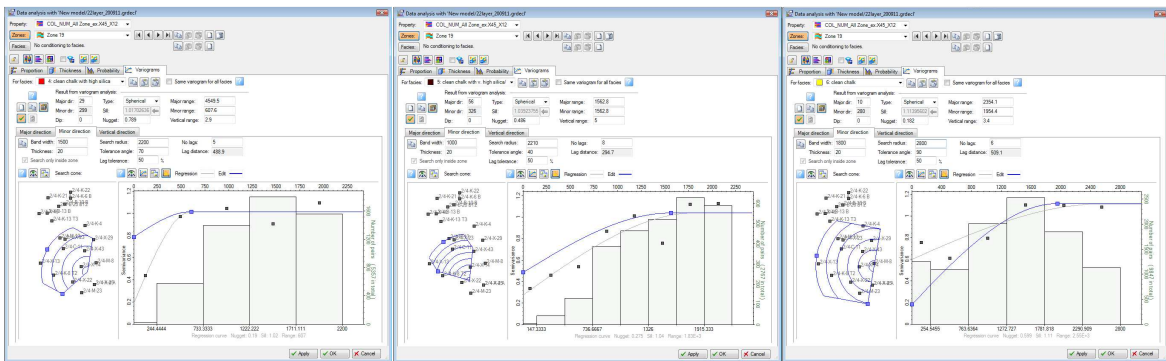
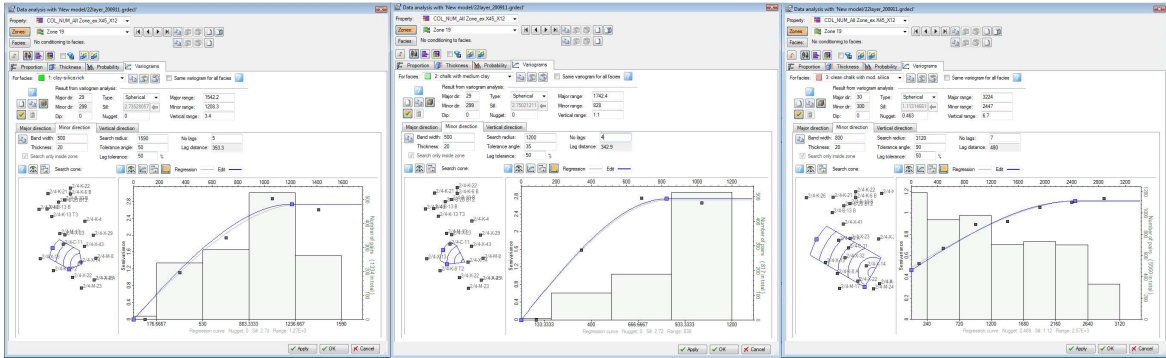
LAYER EEU – Facies 1 to 8 is from left to right in the top to bottom



LAYER EEM – Facies 1 to 8 is from left to right in the top to bottom

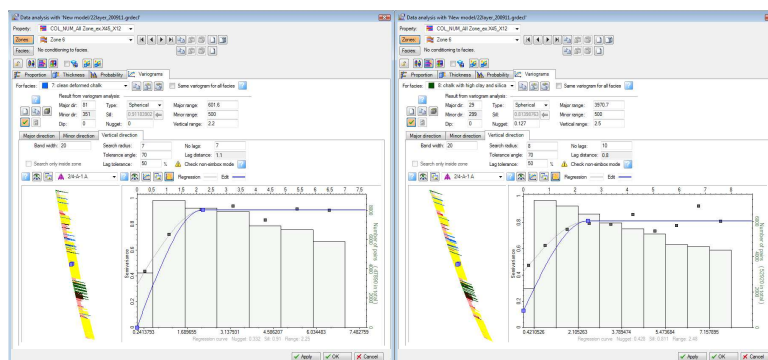
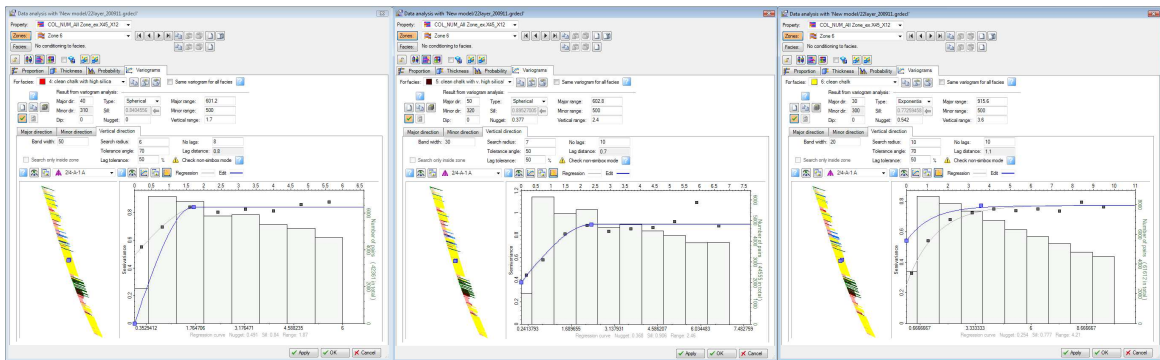
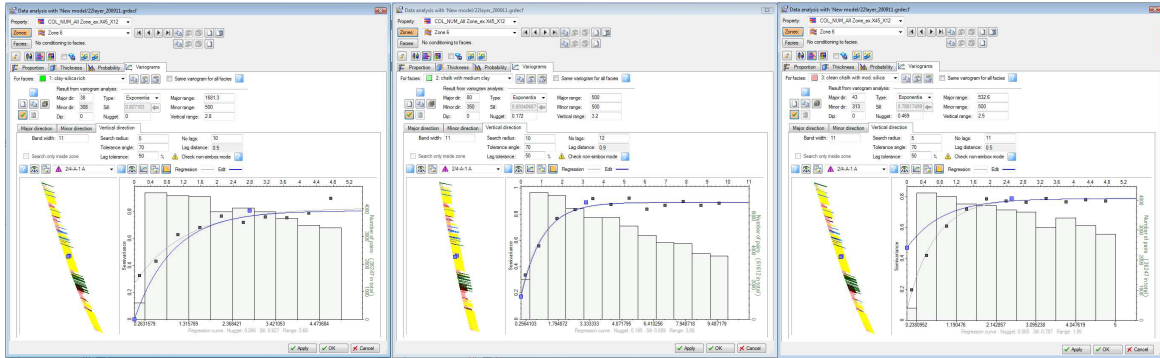


LAYER EEL – Facies 1 to 8 is from left to right in the top to bottom

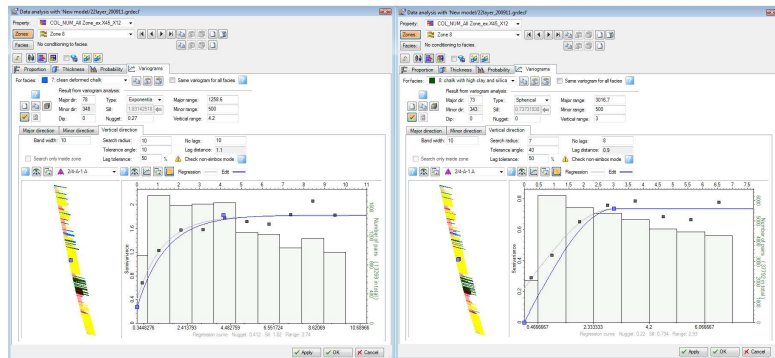
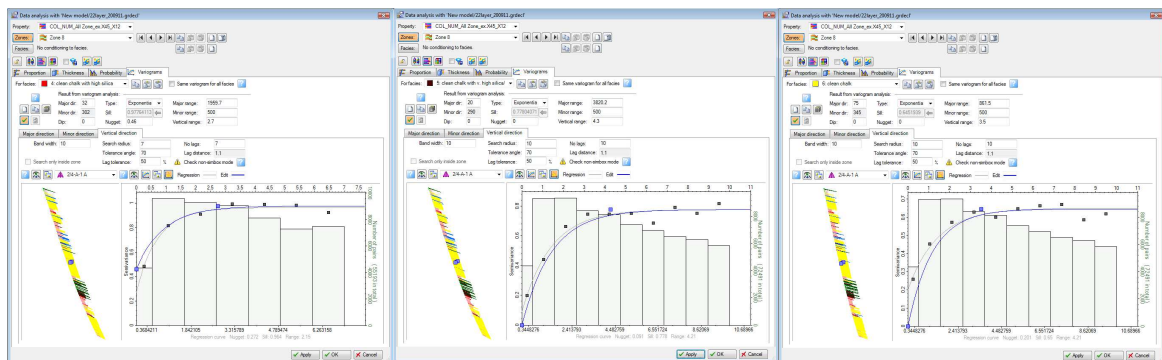
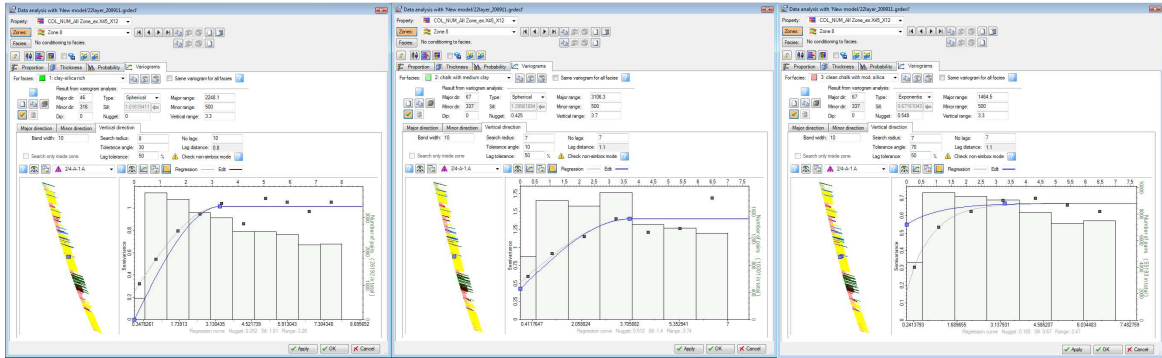


LAYER TBU – Facies 1 to 8 is from left to right in the top to bottom

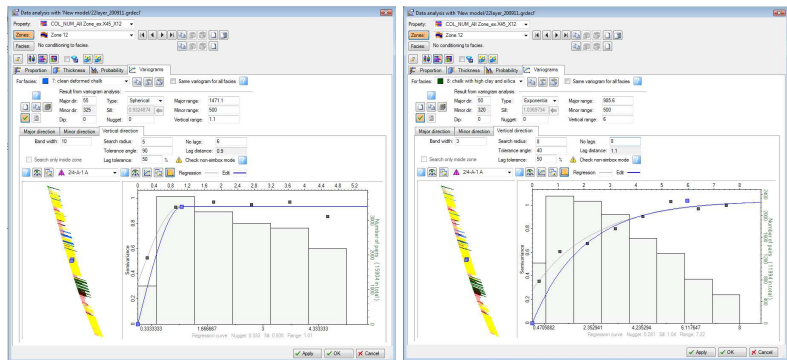
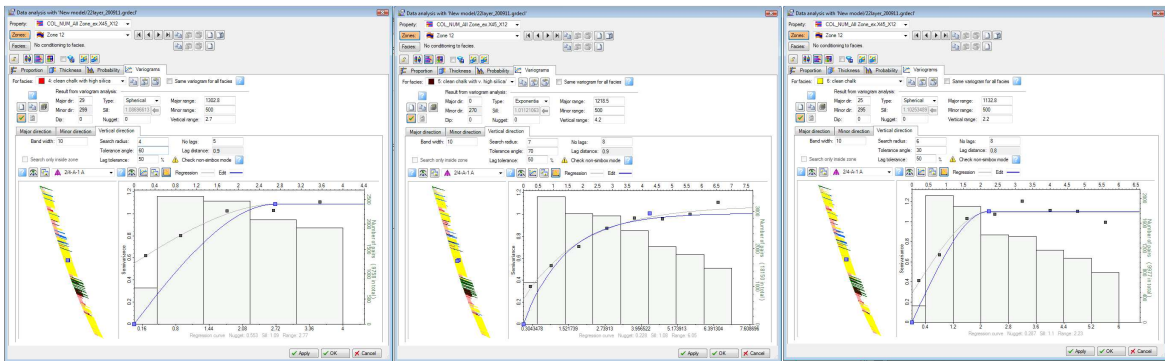
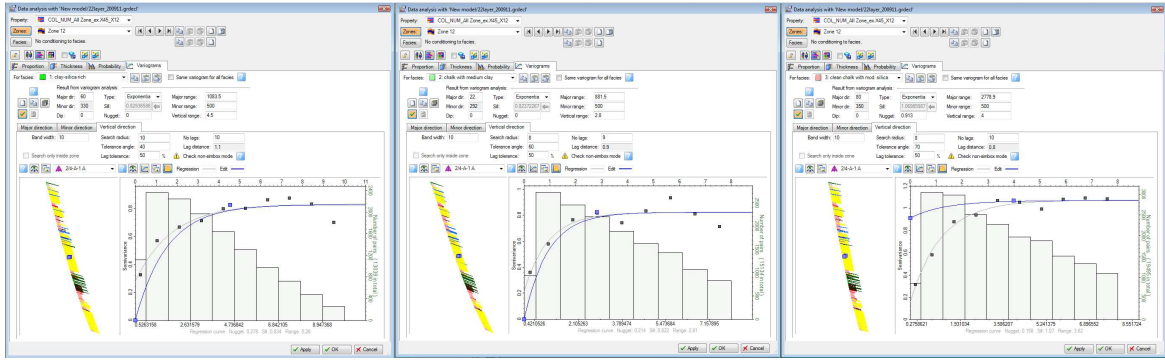
VERTICAL DIRECTION



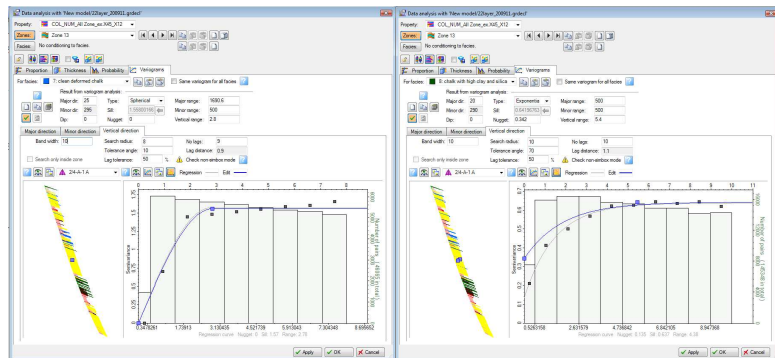
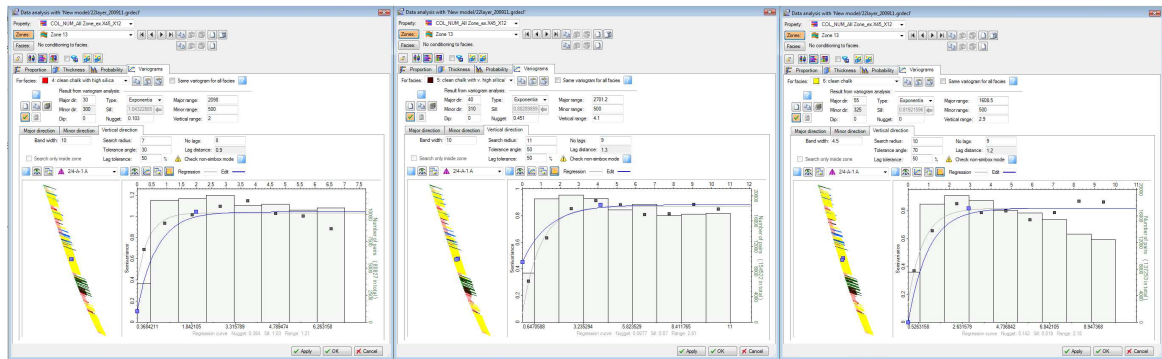
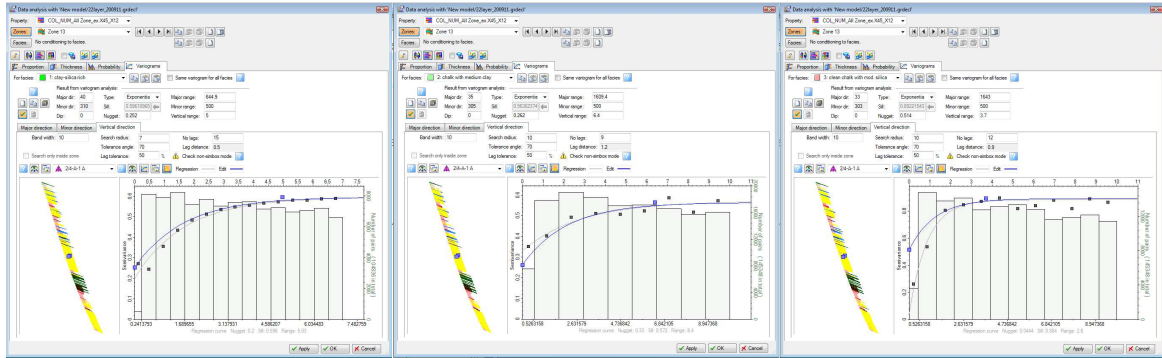
LAYER EM2 – Facies 1 to 8 is from left to right in the top to bottom



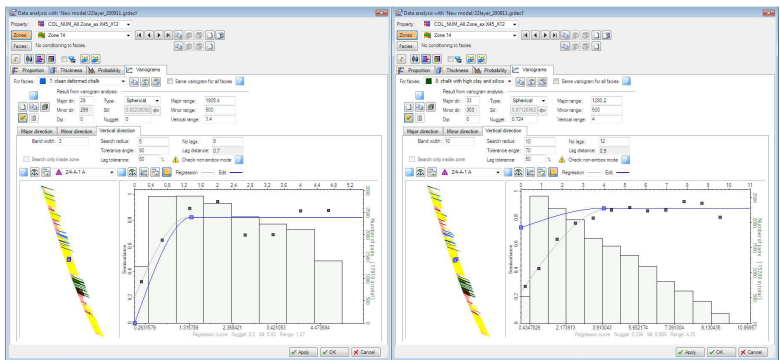
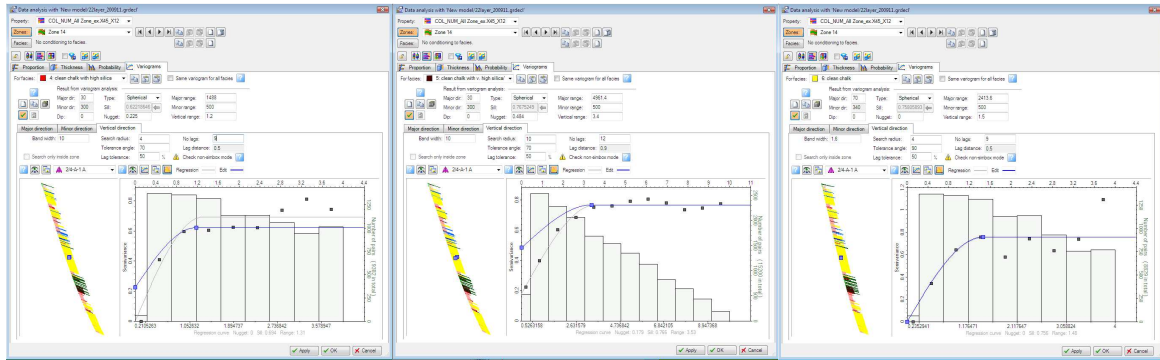
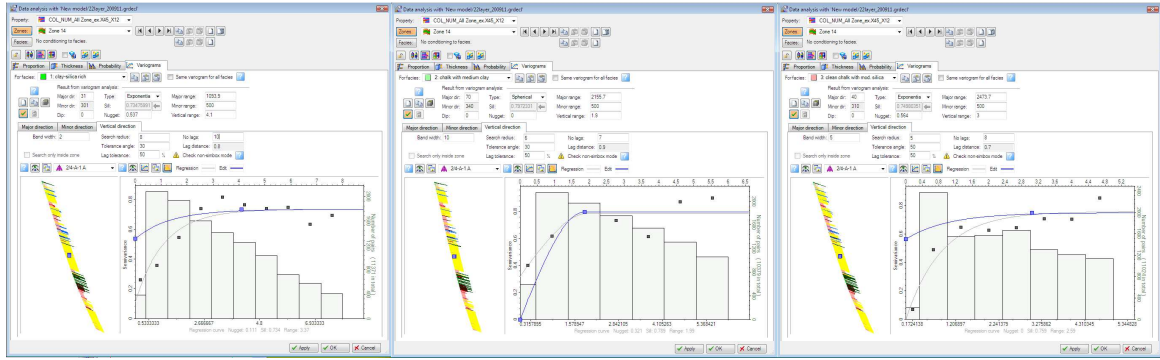
LAYER EM4 – Facies 1 to 8 is from left to right in the top to bottom



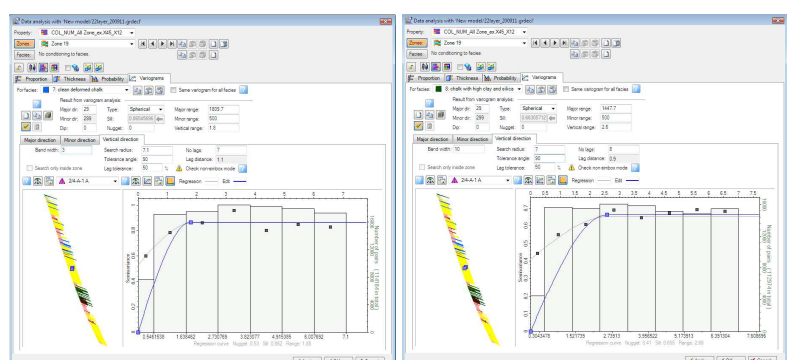
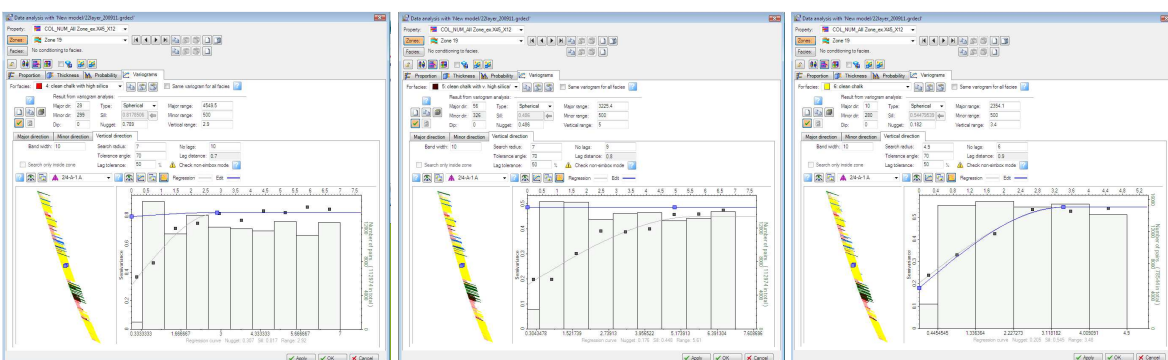
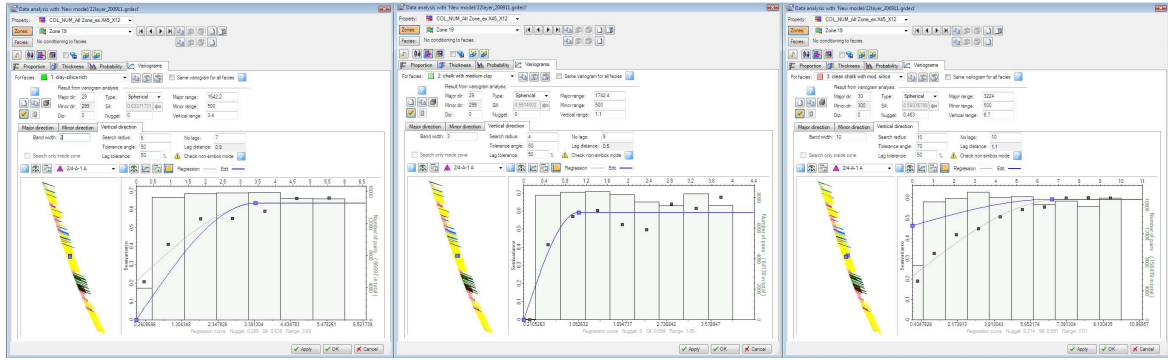
LAYER EEU – Facies 1 to 8 is from left to right in the top to bottom



LAYER EEM – Facies 1 to 8 is from left to right in the top to bottom



LAYER EEL – Facies 1 to 8 is from left to right in the top to bottom



LAYER TBU – Facies 1 to 8 is from left to right in the top to bottom

Appendix 4.5 Parameters from variogram analysis of 3 and 8 facies model

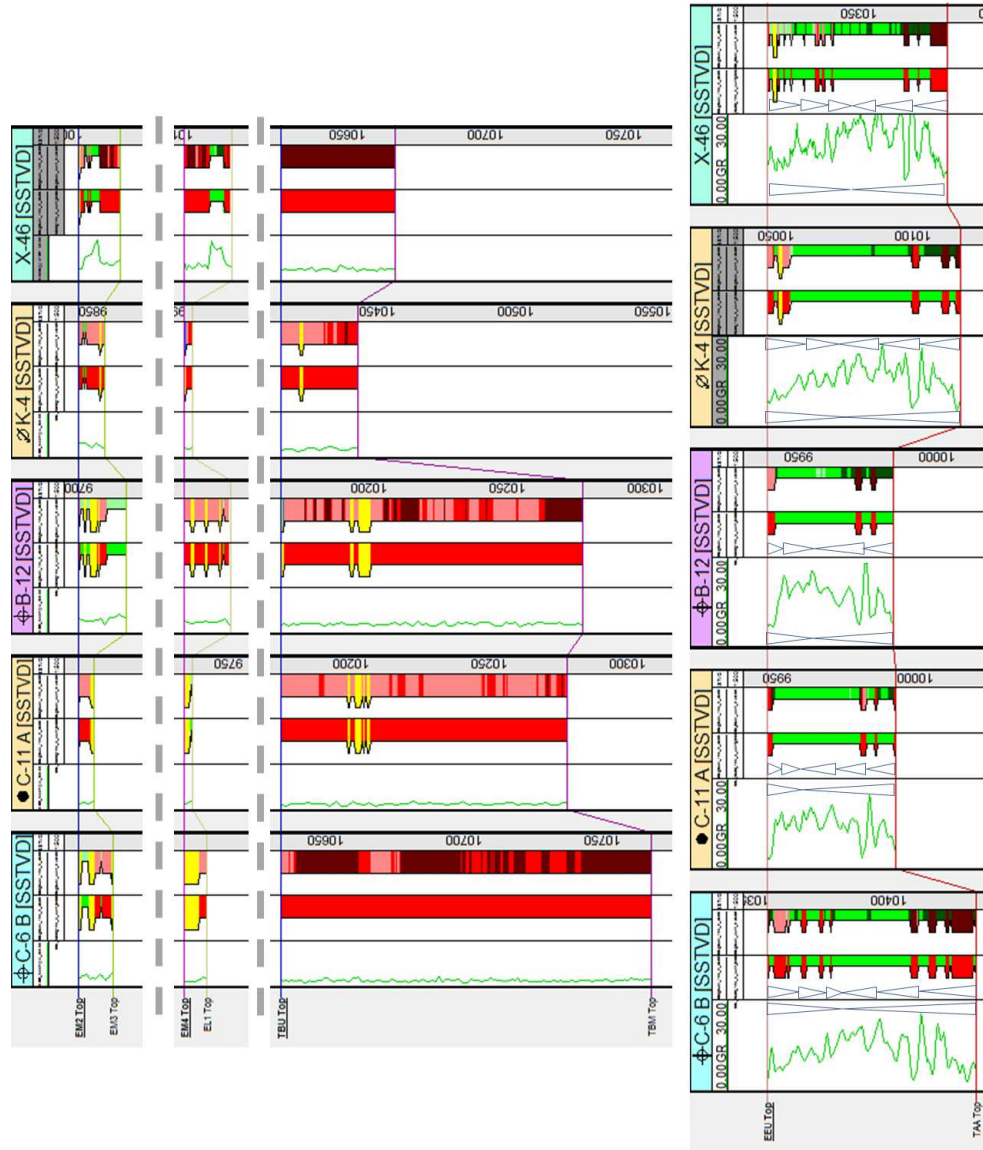
Table of Parameters used in Continuous Facies Modeling for 3 Facies Model

Zone	Facies	Major Direction (deg)	Type	Major Range (m)	Minor Range (m)	Vertical Range (ft/m)	Nugget
6 (EM2)	1	40	Exponential	1048	664	5.6	0.492
	2	30	Exponential	1642	756	4	0.282
	3	60	Exponential	1028	983	5.3	0.59
8 (EM4)	1	76	Exponential	500	500	6.1	0.378
	2	80	Exponential	2278	2178	3.6	0.427
	3	61	Exponential	603	548	4.3	0.459
12 (EEU)	1	5	Exponential	753	375	4.6	0.339
	2	158	Exponential	1410	500	4.3	0.552
	3	35	Exponential	1277	816	2.3	0
13 (EEM)	1	33	Exponential	1724	1360	3	0.389
	2	29	Exponential	2244	852	3.2	0.381
	3	30	Exponential	1431	707	2.2	0
14 (EEL)	1	20	Spherical	5091	3009	3.4	0.639
	2	40	Spherical	3332	2260	2.9	0.654
	3	77	Spherical	3472	812	2.4	0
19 (TBU)	1	29	Exponential	3402	1813	7.9	0.1
	2	5	Spherical	2695	697	2.3	0
	3	51	Spherical	3293	2441	8.8	0.451

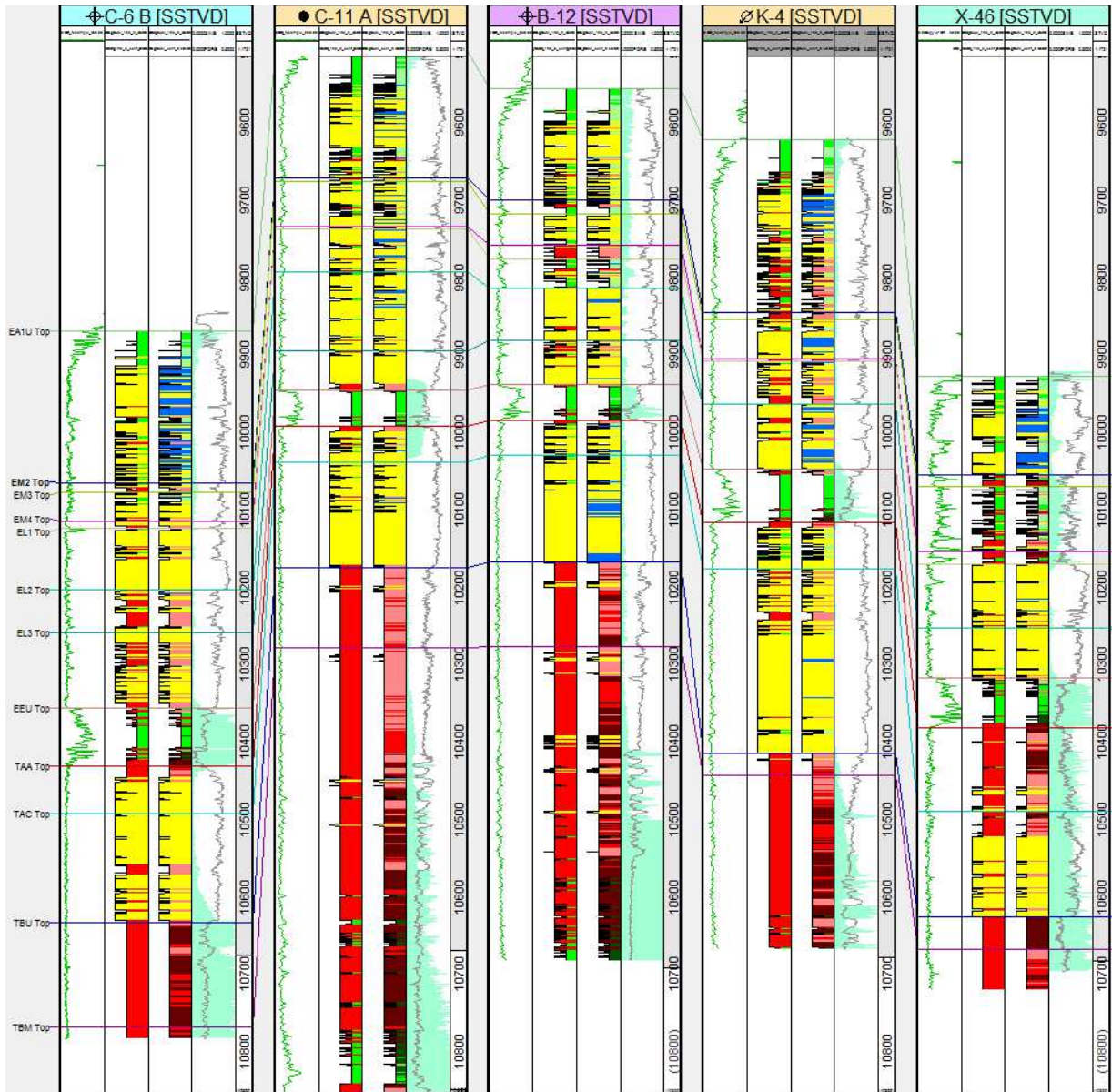
Table of Parameters used in Continuous Facies Modeling for 8 Facies Model

Zone	Facies	Major Direction (deg)	Type	Major Range (m)	Minor Range (m)	Vertical Range (ft/m)	Nugget
6 (EM2)	1	38	Exponential	1681	1013	2.8	0
	2	80	Exponential	600	491	3.2	0.172
	3	43	Exponential	532	443	2.5	0.469
	4	140	Spherical	1440	1036	1.7	0.243
	5	50	Spherical	602	321	2.4	0.377
	6	30	Exponential	915	285	3.6	0.542
	7	171	Spherical	1007	776	2.2	0
	8	29	Spherical	3970	1093	2.5	0.127
8 (EM4)	1	46	Spherical	2248	365	3.3	0
	2	67	Spherical	3106	933	3.7	0.425
	3	67	Exponential	1464	1295	3.3	0.548
	4	32	Exponential	1959	767	2.7	0.46
	5	20	Exponential	3820	1168	4.3	0
	6	75	Exponential	861	371	3.5	0
	7	78	Exponential	1258	1008	4.2	0.27
	8	73	Spherical	3016	1601	3	0
12 (EEU)	1	60	Exponential	1083	1075	4.5	0
	2	22	Exponential	881	881	2.8	0
	3	80	Exponential	2278	1116	4	0.913
	4	29	Spherical	1302	1302	2.7	0
	5	0	Exponential	1218	325	4.2	0
	6	25	Spherical	1132	684	2.2	0
	7	55	Spherical	1471	400	1.1	0
	8	50	Exponential	985	918	6	0
13 (EEM)	1	40	Exponential	644	490	5	0.252
	2	35	Exponential	1609	961	6.4	0.262
	3	33	Exponential	1643	1232	3.7	0.514
	4	30	Exponential	2098	547	1	0.103
	5	40	Exponential	2701	2638	4.1	0.451
	6	55	Exponential	1608	907	2.9	0
	7	25	Spherical	1690	1042	2.8	0
	8	20	Exponential	500	358	5.4	0.342
14 (EEL)	1	31	Exponential	1601	1268	4.1	0.575
	2	70	Spherical	2155	892	1.9	0
	3	40	Exponential	2473	592	3	0.564
	4	30	Spherical	1488	665	1.2	0.225
	5	30	Spherical	4961	2470	3.4	0.484
	6	70	Spherical	2413	1077	1.5	0
	7	29	Spherical	2203	2203	1.4	0
	8	33	Spherical	1280	1060	4	0.724
19 (TBU)	1	29	Spherical	1542	1208	3.4	0
	2	29	Spherical	1742	828	1.1	0
	3	30	Spherical	3224	2447	6.7	0.463
	4	29	Spherical	4549	607	2.9	0.789
	5	56	Spherical	1562	1562	5	0.486
	6	10	Spherical	2354	1954	3.4	0.182
	7	29	Spherical	1809	698	1.8	0
	8	29	Spherical	1447	879	2.6	0

Appendix 5.1 Well correlation



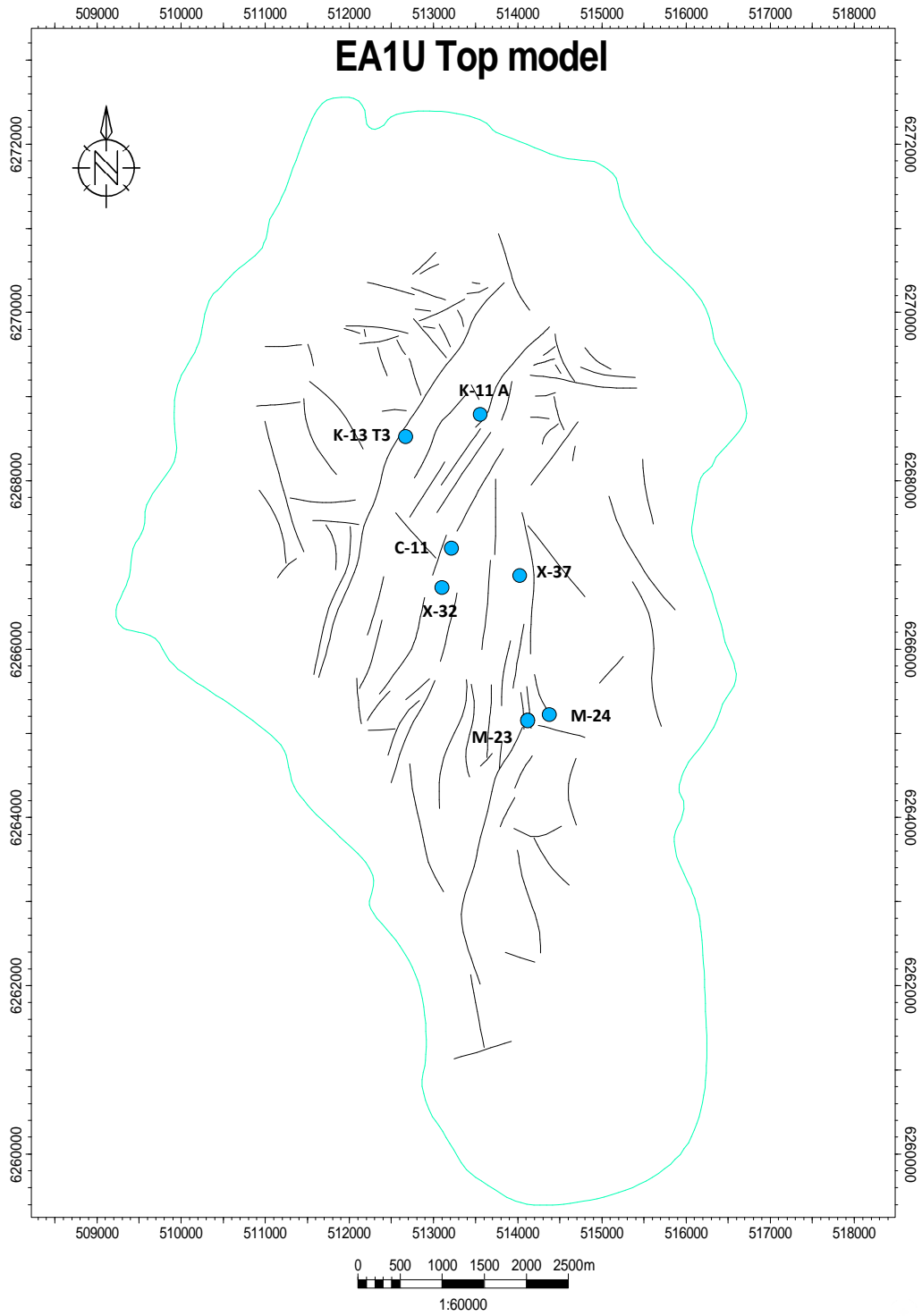
Map of Well Location (left) and Southwest-Northeast Correlation (right)
 Legend of track from is GR (0-30 API), Facies 123, Facies 1-8 and Depth (ft)



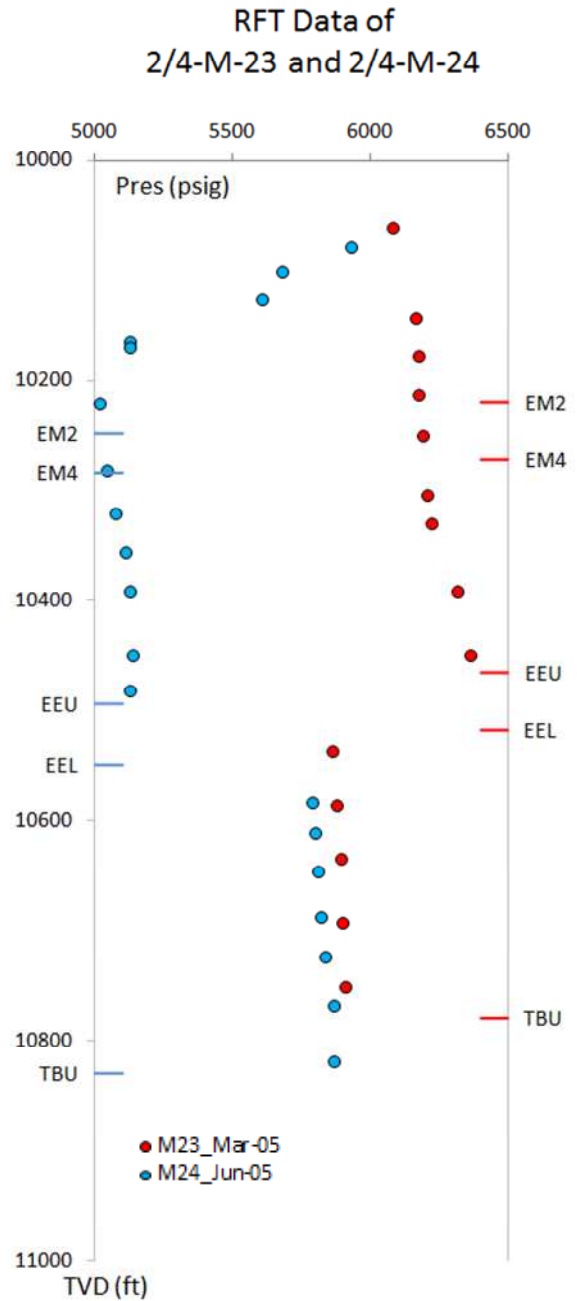
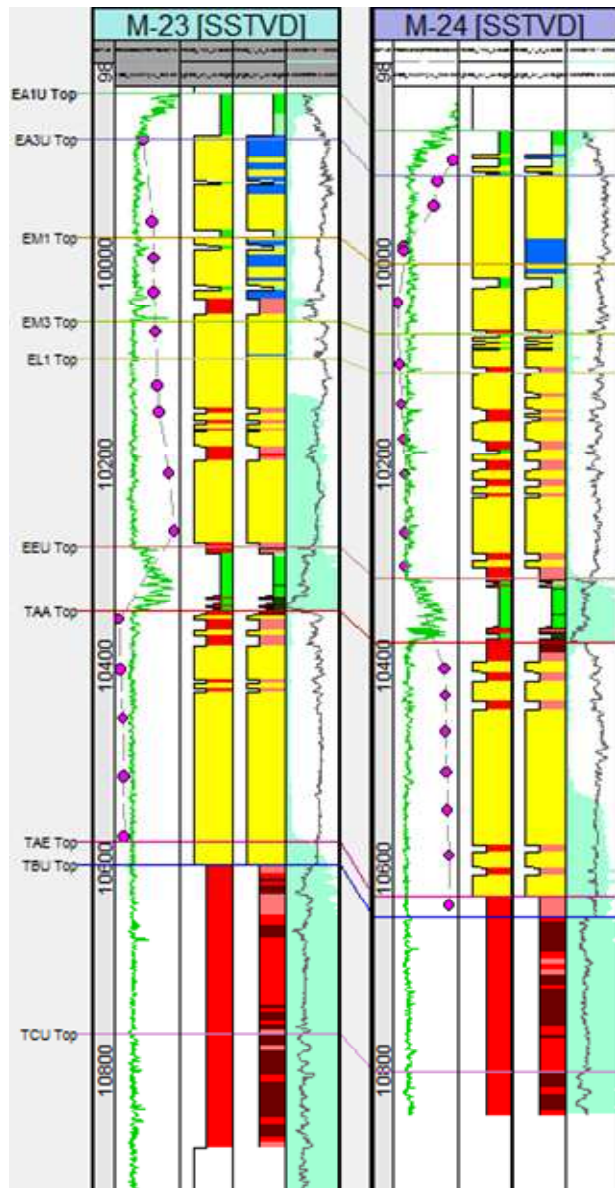
Southwest-Northeast Correlation Flatten at 9000 ftTVD (Legend for the track left to right is GR of 0-30 API, Facies 123 model, Facies 1-8 model and water saturation of 0-1.0 with porosity of 0-0.5)

Appendix 5.2 Observation from well section

Map of Well Reviewed in Facies Characterization

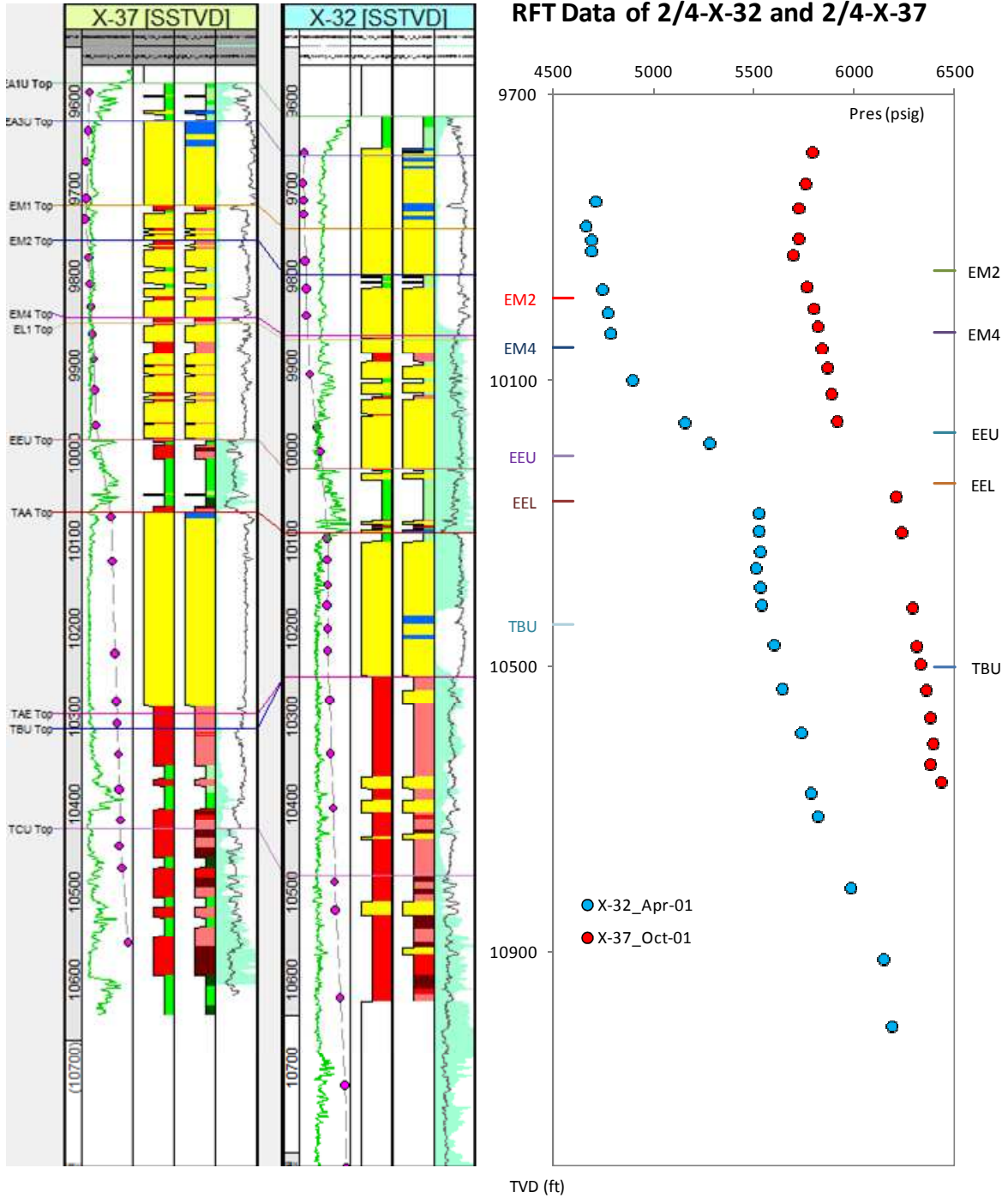


Observation 1 (2/4-M-23 and 2/4-M-24)



Well section and RFT data of 2/4-M-23 and 2/4-M-24
 (Legend for the track from 1st to 5th : depth (ftTVD), GR (0-30 API) with RFT in points (floating psig), 123 facies model, 1-8 facies model and Sw in blue (0-1.0) with porosity in gray (0-0.5))

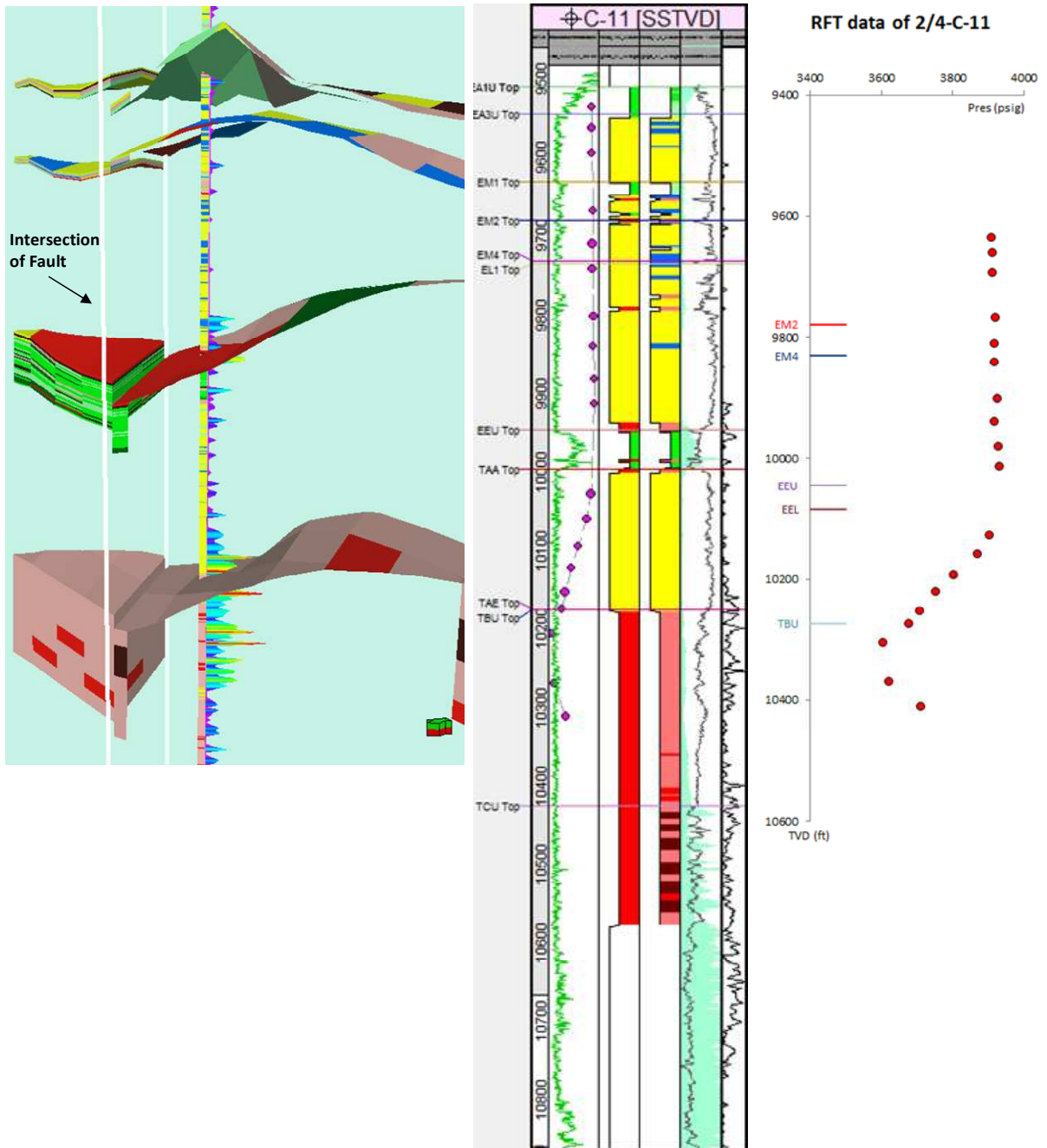
Observation 2 (2/4-X-32 and 2/4-X-37)



Well section and RFT data of 2/4-X-32 and 2/4-X-37

(Legend for the track from 1st to 5th : depth (ftTVD), GR (0-30 API) with RFT in points (floating psig), 123 facies model, 1-8 facies model and Sw in blue (0-1.0) with porosity in gray (0-0.5))

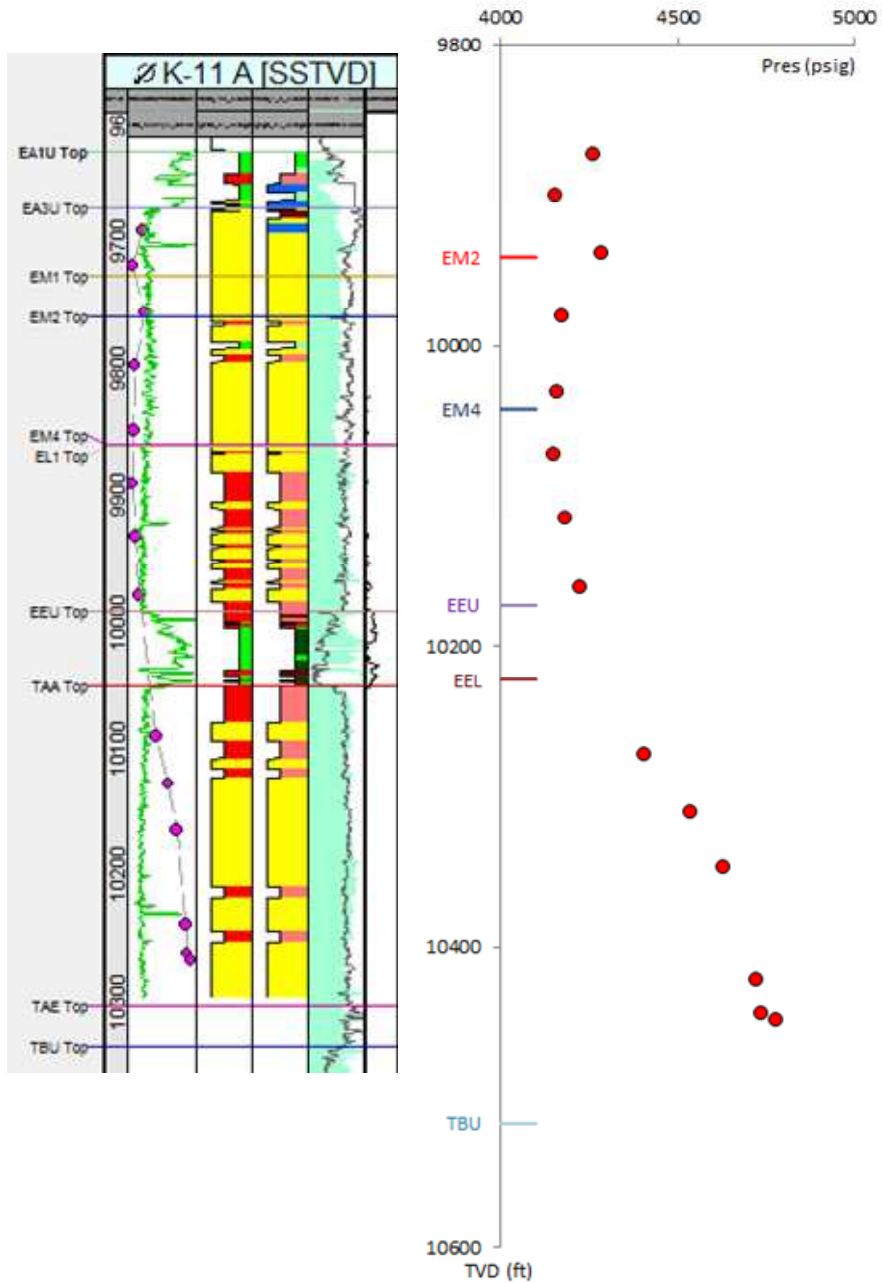
Observation 3 (2/4-C-11 and 2/4-K-11 A)



3D view of 1-8 facies model, well section and RFT data of 2/4-C-11
 (Legend for the track from 1st to 6th : depth (ftTVD), GR (0-30 API) with RFT in points (floating psig), 123 facies model, 1-8 facies model, Sw in blue (0-1.0) with porosity in gray (0-0.5) and fracture intensity (0-40))

Observation 3 cont'd (2/4-C-11 and 2/4-K-11 A)

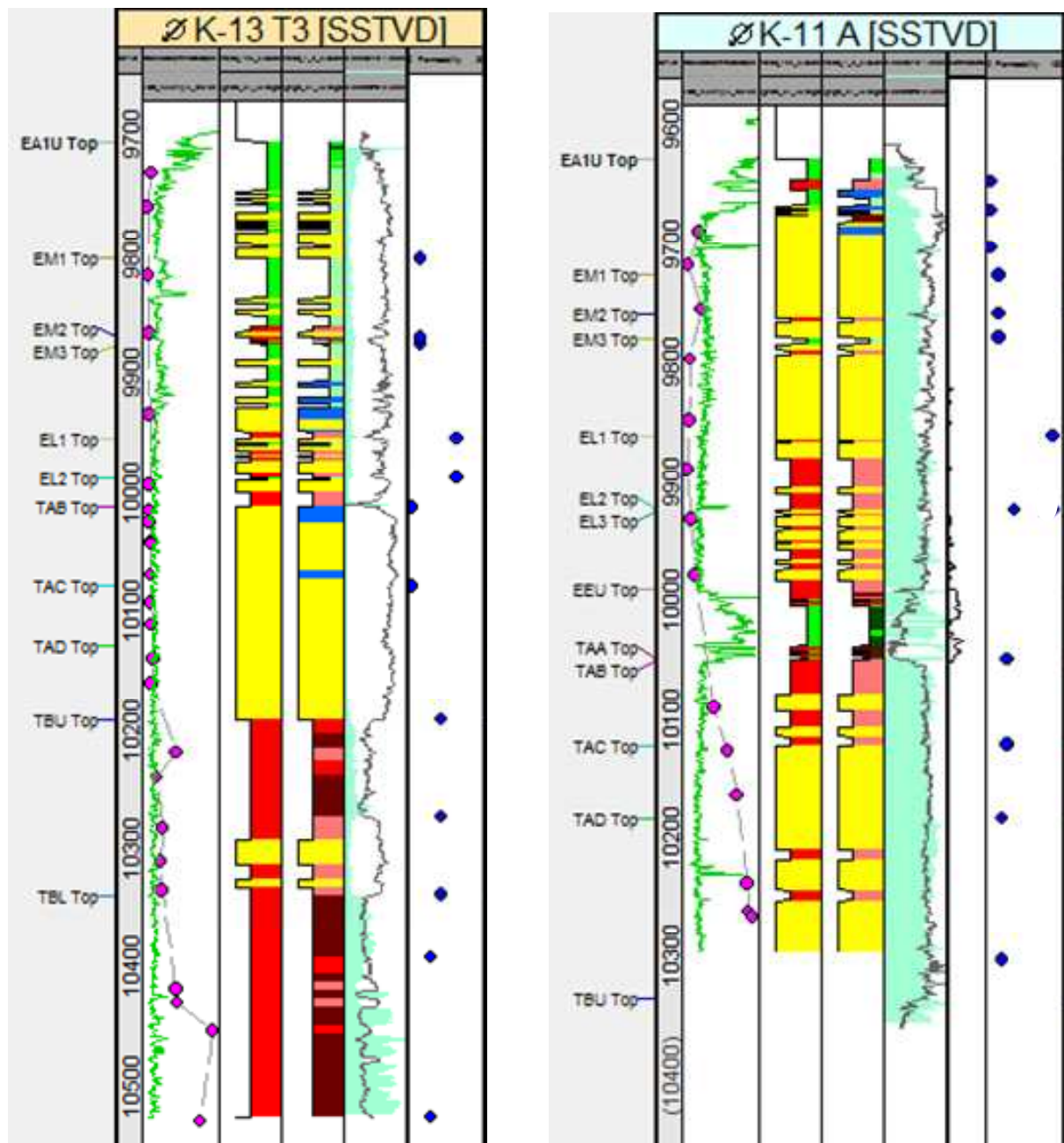
RFT data of 2/4-K-11 A



Well section and RFT data of 2/4-K-11 A

(Legend for the track from 1st to 6th : depth (ftTVD), GR (0-30 API) with RFT in points (floating psig), 123 facies model, 1-8 facies model, Sw in blue (0-1.0) with porosity in gray (0-0.5) and fracture intensity (0-40)

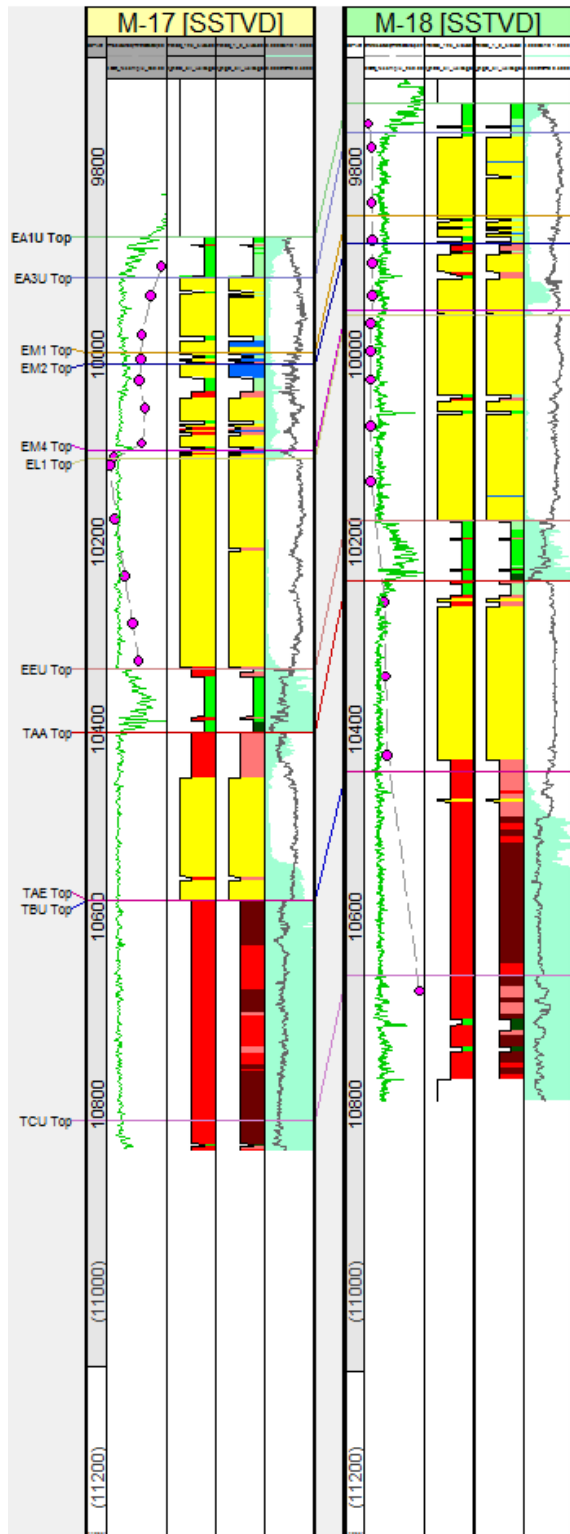
Observation 4 (2/4-K-13 T3 and 2/4-K11 A)



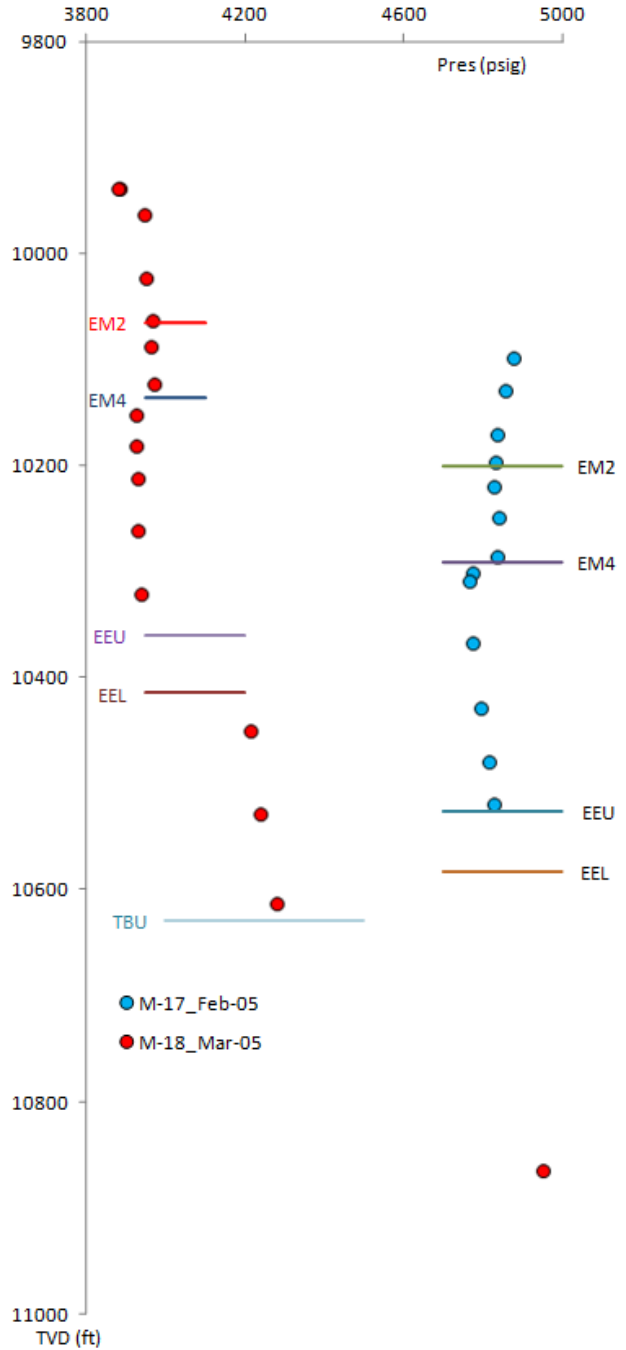
Well section of 2/4-K13 T3 and 2/4-K-11 A

(Legend for the track from 1st to 6th : depth (ftTVD), GR (0-30 API) with RFT in points (floating psig), 123 facies model, 1-8 facies model, Sw in blue (0-1.0) with porosity in gray (0-0.5) and permeability (floating md)

Appendix 6.1 Well section of 2/4-M-17 and 2/4-M-18



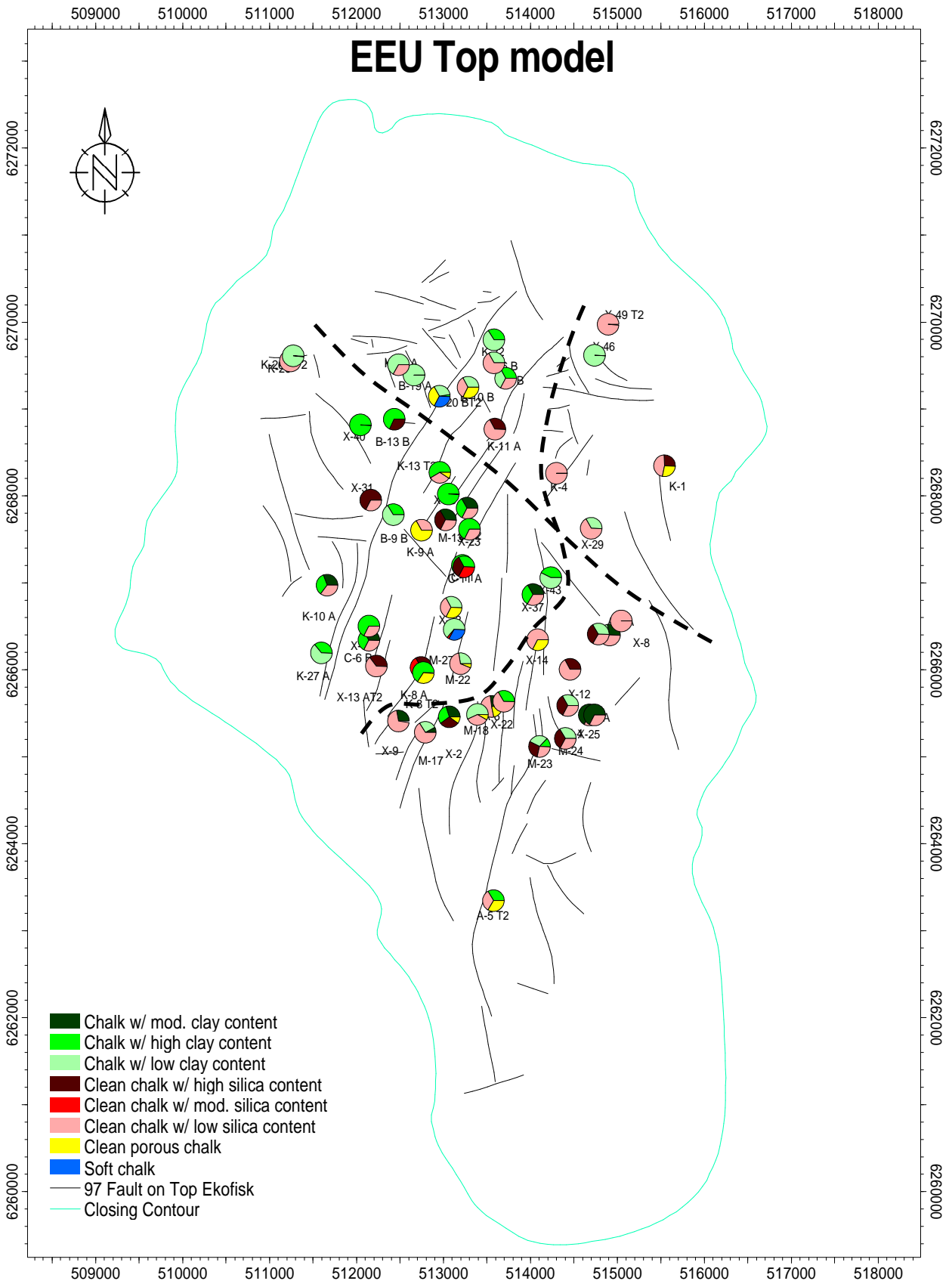
RFT Data of 2/4-M-17 and 2/4-M-18

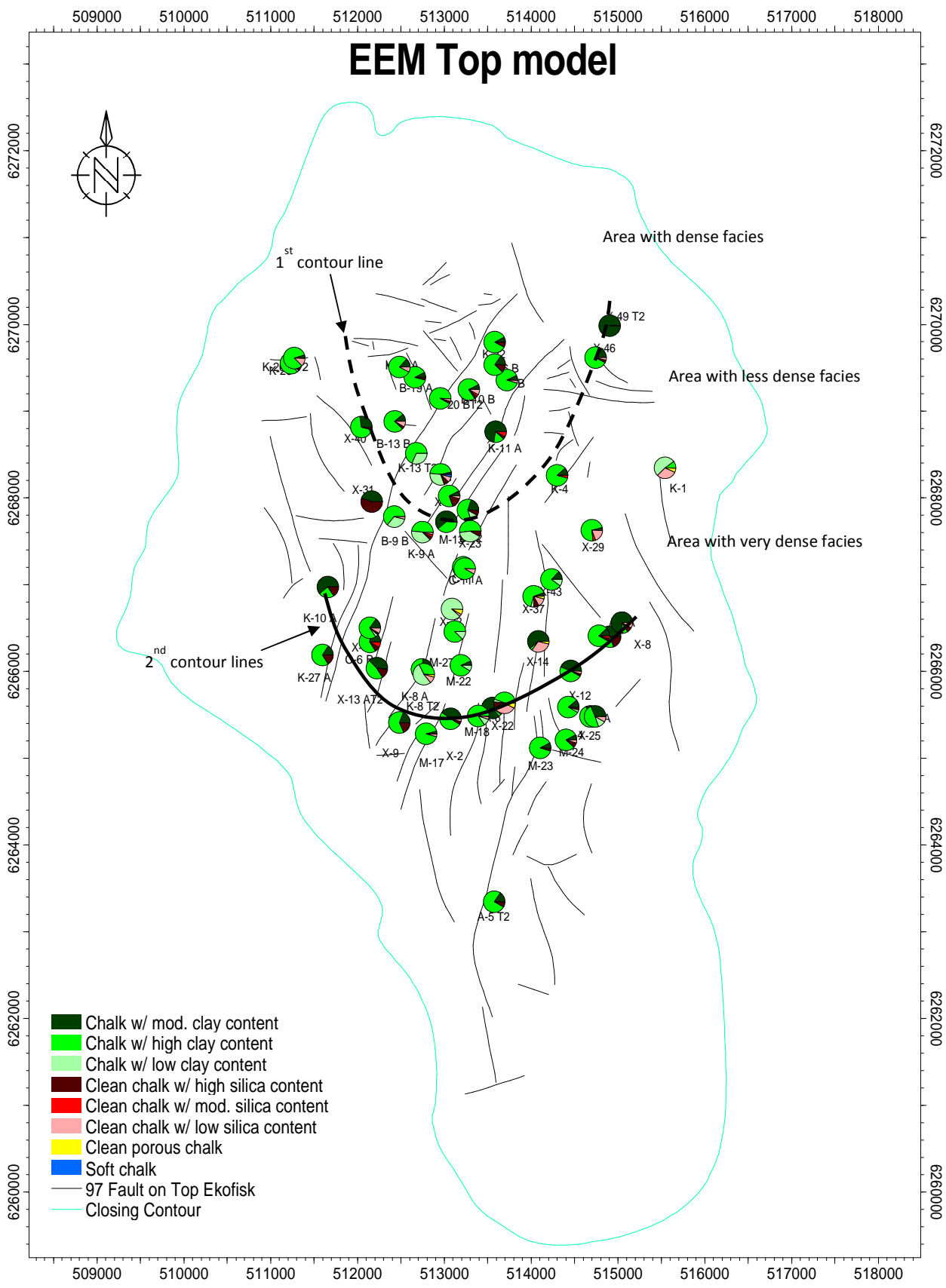


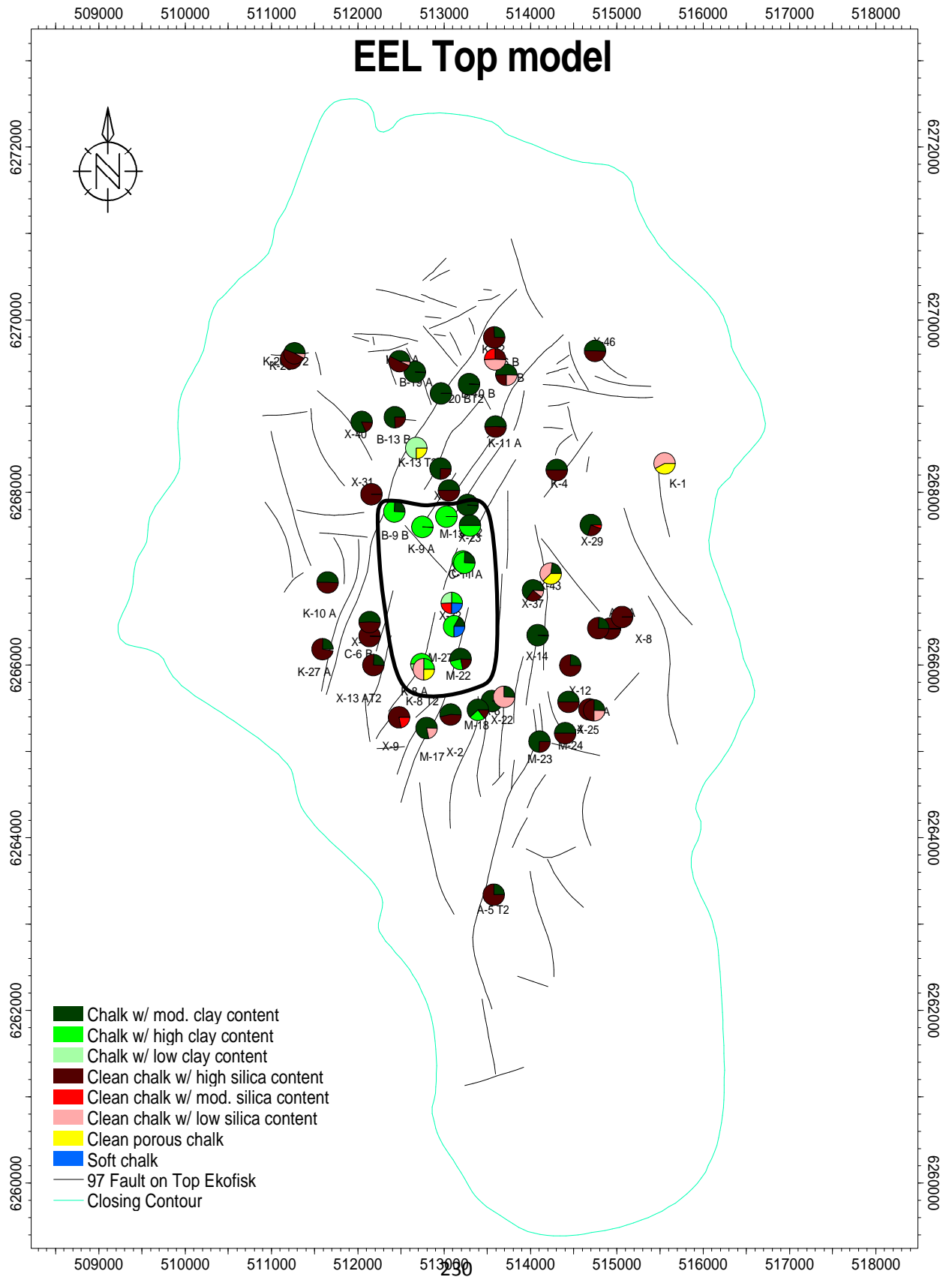
Well section and RFT data of 2/4-M-17 and 2/4-M-18

Appendix 6.2 Trend of facies in layer EEU

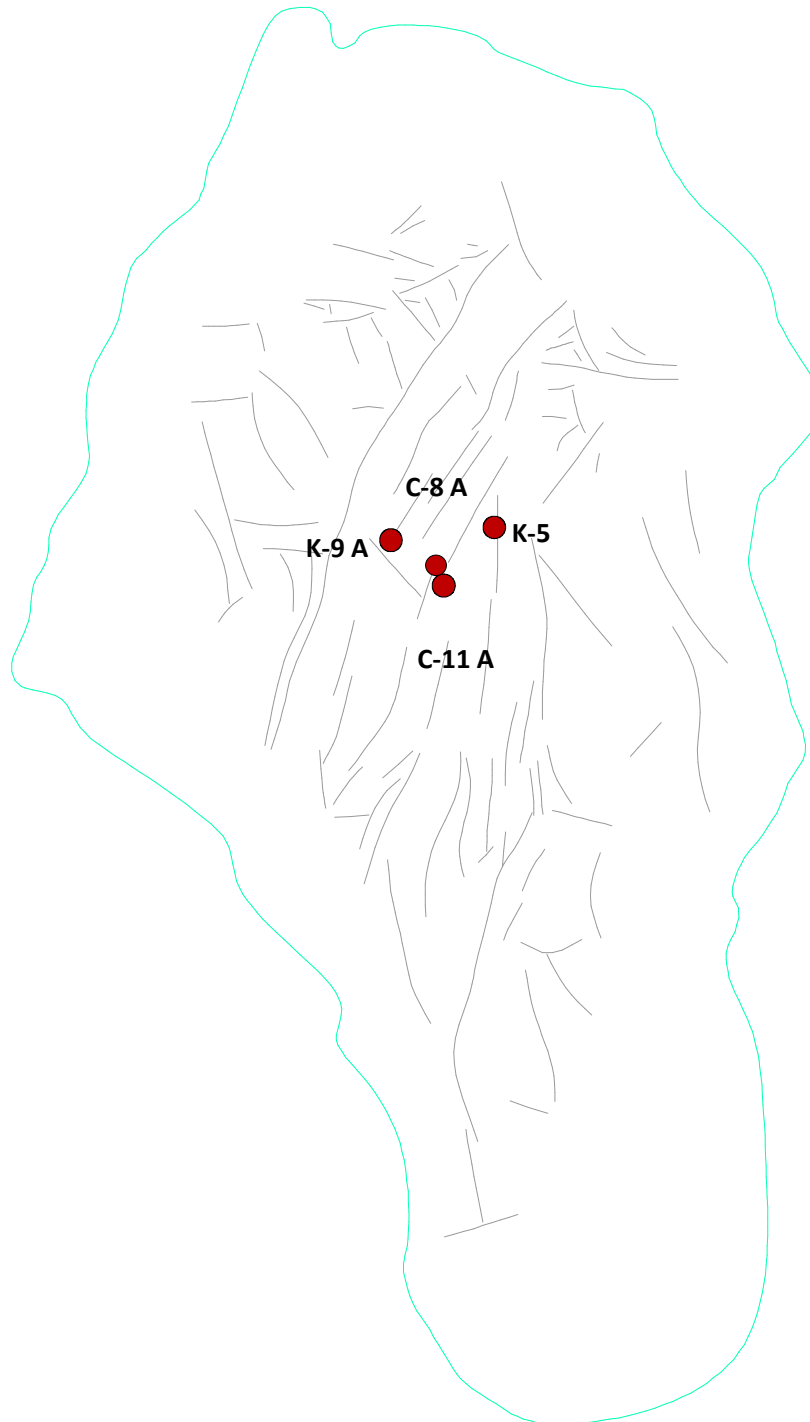
EEU Top model





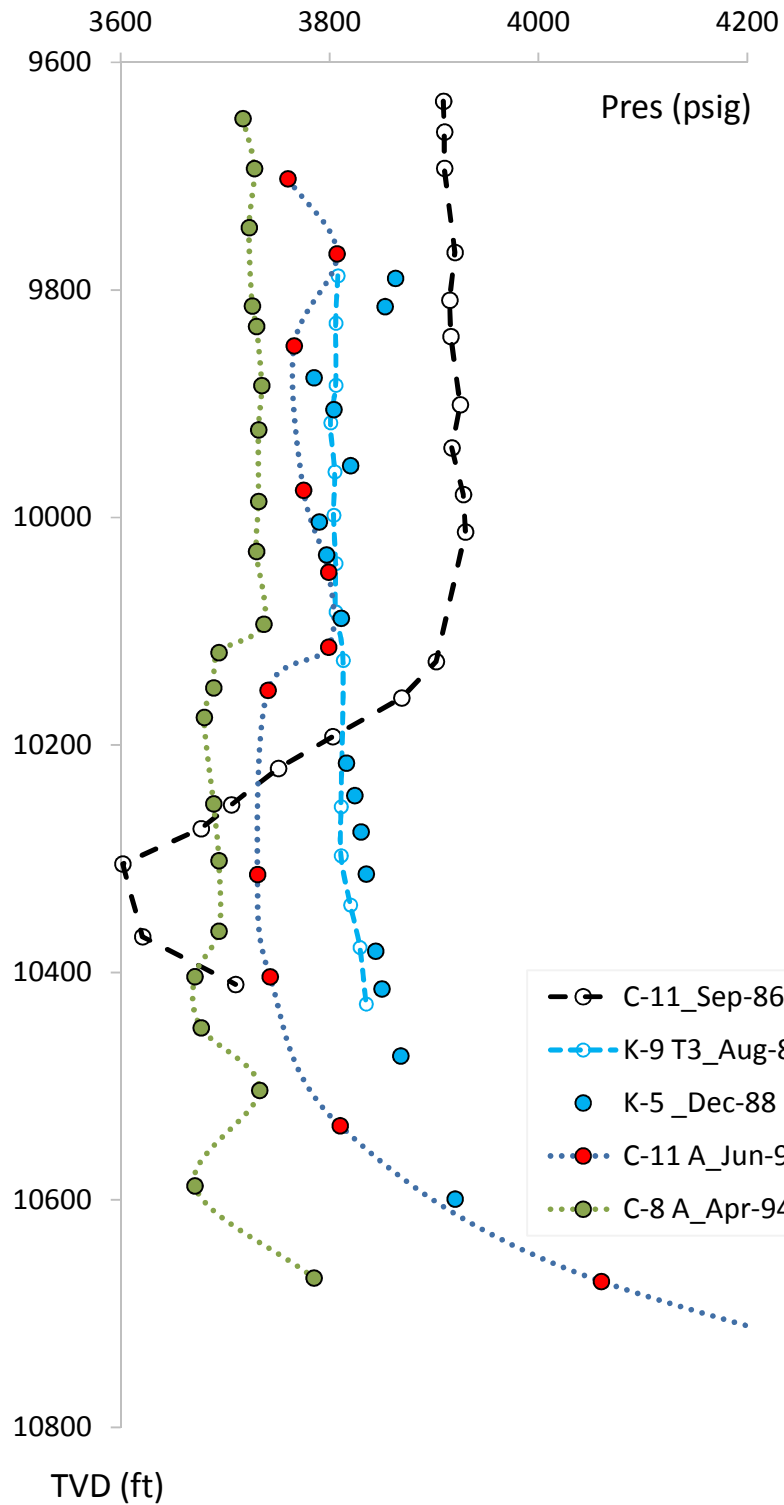


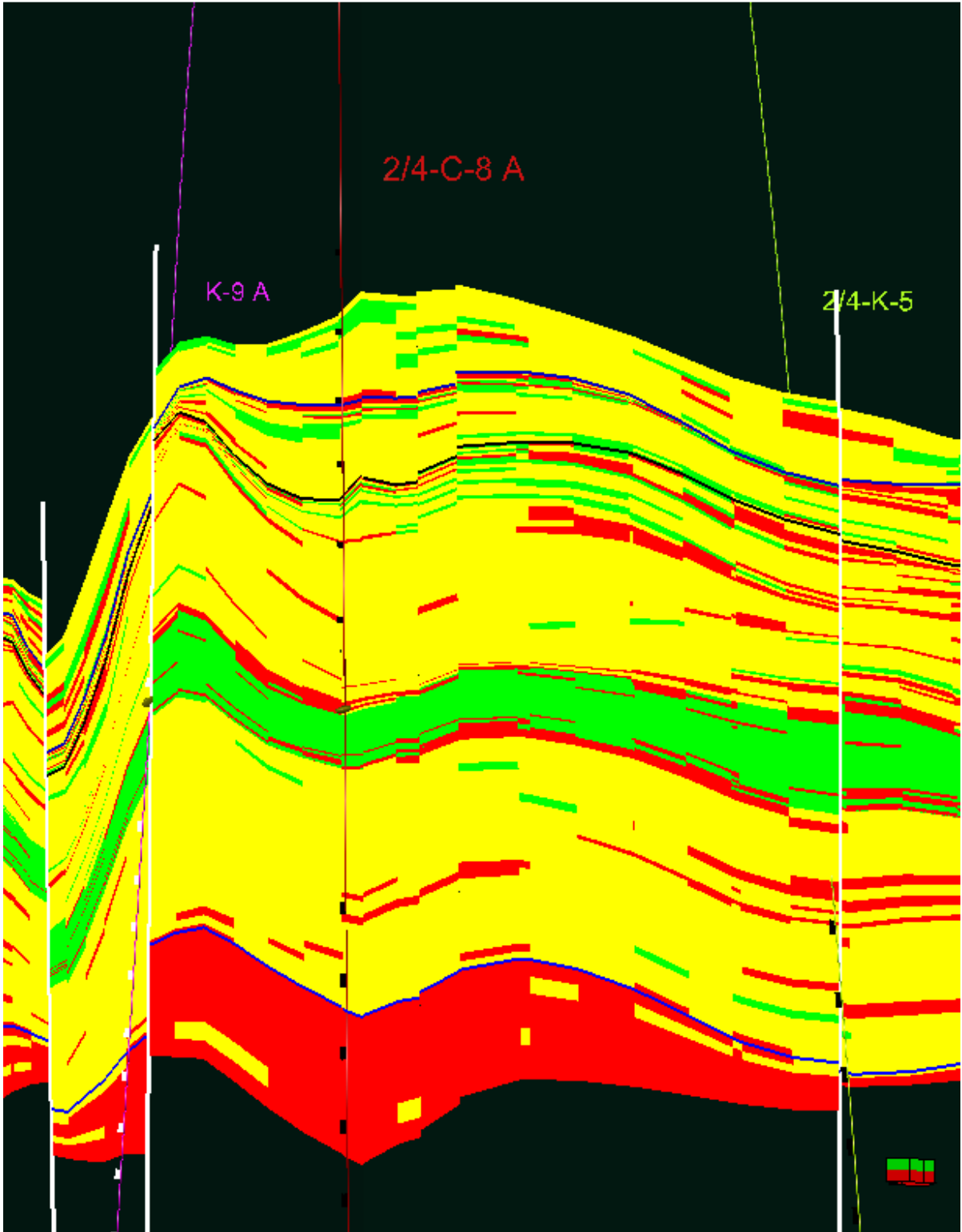
Appendix 6.3 Water imbibition issue on 2/4-C-11 A



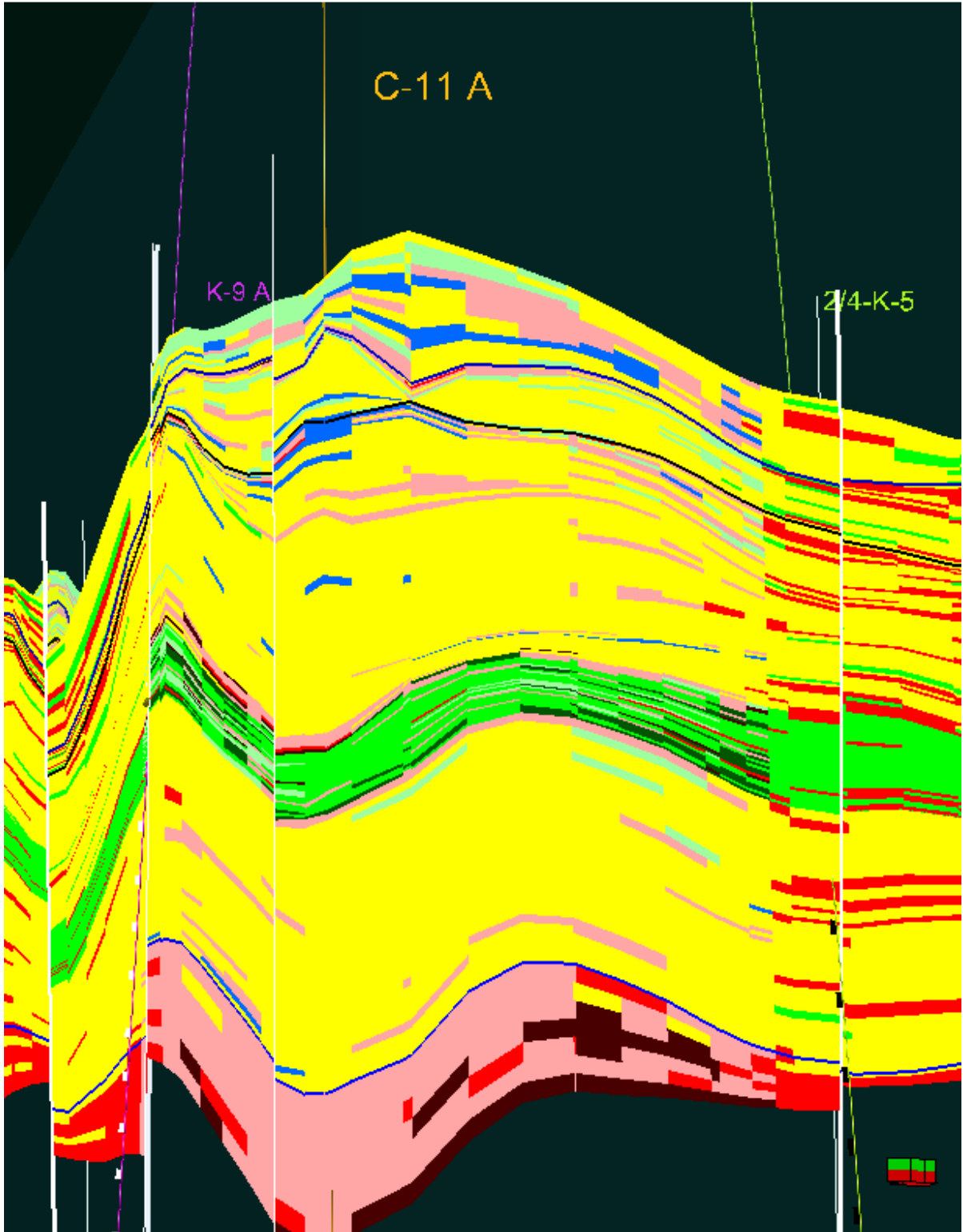
Well location used for the final facies model validation

RFT Data of 2/4-C-11 A & 2/4-C-8 Vicinity

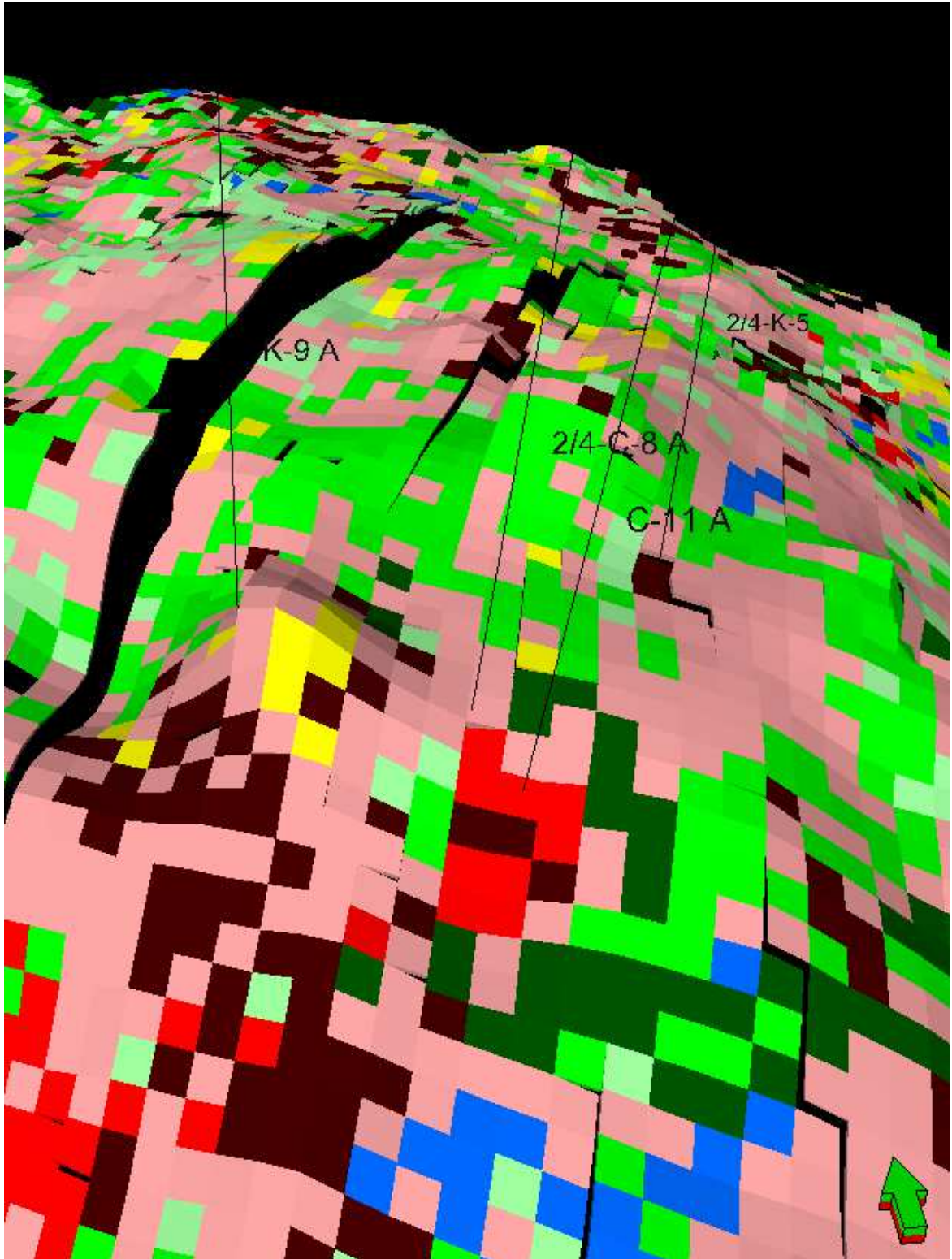




Intersection map of 2/4-C-8 A vicinity in 123 facies model



Intersection map of 2/4-C-11 A vicinity in 1-8 facies model



Facies map of layer EEU in the area of 2/4-C-11 A